

Fatigue Behaviour of Steel Girders Strengthened  
with Prestressed CFRP Strips

by

Farhad Vatandoost

A thesis  
presented to the University of Waterloo  
in fulfilment of the  
thesis requirement for the degree of  
Master of Applied Science  
in  
Civil Engineering

Waterloo, Ontario, Canada, 2010

© Farhad Vatandoost 2010

I hereby declare that I am the sole author of this thesis. This is a true copy of the thesis, including any required final revisions, as accepted by my examiners.

I understand that my thesis may be made electronically available to the public.

## Abstract

Steel bridges and structures often need strengthening due to increased live loads, or repair due to corrosion or fatigue cracking. This thesis explores the use of adhesively bonded prestressed carbon fibre reinforced polymers (CFRP) strips in retrofitting intact steel girders, through experimental and analytical investigations. The first part of the research program investigates the behaviour of CFRP-strengthened steel beams comprised of W Structural Sections (W 310×74) with cover plates welded to the tension flange. Six beams, 2000 mm long, were tested under cyclic loads to examine the effects of CFRP strip strengthening on the fatigue life. The CFRP strip prestressing process, type of CFRP strip, level of prestressing, and the location of the CFRP strips were the main parameters examined in this study.

Debonding at the end of strip was a significant problem that can be controlled by applying a proper end clamp. The maximum increase in fatigue life observed in the experiments was 125 percent, for a specimen strengthened using high modulus CFRP strips bonded onto the cover plates with the highest level of prestressing. An analytical model and a finite element model were developed for analyzing the strengthened beams. A fracture mechanic analysis was performed to investigate the effects of prestressing on the crack growth rates at the critical weld toe. The models were verified using experimental results, and then used to perform parametric studies. It is shown that the effectiveness of reinforcement is greatest for beams with strips on the cover plate, higher CFRP elastic modulus, and higher prestressing level.

In general, this study demonstrates that steel beams can indeed be successfully strengthened or repaired using prestressed CFRP materials.

## **Acknowledgements**

First, I would like to thank my supervisors Dr. K. Soudki and Dr. S. Walbridge for accepting me as their MAsc. student in University of Waterloo and giving me the great opportunity to enhance my knowledge. Without their excellent guidance, engagement, encouragement and wisdom, it would have been so much harder to conduct this work.

I would like to thank our structural laboratory technicians Richard Morrison, Doug Hirst, and Robert Sluban for their great advices and help during my experimental work.

In closing, I thank God. For only through God's grace and blessings has this pursuit been possible.

## **Dedication**

For my parents who I lost eight years ago, who always believed in me and support me through my life with unconditional love, who I deeply feel their absences.

For my wife, Sara, who has always been there through the hard times, who gave me the best gift in my life, our son Milad, who without her patient and encouragement this work was impossible to accomplish.

For my son Milad, who sparked in my life and brought me joy and happiness.

## TABLE OF CONTENTS

Author`s Declaration.....	ii
Abstract .....	iii
Acknowledgments.....	v
Dedication .....	vi
Table of Contents .....	vii
List of Figures .....	xi
List of Tables .....	xiv
CHAPTER 1: INTRODUCTION .....	1
1.1 General .....	1
1.2 Research Objectives .....	4
1.3 Scope.....	4
1.4 Organization.....	5
CHAPTER 2: LITERATURE REVIEW .....	7
2.1 Introduction.....	7
2.2 Conventional Retrofitting of Steel Structures .....	7
2.3 Retrofitting of Steel Structures using FRP Materials .....	9
2.3.1 Surface Preparation .....	12
2.3.2 Retrofitting to Increase Static Strength.....	13
2.3.2.1 Concrete-Steel Composite I Girders .....	13
2.3.2.2 Non-Composite I Girders.....	17
2.3.3 Retrofitting to Enhance Fatigue Performance.....	18
2.3.3.1 Non-Prestressed CFRP Patch on Tension Specimens .....	18
2.3.3.2 Non-Prestressed CFRP Patch on Beam Specimens .....	22
2.3.3.3 Prestressed CFRP Patch.....	23
2.4 Bond of FRP Strengthened Steel .....	28
2.5 Durability of Steel Structures Retrofitted with FRP .....	32
2.6 Field Applications.....	35
2.7 Summary .....	37

CHAPTER 3: EXPERIMENTAL PROGRAM.....	38
3.1 Introduction.....	38
3.2 Materials .....	39
3.2.1 Structural Steel Beam .....	39
3.2.2 Carbon Fibre Reinforced Polymer (CFRP) Strips .....	40
3.2.3 Epoxy Resin .....	41
3.3 Test Specimen.....	41
3.4 Prestressing System .....	43
3.4.1 Griping Tests.....	43
3.4.2 Prestressing System .....	44
3.5 Prestressing Procedure .....	46
3.6 Test Setup.....	54
3.6.1 Instrumentation .....	57
CHAPTER 4: EXPERIMENTAL RESULTS AND DISCUSSION .....	60
4.1 Introduction.....	60
4.2 Prestressing and Load Release Results .....	60
4.2.1 Prestressing Strains .....	60
4.2.2 Shear Stresses at CFRP-Steel Interface andDevelopment length .....	66
4.2.3 Summary .....	68
4.3 Fatigue Test Results .....	69
4.3.1 Fatigue Life.....	69
4.3.2 Deflection versus Life.....	70
4.3.3 Strain vs. Life.....	75
4.3.4 Shear Stress-life .....	103
4.3.5 Crack Growth and Beam Failure .....	107
4.3.6 Summary .....	116
CHAPTER 5: ANALYTICAL AND NUMERICAL MODELLING .....	117
5.1 Introduction.....	117
5.2 Static Analysis of Prestressed Cross Section (before Flexural Loading) .....	117
5.2.1 Analysis Description.....	118
5.2.1.1 Evaluation of Sections Strain/Stress .....	118
5.2.1.2 Prestressing Camber Calculation .....	121
5.2.2 Comparison of Predicted and Measured Strain and Deflection.....	123



5.3 Static Analysis of the Bending Test.....	126
5.3.1 Analysis Description.....	126
5.3.2 Comparison of Predicted and Measured Strain and Deflection.....	127
5.4 Bond Behaviour and Analytical Solutions for Shear Stress Distributions .....	130
5.5 Elastic Finite Element Analysis (FEA) of Fatigue Specimens .....	136
5.5.1 FEA Model Description.....	136
5.5.2 Predicted and Measured Strain and Deflection Comparison .....	143
5.5.3 Predicted Stress Distributions along the Crack Path.....	146
5.5.4 Predicted Stress Distributions along the Crack Path for Full-scale Girders .....	150
5.6 FEA Modelling of CFRP Strips End Debonding.....	151
 CHAPTER 6: FATIGUE AND FRACTURE MECHANICS ANALYSIS .....	 154
6.1 Introduction.....	154
6.2 Comparison of Test Results with Design S-N Curves.....	154
6.3 LEFM Analysis of Fatigue Tests .....	156
6.3.1 Model Description .....	156
6.3.4 Sensitivity Studies of Key Model Parameters for Control Specimen.....	161
6.3.5 Analysis of Retrofitted Specimens using the LEFM Model.....	167
6.4 Parametric Study with the LEFM Model.....	169
6.4.1 Applied Stress Range and Ratio .....	169
6.4.2 Prestressing Level Study.....	171
6.4.3 Analysis of Full-Scale Retrofitted Girder .....	173
 CHAPTER 7: SUMMARY AND CONCLUSIONS.....	 175
7.1 Summary.....	175
7.2 Conclusions.....	176
7.2.1 Prestressing and Prestressing Force release Procedures .....	176
7.2.2 Fatigue Tests and Analytical Studies.....	177
7.3 Recommendations for Future Work.....	179
 REFERENCES .....	 180
 APPENDIX A.....	 191
A.1 Material Mechanical Properties .....	191

A.2 Gripping Tests .....	193
A.2.1 Observations.....	193
A.2.2 Load vs. Displacement Behaviour .....	196
APPENDIX B .....	197
APPENDIX C .....	197
C.1 Sample Strain Calculation.....	203

## LIST OF FIGURES

Figure 2.1. Typical stress-strain curves for FRP reinforcement (Rizkalla et al. 2003) .....	11
Figure 2.2. Various techniques of introducing artificial damage to steel girders. ....	14
Figure 2.3. Calculation of allowable live load for typical strengthened beam. ....	16
Figure 2.4. Specimen geometries with edge notch and drilled hole and loading range (Jones et al. 2003). ....	18
Figure 2.5. Schematic view of double strap joints between CFRP and plates (not to scale)..	20
Figure 2.6. Notch steel plate test specimen, Colombi et al. (2003). ....	25
Figure 2.7. Schematic three layers model or elaminated plate, Colombi et al. ....	25
Figure 2.8. FEM results -normalized SIF vs. crack length, Colombi et al. (2003).....	26
Figure 2.9. Reinforced steel plate specimens configuration, Täljsten et al. (2008).....	27
Figure 2.10. Schematic view of failure modes, Zhao et al. (2006).....	29
Figure 2.11. Finding of the study by Dawood et al. (2006).....	31
Figure 2.12. Finding of the study by Dawood et al. (2006).....	32
Figure 3.1. Section geometric and nominal material properties .....	40
Figure 3.2. Tensile stress vs. strain of the CFRP strip .....	40
Figure 3.3. Specimens configuration .....	42
Figure 3.4. Schematic view of the loading arrangement .....	42
Figure 3.5. A schematic view of prestressing system .....	44
Figure 3.6. Prestressing anchor configuration .....	45
Figure 3.7. The completely assembled prestressing system .....	45
Figure 3.8. Epoxy spreader .....	46
Figure 3.9. Prestressing process preparation.....	47
Figure 3.10. Prestressing stages .....	47
Figure 3.11. The jacking (live) end details .....	48
Figure 3.12. Step loading procedure .....	49
Figure 3.13. CFRP strip clamped to the beam after prestressing.....	50
Figure 3.14. A total debonding as the result of immediate load release .....	51
Figure 3.15. End clamps to mitigate shear and peeling stresses .....	51
Figure 3.16. End clamps configuration.....	52
Figure 3.17. Strain losses in beam at ends at release for specimen 35%-F-M .....	53
Figure 3.18. The fixed clamp anchor used for specimen 35%-F-M .....	53
Figure 3.19. Losses at the strip ends during load release for sepecimen 37%-C-M.....	54
Figure 3.20. The loading frame.....	54
Figure 3.21. Test setup.....	55
Figure 3.22. Test setup and support configurations .....	56
Figure 3.23. Specimen in the loading frame .....	56
Figure 3.24. LVDTs at the midspan during fatigue tests .....	57
Figure 3.25. Strain gauges on the beam and strips .....	58
Figure 3.26. Location of strain gauges on the beam .....	58
Figure 3.27. Location of strain gauges on the CFRP strips attached to the flange. ....	58
Figure 3.28. Location of strain gauges on the CFRP strips attached on the cover plate. ....	59
Figure 4.1. Strain profile along the strips (specimen 15%-F-M).....	61
Figure 4.2. Strain profile along the strips (specimen 14%-F-M).....	62

Figure 4.3. Strain profile along the strips (specimen 35%-F-M).....	64
Figure 4.4. Strain profile along the strips (specimen 37%-C-M) .....	65
Figure 4.5. Average shear stress profile between the strain gauges .....	68
Figure 4.6. Deflection vs. number of cycles .....	72
Figure 4.7. Deflection vs. number of cycles for all specimens .....	74
Figure 4.8. Strain vs. number of cycles for control specimen .....	76
Figure 4.9. Strains vs. Number of Cycles for specimen 15%-F-S.....	78
Figure 4.10. Strain variation along the CFRP strip length for specimen 15%-F-S .....	82
Figure 4.11. Strain variation along the CFRP strip length for specimen 15%-F-S .....	83
Figure 4.12. Strain vs. number of cycles for specimen 14%-F-M.....	84
Figure 4.13. Strain vs. number of cycles for specimen 35%-F-M.....	87
Figure 4.14. Strain variation along the CFRP strip length for specimen 35%-F-M .....	92
Figure 4.15. Strain variation along the CFRP strip length for specimen 35%-F-M.....	92
Figure 4.16. Strain vs. number of cycles for specimen 0%-C-M. ....	94
Figure 4.17. Strain variation along the CFRP strip length for specimen 0%-C-M.....	97
Figure 4.18. Strain variation along the CFRP strip length for specimen 0%-C-M.....	97
Figure 4.19. Strain vs. number of cycles for specimen 37%-C-M. ....	99
Figure 4.20. Strain variation along the CFRP strip length for specimen 37%-C-M.....	103
Figure 4.21. Strain variation along the CFRP strip length for specimen 37%-C-M.....	103
Figure 4.22. Crack initiation and propagation along the weld for control specimen.....	109
Figure 4.23. Crack from the flange to the web of control specimen. ....	109
Figure 4.24. The location of crack initiation and the crack length at the point of debonding for specimen 14%-F-M.....	110
Figure 4.25. Elliptical crack growth pattern through the thickness of flange and interfacial debonding between epoxy and strips (specimen 14%-F-M).....	111
Figure 4.26. Rapid crack growth in few cycles in the web causing a catastrophic failure of specimen 14%-F-M.....	111
Figure 4.27. Debonding of strips for specimen 15%-F-SM.....	112
Figure 4.28. Crack growth pattern along the weld and through the flange (specimen 15%-F- S).....	112
Figure 4.29. Crack growth in both sides of the flange (specimen 35%-F-M). ....	113
Figure 4.30. Debonding of the strips after failure for specimen 0%-C-M.....	114
Figure 4.31. Crack growth and strip fracture for specimen 37%-C-M.....	115
Figure 4.32. Performance of end clamps after failure for specimen 37%-C-M. ....	115
Figure 5.1. Cross section analysis at $x = L/2$ (midspan).....	120
Figure 5.2. Cross section analysis at $x = L/4$ (quarter point).....	120
Figure 5.3. Deflection Due to Prestressing .....	121
Figure 5.4. Deflection Due to Self Weight .....	122
Figure 5.5. Bent element from which relation for elastic curve is obtained.....	123
Figure 5.6. Fatigue test scheme and formulations (NDS, 2005).....	126
Figure 5.7. Schematic view of single lap joint model: geometric parameters .....	132
Figure 5.8. Shear stress variation along the bond length .....	133
Figure 5.9. Schematic view of single lap joint model: debonding failure .....	134

Figure 5.10. Peel stress variation at the end of strips (37% prestressing) with and without end clamp.....	135
Figure 5.11. Symmetrical modelling of quarter beam and boundary conditions.....	137
Figure 5.12. Various iterations of the beam specimen FEA model.....	138
Figure 5.13. Stress path through the flange thickness at the weld toe.....	140
Figure 5.14. Comparison between optimized and most accurate models.....	140
Figure 5.15. Shell element modelling of the strip.....	141
Figure 5.16. Prestressing Step 1 – introduction of prestressing force.....	142
Figure 5.17. Prestressing Step 2 – camber in beam after force released.....	142
Figure 5.18. Deformed shape of the beam model under vertical load.....	143
Figure 5.19. Applied stress distribution along crack path for 0%-C-M specimen.....	147
Figure 5.20. distribution along crack path for 37%-C-M specimen.....	147
Figure 5.21. Net stress distributions for 37%-C-M specimen.....	148
Figure 5.22. Applied stress distribution along crack path for 0%-F-M case.....	148
Figure 5.23. Stress distribution along crack path for 14%-F-M specimen.....	149
Figure 5.24. Net stress distributions for 15%-F-S specimen.....	149
Figure 5.25. Applied stress distribution along crack path for different girder depths.....	150
Figure 5.26. Effect of girder depth on stress distribution due to prestressing.....	151
Figure 5.27. End bond deformation modelled using FEA.....	152
Figure 5.28. Peel stress distribution obtained using analytical and FEA methods.....	153
Figure 5.29. Shear stress comparison obtained using analytical and FEA methods.....	153
Figure 6.1. Comparison of design S-N curves and test results.....	156
Figure 6.2. Schematic view of stresses distributions through the flange thickness.....	159
Figure 6.3. S-N curves for various $C$ and $m$ values.....	162
Figure 6.4. S-N curves for various $\Delta K_{th}$ values.....	164
Figure 6.5. S-N curves for various $a_i$ values.....	165
Figure 6.6. S-N curves for various $a/c$ values.....	165
Figure 6.7. The upper, lower and best fit S-N curves.....	166
Figure 6.8. Comparison of LEFM analysis and test results.....	168
Figure 6.9. Comparison of $\Delta K_{eff}$ and $\Delta K_{rds}$ versus crack depth curves.....	169
Figure 6.10. Stress range and ratio results for 0%-C-M case.....	170
Figure 6.11. Stress range and ratio results for 37%-C-M case.....	171
Figure 6.12. Stress range and ratio results for 40%-C-M case.....	172
Figure 6.13. Stress range and ratio results for 60%-C-M case.....	172
Figure 6.14. Stress range and ratio results for 75%-C-M case.....	173
Figure 6.15. Results of full-scale retrofitted girder analysis ( $d = 600$ mm, 40%-C-M).....	174
Figure 6.16. Results of full-scale retrofitted girder analysis ( $d = 900$ mm, 40%-C-M).....	174
Figure A.1. Elastic modulus calculation based on stress-strain diagram for S-CFRP strip..	191
Figure A.2. Elastic modulus calculation based on stress-strain diagram for S-CFRP strip..	192
Figure A.3. Poisson`s ratio calculation for S-CFRP and M-CFRP strips.....	192
Figure A.4. Gripping test setup.....	193
Figure A.5. Failure of gripping test.....	194
Figure A.6. Sliding at the edges.....	195
Figure A.7. A schematic view of gripping.....	195
Figure A.8. Tensile load Vs. displacement curves for CFRP strip-anchor assemble.....	196

## LIST OF TABLES

Table 2.1. Field application .....	35
Table 3.1. Test matrix .....	39
Table 4.1. Strains and stresses along the strips after all losses (specimen 15%-F-S).....	62
Table 4.2. Strains and stresses along the strips after all losses (specimen 14%-F-M) .....	63
Table 4.3. Strains and stresses along the strips after all losses (specimen 35%-F-M). .....	64
Table 4.4. Strains and stresses along the strips after all losses (specimen 37%-C-M).....	65
Table 4.5. Shear stresses along the strips (MPa) .....	67
Table 4.6. Fatigue life for all specimens.....	69
Table 4.7. Deflections ranges.....	71
Table 4.8. Summary of strain-life results for the control specimen.....	78
Table 4.9. Summary of strain-life results for the specimen 15%-F-S. ....	82
Table 4.10. Summary of strain-life results for specimen 14%-F-M.....	86
Table 4.11. Summary of strain-life results for the specimen 35%-F-M. ....	90
Table 4.12. Summary of strain-life results for the specimen 0%-C-M.....	96
Table 4.13. Summary of strain-life results for the specimen 37%-C-M.....	102
Table 4.14. Total shear stress variation along the beam length during prestressing and fatigue testing for specimen 15%-F-S.....	104
Table 4.15. Total shear stress variation along the beam length during prestressing and fatigue testing for specimen 35%-F-M. ....	105
Table 4.16. Shear stress variation along beam length during fatigue test for specimen 0%-F-M. ....	106
Table 4.17. Total shear stress variation along the beam length during prestressing and fatigue testing for specimen 37%-C-M.....	106
Table 5.1. Analytically and experimental change in strain after prestressing release .....	122
Table 5.2. Prestressing camber calculation based on equivalent load method .....	124
Table 5.3. Prestressing camber calculation based on measured strains .....	125
Table 5.4. Calculated strains under flexural loading .....	128
Table 5.5. Measured total strains under flexural loading.....	129
Table 5.6. Analytical and experimental deflections.....	130
Table 5.7. Comparison of the experimental and FEA applied force .....	143
Table 5.8. Comparison of prestressing cambers determined by various means .....	144
Table 5.9. The prestressing and bending strains from FEA.....	144
Table 5.10. Total strain comparison at three strain gauge locations.....	145
Table 6.1. Model parameters assumed for LEFM analysis. ....	160
Table 6.2. Values for $C$ and $m$ reported or assumed by others. ....	161
Table 6.3. Values for $\Delta K_{th}$ reported or assumed by others. ....	163
Table 6.4. Parameters used for upper, lower, and assumed S-N curves. ....	166
Table B.1. Stress distributions through the flange thickness for the specimen strengthened using attached M-CFRP strips on the cover plates. ....	197
Table B.2. Stress distributions through the flange thickness for the specimen strengthened using attached M-CFRP strips on the flanges.....	198
Table B.3. Stress distributions through the flange thickness for the specimen strengthened using attached S-CFRP strips on the flanges. ....	199

Table B.4. Stress distributions through the flange thickness for unreinforced full-scale girders under a vertical applied unit load.....	200
Table B.5. Stress distributions through the flange thickness for reinforced full-scale girders under a vertical applied unit load.....	201
Table B.6. Stress distributions through the flange thickness for 37% prestressed full-scale girders under. ....	202
Table C.1. Geometric properties of specimens at midspan ( $x = L/2$ ).....	200
Table C.2. Geometric properties of specimens at the quarter points ( $x = L/4$ ).....	200
Table C.3. Stress/Strain calculation ( $x = L/4$ ).....	205
Table C.4. Stress/Strain calculation ( $x = L/4$ ).....	207





# **Chapter 1: Introduction**

## **1.1 General**

Many of our aging cyclically loaded steel structures, including bridges, buildings, offshore platforms, large mining equipment, and towers, are in need of repair or replacement. This requirement for structural rehabilitation is the result of severe deterioration under in-service loading conditions. A variety of factors can contribute to the deterioration of steel structures over time, including: increasing traffic volumes and loads, corrosion (in particular in marine environments or resulting from the use of de-icing salts in winter), and lack of proper maintenance. All of these factors, in combination with the presence of cyclic loads, can result in metal fatigue – a process starting with the formation of micro-cracks, which can eventually grow into larger cracks sufficient to eventually cause structural failure. This problem, along with the limited funding available for replacement of structures, has created a pressing need for reliable and durable systems for the strengthening and repair of these types of structures.

A number of conventional methods for the strengthening and repair of deteriorating steel structures exist. However, each of these methods has potential drawbacks and limitations. Welding or bolting steel reinforcing plates to existing structures is labour intensive and time consuming. Welding is not always possible in the case of older structures and in newer ones may result in new local stress concentrations from which fatigue cracks can eventually initiate. Bolting can be inefficient, since the required holes result in a reduction in the area of the original cross section. What's more, the attached reinforcing steel plates may eventually experience the same corrosion issues as the original structure. For enhancing the fatigue performance of existing welds, post-weld treatment methods may be used, including

grinding, dressing, and peening. While effective in delaying the propagation of small cracks, these treatment methods are generally of no use in delaying crack growth beyond a crack size of a millimetre or so. Based on these limitations, it seems that there is a need for better methods for rehabilitating steel structures subjected to cyclic (fatigue) loading.

Advanced composite materials are arguably the newest materials to enter the construction industry and their utilization is growing rapidly. Fibre reinforced polymers (FRPs) have been recently researched and used for various structural applications including: increasing the static strength of structures made from lower stiffness materials such as wood and concrete, fabricating entire new pultruded structural sections, and more recently for the retrofitting of steel structures. A variety of reasons are given for the increased use of FRPs in structural retrofitting applications. Among these are: their durability against corrosion, their limited impact on aesthetic appearance, and their limited effect on clearances underneath retrofitted slabs or girders. The flexibility and light weight of FRPs makes their use appealing, in particular when access is limited. The use of FRPs for the strengthening of metal structures was first used in the aircraft industry – initially on lower stiffness metals, such as aluminum.

The use of FRPs for the retrofitting of steel structures has its challenges. Early FRPs had stiffness properties lower than steel, thus severely limiting their efficiency. This problem has been addressed more recently with the development of newer FRP products with elastic moduli greater than that of steel ( $E > 200$  GPa). High modulus carbon fibre reinforced polymers (CFRPs), in particular, have received increasing interest for steel applications for this reason.

Recent research on the use of CFRPs for the fatigue retrofitting of steel structures has shown that these materials have potential in this application. These studies have been limited for the most part, however, to fatigue tests of reinforced specimens with fatigue cracks initiating from regions of local stress concentration created by drilling holes or machining notches in the steel. Fatigue performance improvements have been seen in most cases. However, these improvements were modest in some cases, and the findings of these studies cannot be directly extended to more practical situations. A smaller number of studies have found that the benefit of this retrofit can be significantly improved by first prestressing the CFRP and then bonding it to the steel. This results in the introduction of compressive residual stresses in the steel, which can play an active (rather than a passive) role in slowing down the initiation and growth of cracks. Until now, these studies have focused on applications involving riveted structures. The application of a similar approach to welded steel structures has yet to be investigated.

In this thesis, the development of a prestressing system for CFRP strips is described and a fatigue test-based study of steel beams with welded cover plates retrofitted using pre-stressed CFRP strips is presented. The investigated weld detail is a common one on older steel bridge structures that is known to exhibit particularly poor fatigue performance. In addition to fatigue testing, analytical and numerical models are used to determine the effect of the pre-stressed CFRP strips on the local stresses in the vicinity of the critical crack location in the welded beams. The stresses obtained using these models are then used as input for a fracture mechanics analysis. The fracture mechanics model is validated using the test data and parametric studies are performed using the validated model.

## **1.2 Research Objectives**

The objectives of this study are:

- to develop a system for prestressing CFRP strips and appropriate procedures for adhering them to steel surfaces for the purpose of fatigue retrofitting,
- to evaluate the fatigue performance under cyclic flexural loading conditions of steel beams with welded cover plates strengthened using pre-stressed CFRP strips,
- to develop analytical and numerical models for predicting the stress distributions in CFRP-strengthened steel beams, including the residual stresses due to the prestressing of the CFRP strips and the stresses due to externally applied cyclic loads,
- to perform linear elastic fracture mechanics (LEFM) analyses of cyclically loaded CFRP-strengthened steel beams to predict their fatigue performance, and
- to perform parametric studies using the developed models in order to determine the conditions under which the strengthening of welded cover plates with pre-stressed CFRP strips can be most effective in improving fatigue performance.

## **1.3 Scope**

The scope of this study includes: experimental testing, analytical and numerical modelling, and LEFM analysis to examine the use of prestressed CFRP composite materials for the fatigue retrofitting of steel girders with welded cover plates.

The fatigue tests are limited to the study of one steel beam geometry and fatigue detail (a welded cover plate). All of the tests have been conducted under constant amplitude loading at

one stress range and stress ratio. Two CFRP grades and several prestressing levels are investigated.

The analytical, numerical, and LEFM models employed herein are used for the prediction of the test specimen behaviour and for parametric studies, to extend the results beyond the testing conditions and identify the conditions under which the investigated retrofitting method can be most effective in improving fatigue performance.

#### **1.4 Organization**

The following is a brief explanation of the thesis organization:

**Chapter 2** presents a literature review on the static strength or fatigue retrofitting of steel structures using conventional means or composite materials such as CFRP.

**Chapter 3** describes the test specimens, procedures, and experimental program employed for the CFRP grip static tests and the retrofitted steel beam fatigue tests.

**Chapter 4** presents the results of the experimental work including prestressing procedure results and fatigue test results.

**Chapter 5** presents the analytical and numerical modelling work conducted for this thesis. Specifically, the various modelling procedures and models are described. The models are validated using strain and displacement measurements obtain from the fatigue tests.

**Chapter 6** presents the LEFM analysis conducted to predict the performance of the steel girders strengthened using FRP materials. The LEFM model is first described and then validated using the available fatigue test results. Parametric studies are then performed to

evaluate the influences of various parameters on the predicted fatigue lives of the retrofitted beams, and to extend the results to other prestressing levels and girder depths.

**Chapter 7** presents a summary of the thesis, along with conclusions resulting from the experimental and analytical studies and recommendations for future work.

## **Chapter 2: Literature review**

### **2.1 Introduction**

In this chapter, literature on the rehabilitation of steel structures by conventional methods is first reviewed. Then previous research on the use of FRP for strengthening of steel structures is summarized. Specifically topics on static and fatigue strengthening, surface preparation, bond issues, and durability of the reinforcing system are discussed in detail. Field applications on the use of FRPs to strengthen steel structures are presented. The chapter concludes with a summary of the key findings in the literature and highlights areas where the current state-of-the-art is still lacking.

### **2.2 Conventional Retrofitting of Steel Structures**

In general, a structure may need repair due to deterioration over time, change in design code, change of usage, or increase in load spectra. In steel bridge structures, the deterioration of the structural capacity over time may be due to corrosion, impact damage, and/or fatigue cracking (Hollaway et al. 2002, Jones et al. 2003, Liu et al. 2005, Schnerch et al. 2005).

The conventional methods for increasing the static strength of steel structures typically involve welding or bolting steel plates to the existing structure, in order to increase the effective cross sectional area or the buckling resistance of the structure (Allen et al. 1980, Bakht et al. 1979). Examples for retrofitting steel structures include the following:

- welding cover plates to the critical flange areas of bridge floor beams,
- adding more bolts or substituting larger bolts when flange material is added,

- reinforcing bearing stiffeners by bolting or welding additional angles,
- adding supplementary bolted or welded intermediate stiffener plates,
- splicing webs to resist moment by adding plates, and/or reinforcing truss members by adding adjustable bars or cover plates.

Compression members can be strengthened by adding cover plates, either to increase the section moment of inertia, to convert unsymmetrical cross sections to symmetrical ones, or to reduce the width-to-thickness ratios of the plates that comprise the cross section, in order to avoid local buckling and fully utilize the yield strength of the steel.

Conventional methods have associated constructability and durability issues. In many cases, welding is not a desirable solution due to the poor fatigue performance associated with welds and the associated weld defects (Manteghi et al. 2006). Welding is labour intensive and can only be performed by trained and certified welders. Also, in older structures, the existing steel may not be weldable, thus necessitating the use of bolted plates or some other approach. Although bolted connections have better fatigue performance, they are not proficient from a cost and time point of view, due to the significant labour associated with the field drilling and alignment of the bolt holes. There is also a cross sectional loss associated with drilling bolt holes in existing structural members, which reduces the efficiency of this rehabilitation approach. The use of steel plates for reinforcing existing structures has the additional disadvantage that the new steel plates may be just as susceptible to corrosion or fatigue as the existing steel structure (Colombi et al. 2003b).



For increasing the fatigue strength of existing steel structures, steel plates may also be used to increase the cross section area and thus reduce the applied stress range level. Several alternative techniques have also been investigated for improving the fatigue performance of welded steel structures, including: hammer peening, burr grinding, and mechanized tungsten inert gas (TIG) dressing (Colombi et al. 2003a,b). These so-called “post-weld treatment methods” work by either modifying the weld toe geometry and thus reducing the stress concentration at the weld toe, removing micro-defects, or introducing compressive residual stresses, which have the effect of reducing the growth rates of small cracks subjected to cyclic loading conditions (Allen et al. 1980, Dowling et al. 2009). However, there are still many unresolved issues regarding these methods such as, labour costs, practical difficulties due to use of heavy duty equipments and material weight, corrosion sensitivity and inconsistency in section geometry.

### **2.3 Retrofitting of Steel Structures using FRP Materials**

The first use of fibre reinforced polymer (FRP) products for structural strengthening was Glass FRP (GFRP) reinforcement in reinforced concrete structures in the mid-1950s (Rizkalla et al. 2003). Carbon FRP strips overlay have been used to strengthen metallic structures such as aircraft in the early-1980s (Armstrong et al. 1983). Since their early application, many FRP materials with different types of fibres have been developed and used in various civil engineering applications.

FRPs consist of fibres embedded in a matrix. The fibre type and volume fraction are chosen to satisfy strength and stiffness design requirements, and the surrounding matrix facilitates

the transfer of the load among fibres, provides dimensional stability, and fibre support and protection. Fibres used in composites can be categorized into three main types: carbon fibres, inorganic fibres (i.e. glass fibres), and polymeric fibres (i.e. aramid fibres). The matrix is typically epoxy, vinyl ester, or polyester resin. The matrix can be thermoplastic or partially cured thermo-set resin. The contribution of the matrix to the strength or stiffness of the composite is usually minimal. According to Allan et al. (1988), resin selection controls the manufacturing process, service temperature, flammability characteristics, and corrosion resistance of the composite.

Advantages of FRPs include: High strength to weight ratio, light weight, ease of transport and installation, thermal stability, excellent fatigue characteristics of CFRPs, electromagnetic neutrality, and the ability to tailor mechanical properties, and non-corrosiveness (durability). FRP materials also have potential disadvantages such as: low in-plane transverse strength (shear strength), high initial cost in comparison to steel, low compression strength, low elastic modulus (except for HM-FRPs), low fire resistance, deterioration of mechanical properties due to moisture absorption, and susceptibility to creep and creep rupture (GFRPs).

The main differences among the available FRP products are the damage tolerance and the fibre stiffness. The higher strength of carbon fibre reinforced polymers (CFRPs) compared with the steels is evident in Figure 2.1, while glass fibre reinforced polymers (GFRPs or “fibreglass”) have a relatively low strength (Rizkalla et al. 2003).

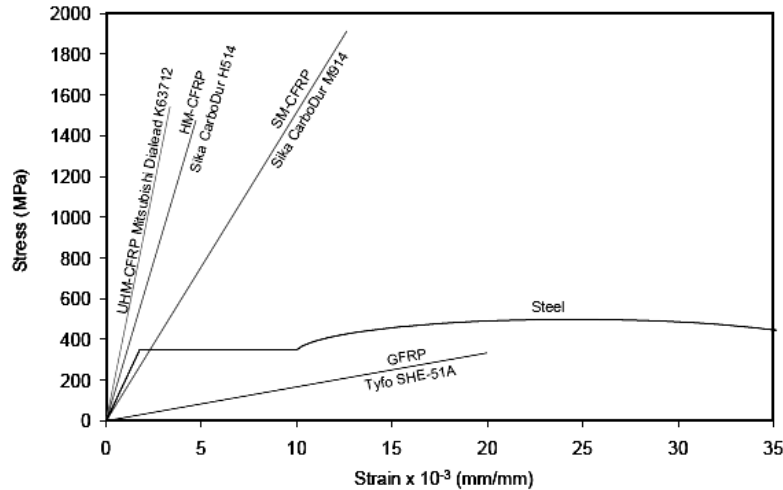


Figure 2.1. Typical stress-strain curves for FRP reinforcement (Rizkalla et al. 2003)

FRP materials are available in a variety of grades, according to the process by which they are manufactured. In the context of this thesis, a CFRP material is classified to by its elastic modulus. CFRP material with an elastic modulus value less than that of steel (i.e.  $E < 200$  GPa) is referred as Standard Modulus-CFRP (SM-CFRP), CFRP material with an elastic modulus ranging between 200 GPa and 400 GPa is referred as High Modulus-CFRP (HM-CFRP). CFRP material with an elastic modulus larger than 400 GPa is referred to as Ultra High Modulus-CFRP (UHM-CFRP). A detailed review of the different types of fibres and resins used to develop FRP materials is reported elsewhere (Rizkalla et al. 2003).

Research efforts to examine the feasibility and effectiveness of retrofitting civil steel structures using FRP have generally focused on the following areas:

- surface preparation,
- static strength of tension and compression members,

- fatigue and cyclic load behaviour of retrofitted members,
- bond of FRP strengthened steel, and
- durability and of galvanic corrosion issues.

A brief summary of the key research findings in the literature is presented in the following sections.

### *2.3.1 Surface Preparation*

Proper installation of a CFRP strip onto a steel surface is essential to ensure the design functionality and long-term performance of the strengthened member (Karbhari et al. 1995, Shulley et al. 1994, Liu et al. 2005). To guarantee full utilization of the bonded CFRP strip, surface preparation of the steel must be undertaken to enhance the formation of a chemical bond between the adherent (CFRP, steel) and adhesive. For this purpose, the active steel surface must be free from contaminants and the weak layers removed. The best approach for surface preparation is degrease the steel surface and then sand blasting to remove any weak exterior layers (i.e. millscale or corrosion) and increase the surface roughness. Any remaining dust on the steel and CFRP surfaces should then be removed by vacuuming and wiping. Solvents such as acetone are highly recommended to remove all possible contaminants on the CFRP surface.

### *2.3.2 Retrofitting to Increase Static Strength*

Early studies of bonded CFRP strips to steel structures for strength improvement were mainly focused on static strength and stiffness increases. This is typically what is needed in upgrading applications to accommodate an increase in live load, as discussed in the following sections.

#### *2.3.2.1 Concrete-Steel Composite I Girders*

Sen et al. (2001) investigated the effect of bonding a CFRP strip to a steel bridge girder on its static load capacity. Six 6100 mm long W200 x 36 steel girders ( $f_y = 310 \text{ MPa}$ ) acting compositely with concrete slabs (710 mm x 114 mm) were tested. The girders were loaded beyond their yield stress, unloaded and then repaired. The girders were repaired using SM (standard modulus)-CFRP strips (2 and 5 mm thick). Strength gains of 21% and 52% for the girders strengthened with 2 and 5 mm thick CFRP strips were observed, respectively. The strength increases of similar wide flange steel beams with  $f_y = 370 \text{ MPa}$  and strengthened with CFRP strips (2 mm and 5 mm thick) were 9% and 32%, respectively.

Tavakkolizadeh et al. (2003a) carried out an experimental investigation on CFRP strengthening of steel bridge girders. They tested three 4780 mm long composite girders. The steel sections were W355 x 13.6 and the concrete slabs were 910 mm x 75 mm. The tension flange area of the girder was reduced as shown in Figure 2.2 to simulate 25, 50, and 100 percent loss of its tensile capacity. The specimens were repaired with SM-CFRP strips with an average tensile strength of 2,137 MPa, tensile modulus of elasticity of 144 GPa, Poisson's ratio of 0.34, and length of 3950 mm. CFRP cross sectional areas ranged from 97 mm<sup>2</sup> for

the girder with 25 percent loss and 483 mm<sup>2</sup> for the girder with 100 percent loss. Following the strengthening, the beams were tested in flexure to failure.

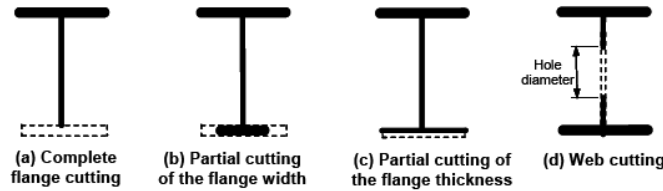


Figure 2.2. Various techniques of introducing artificial damage to steel girders  
(Edberg et al., 1996 and Gillespie et al. 1996a)

It was found that the strength was not only restored but also increased by 20, 80, and 100 percent, using CFRP strip areas of 97, 290, and 483 mm<sup>2</sup>, respectively, compared to a calculated value for the intact (control) specimen. On the other hand, no extra gain in stiffness was noticed, where the measured stiffness values were 91, 102, and 86 percent, of that of the intact girder. It was also found that rupture of CFRP strip occurred in the girder with 25 percent loss in tension flange and repaired with 97 mm<sup>2</sup> of CFRP strip. The girder having 50 percent loss in tension flange and repaired with 290 mm<sup>2</sup> of CFRP strip failed by crushing of the concrete slab, followed by a limited debonding of the CFRP strip at midspan. The girder with 100 percent loss in tension flange and repaired with 483 mm<sup>2</sup> of CFRP strip exhibited complete debonding of CFRP strip. It should be noted that the change in failure mode of specimens could be related to the degree of damage and the area of the CFRP strip.

Al-Saidy et al. (2004), investigated the use of CFRP strips to strengthen damaged steel-concrete composite beams. A total of six steel-concrete composite beams were tested in this study. The steel beams were W83×15 grade A572 structural steel. A composite concrete slab

812 mm wide by 76 mm thick was used in all beams. The damaged beams were repaired using CFRP plates with elastic modulus of 200 GPa, 1.4 mm thickness and 50 mm width. The elastic flexural stiffness of the CFRP strengthened damaged composite beams was restored up to 50% of the undamaged beams. The strength of the damaged beams was fully restored to their original undamaged state with the use of CFRP strengthening. Ductility was reduced by adding multiple CFRP strips, however, stiffness was increased.

Dawood (2005) used UHM-CFRP strips with elastic modulus of 460 GPa to strengthen 3050 mm long concrete-steel composite beams consisting of a W200×19 steel specimen and 525 mm × 65 mm concrete slab. CFRP end wraps were used to prevent debonding of the CFRP plates. Substantial increases in both stiffness and strength of 46 and 66 percent, respectively, were achieved. Rupture of the CFRP strips was the dominant failure mode.

Schnerch et al. (2005) developed a model based on strain compatibility and constitutive material properties to predict the stiffness increase, ultimate strength increase, and failure mode of reinforced flexural members. The study showed a significant stiffness increase while maintaining the ductility of the original section. The developed model was used to show the importance of using high modulus (HM) strips to generate significant stiffness increases. The axial stiffness and rupture strength of the CFRP strips were found to be most important parameters in the performance of the strengthened system. To verify the model, externally bonded HM- and UHM-CFRP strips were used to strengthen two large-scale steel-concrete composite beams. The beams consisted of W310 × 45 steel sections and 840 mm × 100 mm concrete slabs. The modulus of elasticity of the HM- and UHM-CFRP was 229 GPa and 457 GPa, respectively. A four-point bending load configuration was used with a 6400 mm span

and a 1000 mm constant moment region. The CFRP strips were wrapped at their ends with 330 mm wide CFRP sheets, which were extended up on the web from both sides. The HM-CFRP strips increased the elastic stiffness and flexural strength of the beams by 10 and 16 percent, respectively. On the other hand, the UHM-CFRP strengthening (area of CFRP was 70 percent larger than the HM-CFRP) increased the elastic stiffness and flexural strength of the beams by 36 and 45 percent, respectively. Both beams failed by rupture of the CFRP strips.

Schaech et al. (2007) proposed a procedure to determine the increase in the live load capacity of CFRP strengthened steel composite beams. The authors suggested that the combined effect of the unfactored dead load and the increased live load should not exceed 60% of the increased yield strength to satisfy the three conditions shown in Figure 2.3.

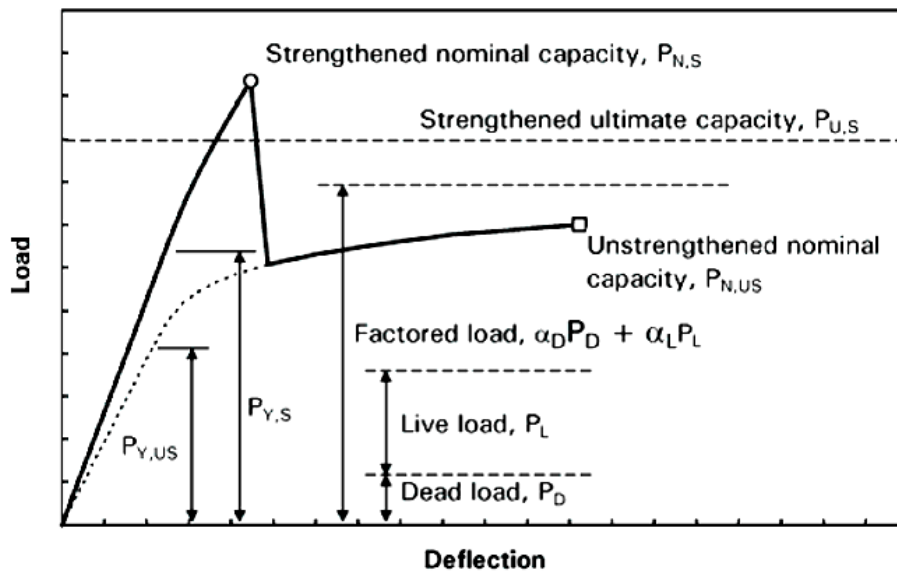


Figure 2.3. Calculation of allowable live load for typical strengthened beam



Also, the total factored load acting on the girder should not exceed the ultimate capacity of the strengthened member. It was recommended that the total increase in the unfactored load acting on the structure should not exceed the ultimate capacity of the un-strengthened beam.

#### *2.3.2.2 Non-Composite I Girders*

Miller et al. (2001) verified the effectiveness of CFRP strips overlay to restore losses of stiffness and strength in deteriorated non-composite bridge girders. Four full-scale American standard steel beams (S24 × 80) 21ft long, taken from an existing damaged bridge were tested. All four girders were rehabilitated with CFRP strips bonded to the inner and outer faces of the tension flange. The CFRP strips used were 37 mm wide, 5.25 mm thick with an elastic modulus of 112 GPa and ultimate strength of 930 MPa. Increases in stiffness of 10 to 37% and 17% to 25% strength increase were achieved for the repaired girders and an 11.6% increase in flexural stiffness due to the retrofit was achieved.

Linghoff et al. (2008) conducted a series of tests on CFRP strengthened steel beams. They tested five HEA180 steel beams of 1800 mm span in four-point bending. The beams were strengthened with two HM-CFRP strips of 80 mm x 1.2 mm attached to the bottom and top sides of the lower flange. They found that the moment capacity increase was limited by the flexural capacity of the beam that was restricted to yielding of the compression flange. The load carrying capacity of the beam dropped after the bottom layer of the HM-CFRP ruptured. The maximum strength increase achieved was 20%.

### 2.3.3 Retrofitting to Enhance Fatigue Performance

A steel structure subjected to cyclic load during its life may eventually experience significant fatigue damage. For stresses above the fatigue limit a finite number of cycles leads to crack propagation and eventual failure. New methods of utilizing CFRP to mitigate this problem have been developed in recent years. Tests in this area have shown significant increases in fatigue life of CFRP strengthened members by up to three times (Colombi et al. 2003, Deng et al. 2005, Jones et al. 2003, Monfared et al. 2008, Nozaka et al. 2005, Täljsten et al. 2008). The following sections present the recent findings in the literature.

#### 2.3.3.1 Non-Prestressed CFRP Patch on Tension Specimens

Jones et al. (2003) performed several fatigue tests on edge notched and hole drilled specimens. The specimens were strengthened with different types of CFRP strips (NM-CFRP, HM-CFRP) and subjected to various cyclic load levels. The test specimen geometry and the load range used in this study are presented in Figure 2.4.

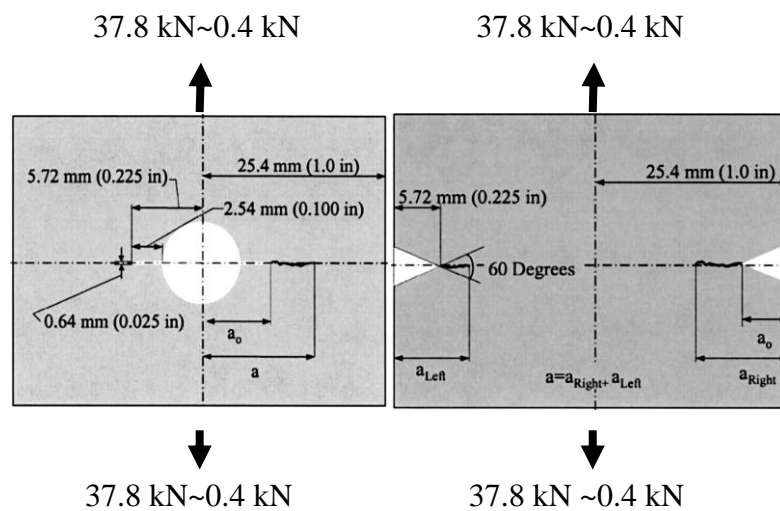


Figure 2.4. Specimen geometries with edge notch and drilled hole and loading range (Jones et al. 2003)

Cold rolled A36 steel bars (yield stress of 340 MPa), nominally 6.5 mm by 51 mm with a length of 510 mm were used to make the specimens. A constant amplitude sine wave of 25 Hz frequency with maximum load of 37.8 kN and minimum load of 0.4 kN was applied. A total of 29 specimens were tested. The strengthening configuration had a 25.5 mm wide by 255 mm long CFRP bonded to each side of a specimen over the center hole and notch (crack starter). Two types of CFRPs were used: SikaWrap Hex 103C and MBRACE CF130 with elastic moduli of 65 GPa and 38 GPa, respectively. The CFRP bonded length was 255 mm or 380 mm. The basic strengthening configuration had a 25.5 mm wide strip bonded to each side of a specimen over the center hole or the notch (crack starters). In some specimens the CFRP strip was split into 13 mm wide strips and applied on either side of the crack starters. The following key findings were noted: (1) A considerable increase in the fatigue life of the strengthened specimens was observed with a maximum increase in fatigue life of 115% obtained with two sided CFRP strip application. (2) The CFRP strips did not fracture. The cracks propagated behind the CFRP strips and failure was by CFRP debonding followed by tension failure in the steel. (3) Surface preparation, proper use of adhesive, and the method of adhesive application can significantly change the behaviour of the test specimen. Sand blasting, vacuuming, and degreasing the steel surface were recommended. (4) Applying CFRP strips to damaged steel specimens not only prolonged the fatigue life, but also delayed the onset of fatigue crack propagation. (5) Fully covering the centre hole resulted in an increase in the fatigue life of the strengthened system about two times that of a specimen with CFRP strips applied on either side of the hole.

Liu et al. (2005) studied the fatigue bond behaviour of CFRP to steel interfaces. Three layers of high modulus CFRP (HM-CFRP) and normal modulus CFRP (NM-CFRP) sheets were

applied to each side of two steel plates with a structural adhesive (Araldite 420) as shown in Figure 2.5.

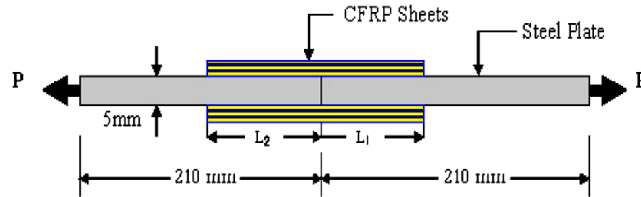


Figure 2.5. Schematic view of double strap joints between CFRP and plates (not to scale)

This adhesive is described as an extremely tough, resilient adhesive with adequate moisture resistance. A total of twelve CFRP/steel joint specimens were designed and tested. CFRP sheets, MBrace CF 130 with the elastic modulus of 240 GPa and MBrace CF 530 with an elastic modulus of 640 GPa, were used as a patch system in this test program. The specimen was loaded in tension at different constant amplitude stress range levels to 0.5 to 6 million cycles. The tension loads applied to such a specimen are carried by the bonding interfaces. Depending on the elastic modulus of the CFRP, two failure modes were observed: (1) interfacial debonding for NM-CFRP, or (2) fibre breakage of HM-CFRP. Based on the results, it was concluded that: (1) No fatigue failure occurred when the maximum applied load was less than 40% of the static strength of the strengthened specimens. (2) The influence of fatigue loading on the bond strength was not significant (less than 10%) if the maximum applied load was less than about 35% of the specimen's static strength. (3) A reduction in the bond-slip stiffness was observed due to the accumulated damage caused by the fatigue loading. (4) The fatigue failure modes were not significantly affected by the range of applied

stresses except for those bonded with high modulus CFRP, where fibres fractured in several locations.

Similar results on retrofitting steel structures using a CFRP patch were reported in a study by Zheng et al. (2006). In this study, the fatigue behaviour of six steel plates strengthened with external bonded CFRP strips was investigated. The three main parameters were: stress range, strengthening method and stiffness of CFRP. The following findings were drawn from the test results: (1) Externally bonding CFRP strips to a steel structure with a fatigue crack can dramatically increase the fatigue life of strengthened specimens by 155~580% over un-strengthened specimens; (2) The application of CFRP strips was more effective when higher modulus CFRP strips were bonded to both sides of the steel plates; (3) Premature debonding of the CFRP strip from the steel surface was observed in specimens strengthened using low elastic modulus CFRP.

Monfared et al. (2008) at University of Waterloo found that the application of a CFRP overlay on one side or two sides of a notched steel plate can increase the fatigue life relative to that of an unreinforced specimen. The main CFRP system used was Sika Wrap Hex 103C with a modulus of elasticity of 65 GPa, and thickness of 1.0 mm. Three un-reinforced notched steel plates, and 18 notched steel plates reinforced with CFRP were tested. Fatigue life improvements in the case of one side CFRP overlay were in the order of 79% and 119% for specimens tested at stress ranges of 144 MPa and 108 MPa respectively. Fatigue life improvements in the case of both sides CFRP overlays were 106%, 94%, and 69% at stress ranges of 108, 126, and 144 MPa respectively. It was also found that surface preparation and the strength of applied CFRP overlay can significantly affect the system's performance.

### *2.3.3.2 Non-Prestressed CFRP Patch on Beam Specimens*

The fatigue life of steel girders was enhanced by using CFRP strips in a study by Tavakkolizadeh et al. (2003b). A total of 21 specimens made of S12734.5 A36 steel beams with 1.3 m long were prepared and tested. Unstrengthened beams were also tested as control specimens. Different constant stress ranges between 69 and 379 MPa were considered. The used CFRP strip had an average tensile strength of 2,137 MPa, tensile modulus of elasticity of 144 GPa, and Poisson's ratio of 0.34 with a width of 76 mm and a thickness of 1.27 mm. The results showed that the CFRP strip overlay not only tended to extend the fatigue life of a detail more than three times, but also decreases the crack growth rate significantly. Strengthened specimens experienced longer fatigue lives of between 2.6 to 3.4 times the unstrengthened specimens for stress ranges of 345 to 207 MPa, respectively. The stable crack growth rates decreased by an average of 65% as a result of strengthening.

In a study by Schnerch et al. (2007), HM-CFRP strips with 450 GPa elastic moduls were used to strengthen 6.4 m long full scale 310×45 W section steel beams. The authors found that the a retrofitted beam was able to sustain three million loading cycles with a 20 percent increase of the simulated live load level. The beams exhibited similar performance to a control beam which was tested at a lower loading range.

Nine small-scale steel beams strengthened with CFRP strips were tested in fatigue by Deng et al. (2007). The steel beams used were 1.2 m long 127 × 76 UB13 with yield strength of 275 MPa. The flange surface that received the CFRP strip was sandblasted and the plate was attached within 4 hours. The CFRP strips used were 3 mm thick and 400 mm long. The adhesive used was a two-part thixotropic epoxy resin (Sikadur-31). The minimum applied

load was 5 kN and the maximum applied load varied in order of 40 kN, 50 kN, 55 kN, 70 kN, 90 kN, 125 kN and 135 kN. A 30% increase in fatigue life was observed for the lowest load range (5 kN~50 kN) applied during the fatigue tests. A higher load range resulted in a lower increase in fatigue life. The comparison of the number of the cycles to crack initiation showed a larger delay in crack initiation for the CFRP strengthened specimen.

#### *2.3.3.3 Prestressed CFRP Patch*

Only a few studies have examined the effect of prestressing on the behaviour of steel structures strengthened with CFRP plates.

Colombi et al. (2003) examined the effects of prestressing in experimental and numerical study. The effectiveness of prestressed CFRP bonded strips to arrest the crack propagation was investigated on the notched steel plates shown in Figure 2.6. Five specimens were tested: one control specimen, one reinforced specimen with non-prestressed CFRP strips, and three specimens reinforced using prestressed CFRP strips were tested. The CFRP strips were Sika Carbodur. The test variables included the thickness of CFRP strip (1.2 mm or 1.4 mm), the modulus of elasticity of CFRP (174 GPa or 216 GPa) and the prestressing force. All of the specimens were tested under constant amplitude loading using a stress range equal to 80 MPa in the nominal section of the unreinforced specimen. The stress ratio was  $R = 0.4$ . By reinforcing the steel plates with non-prestressed CFRP strips (Sika CarboDur S512), the fatigue life of the specimens was increased by a factor of about three, while the maximum fatigue life improvement for the prestressed CFRP specimen was about sixteen. A 2D plane stress finite element analysis was used to model the steel plate, CFRP strips and the adhesive

interface as shown in Figure 2.7. Shear spring elements were used to represent the adhesive layer between the steel plate and the CFRP strip. The experiment conditions were simulated in numerical modelling. The authors carried out parametric studies to investigate the influences of stress ratio ( $R$ ), reinforcement, prestressing, CFRP strip strength, thickness of strip, and adhesive. Results of the FEM simulation are shown in Figure 2.8.



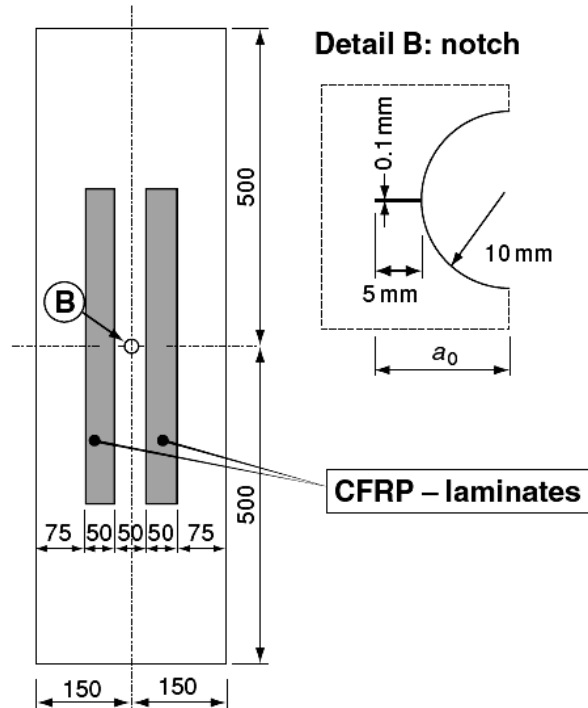


Figure 2.6. Notch steel plate test specimen, Colombi et al. (2003)

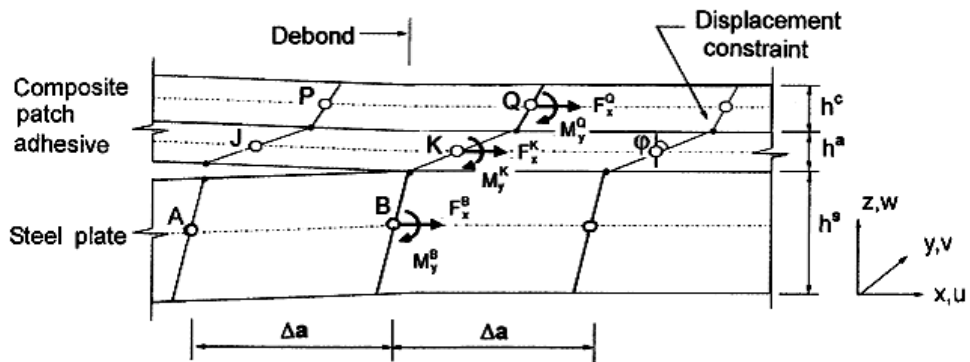
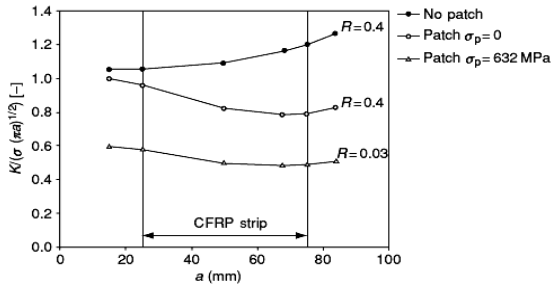
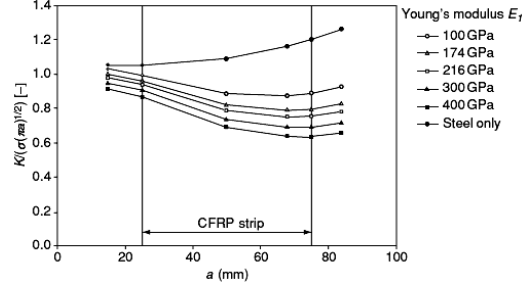


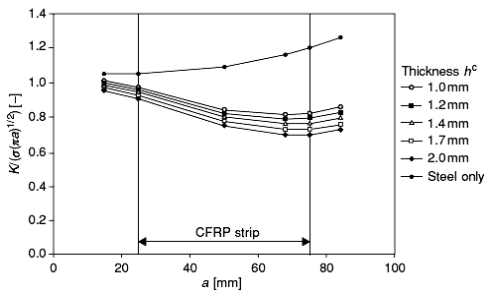
Figure 2.7. Schematic three layers model of elaminated plate, Colombi et al. (2003)



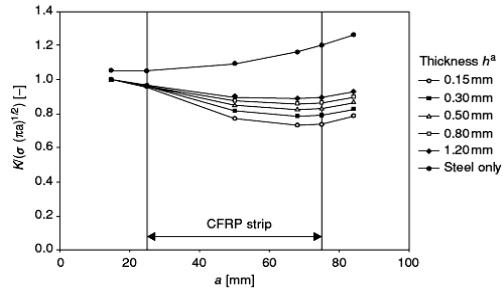
(a) strips with and without prestressing.



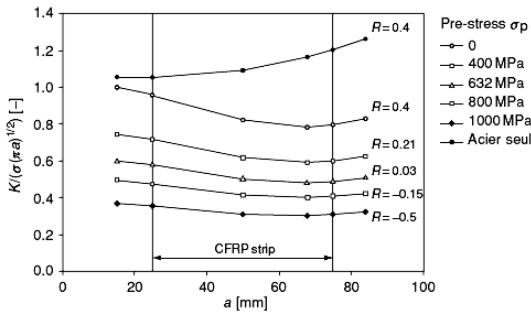
(b) Young`s modulus of CFRP strip



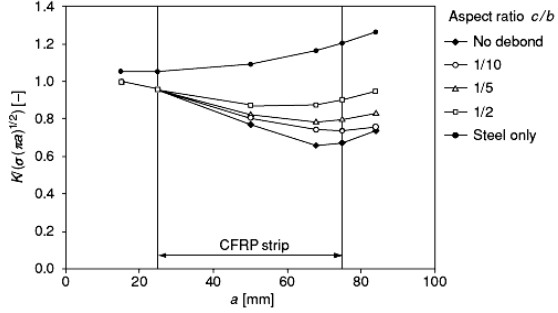
(c) thickness of CFRP strip



(d) adhesive thickness



(e) effect of prestress



(f) effect of CFRP debonding

Figure 2.8. FEM results -normalized SIF vs. crack length, Colombi et al. (2003)

The following findings, were reported: (1) Prestressing a CFRP strip prior to bonding introduces compressive stress, which prevents further cracking growth by promoting the crack closure effect. (2) The application of high stiffness prestressed CFRP strips bonded perpendicular to the crack path modifies the crack geometry by bridging the crack lips. (3)

Prestressing reduces the effective stress ratio. (4) Shear deformation of the adhesive is not negligible so that as adhesive thickness increases, the strengthening efficiency reduces. (5) Reduction in stress ratio for a cracked steel plate by prestressing promotes crack closure, which is more important in the case of short cracks. (6) In long cracks, debonding at the steel plate-adhesive interface is the failure mode.

Täljsten et al. (2008) conducted a series of tests on specimens taken from an old bridge girder to examine the influence of bonded prestressed CFRP plate on the static strength and fatigue life improvement. A total number of ten plate specimens were tested as shown in Figure 2.9.

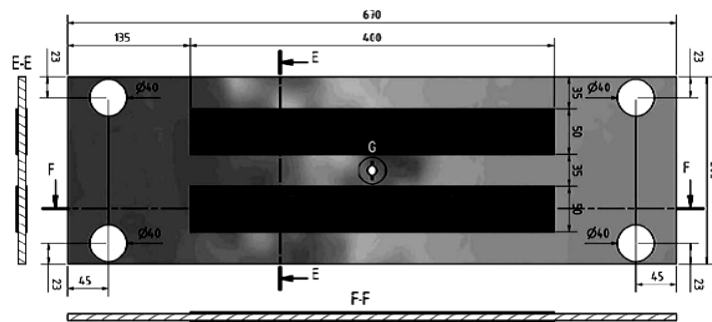


Figure 2.9. Reinforced steel plate specimens configuration, Täljsten et al. (2008)

Test specimens were divided into five different configurations. The specimens configurations based on the type of strip (E or M), adhesive (S or B), thickness of adhesive ( $t_a = 1$  or  $2$  mm), Prestressing force ( $P_{per} = 0, 12, \text{ or } 15$  kN) and applied stress range ( $97.5$  MPa). Two types of CFRP strip were used : E 50 C (E) and M 50 C (M) with elastic modulus of  $155$  GPa and  $260$  GPa, respectively. The adhesives were BPE 567 (B) with elastic modulus of  $4.5$  GPa and Pox SK 41 (S) with elastic modulus of  $9.87$  GPa. The Swedish standard SA21/2 for grit blasting of the metallic surface and acetone cleaning for surface

preparation was used. It was shown that the fatigue life of non-prestressed test specimens was increased about 2 to 4 times vs. the control specimen. Prestressing the CFRP strip reduced the crack propagation and extended the fatigue life of the test specimen to what might be considered as run-out behaviour. The crack propagation rate and fatigue life was found to be dependent on the strip stiffness and, largely, on the prestressing force. It was noted that the prestressing effects can increase as the stress ratio ( $R$ ) decrease. It was also observed that any violation of fabrication tolerances can unpredictably change the result and lead to a very scattered fatigue life.

#### **2.4 Bond of FRP Strengthened Steel**

Debonding has been reported as a main issue associated with strengthening steel structure using CFRP strips, especially when thick or multilayer CFRP strips are used, due to the resulting high magnitude of the applied shear force transferred to the adhesive layer. Because of the high stress concentration at the ends of CFRP strips bonded to the steel surface, end debonding is a critical failure mode. Controlling the end debonding is essential, particularly in the case of prestressed CFRP strips.

Six failure modes can be identified in a CFRP-to-steel bonded system, depending on the elastic modulus, type of adhesive used, and its thickness (Zhao et al. 2006) (see Figure 2.10).

These include:

- (a) steel and adhesive interface failure,
- (b) cohesive failure (adhesive layer failure),

(c) CFRP and adhesive interface failure,

(d) CFRP delamination (separation of carbon fibres from the resin matrix),

(e) CFRP rupture, and

(f) steel yielding.

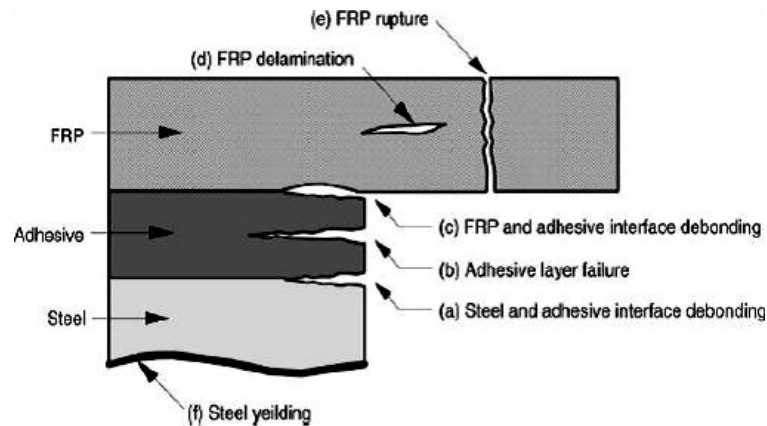


Figure 2.10. Schematic view of failure modes, Zhao et al. (2006)

For normal modulus CFRP, with  $E = 100\sim 250$  GPa, failures usually occur due to mode (a) and (b) but for a high modulus CFRP, with  $E > 250$  GPa, failure mode (e) is more common. Using a thin layer of adhesive tends to cause failure mode (b). However a thick layer of adhesive tends to cause failure mode (d). Failure mode (d) is a more brittle failure than mode (b). Ensuring a sufficient steel plate thickness can avoid the occurrence of failure mode (f). The most desired mode of failure is mode (e) corresponding to the maximum strengthening efficiency.

Several researchers have conducted experimental studies to investigate the bond behaviour of the CFRP to steel interface by using flexural or axial tension tests.

Nozaka et al. (2005) examined five adhesives to bond CFRP to steel. They found that the 3M DP\_460 NS adhesive and Fyfe Tyfo UC CFRP strips achieved the highest strain in the CFRP at failure. The most effective bond length is the shortest one that is able to maximize the load transition into the CFRP strip. Uniform yielding and high ductility throughout the adhesive layer are required to redistribute the stresses successfully within the adhesive layer to avoid debonding.

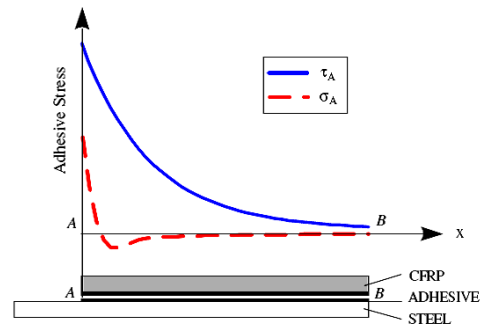
Schnerch et al. (2006) conducted an experimental study to investigate the effects of adhesive properties on the performance of CFRP strengthened steel members. Various types of adhesives were used to examine the bond behaviour and development length of CFRP strips bonded to steel beams in a four point bending test. The development length increased by varying the adhesive type as follows: Weld-On SS620, SP Spabond 345, Vantico Araldite 2015, Jeffco 121, Fyfe Tyfo MB and Sika Sikadur 30. It was also observed that a suitable surface preparation by cleaning the CFRP strip's surface with acetone and sandblasting the steel surface reduces the development length and prevents undesirable debonding failures.

In a study on the bond and splice behaviour of CFRP strengthened steel beams completed by Dawood et al (2006), three parameters were investigated: (1) the length of the CFRP strip, (2) the geometric configuration of the strip ends, and (3) the use of an additional clamping or transverse fibre wrap to act against the out-of-plane stress at the end of CFRP strip known as peeling stress. High modulus HM-CFRP strips, produced by Mitsubishi Chemical Inc, were used to strengthen the steel specimens. Proper surface preparation consisting of sandblasting,

vacuuming, and wiping the steel and CFRP surfaces was performed. The epoxy was left to cure for 12 hrs before testing. Double-lap shear coupon tests and beam tests were carried out. Figures 2.11 and 2.12 shows the key findings of the study. The typical debonding failure is shown in Figure 2.11(a). The calculated shear and peeling stress distributions are shown in Figure 2.11(b). Figure 2.12(a) and Figure 2.12(b) show the different geometric configurations and the transverse wrapping that were used to reduce premature debonding. It was found that introducing a reverse taper at both ends and the centre of the splice joint increases the capacity of the bond joint by two times through eliminating the abrupt geometry changes, which introduces the local stress concentration. Using a reverse taper, rounded end taper, or steel clamps at the end of CFRP strips increased the capacity of the CFRP bonded-steel joint up to 80% by mitigation of peeling off action.



(a) Peeling off action at the end of CFRP strip)



(b) Adhesive shear and peel stress distributions in the adhesive joint along the path

Figure 2.11. Findings of the study by Dawood et al. (2006)



(c) (1) square, (2) tapered, (3) rounded and (4) clamped plate ends.

(d) Transverse fibre wrap

Figure 2.12. Findings of the study by Dawood et al. (2006)

From the above, it is evident that strengthening a steel member using bonded CFRP strips, requires special attention to avoid the CFRP debonding failure mode. A proper surface preparation is very important. The critical location of debonding is the very close to the end joint. Thus, controlling the shear and peel stresses at the end of the CFRP strip are essential for having a good performance for the strengthened members.

## 2.5 Durability of Steel Structures Retrofitted with FRP

In spite of the excellent resistance of FRPs to corrosion and chemical attack, the steel in contact with the adhesive may be attacked by long-term exposure to moisture especially in conjunction with the salt resulting from de-icing of roadways or ocean spray (Brown et al. 1974). Moisture diffuses through the adhesive layer to the substrate surface at the edges of a joint leading to a reduction of the joint strength. Humidity in conjunction with high temperature were found to significantly degrade the bond durability of FRP repaired steel aircraft wings (Armstrong et al. 1983). Shulley et al. (1994), investigated the durability of



bonded FRP strengthened systems using the wedge test method (ASTM, D3762-03). Five different types of carbon and glass fibres were subjected to various environmental conditions (hot water, freezing, freeze/thaw, salt water, and room temperature water) for a period of two weeks before initiation of the wedge test. The tests showed that the GFRP reinforced systems had a more durable bond with steel than CFRP reinforced systems. Low temperature exposure had the least significant effect on the performance of the reinforcing systems. The most durable bond systems were those subjected to a sub-zero environment.

It was suggested that the use of adhesion promoters such as Silanes may increase the durability of steel-epoxy bond without affecting the initial bond strength (Bisby et al. 2003, Brown et al. 1974, Karbhari et al. 1995).

Galvanic corrosion happens when a direct electrical contact exist between two adherents, which have anodic and cathodic potentials with corrosion taking place on the anodic metal surface. In a composite CFRP-steel joint, steel plays the role of the anode and the CFRP acts as the cathode so that a high potential for galvanic corrosion exists. Electrolytic solutions like water with salt, acid, or combustion products promote corrosion of the joint. Corrosion of CFRP bonded to metals in saline environments for different types of metallic subsurface was examined by Brown et al. (1974). Specimens were fabricated by either bolting the CFRP laminate or bonding it with epoxy resin to aluminum, steel, stainless steel, and titanium plates. To accelerate the corrosion, the specimens were placed in a continuous fog of neutral sodium chloride solution at a temperature of 350°C for 42 days. No deterioration due to accelerated corrosion was observed for the adhesively bonded specimens, while a more severe deterioration was observed for the bolted specimens. Tavakkolizadeh et al. (2001)

examined how the thickness of epoxy can change the corrosion durability of the bonded CFRP reinforcing system. Test results showed that applying a thin film of epoxy coating (0.1 mm) decreased the corrosion rate in seawater by sevenfold, relative to specimens with direct contact (i.e. no epoxy) between steel and CFRP. Furthermore, by applying a thicker epoxy coating (0.25 mm) the corrosion rate was decreased by 21 times.

New methods to mitigate corrosion of the CFRP-steel composite include: selection of an adhesive with good isolation properties (Zhao et al. 2006), using thicker epoxy, water resistant sealant, a non-conductive barrier plus a sealant, or bonding a GFRP layer before applying the CFRP layer onto the steel surface (Dawood et al. 2006, Allan et al. 1988).

Other durability issues such as creep and exposure to extreme temperatures, ultraviolet light, or fire can also have significant effects on the response and durability of the FRP strengthened member. Intentional temperature increases up to a certain level can be employed as a beneficial post-cure procedure for the FRP composite and adhesive. However, very high temperatures can increase the sensitivity of bond to moisture penetration and galvanic corrosion (Bisby et al, 2003).



All structural materials undergo some degree of mechanical degradation when exposed to a severe fire. For FRP-retrofitted structures under fire, particularly steel structures, the resin can lose its ability to protect the fibres and transfer loads between them. In addition to degradation within the FRP composite itself, the bond between the FRP and the substrate will eventually fail and expose the member to the full fire effect. Supplementary insulation




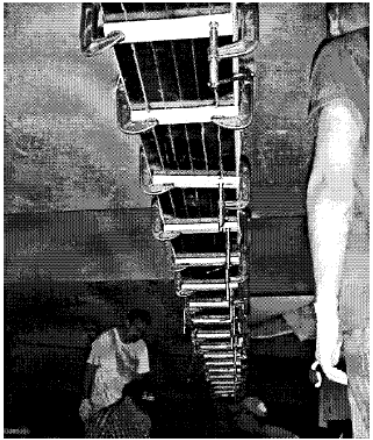
systems can, however, significantly improve the FRP performance at high temperatures (Dawood et al, 2006).

## 2.6 Field Applications

Table 2.1 summaries the examples of field applications involving the reinforcement of steel structures using CFRP reported in the literature to date.

Table 2.1. Field applications

PROJECT INFORMATION (REFERENCE)	SYSTEM DESCRIPTION	PICTURE
<p>Steel bridge girder strengthened in the field Phares et al. (2003)</p>	<p>Externally post-tensioned CFRP rods. The anchorage assemblies were bolted to the webs of the beams.</p>	
<p>Steel bridge girder strengthened in the field Phares et al. (2003)</p>	<p>Bonded CFRP strips applied to the inner side of a W section steel girder.</p>	

PROJECT INFORMATION (REFERENCE)	SYSTEM DESCRIPTION	PICTURE
<p>Slattocks Canal Bridge, a historic steel bridge in Uk. Hollaway et al. (2002)</p>	<p>Upgraded bridge using bonded CFRP Strips. The upgrading maintained the navigable clearance required for the canal.</p>	
<p>Upgrading of a principal curved beam, Nottingham, UK. Hollaway et al. (2002)</p>	<p>Strengthening a damaged steel girder using CFRP sheet wrap around the beam.</p>	
<p>Composite steel-concrete bridge (Hythe bridge) in UK. Hollaway et al. (2002)</p>	<p>Prestressed CFRP strip overlays applied to steel-concrete composite bridge.</p>	
<p>Christina Creek bridge, Newark (New Jersey State). Miller et al. (2001)</p>	<p>SM-CFRP strips bonded to the outer face of the tension flange along the girder span. Tapered CFRP strips at the ends.</p>	

## **2.7 Summary**

Using bonded CFRP reinforcement is as a very promising approach for retrofitting metallic structures. Durability, debonding prevention, developing application, and design are challenges preventing their wide spread use. Steel surface sandblasting, vacuuming, and wiping the CFRP surface are effective to prevent debonding along the bond interface. End transverse wrapping, tapering and/or the use of a physical end clamp are recommended, especially in the case of prestressing the CFRP. Previous research shows a significant increase in the static strength and fatigue life of CFRP strengthened steel members. Stiffness increases can be achieved only when a sufficiently high CFRP reinforcement ratio is used. However using a high reinforcement ratio may be an uneconomical solution. Further study focusing on actual steel structures such as bridge girders strengthened using prestressed CFRP reinforcement is required to develop optimal reinforcing procedure and design methods. The use of prestressed CFRP strips has been examined in previous studies and found to be a highly effective approach. Developing a proper and practical prestressing procedure and method for predicting the fatigue life improvement are the main concerns of the current thesis.

## Chapter 3: Experimental Program

### 3.1 Introduction

An experimental research program was conducted to investigate the performance of steel beams retrofitted using carbon FRP (CFRP) plates subjected to flexure fatigue loads. The program consisted of six specimens: one control and five reinforced specimens. The specimens consisted of W Structural Section (W310×74) steel beams strengthened using two CFRP plates. Two different types of CFRP were examined. The steel beams were stiffened using two welded cover plates on the bottom flange. The test parameters considered were the effect of prestressing level, location of CFRP strip, and CFRP modulus. The CFRP strips were prestressed using special fixtures that were mounted at either end of the steel beam. The specimens were instrumented by strain gauges, LVDTs, and load cells. All specimens were tested in four-point bending under fatigue loads, to investigate the effectiveness of prestressed CFRP in increasing the fatigue life of steel beams. The level of prestressing was decided based on the results of studies done on the strengthening of steel members using prestressed CFRP strips (Colombi et al. 2003, Täljsten et al. 2008). The maximum stress in the CFRP strip including the stress due to prestressing and fatigue test should not exceed the ultimate strength of CFRP strip. In addition, the prestressing level was limited by debonding issues, as discussed in Chapter 4 of this thesis. The test specimens are described in Table 3.1. The specimen nomenclature used to identify the specimens during the study is as follows:

The first number refers to the level of prestressing stress as a percentage of the ultimate strength of the CFRP strip. The second letter refers to the location of the applied CFRP strips.

“F” indicates that the strips are bonded to the inner side of the flange and “C” indicates that the strips are attached to the cover plate. The last notation refers to the elastic modulus of the CFRP strip used. “S” is a CFRP strip with a standard modulus equal to 165 GPa and “M” is a CFRP strip with moderate modulus equal to 210 GPa.

Table 3.1. Test matrix

Test	Specimen ID	% Prestressing	Type of Strip	Loading	Loading Range (kN)
1	Control	0%	--	fatigue	32-280
2	14%-F-M	14%	M	fatigue	32-280
3	15%-F-S	15%	S	fatigue	32-280
4	35%-F-M	35%	M	fatigue	32-280
5	0%-C-M	0%	M	fatigue	32-280
6	37%-C-M	37%	M	fatigue	32-280

\* Prestressing stress as a percentage of ultimate strength of CFRP strip

\*\* Modulus of S strip = 165 GPa, Modulus of M strip = 210 GPa

The following sections of this chapter present the properties of the materials used to fabricate the specimens, details of the fabrication processes, testing configurations, and instrumentation. The laboratory testing are presented in Chapter 4.

## 3.2 Materials

This section describes the properties of the various materials used in the experimental program. A hot-rolled steel W-section and two different types of CFRP plates were used.

### 3.2.1 Structural Steel Beam

W310x74 hot-rolled sections of weldable steel (Type 350W) were used. A schematic of the

cross section and constitutive model of steel specimens are shown in Figure 3.1. The nominal yield and ultimate strengths of the beam were 350 and 450 MPa, respectively.

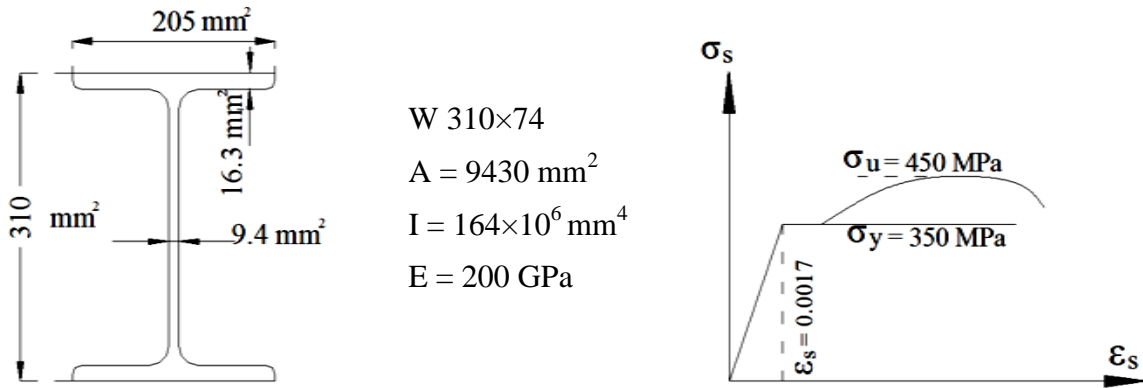


Figure 3.1. Section geometric and nominal material properties

### 3.2.2 Carbon Fibre Reinforced Polymer (CFRP) Strips

Two types of pultruded CFRP strips were used (Sika Canada Inc., 2009). The first type was Sika CarboDur M514 with strip width of 50 mm and 1.4 mm thickness. The second type was Sika CarboDur S512 with a strip width of 50 mm and thickness of 1.2 mm. The constitutive properties of CFRP strips as reported by the manufacture are shown in Figure 3.2.

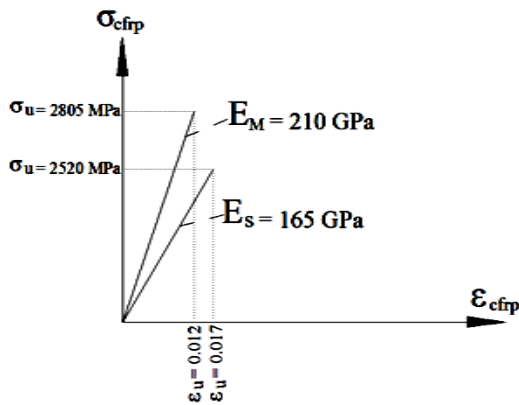


Figure 3.2. Tensile stress vs. strain of the CFRP strip



The actual elastic modulus and poisson's ratio of the CFRP strip were calculated using the strains recorded during the prestressing procedure. See Appendix A for details.

### *3.2.3 Epoxy Resin*

An epoxy resin, commercially known as Sikadur-30 (Sika Canada, 2009), was used to bond the CFRP strips to the steel surface. This is essentially a thixotropic adhesive mortar based on a two-component solvent free epoxy resin. The mixing ratio by weight is 3:1 of Component A (resin) and Component B (hardener).

## **3.3 Test Specimen**

The specimen was designed according to the steel structures design code (CAN/CSA-S16-01). The test specimen was a W310 × 74 steel beam, with two 500 × 150 × 12 cover plates welded on the beam flange (as stiffeners) as shown in Figure 3.3. The size of the specimen was selected according to the load capacity of the test frame (290 kN) and the loading arrangement (Figure 3.4). A load range of  $\Delta P = 252$  kN ( $R = 0.1$ ) was used. This load range corresponded to a tensile stress range of 95.3 MPa. This specimen configuration represents a load fatigue detail (Category E7 in CAN/CSA-S16-01).

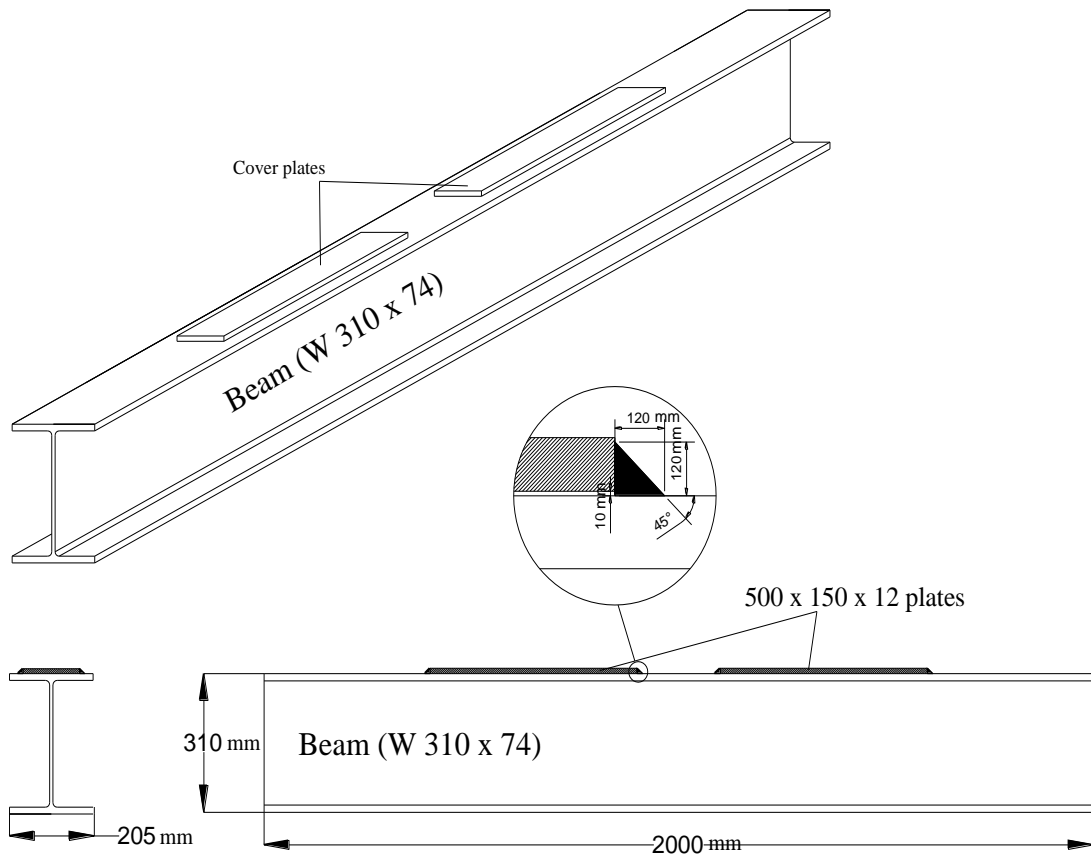


Figure 3.3. Specimen configuration

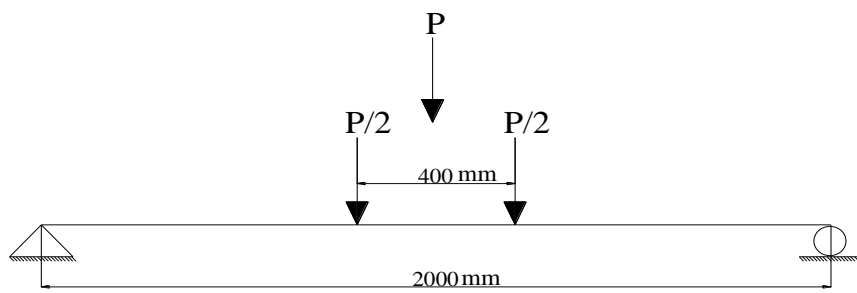


Figure 3.4. Schematic view of the loading arrangement

Consequently, the number of cycles to failure, computed using the fatigue constants for Detail Category E', was determined to be about 435000 cycles.

### **3.4 Prestressing System**

Five of the test specimens were strengthened using CFRP strips. The specimen configuration allows two possibilities of CFRP strip application: (1) on the cover plates and (2) on the flanges. To prestress the strips, a self supporting prestressing system that mounts onto the beam was designed. Surface preparation was carried out for better bond, consisting of sandblasting the steel surface and wiping the strips clean with acetone. The beam was placed in the self supporting system and the epoxy was applied onto the strips and steel surface. The strips were gripped at either end using a clamp anchor. The prestressing force was applied gradually using a hydraulic jack, and it was held for five days while the epoxy cured. The prestress losses were recorded for three days after releasing the prestressing force to the beam. The components of the prestressing system and the prestressing procedure are described in detail in the following sections.

#### *3.4.1 Gripping Tests*

Gripping tension tests were carried out to examine the efficiency of the end grips that were used to maintain the tension force in the CFRP strips during the prestressing processes. The grip was a clamped anchor consisting of two steel plates, aluminum sleeves, and six bolts three on either side of the CFRP strip. The anchor was used to grip two CFRP strips at one time. Based on trial and error, the optimum gripping force required to prevent sliding of the

CFRP strip was found to be 25.45 kN(equal to 70 ft·lb torque per bolt). Later, the aluminum sleeve was replaced by sandpaper (grade 240) to act as a soft material sandwiching the CFRP strip and providing load transfer by friction. See Appendix A for more details regarding the gripping tests.

### 3.4.2 Prestressing System

A schematic view of the system used for prestressing the CFRP strips is shown in Figure 3.5.

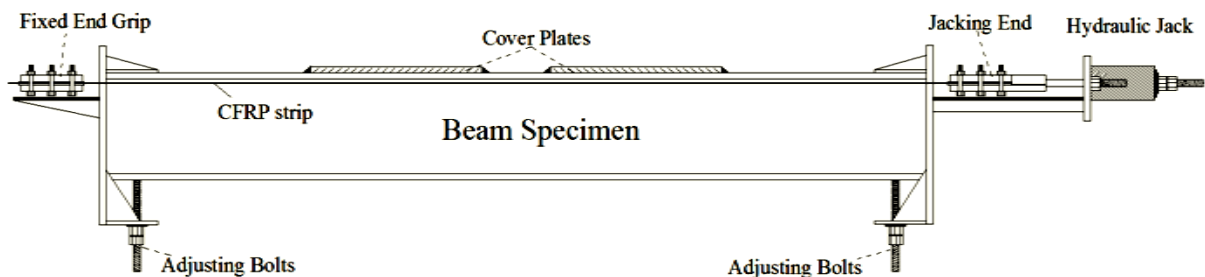


Figure 3.5. A schematic view of prestressing system

The prestressing system consisted of anchorage blocks at both ends of the beam. The anchorage blocks were firmly fitted onto the beam using adjustable bolts. The strips were anchored using clamped anchors (Section 3.4.1). The dead and live end anchors are shown in Figure 3.6. The prestressing force was applied using a hydraulic jack mounted on the main rod connected to the live anchorage and two side rods were used to adjust the applied load in the strips and to lock the force in the strips after prestressing.



(a) Dead end anchorage



(b) Live end anchorage

Figure 3.6. Prestressing anchor configuration

Three load cells, one on each welded rod to the live anchor, were used to monitor the prestressing force during and after prestressing process. The assembled prestressing system including the end clamps used to prevent debonding are shown in Figure 3.7 for both cases of strip applications, on the flange and on the cover plates.



(a) Completed prestressing system for the strips on the cover plates.



(b) Completed prestressing system for the strips on the inner side of the flange.

Figure 3.7. The assembled prestressing system

### 3.5 Prestressing Procedure

The prestressing process including the prestressing, curing the epoxy, load release and relaxation are discussed in this section.

The surface preparation is an essential step for an effective bond behaviour. As mentioned in Chapter 2, proper surface preparation is required to prevent premature CFRP debonding. For this purpose, the steel surface was sandblasted to increase the friction and improve the bond between the epoxy and steel surface. The CFRP strips were carefully cleaned with acetone prior to applying the epoxy. The epoxy components were mixed according to the manufacture`s data sheet. The thickness of the epoxy plays an important role on the bond behaviour. Epoxy thicker than 2 mm reduces the bond strength and a thinner layer is not practical. For this purpose an epoxy spreader shown in Figure 3.8, was fabricated and used to apply the epoxy.

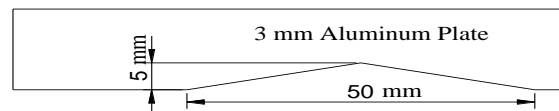
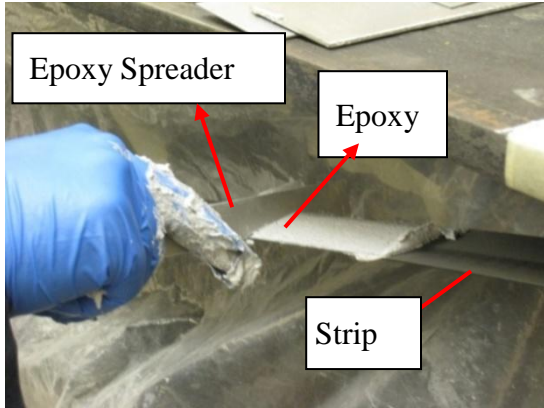


Figure 3.8. Epoxy spreader

The triangular shaped profile ensures a uniform epoxy layer after the excess epoxy is squeezed out by clamping the strips on to the steel beam (Figure 3.9(a)).

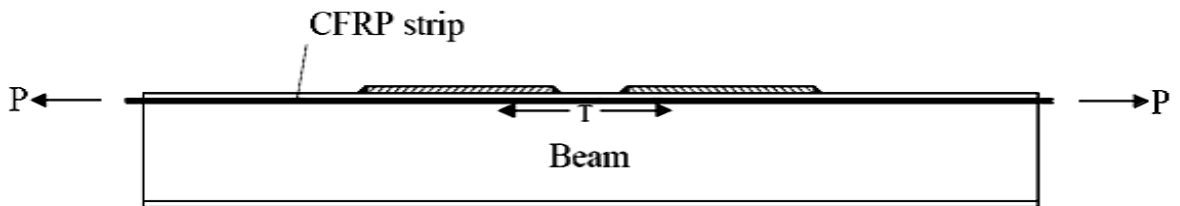
The prestressing sequence on the beam specimen is illustrated in Figure 3.10.



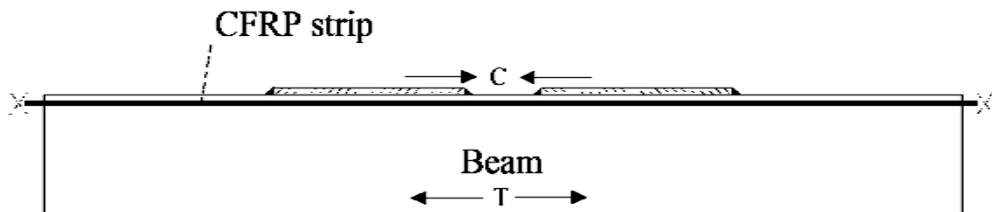
(a) Application of epoxy on the strip

(b) Clamped strips to the beam after prestressing

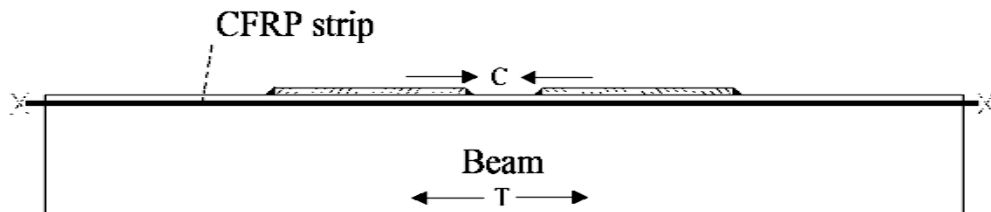
Figure 3.9. Prestressing preparation process



(a) Stage 1: @ prestressing



(b) Stage 2: @ release



(c) Stage 3: @ three days relaxation

Figure 3.10. Prestressing stages

The prestressing process involved three stages: (1) prestressing the CFRP strips, (2) releasing the prestressing force to the beam, (3) allowing three days of stress relaxation prior to testing. To maintain equal prestressing force in both CFRP strips, two side bolts were used to adjust the applied force during prestressing. Figure 3.11 shows the jacking end (live end) configuration. Prestressing the strips was done in steps by loading the two strips using a single hydraulic jack. At a certain prestressing force ( $\sim 15$  kN) the side bolts were tightened and the load was released to the strips by unloading the hydraulic jack. The strains in the strips were adjusted to the same level using the adjustable bolts. The step loading process was repeated two or more times until the desired prestressing force was achieved. Following this, the jack was totally unloaded and the side bolts were tightened.

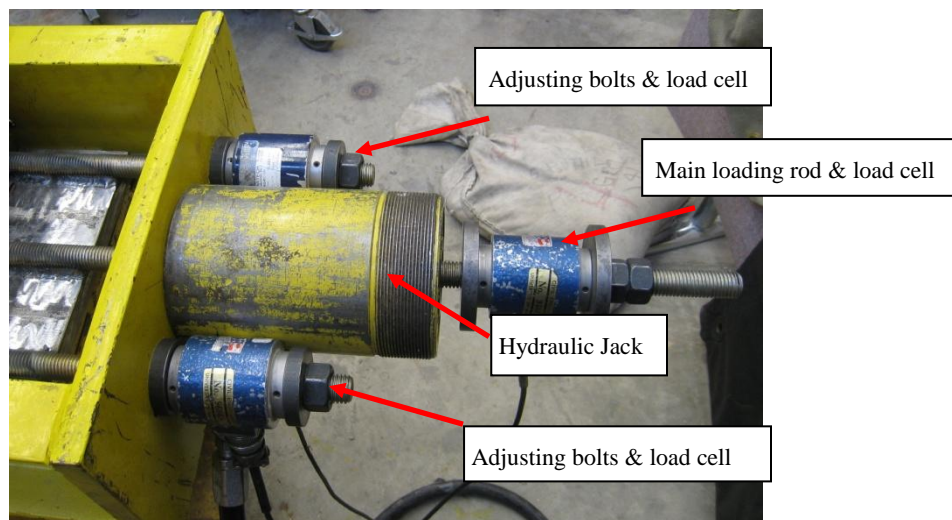
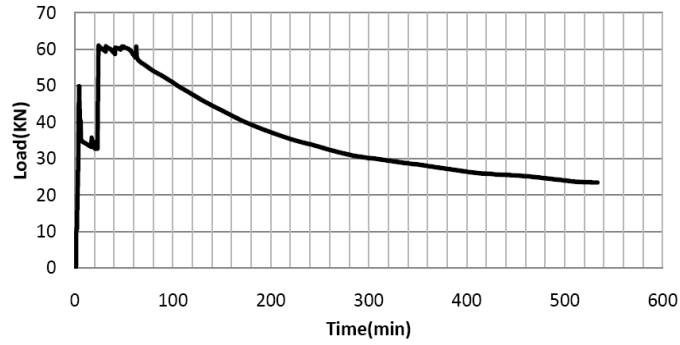


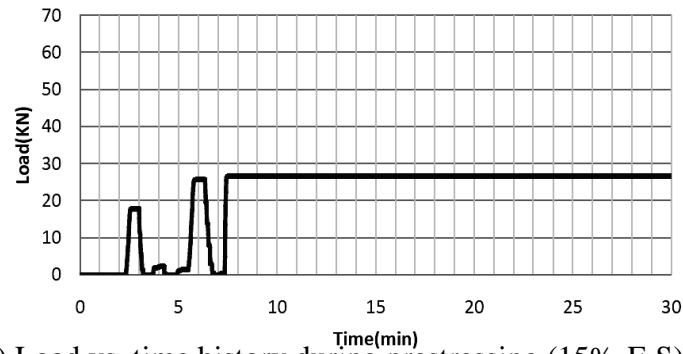
Figure 3.11. The jacking (live) end details

The prestressing force versus time history for all four prestressed specimens, except specimen 35%-F-M, are plotted in Figure 3.12.

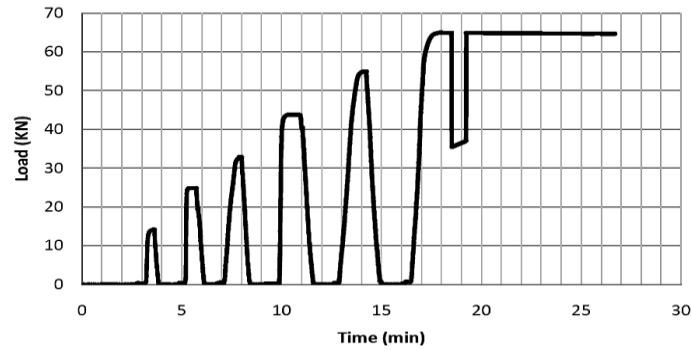




(a) Load vs. time history during prestressing (14%-F-M)



(b) Load vs. time history during prestressing (15%-F-S)



(c) Load vs. time history during prestressing (37%-C-M)

Figure 3.12. Step loading procedure

Due to a power outage, the data for specimen 35%-F-M were lost. The first specimen was prestressed to 60 kN per strip (35% of strip ultimate strength) as shown in Figure 3.12(a). The prestressing force dropped dramatically because of an improper end anchorage, which

was modified for the next specimens. The target loads were 26 kN and 62 kN for the 15%-F-S specimen and the 37%-C-M specimen, respectively. As shown in Figure 3.12(b) and Figure 3.12 (c) the target loads were achieved successfully.

The strips were clamped along the strip/epoxy/steel bond line for five days to cure the epoxy. (Figure 3.13).



Figure 3.13. CFRP strip clamped to the beam after prestressing

After 5 days, the prestressing force was released to the beam specimens by loosening the bolts in both end anchorages. The load release process tended to be very critical for specimens with higher prestressing levels. No significant losses at the CFRP strip end was observed for specimens 14%-F-M and 15%-F-S while significant losses was experienced for specimens 35%-F-M and 37%-C-M. The epoxy bond line was susceptible to premature failure when the load was released very rapidly as shown in Figure 3.14. According to the literature on the bond behaviour of CFRP strip to steel interfaces, controlling the out-of-plane

peel stress, and the shear stress at the ends of strips is very critical for maintaining the bond (Schnerch et al., 2005).

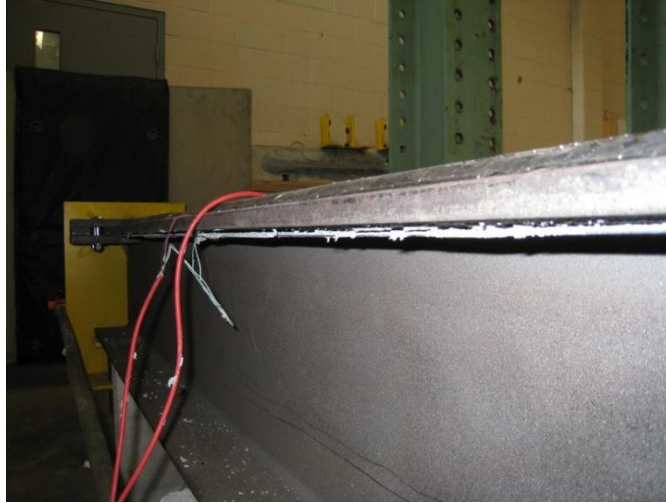


Figure 3.14. A total debonding as the result of rapid load release

To mitigate this problem, a clamping system was applied at the end of the strips for all specimens, as shown in Figure 3.15, to reduce the out-of-plane (peel) and shear stresses during load release. The required pressure to alleviate the peel/shear stress was applied by clamping the end of the strip. This system remained on the specimens during the fatigue test.



Figure 3.15. End clamps to mitigate shear and peel stresses

A calibrated torque wrench was used to tighten the bolt and measure the applied force. For example, the peel stress for specimen 37%-C-M was numerically determined to be 45 MPa (Chapter 5). However, the tensile strength of the epoxy is 25 MPa (Sika Canada, 2009). Therefore, a clamping stress of 20 MPa corresponding to 137.5 lb·ft torque is needed to mitigate the premature debonding. The clamp configuration is illustrated in Figure 3.16.

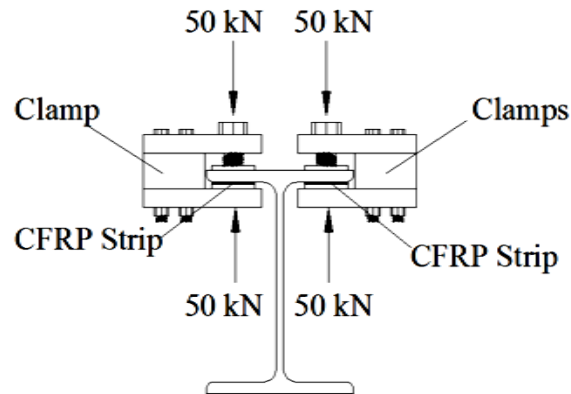


Figure 3.16. End clamp configuration

Using the clamps at the ends of the strips prevented the debonding, but strain transfer to the epoxy at the strip ends was recorded. Similar trends for the strain transfer at the ends of strips were observed during release of the prestressing force. As shown in Figure 3.17, for the specimen 35%-F-M, the strain transfer at release was much higher at the dead end than at the live end. The load was released very slowly at the live end by gradually releasing the pressure on the hydraulic jack. The load released at the dead end was achieved by loosening the anchorage bolts, which resulted in the sudden loss of strain (see curve A in Figure 3.17).

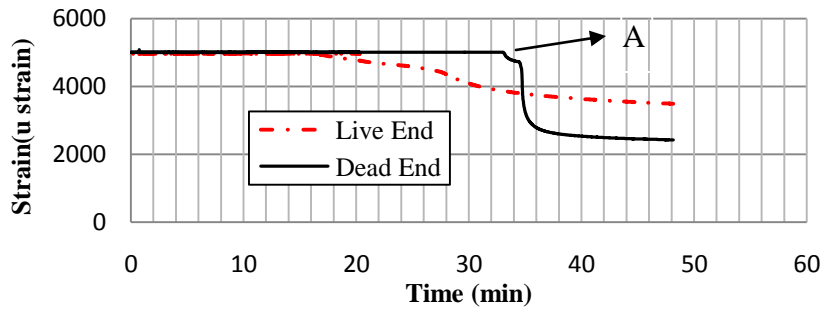


Figure 3.17. Strain transfer at the strip ends at release for specimen 35%-F-M

To mitigate the debonding at the ends of the strips, fixed clamped anchors shown in Figure 3.18, used at the strip ends for specimen 37%-C-M. As a result, no major strain transfer was recorded at the dead end and the strain transfer at the live end was reduced significantly as shown in Figure 3.19. The strain transfer at the live end for specimen 35%-F-M was 75% compared to 33% for specimen 37%-C-M.

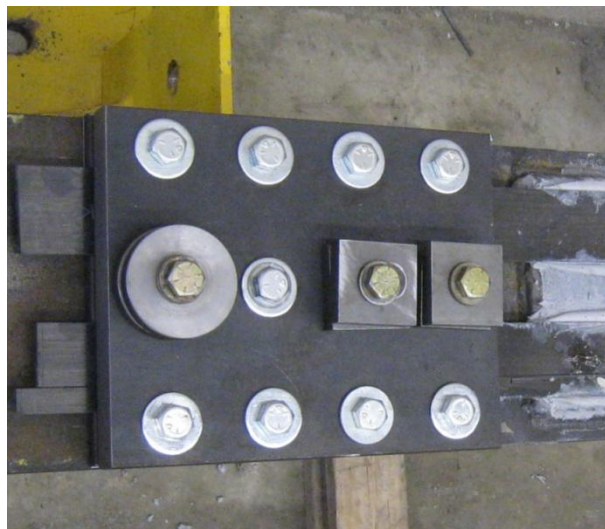


Figure 3.18. The fixed clamp anchor used for specimen 37%-C-M

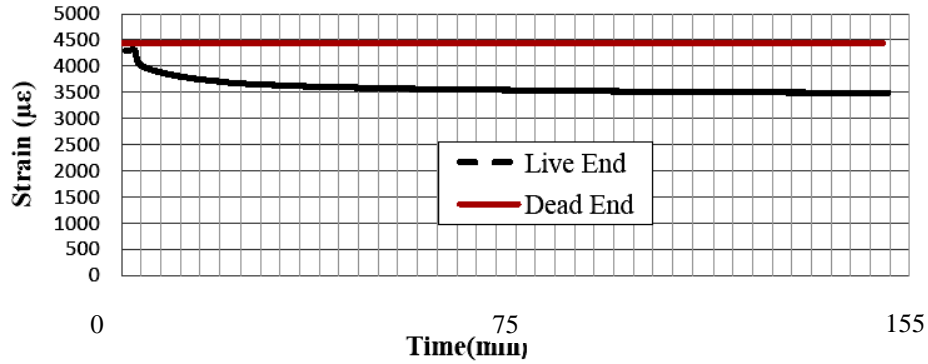


Figure 3.19. Strains at the strip ends during load release for specimen 37%-C-M

### 3.6 Test Setup

A special loading frame designed for fatigue tests was used to test the specimens as shown in Figure 3.20. The maximum loading capacity of frame is 290 kN (static load). A sinusoidal cyclic load range of 252 kN ( $P_{\max} = 280$  kN and  $P_{\min} = 28$  kN) with a load ratio of  $R = 0.1$  was applied. The loading frequency was set at 0.8 Hz and the sampling frequency was 10 reading/sec or 10 Hz. to capture the load peaks.

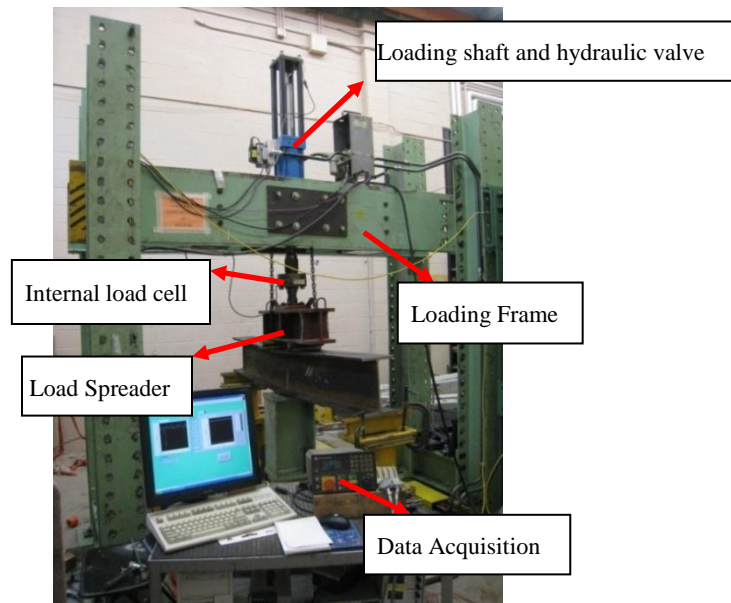
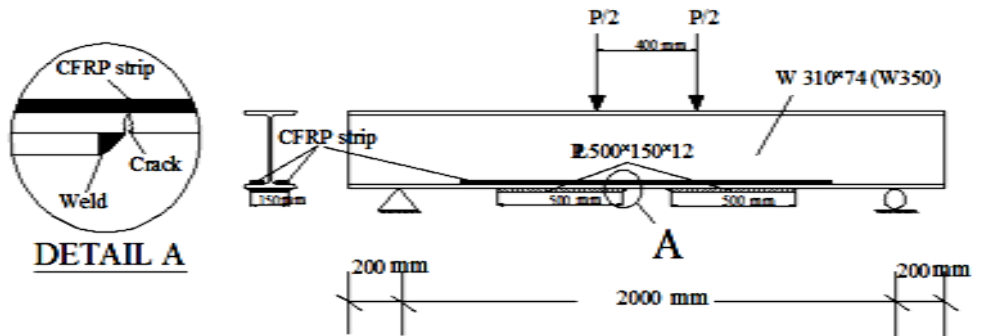
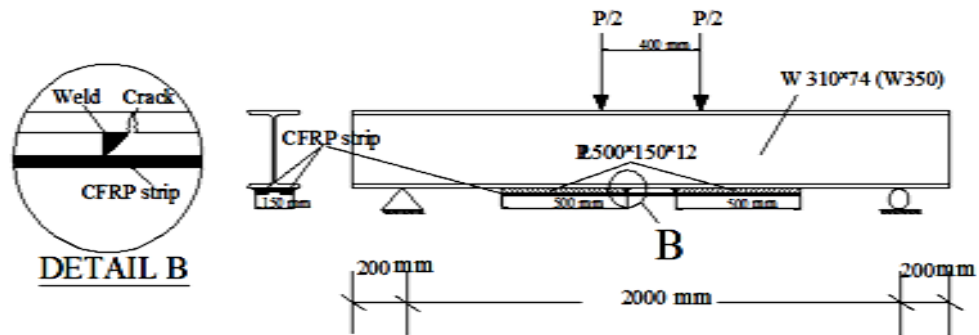


Figure 3.20. The loading frame

The specimens were tested in flexure in a four point bending configuration with a span of 2000 mm between the centerline of the supports. The distance between the two applied loads was 400 mm. The loads were applied using a stiff W section steel spreader beam. The two point loads were applied over two transverse steel plates, which covered the entire width of the specimen. The test setup is shown in Figure 3.21.



(a) Test setup for the specimens strengthened using strips on the flange



(b) Test setup for the specimens strengthened using strips on the cover plates

Figure 3.21. Test setup

Steel rollers were placed between the spreader beam and each of the steel plates. The specimen was supported on a roller support at one end and a hinged support at the other end (Figure 3.22). Both supports were elevated using heavy HSS square stubs to accommodate the expected large deflection at midspan. A strong HSS vertical post was mounted under the

specimen for safety purposes. The specimens were loaded under stroke control. The details of the test setup are shown in Figure 3.23.



(b) Simple support (c) Roller support  
Figure 3.22. Test setup and support configurations

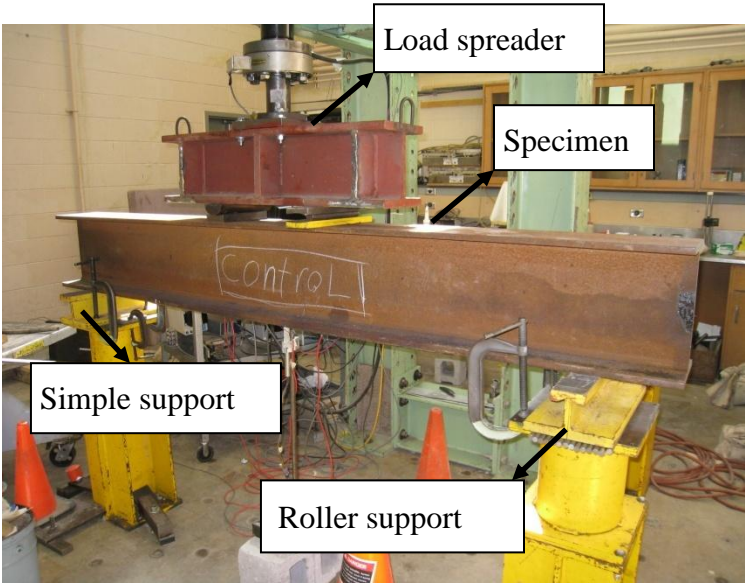


Figure 3.23. Specimen in the loading frame



### 3.6.1 Instrumentation

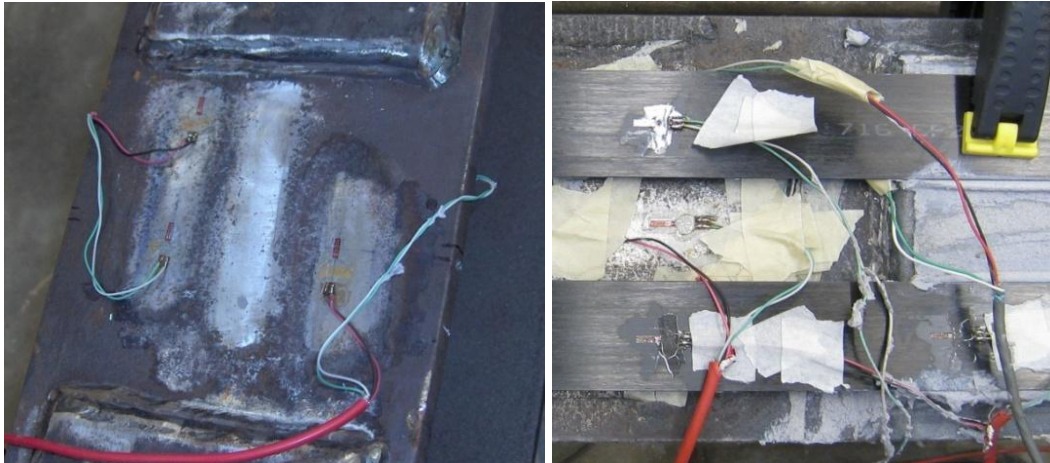
Two LVDTs were placed at both sides of the girder, at midspan to measure the vertical deflection as shown in Figure 3.24. Due to the very small predicted deflection for the specimens, the LVDTs were calibrated for a maximum deflection of 4 mm.



Figure 3.24. LVDTs at the midspan during fatigue tests

The longitudinal strains along the steel girder and CFRP plates were measured using 5 mm long  $120 \Omega$  electrical resistance strain gauges. Three strain gauges were attached on to the steel surface at midspan, as shown in Figure 3.25(a). Several strain gauges were attached to the CFRP strips, and are spaced as shown schematically in Figure 3. 25(b). The strain gauges are numbered as depicted in Figure 3.26, Figure 3.27 and Figure 3.28. The strain gauges located on the steel beam are denoted with (GB#) and on the CFRP strips with (GS#). The data measured by the strain gauges, LVDTs, load and stroke of the loading machine were recorded using a Data Acquisition System (DAS). The DAS recorded the load, stroke and LVDTs readings through a high-level input card with an accuracy of  $\pm 5$  mV. Strain gauge

readings were recorded through a strain gauge card with an accuracy of  $\pm 5$  mV. The test data was collected and stored using the computer program LabVIEW.



(a) Strain gauges on the beam

(b) Strain gauges on the strips

Figure 3.25. Strain gauges on the beam and strips

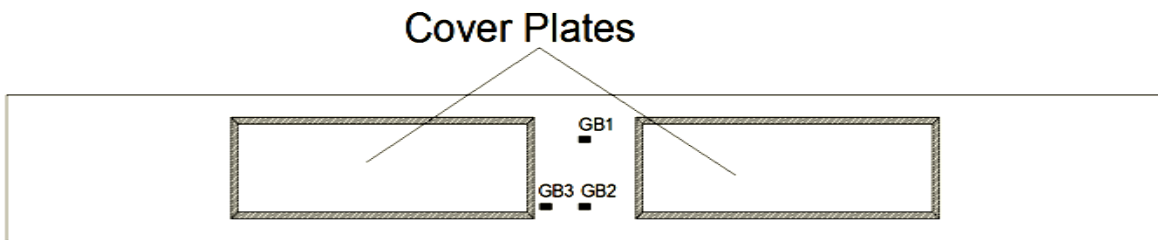


Figure 3.26. Location of strain gauges on the beam

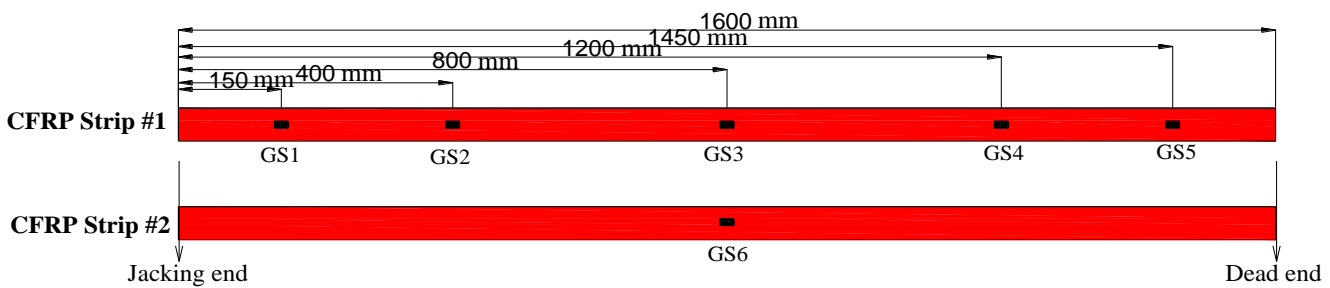


Figure 3.27. Location of strain gauges on the CFRP strips attached to the flange.

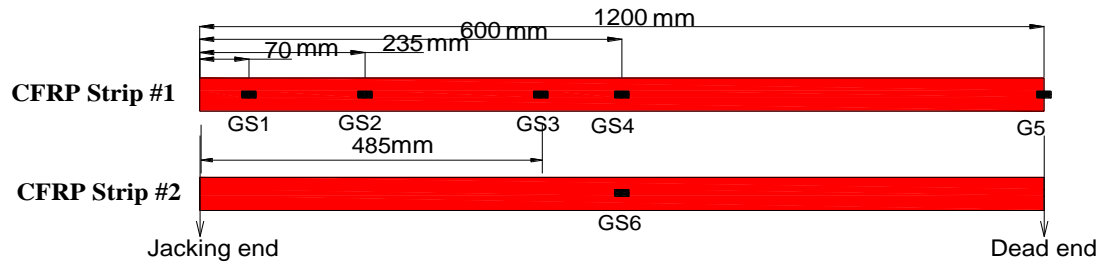


Figure 3.28. Location of strain gauges on the CFRP strips attached on the cover plates

## **Chapter 4: Experimental Results and Discussion**

### **4.1 Introduction**

This chapter presents the results of the experimental program. A total of six steel beams were tested: one beam was unstrengthened, one beam was strengthened with non-prestressed CFRP strips and four beams were strengthened with prestressed CFRP. The non- prestressed CFRP strips were placed on the cover plates at the outer flange of the strengthened specimen. For the prestressed strengthened specimens, three beams were reinforced with prestressed CFRP strips on the inside face of the flange and one beam was reinforced with prestressed CFRP strips bonded on the cover plates. The prestressing and load release results are presented first, followed by the fatigue test results.

### **4.2 Prestressing and Load Release Results**

This section presents the results of the prestressing and load release steps, including measured strains and calculated shear stresses for all prestressed specimens.

#### *4.2.1 Prestressing Strains*

The tensile strains in the CFRP strips along the beam are presented for three stages: 1) at prestressing, 2) at the time the prestressing force was released to beam, and 3) three days after release of the prestressing force. Based on experimental observation of prestressed specimens monitored to measure the strain losses after load release, the most significant losses occurred within three days of prestressing release. Consequently, to account for time dependent losses after load release, all specimens were monitored for three days to measure

the major possible losses. Based on specimen configuration, material properties, and prestressing level, the time dependent losses are thought to be mostly due to creep of the epoxy and a small amount of elastic shortening. For simplicity, all the losses are referred to herein simply as “losses”.

The corresponding stresses were calculated using equation (4.1).

$$\sigma = E \times \varepsilon \quad (4.1)$$

where the elastic modulus (E) for type M-CFRP is 210 GPa and for type S-CFRP is 165 GPa.

In this section, the results from 15%-F-S, 14%-F-M, 35%-F-M, 37%-C-M are discussed.

1) Specimen 15%-F-S

The strain profile along the strips for specimen 15%-F-S is shown in Figure 4.1. It is evident that the maximum transfer of prestressing strain to the epoxy occurred near the end of the strips, where the shear and out-of-plane stresses (peel stresses) are highest. From Figure 4.1, it is evident that the transfer length was less than or equal to 150 mm.

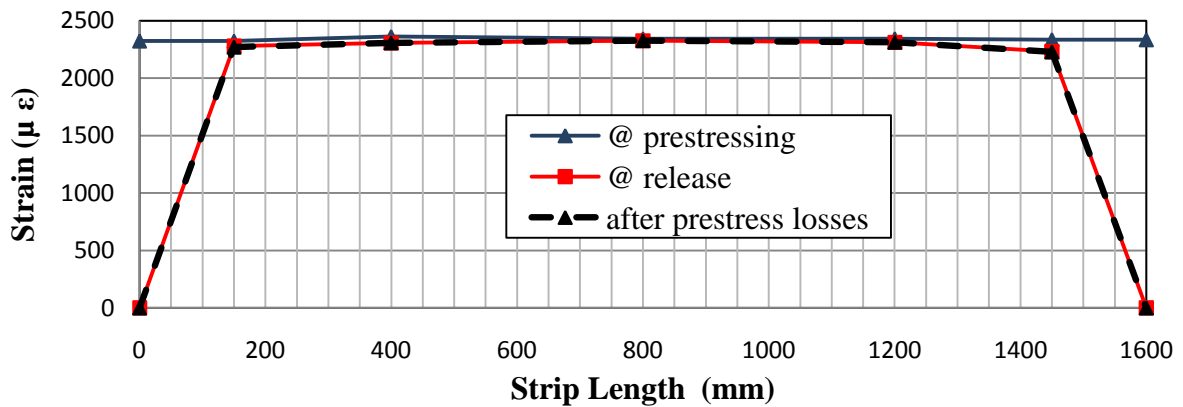


Figure 4.1. Strain profile along the strips (specimen 15%-F-S)

Table 4.1. Strains and stresses along the strips after all losses (specimen 15%-F-S)

	Distance from Beam End (mm)				
	150	400	800*	1200	1450
Strains at prestressing ( $\mu\epsilon$ )	2325	2365	2343 2322	2345	2336
Strains at release ( $\mu\epsilon$ )	2271	2309	2329 2326	2314	2229
% Transferred stress & losses	2.3	2.4	0.6	1.3	4.6
Average prestressing stress (MPa)	375	381	384	382	368
% $F_u$	15	15	15	15	15

\* Strains measured in strips 1 & 2

Table 4.1 gives the final prestressing strains/stresses. The stress at the middle of the CFRP strip in specimen 15%-F-S was equal to 384 MPa or 15.2% of  $F_u$ .

### 2) Specimen 14%-F-M

Figure 4.2 shows the CFRP strain profile along the beam length for specimen 14%-F-M. The general trend in prestressing strains was similar to that of specimen 15%-F-S. The final prestressing strains and stresses in the strips are given in Table 4.2. The highest measured prestress losses occurred near the ends of the strips. The average stress in the CFRP strips at midspan for specimen 14%-F-M was equal to 332 MPa or 13.9% of  $F_u$ .

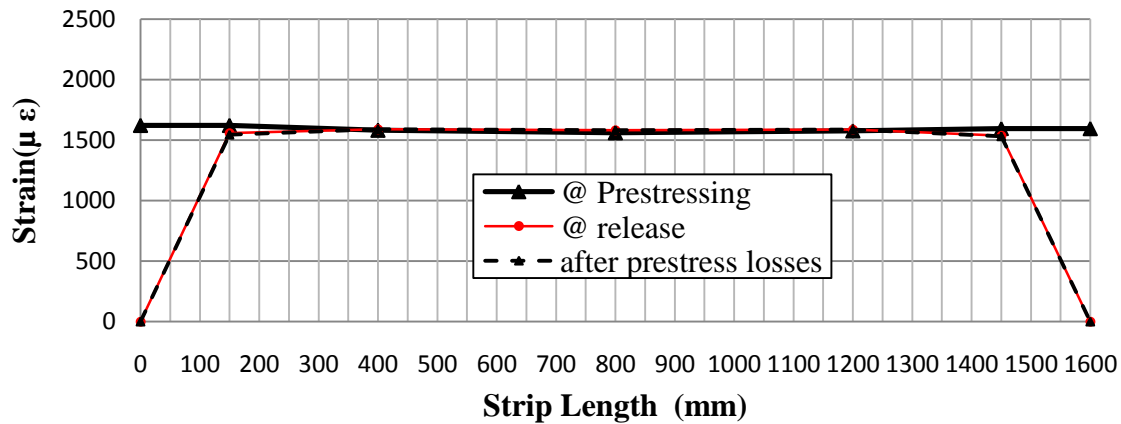


Figure 4.2. Strain profile along the strips (specimen 14%-F-M)

Table 4.2. Strains and stresses along the strips after all losses (specimen 14%-F-M)

	Distance from Beam End (mm)				
	150	400	800*	1200	1450
Strains at prestressing ( $\mu\epsilon$ )	1621	1582	1561 1751	1577	1596
Strains at release ( $\mu\epsilon$ )	1545	1591	1582 1745	1587	1533
% Transferred stress & losses	4.7	-0.6	-1.3	-0.6	3.9
Average prestressing stress (MPa)	324	334	332	333	322
% $F_u$	12.88	13.26	13.19	13.22	12.77

\* Strains measured in strips 1 & 2

### 3) Specimen 35%-F-M

At higher prestressing levels, greater shear and peel stresses developed at the ends of the strips resulting in much higher prestressing strain transferred in specimen 35%-F-M compared to the specimens prestressed to lower prestressing levels, as shown in Figure 4.3. After load release, prestressing strain transfer occurred within the development length of the strips: 43.2% at the jacking end (live end), and 56% at the fixed end (dead end). After 3 days, the strain changes were relatively small compared to the changes at the load release. From Figure 4.3 it is evident that the transfer length was approximately 400 mm. The obtained strains and stresses along the strips are given in Table 4.3. The prestressing stress at midspan was 894 MPa or 35.6% of  $F_u$ .

The clamping system applied at the end of CFRP strips mitigated the debonding. However significant transferred strain and prestress losses still were measured. The development length at the live end (~400 mm from beam end) where the prestress force was gradually released to the beam was lower than that at the dead end (~450 mm from beam end) when the force release was more rapid. Although the critical fatigue detail (weld toe) is still far from

the development length, the application of clamps is still necessary to prevent the debonding at the ends of the prestressed CFRP strips.

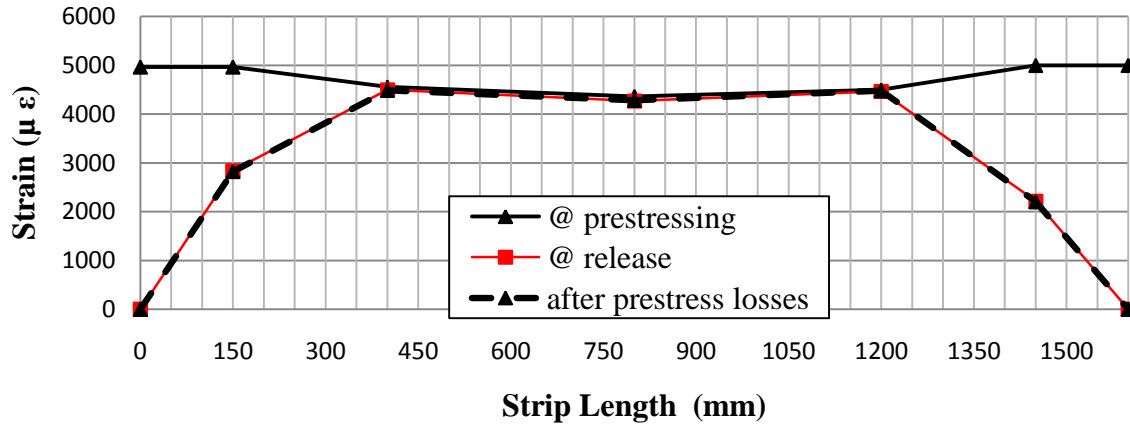


Figure 4.3. Strain profile along the strips (specimen 35%-F-M)

Table 4.3. Strains and Stresses along the strips after all losses (specimen 35%-F-M)

	Distance from Beam End (mm)				
	150	400	800*	1200	1450
Strains at prestressing (μ ε)	4967	4562	4364 4277	4503	4998
Strains at release (μ ε)	2824	4485	4284 4258	4479	2204
% Transferred stress & losses	43.2	1.7	1.8	0.5	55.9
Average prestressing stress (MPa)	593	942	894	941	463
% $F_u$	24	37	35	37	18

\* Strains measured in strips 1 & 2

### Specimen 37%-C-M

To reduce the transfer length at the ends of the strips and mitigate debonding, a fixed clamping system (described in Chapter 3) was employed for the dead end on specimen 37%-C-M while the same clamp was used for the live end as was used for specimen 35%-F-M. The prestressed CFRP strips were bonded on the cover plates on the outer flange of this



specimen. As a result of using a fixed clamp, the transfer length was significantly reduced. The losses at the live end were also reduced as illustrated in Figure 4.4. The strain transferred to the epoxy and prestress losses at the jacking end for specimen 35%-F-M were 33% compared to losses of 75% for specimen 37%-C-M. The strains and stresses along the strips for specimen 37%-C-M are given in Table 4.4. The final stress in the middle of the strips was 933 MPa or 37% of  $F_u$ .

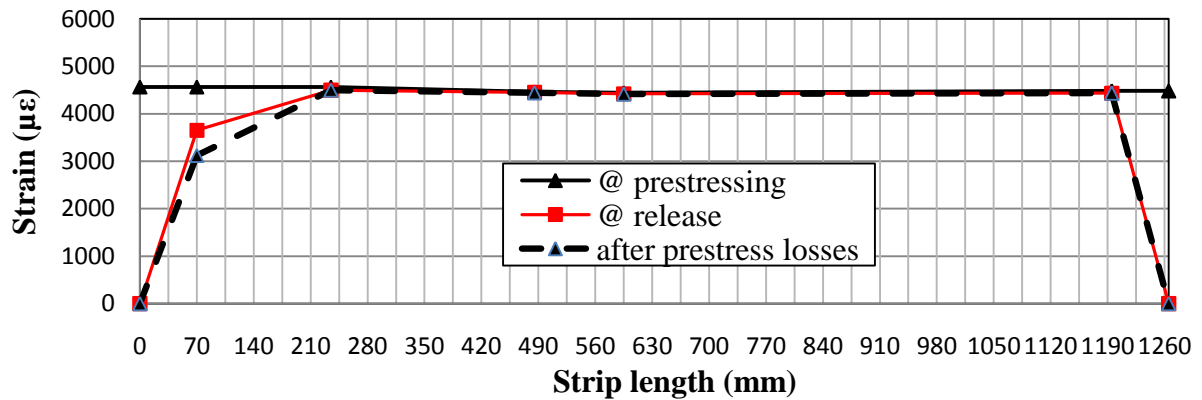


Figure 4.4. Strain profile along the strips (specimen 37%-C-M)

Table 4.4. Strains and Stresses along the strips after all losses (specimen 37%-C-M)

	Distance from Beam End (mm)				
	70	225	485	600*	1195
Strains at prestressing ( $\mu\epsilon$ )	4182	4568	4462	4441 4452	4482
Strains at release ( $\mu\epsilon$ )	3124	4501	4443	4414 4435	4435
% Transferred stress & losses	33.9	1.5	0.4	0.6	1.1
Average prestressing stress (MPa)	656	945	933	930	931
% $F_u$	26	38	37	37	37

\* Strains measured in strips 1 & 2

#### 4.2.2 Shear Stresses at CFRP-Steel Interface and Development Length

The shear stress transferred to the epoxy at the CFRP-steel interface can be calculated using the measured tensile strains along the CFRP strip which identify the development length. The average shear stress between two locations produced during prestressing is calculated based on the measured strains at those locations using equation 4.1 (Schnerch et al. 2006).

$$\tau_x = \frac{(\varepsilon_i - \varepsilon_{i-1})}{(x_i - x_{i-1})} \cdot t_{cfpr} \cdot E_{cfpr} \quad (4.1)$$

The shear stresses between two strain gauges locations were determined for all specimens and are given in Table 4.5. It is evident from Table 4.5 that the shear stresses at both ends are higher than that at the middle of strips. This confirms that a transfer length is required to transfer the prestressing force from the CFRP strip to the steel beam. Specimen 37%-C-M, with fixed end clamps, exhibited very low shear stresses at the GS4-GS5 locations where the fixed clamps were located compared to the other specimens. Consequently, the transfer length at the fixed end was significantly reduced for this specimen.

The average shear stress profiles along the CFRP strips are shown in Figure 4.5. As can be seen in this figure, the shear stresses at the beam ends, and consequently the transfer lengths, generally increase with the prestressing level.

Table 4.5. Shear stresses along the strips (MPa)

Location	$(\sigma_2 - \sigma_1)$ (MPa)	$\Delta x$ (mm)	$\Delta \tau_p$ (MPa)
Specimen	15%-F-S		
End-GS1	324-0	150	4.54295
GS1-GS2	324-334	250	0.05420
GS2-GS3	334-332	400	0.00656
GS3-GS4	332-333	400	0.00331
GS4-GS5	333-322	250	0.06390
GS5-End	322-0	150	4.50567
Specimen	14%-F-M		
End-GS1	375-0	150	4.49717
GS1-GS2	375-381	250	0.02970
GS2-GS3	381-384	400	0.00980
GS3-GS4	384-382	400	0.00708
GS4-GS5	382-368	250	0.06740
GS5-End	368-0	150	4.41382
Specimen	35%-F-M		
End-GS1	593-0	150	8.30
GS1-GS2	593-942	250	1.95
GS2-GS3	942-894	400	0.147
GS3-GS4	894-941	400	0.143
GS4-GS5	941-463	250	2.67
GS5-End	463-0	150	6.47
Specimen	37%-C-M		
End-GS1	656-0	100	9.18
GS1-GS2	656-945	165	2.45
GS2-GS3	945-933	250	0.067
GS3-GS4	933-930	110	0.079
GS4-GS5	930-931	600	0.010

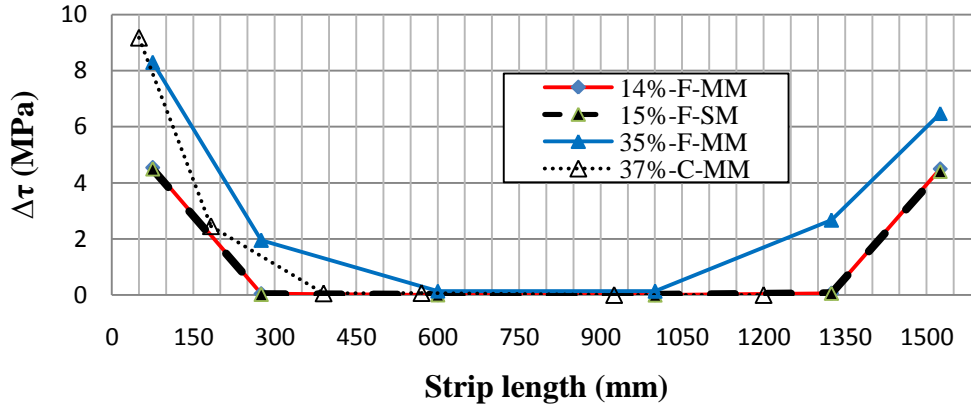


Figure 4.5. Average shear stress profile between the strain gauges

#### 4.2.3 Summary

The following key findings can be drawn for the behaviour of the specimens during prestressing: (1) significant transfer stresses/strains were always observed during load release. (2) 3 days after load release, the prestress losses were negligible. The main source of the losses during this time is thought to be creep of the epoxy. The loss values were very small, except for those at the live end of specimen 37%-C-M. (3) The stress losses and the shear stress transferred to the epoxy are relatively high at the strip ends, causing this to be allocation vulnerable to debonding. The transfer length is dependent on the prestressing level. (4) End clamping mitigates the debonding of the CFRP strips and maintains the prestressing force, hence also reducing the transfer length.

### 4.3 Fatigue Test Results

The fatigue test results are discussed in this section. The strains vs. fatigue life, deflection vs. fatigue life, test observations (CFRP strip debonding, crack observation, crack growth, mode of failure), and observed effects of prestressing level and CFRP strip location are presented.

#### 4.3.1 Fatigue Life

The fatigue lives for all specimens are given in Table 4.6. The fatigue life is determined as the number of cycles corresponding to the point when a crack propagated from the flange to the web-flange region. Beyond this point, unstable crack growth occurred, with the crack propagating to the middle of the web in less than 10 cycles for all specimens.

Table 4.6 shows that the fatigue life improvement varied but that the prestressed CFRP reinforcement considerably increased the fatigue life of steel beam with welded cover plates in all cases.

Table 4.6. Fatigue life for all specimens

Strip Location	Specimen*	Reinforcement Ratio(%)**	Fatigue Life (No. of Cycles)	Improvement (%)
	Control	0.74	409600	-----
Strips on inner Flange	15%-F-S	0.64	490900	19.8
	14%-F-M	0.74	576800	40.8
	35%-F-M	0.74	558600	36.4
Strips on cover plates	0%-C-M	0.74	646500	57.8
	37%-C-M	0.74	914750	123.3

\*C-cover plate, F-flange

\*\* Reinforcement Ratio(%) = the area section of CFRP strip / the area section beam

It is evident that the fatigue life improvement was affected by the stiffness of CFRP strips, level of prestressing and the location of CFRP strips. The low fatigue life improvement for specimen 15%-F-S was likely due to using S (standard modulus) CFRP strip. The unexpected low fatigue life for specimen 35%-F-M was possibly due to a poor epoxy application or perhaps because of the wide scatter normally seen in fatigue test of welded specimens.

The highest fatigue life was achieved by specimen 37%-C-M with the prestressed CFRP strips bonded on the cover plates.

#### *4.3.2 Deflection versus Life*

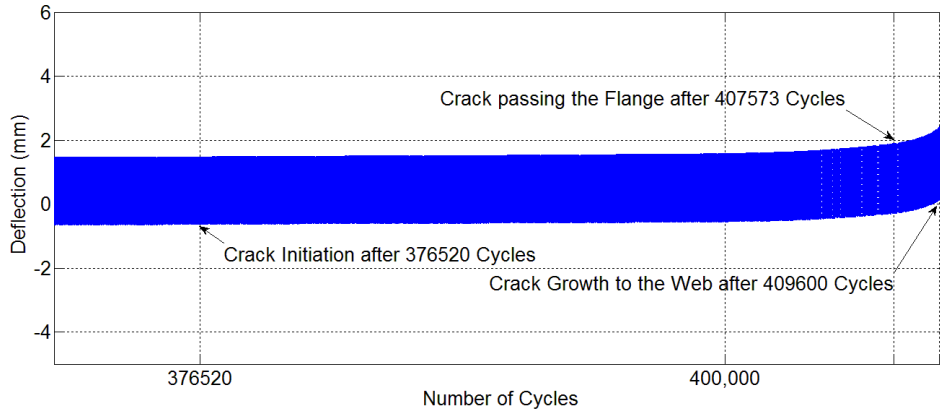
Table 4.7 gives the deflection range ( $\Delta\delta = \delta_{\max} - \delta_{\min}$ ) for all specimens during the fatigue tests. This deflection range was calculated based on the displacements measured by the LVDT at midspan at the beginning of fatigue testing. The deflection was measured for a cyclic load range of 248 kN, with a minimum load of 32 kN and maximum load of 280 kN ( $R = 0.114$ ).

It is evident from Table 4.7 that the deflection is inversely proportional to the stiffness of the reinforcement. Specimens strengthened with medium modulus strips exhibited lower deflections. The deflection of specimen 35%-F-M was much higher than that for specimen 14%-F-M which would explain the lower fatigue life for specimen 35%-F-M. No explanation can be given to why specimen 14%-F-M had a lower deflection range. The smallest deflection range was recorded for specimen 37%-C-m with strips placed on the cover plates.

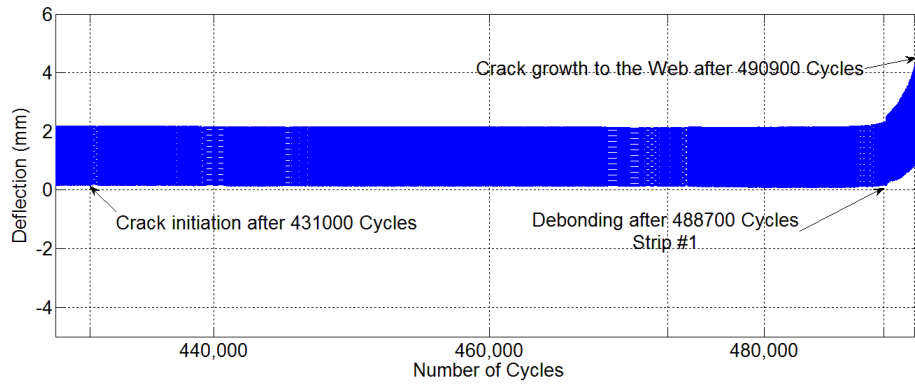
Table 4.7. Deflections ranges

Beam	$\Delta\delta$ (mm)
Control	2.15
15%-F-S	2.14
14%-F-M	1.57
35%-F-M	2.12
0%-C-M	1.90
37%-C-M	1.46

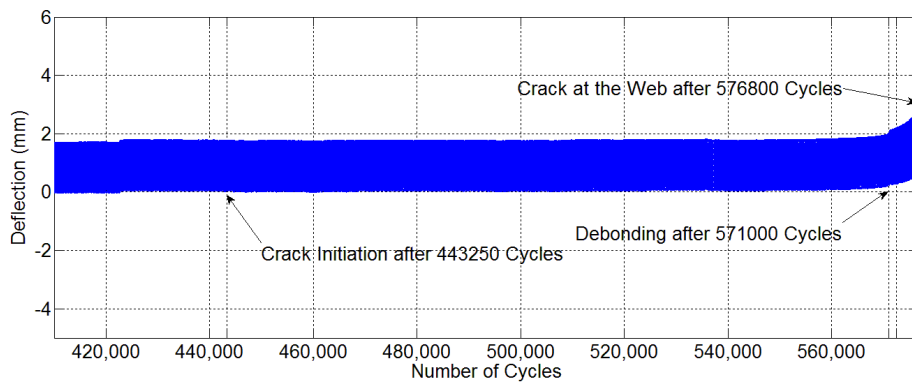
The deflection vs. number of cycles for all specimens during the fatigue tests are shown in Figure 4.6(a)-(f). These figures document critical stages for the specimens in terms of crack initiation, debonding of CFRP strip(s), and crack growth. A similar trend for deflection vs. number of cycles is observed for all specimens. The deflection gradually increases after crack initiation. Looking at Figure 4.6, the deflection increase is more rapid when the crack reaches the web neck for the control specimen and specimen 0%-C-M. The deflection increases for all prestressed specimens occur after CFRP strip debonding, while the crack is still within the flange thickness. The deflection range increases after partial debonding (one strip debonded), followed by a sudden increase in deflection when the strip fractured for all prestressed specimens, while an upward shift in the deflection range was measured for the control beam after crack initiation (see Figure 4.6 (a)).



(a). Control specimen



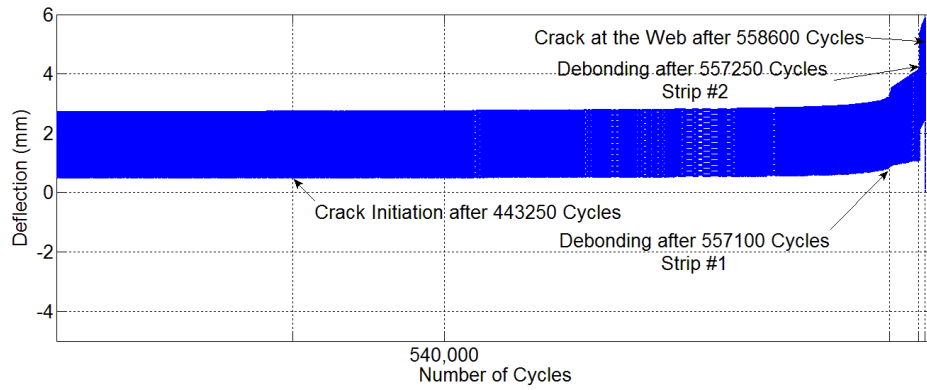
(b) 15%-F-S specimen



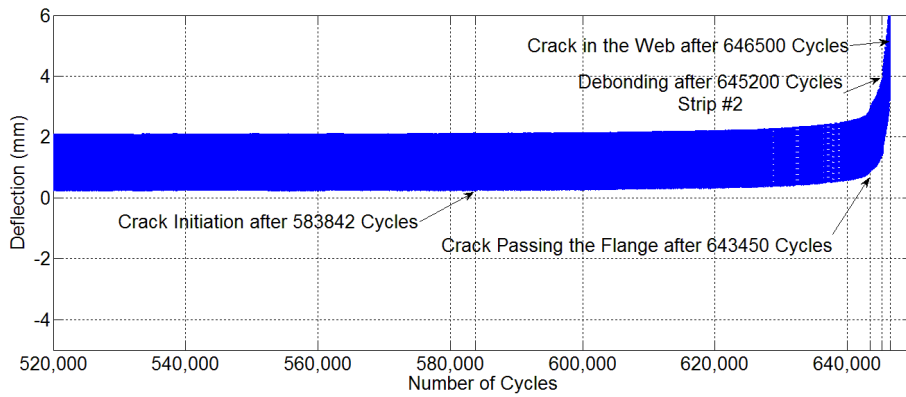
(c) 14%-F-M specimen

Figure 4.6. Deflection vs. number of cycles

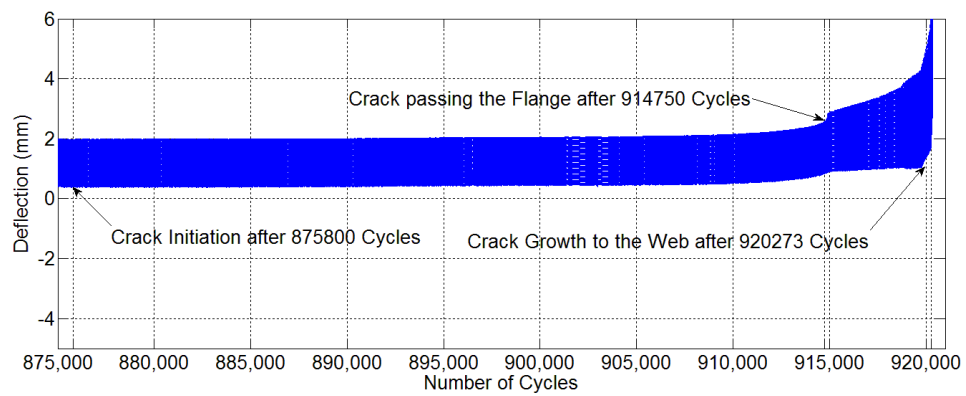




(d) 35%-F-M specimen



(e) 0%-C-M specimen



(f) 37%-C-M specimen

Figure 4.6(continued). Deflection vs. number of cycles

The deflection range variation vs. number of cycles for all specimens are shown in Figure 4.7. The deflection range curves are drawn for the last 45000 cycles. Looking at Figure 4.7, it can be seen that: (1) the highest deflection range belongs to the control specimen while the lowest deflection range belongs to specimen 37%-C-M indicating the highest stiffness increase for that specimen. (2) the deflection ranges are dramatically increased at the end of fatigue life. (3) the lower deflection range for the specimens with CFRP strips on the cover plates confirms the influence of the CFRP strip location on the specimen stiffness.

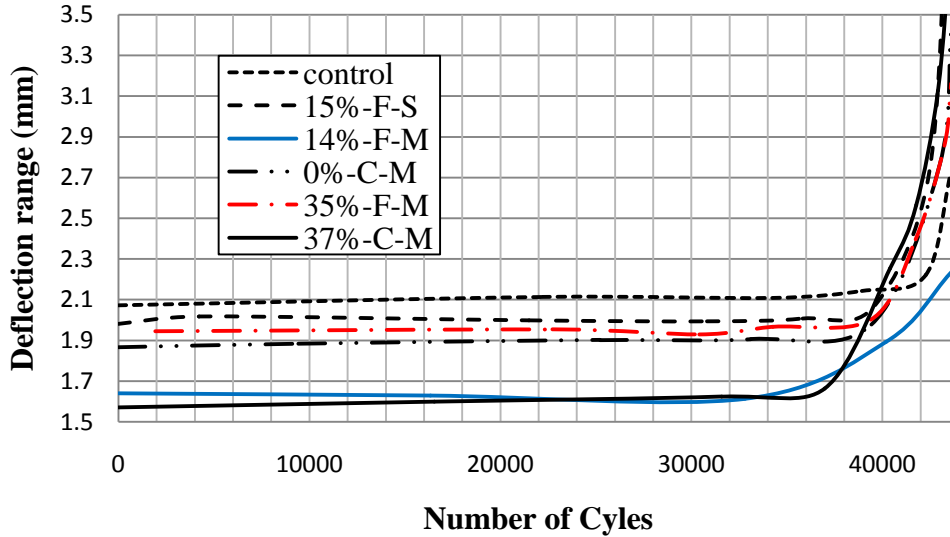


Figure 4.7. Deflection vs. number of cycles for all specimens

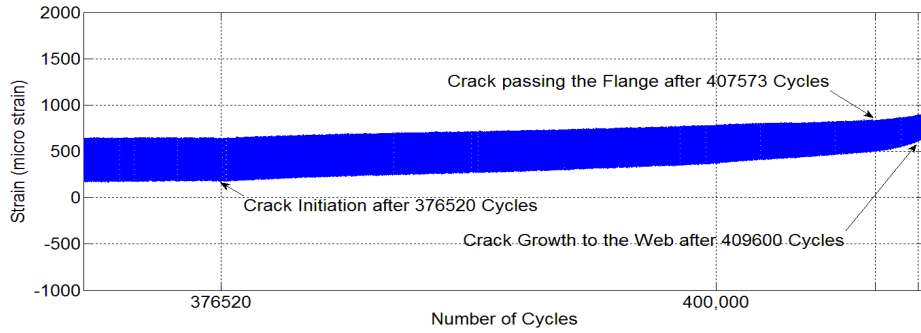
### 4.3.3 Strain vs. Life

This section presents of the measured strains vs. number of cycles at critical stages (crack initiation, crack growth or debonding, fracture) for all specimens. Results for strains measured on the CFRP strips (GS1→GS6) and those on the beam at midspan (GB1→GB3) are presented in detail.

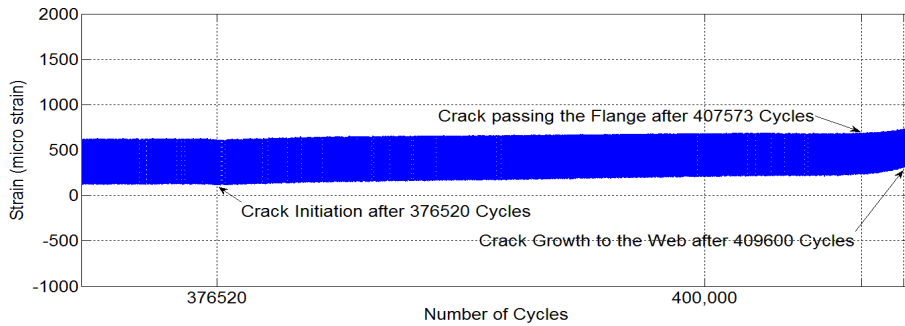
#### 1) Control specimen

The crack was initiated after 376520 cycles (91.9% of fatigue life) and propagated through the flange thickness towards the web after 407573 cycles (99.5% of fatigue life). The beam failed after 409600 cycles.

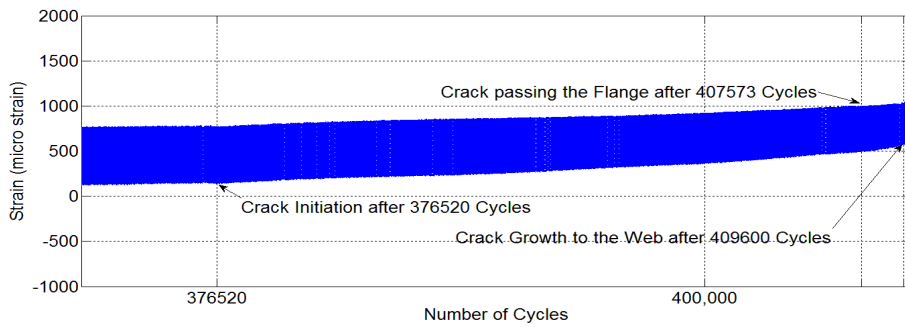
Figure 4.7 shows the strain vs. life curved for each strain gauge on the control beam. As shown in Figure 4.7, the slopes of the curves changed as the number of cycles increased. The strains rapidly increased as the crack propagated into the flange at 407573 cycles. The beam failed shortly after 2000 cycles (less than 0.5% of the total fatigue life). Comparing the strain data from the gauge located close to the weld-toe (GB3) to those of strain gauges at the middle of the beam (GB1, GB2), it can be seen that the strain range ( $\Delta\varepsilon$ ) decreased as the level of strain increased near the crack. Although the strain gauge was not placed close enough to capture the peak stress at the weld-toe as this is impossible for practical reasons, the strain range at the location close to the weld toe decreased as the crack depth increased. From this, it can be deduced that the tensile (bottom) flange near the crack location contributes less and less in resisting the applied loads as the crack grows through it.



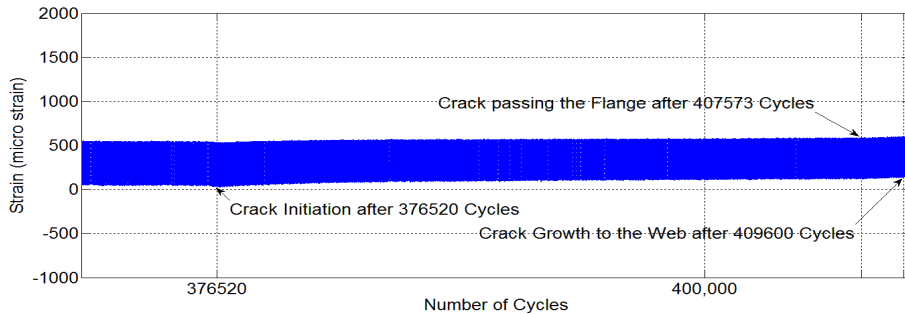
(a) Strain gauge (GB1)



(b) Strain gauge (GB2)



(c) Strain gauge (GB3)



(d) Strain gauge (GBI2)

Figure 4.8. Strains vs. number of cycles for Control Beam

A summary of the strains recorded for the control beam is given in Table 4.8.

Table 4.8. Summary of strain-life results for the control specimen

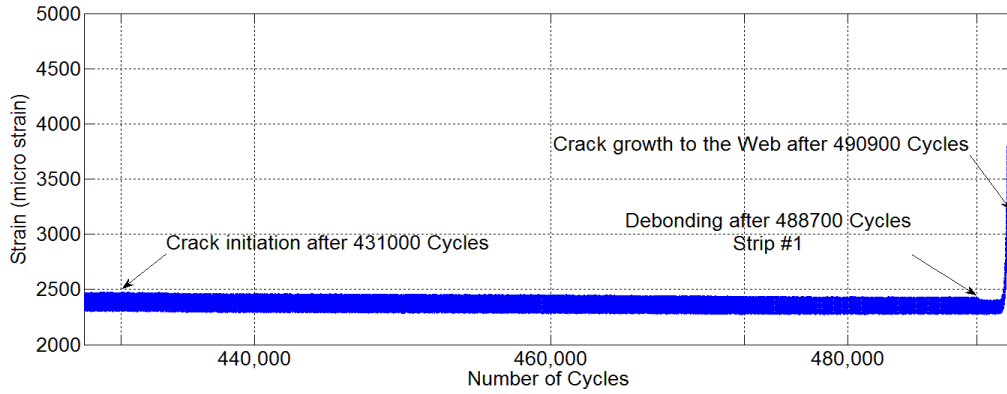
Gauge #	Occurrence	Cycle #	% life	$\epsilon$ min ( $\mu\epsilon$ )	$\epsilon$ max ( $\mu\epsilon$ )	$\Delta\epsilon$ ( $\mu\epsilon$ )
GB1 (midspan)	Crack Initiation	376520	91.9	183	635	452
	Crack Growth to web	407573	99.5	509	836	327
	Fracture	409600	100	621	888	267
GB2 (midspan)	Crack Initiation	376520	91.9	124	610	487
	Crack Growth to web	407573	99.5	236	677	441
	Fracture	409600	100	314	722	408
GB3 (close to weld toe)	Crack Initiation	376520	91.9	147	763	616
	Crack Growth to web	407573	99.5	500	991	491
	Fracture	409600	100	577	1029	452
GBI2 (inner side) (midspan)	Crack Initiation	376520	91.9	44	527	483
	Crack Growth to web	407573	99.5	129	578	441
	Fracture	409600	100	144	590	446

\* GB---GB3 are located on the beam

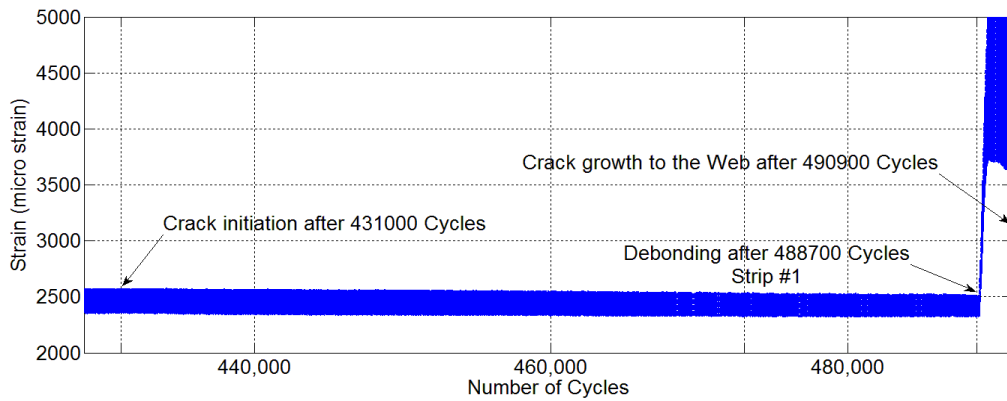
## 2) Specimen 15%-F-S

The crack initiated at the weld toe after 431000 cycles (87.8% of fatigue life) and propagated through the flange thickness towards the web while strip #1 debonded at the midspan after 488700 cycles (99.6% of fatigue life). The specimen failed after 490900 cycles. The strain-life curves for all gauges are shown in Figure 4.9. The strain-life histories show that there is a shift in strain at the onset of debonding. Debonding of the strip occurred on the side of the cracked weld-toe, revealing the significant effect of cracking on debonding initiation. Gauge GS6 recorded the strain at the middle of strip #2 as shown in Figure 4.9 (f). Increase in the strain range after debonding indicates that crack growth was at the other side. This behaviour was caused by unsymmetrical loading of the specimen. Looking at Figure 4.9 (g), Figure 4.9 (h) and Figure 4.9 (i), it can be seen that as the strain ranges for gauges GB1, 2, and 3 decreased, the strain values increased, indicating crack growth into the web. As the crack

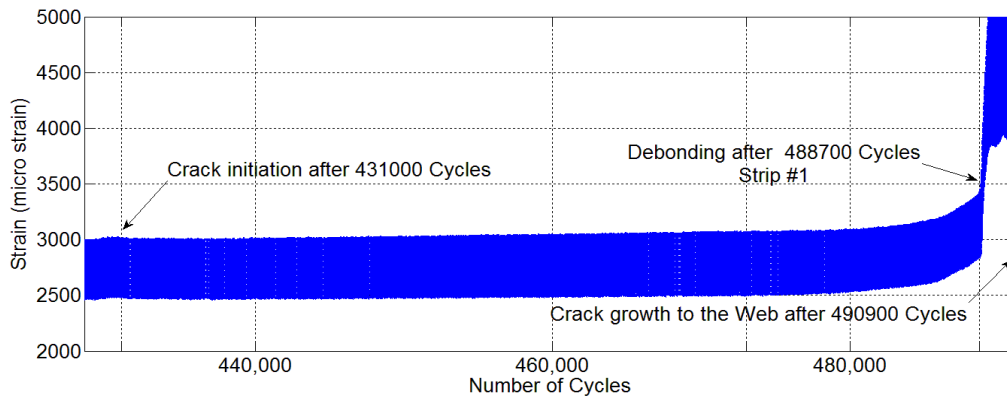
grows towards the web, the strain on the flange tends to decrease as recorded by gauges GB1 and GB2.



(a) Strain gauge (GS1)

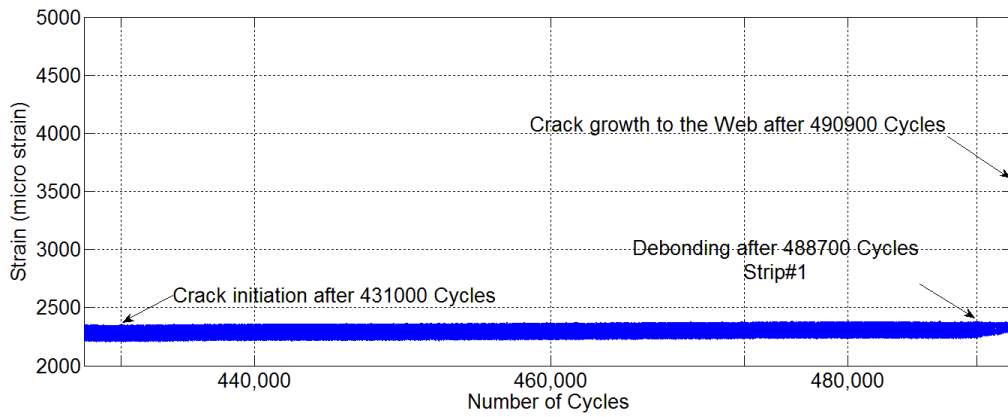


(b) Strain gauge (GS2)

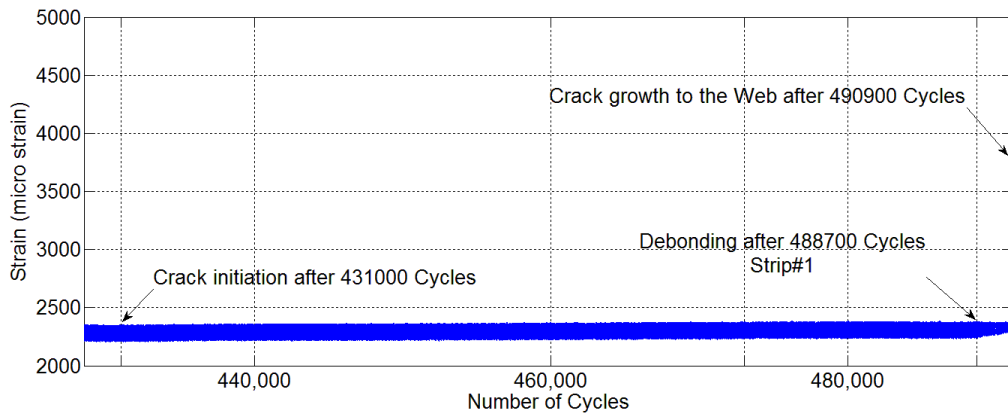


(c) Strain gauge (GS3)

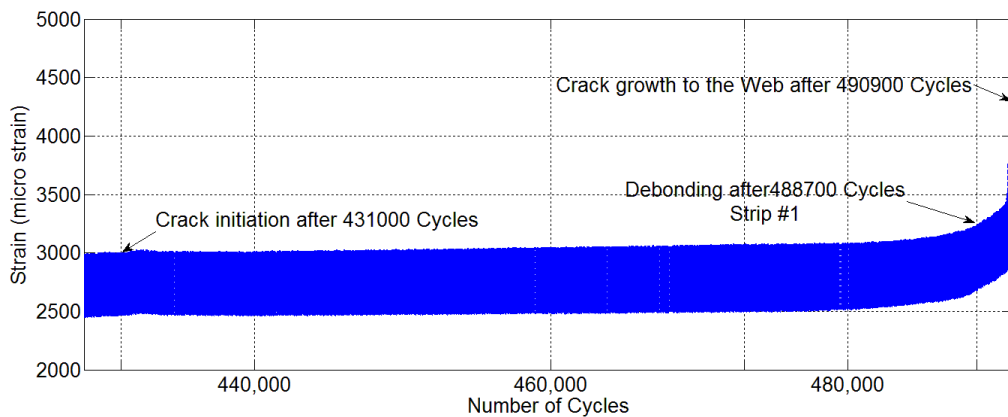
Figure 4.9. Strains vs. number of cycles for specimen 15%-F-S



(d) Strain gage (GS4)

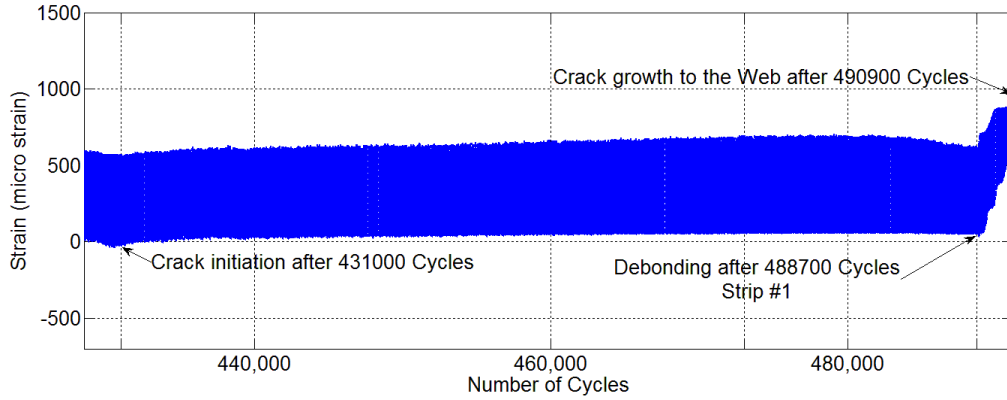


(e) Strain gage (GS5)

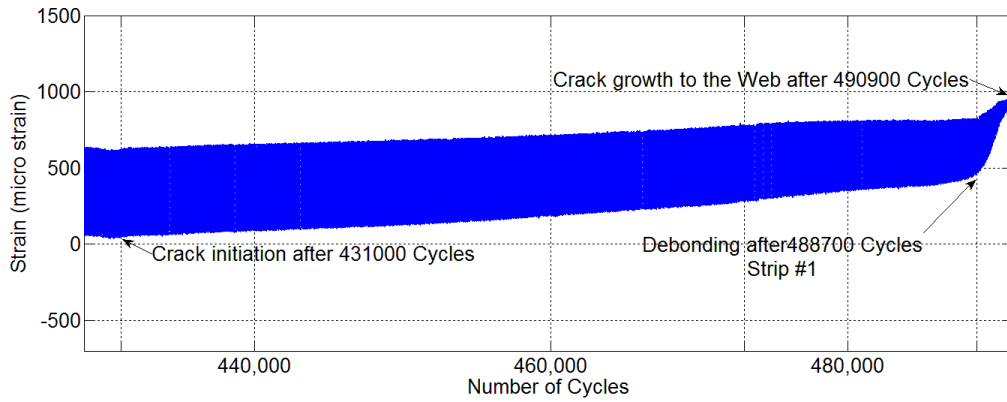


(f) Strain gage (GS6)

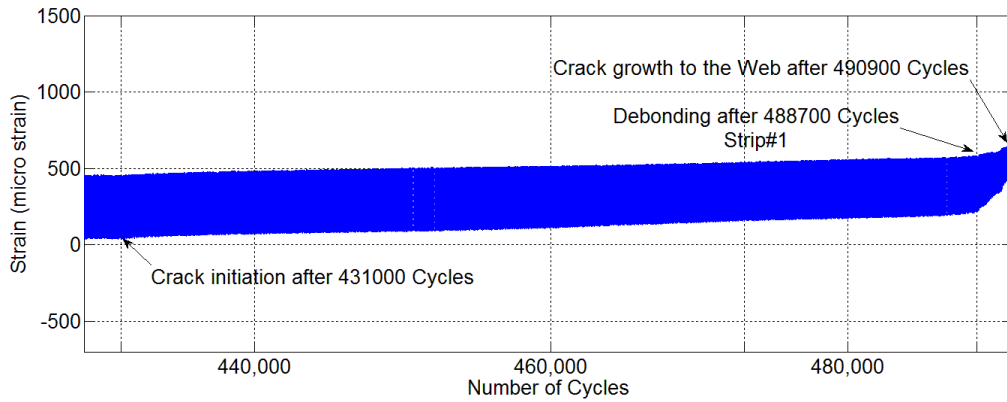
Figure 4.9 (continued). Strains vs. number of cycles for specimen 15%-F-S



(g) Strain gague (GB1)



(h) Strain gague (GB2)



(i) Strain gague (GB3)

Figure 4.9 (continued). Strains vs. number of cycles for specimen 15%-F-S



The critical strains recorded during the fatigue test of 15%-F-S specimen are summarized in Table 4.9. Strains along the length of CFRP strips at critical stages in the fatigue life corresponding to the maximum and minimum applied load are plotted in Figure 4.10 and Figure 4.11. A sudden change in the strains after debonding was followed by a dramatic increase in the strain range as observed in these figures. This phenomenon was only observed for gauges GS2 and GS3, indicating that debonding of strip #1 was initiated over half of the strip length while the other part of the strip was still bonded.

Table 4.9. Summary of strain-life results for the specimen 15%-F-S

Gauge #	Occurrence	Cycle #	% life	$\epsilon$ min ( $\mu\epsilon$ )	$\epsilon$ max ( $\mu\epsilon$ )	$\Delta\epsilon$ ( $\mu\epsilon$ )
GS1 150 mm from end of strip #1	Crack Initiation	431000	87.8	2310	2466	156
	Debonding	488700	99.6	2284	2418	134
	Fracture	490900	100	3546	4743	1197
GS2 400 mm from end of strip #1	Crack Initiation	875800	87.8	2360	2569	209
	Debonding	914750	99.6	2327	2500	173
	Fracture	920273	100	3633	5452	1819
GS3 middle of strip #1	Crack Initiation	875800	87.8	2485	3005	520
	Debonding	914750	99.6	2853	3427	574
	Fracture	920273	100	3882	6072	2189
GS4 1200 mm from end of strip #1	Crack Initiation	875800	87.8	2298	2515	217
	Debonding	914750	99.6	2354	2547	193
	Fracture	920273	100	2414	2559	145
GS5 1450 mm from end of strip #1	Crack Initiation	875800	87.8	2215	2348	132
	Debonding	914750	99.6	2247	2367	120
	Fracture	920273	100	2307	2367	60
GS6 middle of strip #2	Crack Initiation	875800	87.8	2331	2851	520
	Debonding	914750	99.6	2483	2884	401
	Fracture	920273	100	2719	3683	964
GB1 middle of beam	Crack Initiation	875800	87.8	70	627	557
	Debonding	914750	99.6	474	814	340
	Fracture	920273	100	919	938	19
GB2 middle of beam	Crack Initiation	875800	87.8	-3	568	571
	Debonding	914750	99.6	54	616	562
	Fracture	920273	100	548	878	330
GB3 Close to weld toe	Crack Initiation	875800	87.8	52	445	393
	Debonding	914750	99.6	226	575	349
	Fracture	920273	100	441	643	201

\* GBs are located on the beam and GSs are located on the strip

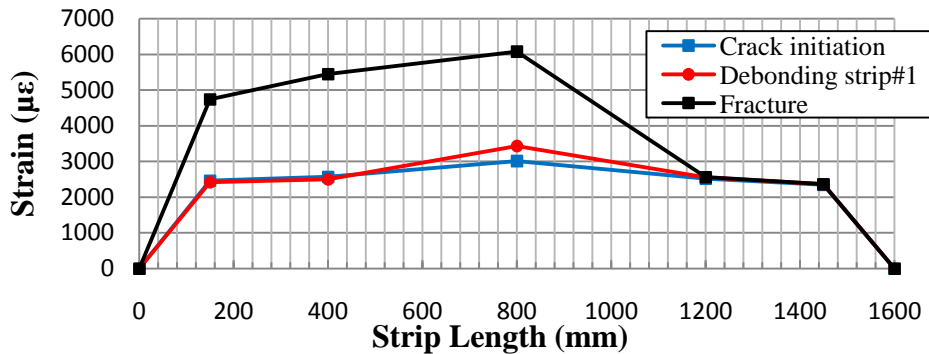


Figure 4.10. Strain variation along the CFRP strip length for specimen 15%-F-S  
( $P_{max} = 280$  kN)

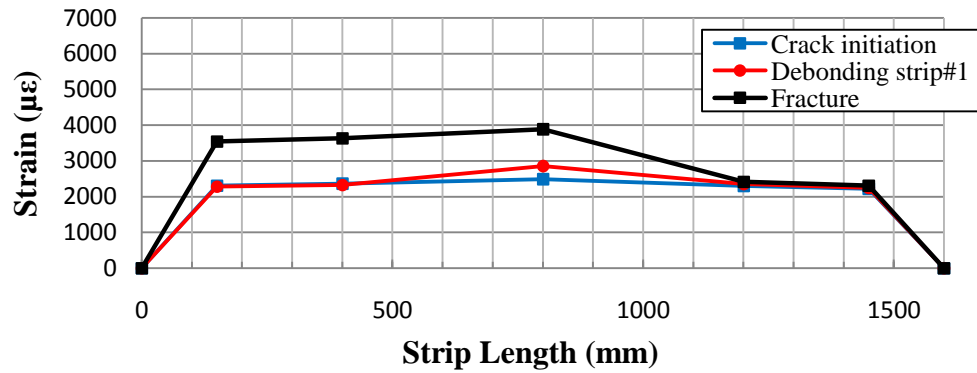


Figure 4.11. Strain variation along the CFRP strip length for specimen 15%-F-S ( $P_{min} = 32$  kN)

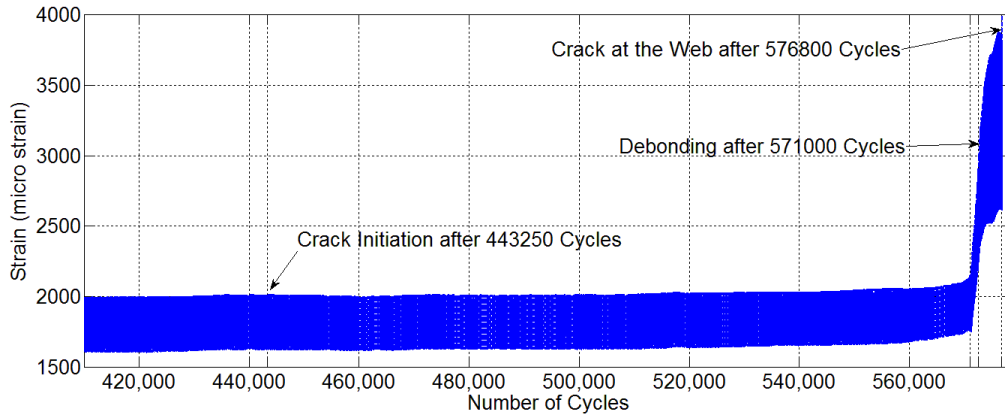
### 3) Specimen 14%-F-M

The crack at the weld-toe was initiated at 443250 cycles and propagated into the web. CFRP strip debonding occurred after 571000 cycles, followed by specimen failure after 576800 cycles.

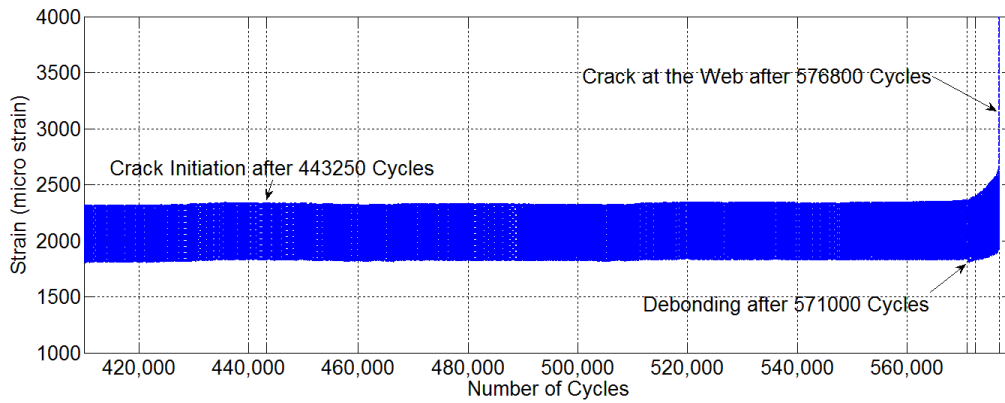
The plots of strain vs. life for all gauges on the beam are shown in Figure 4.12. For this specimen, data for only two strain gauges on the CFRP strips are plotted, GS3 and GS6. The strain variation vs. life was stable until debonding occurred and was accompanied by a sharp increase in strain (GS3 at middle strip). Strain gauge GS3, at the middle of strip #1, exhibited a sudden increase in strain at debonding of the strip while gauge GS6, at the middle of other strip (strip #2), did not record high strains indicating no debonding for strip #2. Comparing the strain values of GS3 and GS6, a huge difference in strains after debonding and up to failure can be seen. Looking at Figure 4.12(c)-(e), a shift up in strain values is observable for

GB1, GB2, and GB3 after crack initiation, particularly after debonding. GB3, the strain gauge close to weld, recorded a drop in strain range after debonding.

The strain-life results are summarized in Table 4.10 for specimen 14%-F-M.

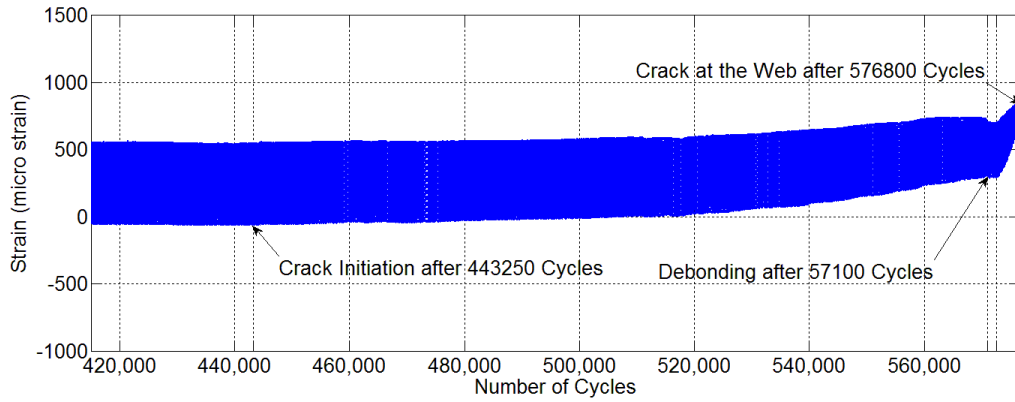


(a) Strain gauge (GS3)

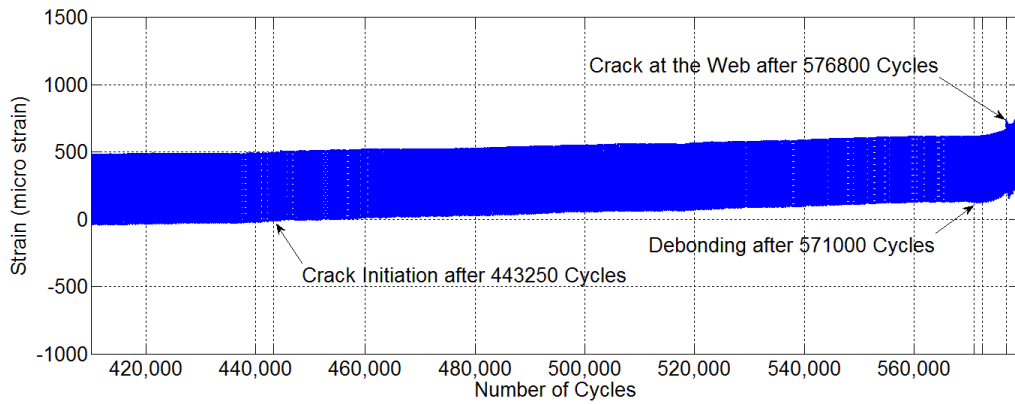


(b) Strain gauge (GS6)

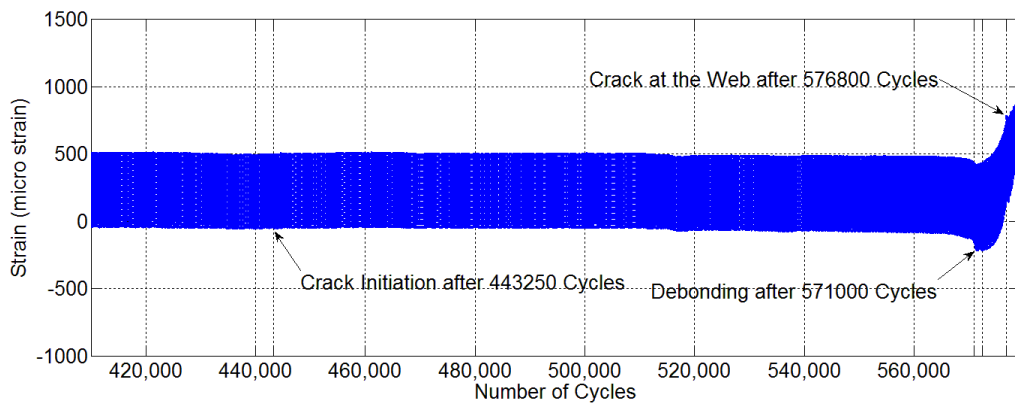
Figure 4.12. Strains vs. number of cycles for specimen 14%-F-M



(c) Strain gauge (GB1)



(d) Strain gauge (GB2)



(e) Strain gauge (GB3)

Figure 4.12 (continued). Strains vs. number of cycles for specimen 14%-F-M

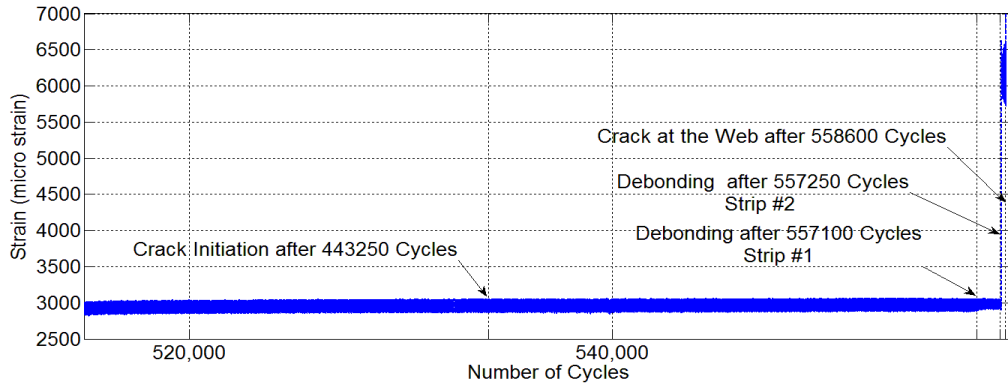
Table 4.10. Summary of strain-life results for specimen 14%-F-M

Gauge #	Occurrence	Cycle #	% life	$\epsilon$ min ( $\mu\epsilon$ )	$\epsilon$ max ( $\mu\epsilon$ )	$\Delta\epsilon$ ( $\mu\epsilon$ )
GB1 middle of beam	Crack Initiation	443250	77	-34	551	585
	Debonding	571000	99	306	713	407
	Fracture	576800	100	712	856	144
GB2 middle of beam	Crack Initiation	443250	77	-24	568	592
	Debonding	571000	99	126	618	492
	Fracture	576800	100	196	671	475
GB3 close to weld toe	Crack Initiation	443250	77	0	514	514
	Debonding	571000	99	-163	437	600
	Fracture	576800	100	125	725	600
GS3 middle of strip #1	Crack Initiation	443250	77	1629	2123	493
	Debonding	571000	99	1754	2137	382
	Fracture	576800	100	2614	3041	426
GS6 middle of strip #2	Crack Initiation	443250	77	1817	2315	499
	Debonding	571000	99	1833	2369	536
	Fracture	576800	100	1955	2664	709

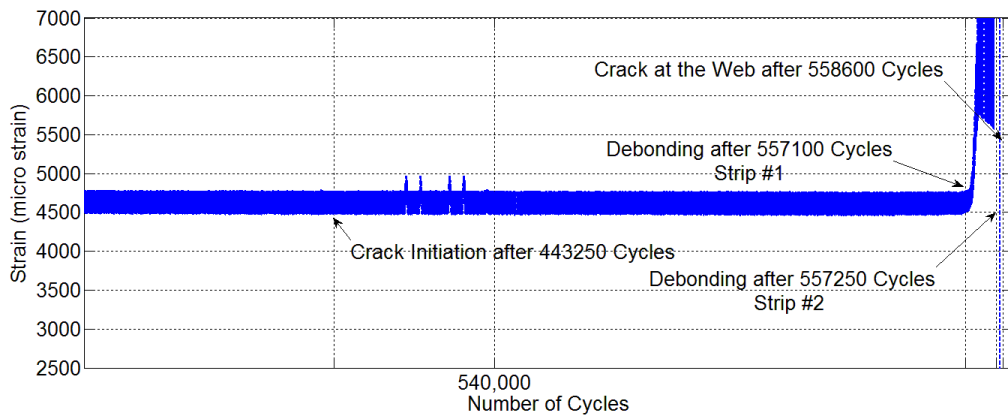
\* GBs are located on the beam and GSs are located on the strip

#### 4) Specimen 35%-F-M

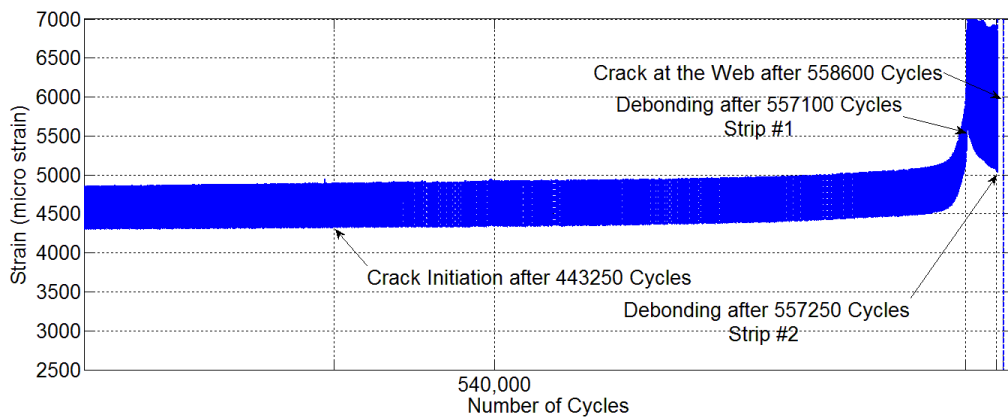
Crack initiation in specimen 35%-F-M was observed at the weld-toe after 443250 cycles. After 557100 cycles strip #1 was debonded followed by debonding of strip #2 after only 150 cycles. The specimen failed by fracture in the web after 558600 cycles. Figure 4.13 shows the strain life data for all gauges. Looking at Figure 4.13 (b) and (c), the strain values and strain ranges dramatically increase after debonding of the second strip. However the strain changes at both ends (GS1 and GS5) exhibit a stable response or good bond until failure. Unsymmetrical loading led to crack initiation at the same side as the debonded strip (strip#1). Comparing strain curves on the beam for gauges GB1 and GB2, the rapid strain increase for GB1 suggests an unsymmetrical loading. A stress range decrease was observed for GB3 around the time of crack initiation.



(a) Strain gauge (GS1)

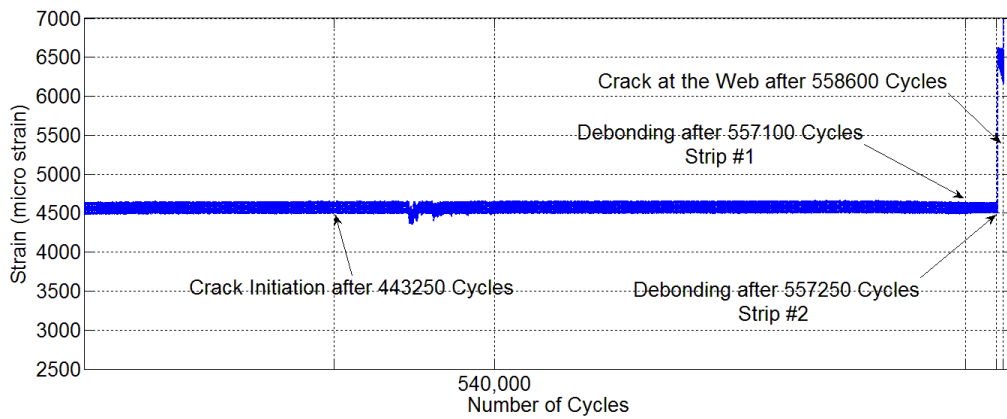


(b) Strain gauge (GS2)

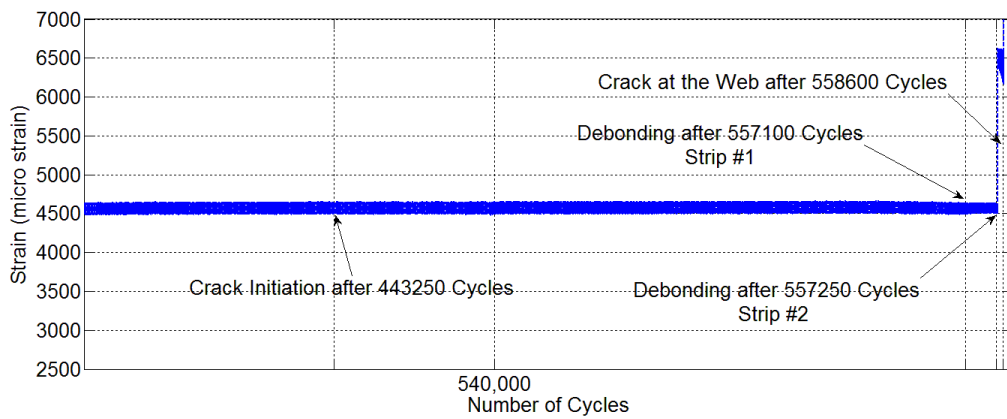


(c) Strain gauge (GS3)

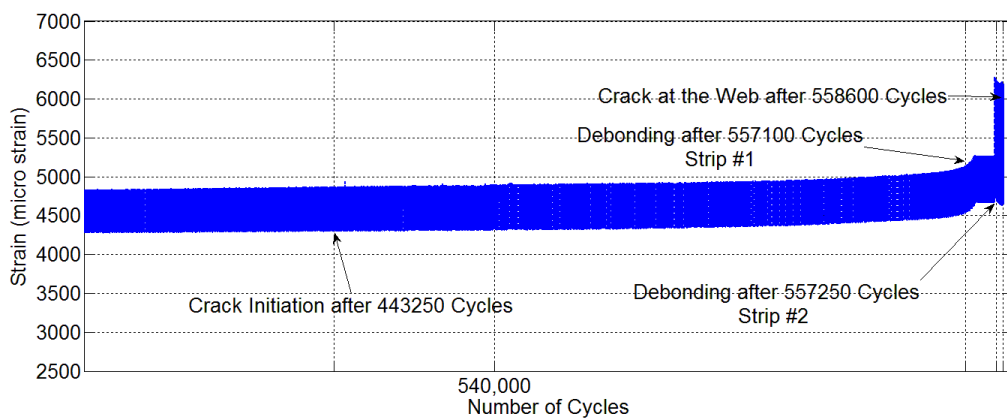
Figure 4.13. Strains vs. number of cycles for specimen 35%-F-M



(d) Strain gauge (GS4)



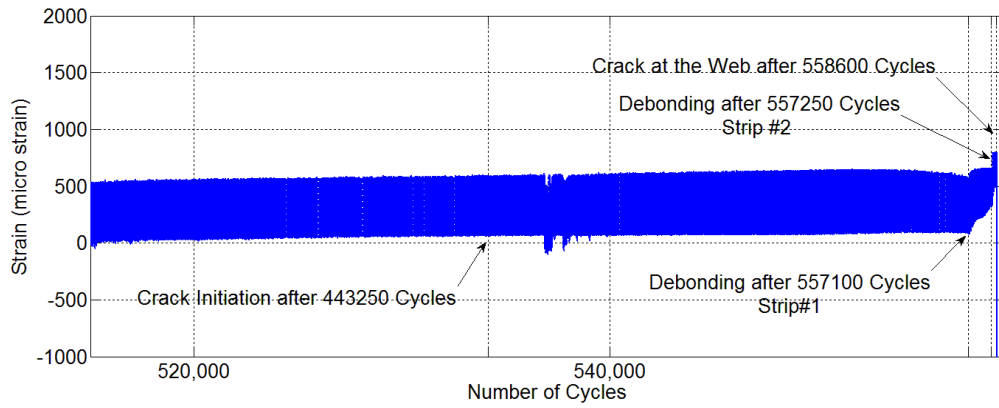
(e) Strain gauge (GS5)



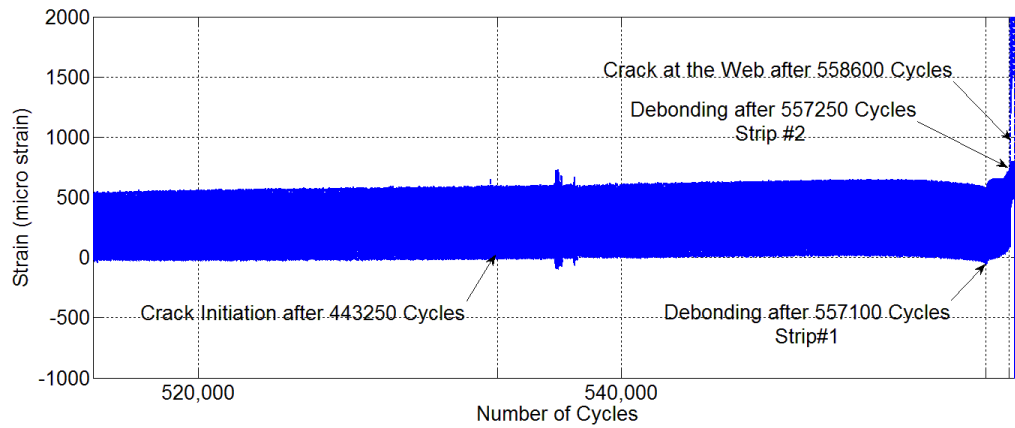
(f) Strain gauge (GS5)

Figure 4.13 (continued). Strains vs. number of cycles for specimen 35%-F-M

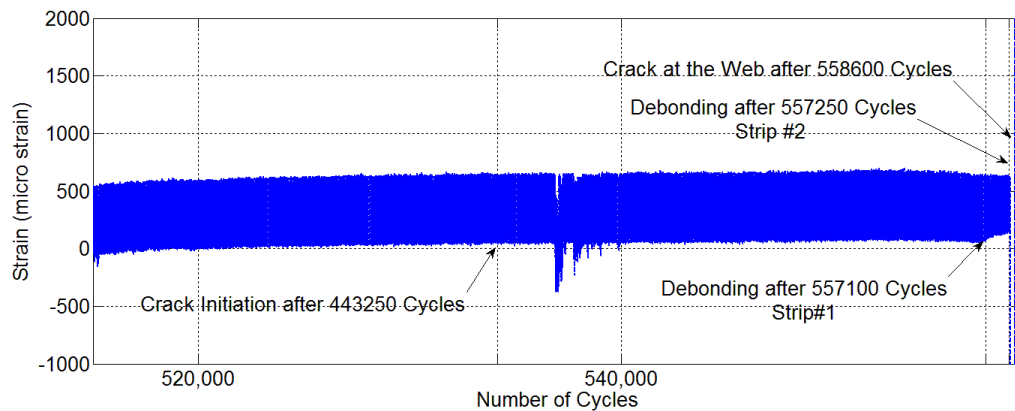




(g) Strain gauge (GB1)



(h) Strain gauge (GB2)



(i) Strain gauge (GB3)

Figure 4.13 (continued). Strains vs. number of cycles for specimen 35%-F-M

The summary of strain changes along the strips is shown in Table 4.11 and illustrated in Figure 4.14 and Figure 4.15. Looking at strain values and strain profiles along the strips, it can be seen that the strain values are generally higher at midspan. After crack initiation, strain values of GS2 and GS3 (at midspan) increases while the other strains were almost constant. Debonding of the CFRP strips caused a sudden increase in strain.

Table 4.11. Summary of strain-life results for the specimen 35%-F-M

Gauge #	Occurrence	Cycle #	% life	$\epsilon$ min ( $\mu\epsilon$ )	$\epsilon$ max ( $\mu\epsilon$ )	$\Delta\epsilon$ ( $\mu\epsilon$ )
GB1 middle of beam	Crack Initiation	443250	79.4	22	505	483
	Debonding Strip#1	557100	99.7	102	575	473
	Debonding Strip#2	557250	99.8	89	555	466
	Fracture	558600	100	795	504	-291
GB2 middle of beam	Crack Initiation	443250	79.4	-12.2	509.143	521
	Debonding Strip#1	557100	99.7	-29	584	613
	Debonding Strip#2	557250	99.8	-44	575	619
	Fracture	558600	100	3037	1539	-1498
GB3 Close to weld toe	Crack Initiation	443250	79.4	51	589	538
	Debonding Strip#1	557100	99.7	90	593	503
	Debonding Strip#2	557250	99.8	105	621	516
	Fracture	558600	100	-	-	1

\* GBs are located on the beam and GSs are located on the strip

\*\* (-) gauge was failed

Table 4.11(continued). Summary of strain-life results for the specimen 35%-F-M

Gauge #	Occurrence	Cycle #	% life	$\epsilon$ min ( $\mu\epsilon$ )	$\epsilon$ max ( $\mu\epsilon$ )	$\Delta\epsilon$ ( $\mu\epsilon$ )
GS1 150 mm from end of strip#1	Crack Initiation	443250	79.4	2837	2989	152
	Debonding Strip#1	557100	99.7	2893	3047	153
	Debonding Strip#2	557250	99.8	2892	3054	161
	Fracture	558600	100	5746	6576	830
GS2 400 mm from end of strip#1	Crack Initiation	443250	79.4	4543	4792	249
	Debonding Strip#1	557100	99.7	4483	4754	272
	Debonding Strip#2	557250	99.8	4528	4777	249
	Fracture	558600	100	-5175	-5175	-
GS3 middle of strip#1	Crack Initiation	443250	79.4	4305	4843	538
	Debonding Strip#1	557100	99.7	4940	5630	690
	Debonding Strip#2	557250	99.8	5178	5964	787
	Fracture	558600	100	-	-	-
GS4 1200 mm from end of strip#1	Crack Initiation	443250	79.4	4462	4595	132
	Debonding Strip#1	557100	99.7	4498	4629	132
	Debonding Strip#2	557250	99.8	4511	4625	114
	Fracture	558600	100	6206	6600	395
GS5 1450 mm from end of strip#1	Crack Initiation	443250	79.4	2212	2367	155
	Debonding Strip#1	557100	99.7	2683	2698	15
	Debonding Strip#2	557250	99.8	2678	2736	58
	Fracture	558600	100	2674	2726	52
GS6 middle of strip#2	Crack Initiation	443250	79.4	4312	4775	463
	Debonding Strip#1	557100	99.7	4586	5156	570
	Debonding Strip#2	557250	99.8	4673	5184	511
	Fracture	558600	100	4615	6208	1593

\* GBs are located on the beam and GSs are located on the strip

\*\* (-) gauge was failed

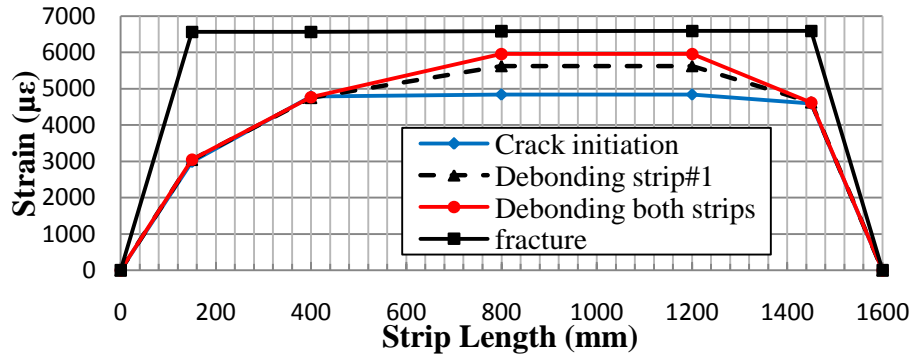


Figure 4.14. Strain variation along the CFRP strip length for specimen 35%-F-M  
( $P_{\max} = 280$  kN)

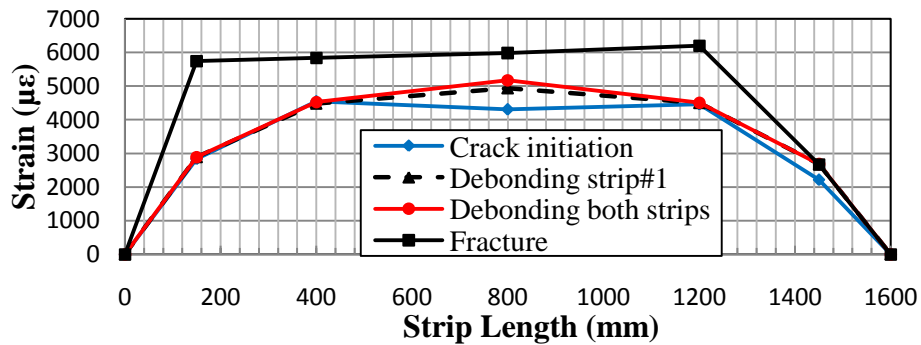


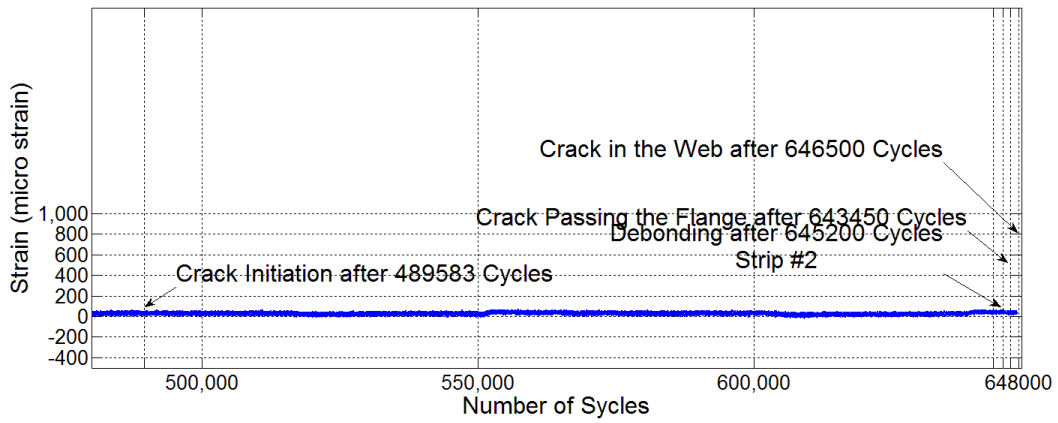
Figure 4.15. Strain variation along the CFRP strip length for specimen 35%-F-M  
( $P_{\min} = 32$  kN)

### 5) Specimen 0%-C-MM

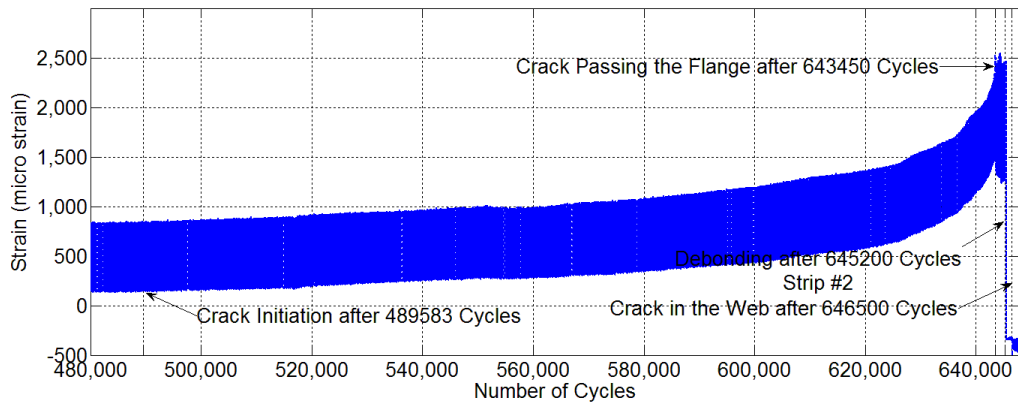
Crack initiation in specimen 0%-C-M was observed after 583842 cycles (90% of life). Debonding of CFRP strip #1 occurred after 645200 cycles (99.8% of fatigue life) when the crack already propagated through the flange. The specimen failed at 646500 cycles.

The strain vs. life data for the gauges on the strips is shown in Figure 4.16. A stable strain variation until specimen failure is observable from Figure 4.16 (a) for the gauges at the end of strips indicating no debonding. The strain values increased gradually for all the gauges located along the CFRP strips (Figure 4.16 (b), (c) and (d)). However the strain ranges

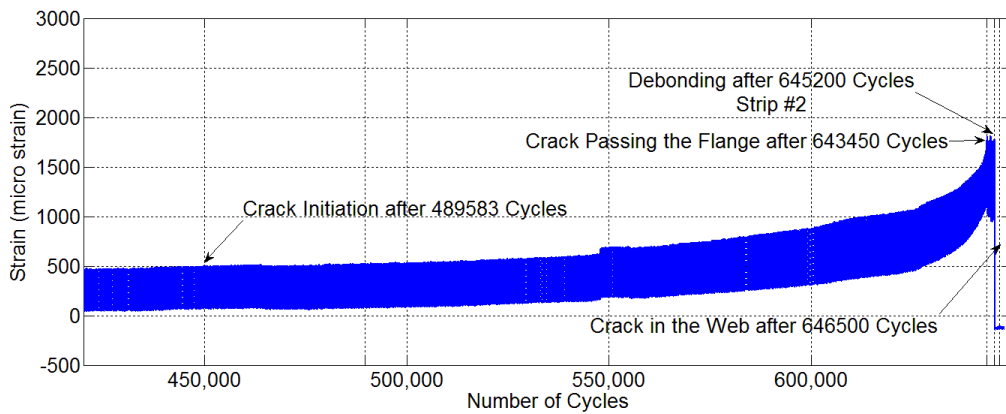
increase more rapidly as the number of cycles increases. Gauges mounted on the beam showed that the strain level at the gauge closest to the crack (Figure 4.16 (f)) increased more than those away from the crack (Figure 4.16 (e)). The strain profile along the CFRP strips is shown in Figure 4.17 and Figure 4.18 for maximum and minimum fatigue load levels. Crack growth into the web and strip debonding was accompanied by a significant increase in strain of the strip prior to failure. A summary of the strain-life results at critical stages for specimen 0%-C-M is given in Table 4.12.



(a) Strain gauge (GS1)

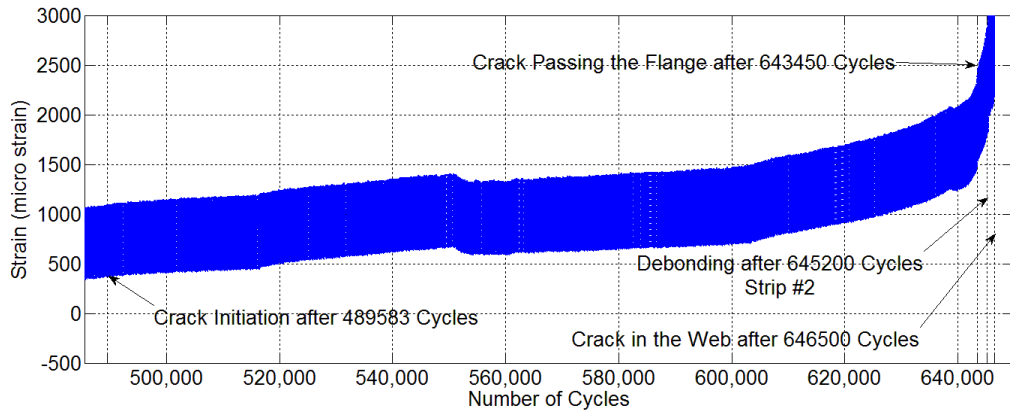


(b) Strain gauge (GS2)

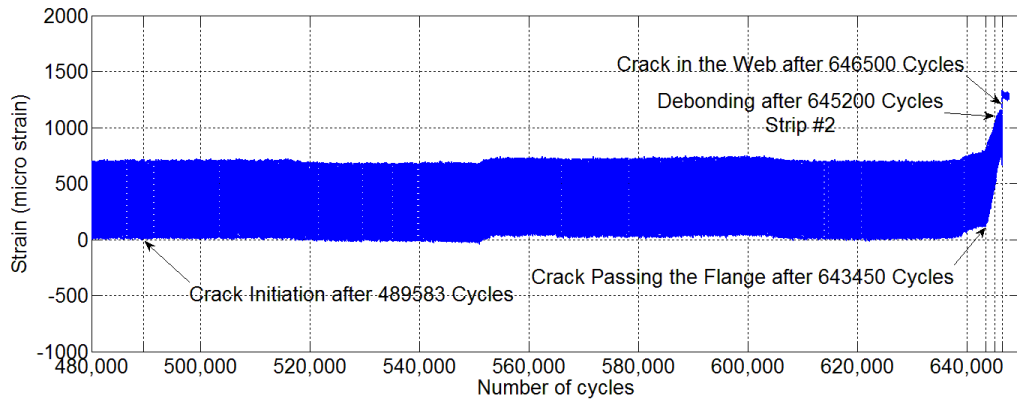


(c) Strain gauge (GS3)

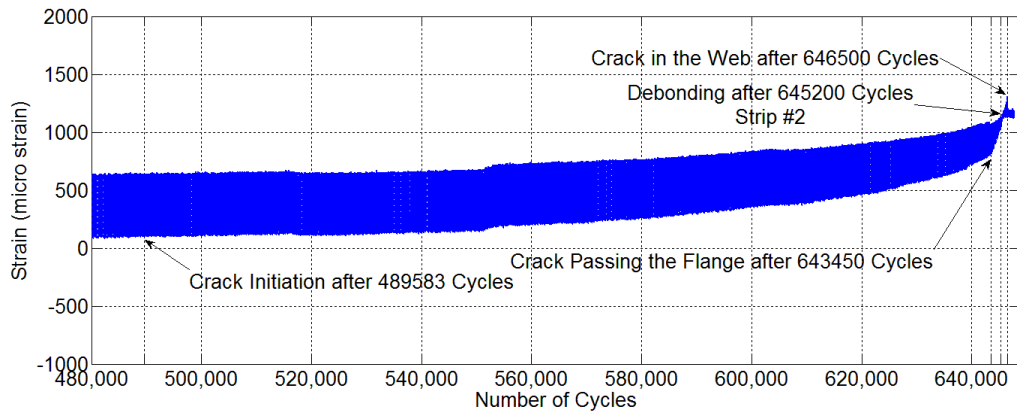
Figure 4.16. Strains vs. number of cycles for specimen 0%-C-M



(d) Strain gauge (GS4)



(e) Strain gauge (GB1)



(f) Strain gauge (GB3)

Figure 4.16 (continued). Strains vs. number of cycles for specimen 0%-C-M

Table 4.12. Summary of strain-life results for the specimen 0%-C-M

Gauge #	Occurrence	Cycle #	% life	$\epsilon$ min ( $\mu\epsilon$ )	$\epsilon$ max ( $\mu\epsilon$ )	$\Delta\epsilon$ ( $\mu\epsilon$ )
GS1 at the end on strip#1	Crack Initiation	583842	90.3	26	43	17
	Crack in the Web	643450	99.5	47	52	5
	Debonding Strip#1	645200	99.8	42	55	13
	Fracture	646500	100	39	42	3
GS2 250 mm for end of strip#1	Crack Initiation	583842	90.3	386	1070	684
	Crack in the Web	643450	99.5	1532	2417	884
	Debonding Strip#1	645200	99.8	1273	2447	1174
	Fracture	646500	100	-	-	-
GS3 500 mm from end of strip#1	Crack Initiation	583842	90.3	254	787	533
	Crack in the Web	643450	99.5	1159	1719	560
	Debonding Strip#1	645200	99.8	986	1765	779
	Fracture	646500	100	-	-	-
GS4 at the middle of strip#1	Crack Initiation	583842	90.3	681	1392	711
	Crack in the Web	643450	99.5	1528	2350	822
	Debonding Strip#1	645200	99.8	1835	2836	1000
	Fracture	646500	100	140702	157760	17058
GB1 at the middle of beam	Crack Initiation	583842	90.3	62	702	640
	Crack in the Web	643450	99.5	137	754	617
	Debonding Strip#1	645200	99.8	508	1031	523
	Fracture	646500	100	675	1084	409
GB3 Close to the weld toe	Crack Initiation	583842	90.3	288	757	469
	Crack in the Web	643450	99.5	822	1044	222
	Debonding Strip#1	645200	99.8	1038	1106	68
	Fracture	646500	100	1177	1283	105

\* GBs are located on the beam and GSs are located on the strip

\*\* (-) gauge was failed



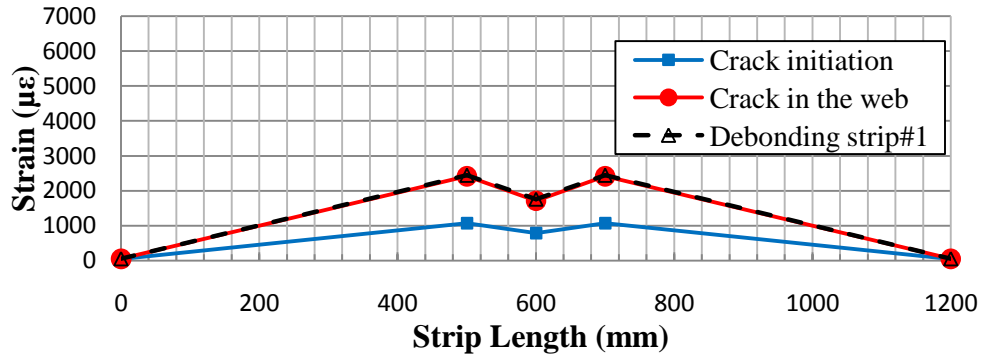


Figure 4.17. Strain variation along the CFRP strip length for specimen 0%-C-M ( $P_{max} = 280$  kN)

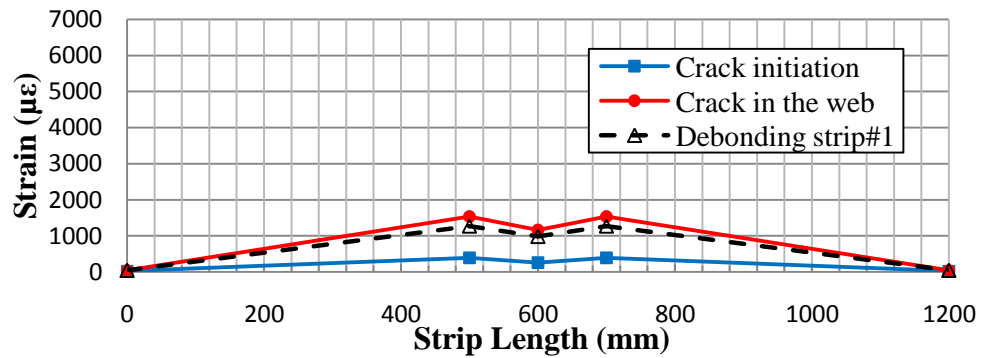


Figure 4.18. Strain variation along the CFRP strip length for specimen 0%-C-M ( $P_{min} = 32$  kN)

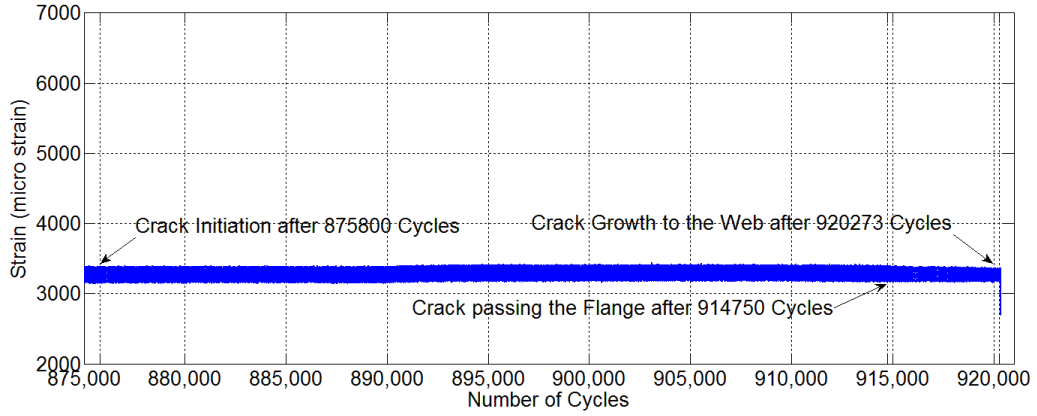
6) Specimen 37%-C-M

Cracking at the weld-toe was initiated after 875800 cycles (95.2% of fatigue life) and grew through the flange thickness to reach the web-flange joint at 914750 cycles (99.4% of fatigue life). The CFRP strip debonding was coincident with failure of specimen after 920273 cycles.

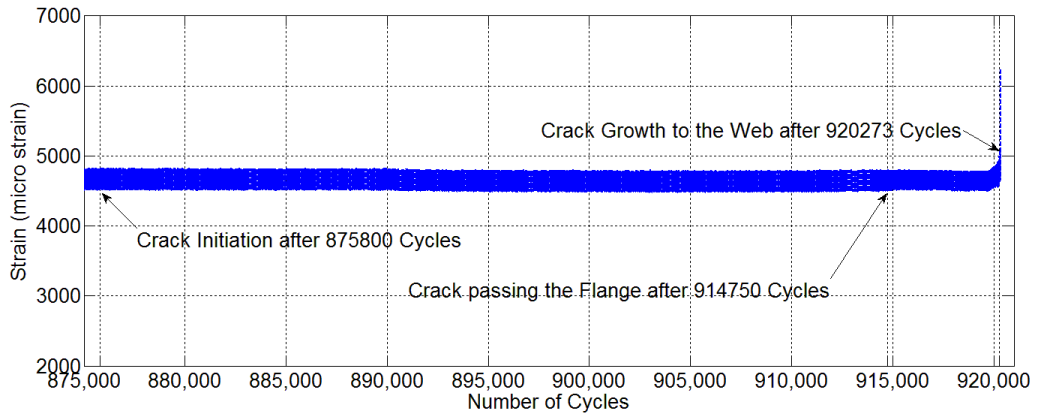
Figure 4.19 shows the strain-life data for all gauges. It is seen that the strain increase the crack growth to the web followed by a sudden drop in strain at the failure for gauges GS 3 and #4 (Figure 4.19 (c) and (d)). An almost constant strain amplitude was measured for GS

#1(Figure 4.19 (a)) indicating no debonding during the test. A strain fluctuation at the end of fatigue life shown in Figure 4.19 (e) indicates debonding at this end (GS5) while the other end is still bonded (GS1).

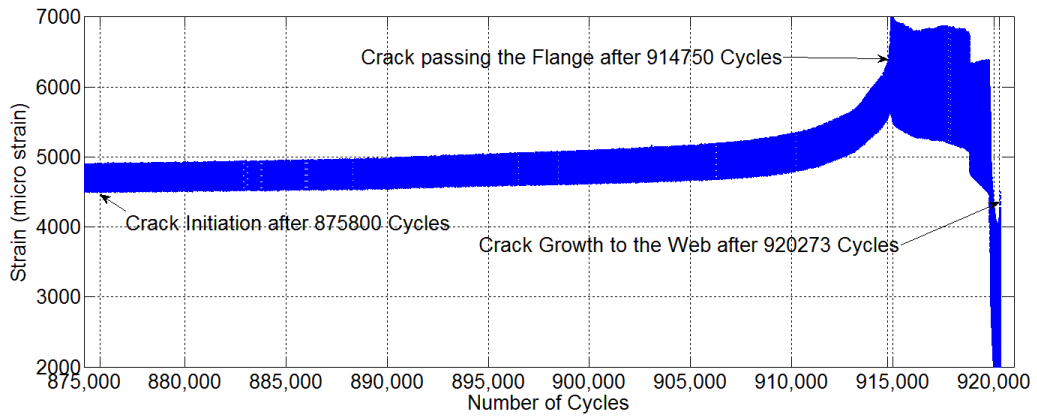
The strain-life data corresponding to critic stages for all specimen 37%-C-M are presented in Table 4.13. The strain profiles along the strips for the maximum and minimum applied loads are shown in Figure 4.20 and Figure 4.21, respectively. These figures show that the strains along the beam length jump as the crack grows into the web and then drops at beam failure.



(a) Strain gauge (GS1)

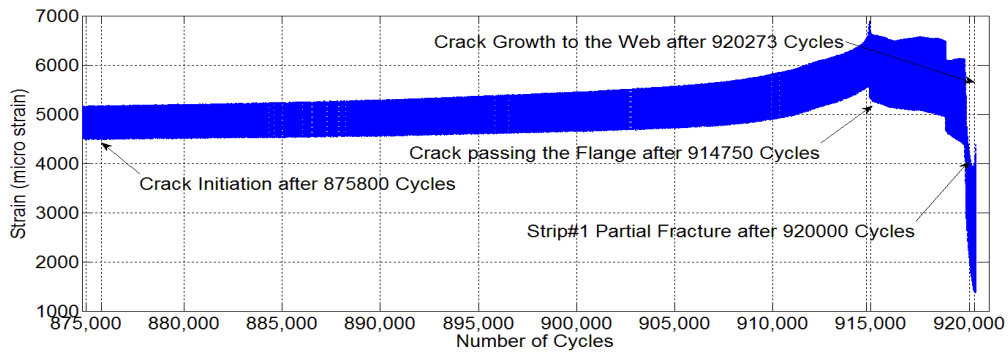


(b) Strain gauge (GS2)

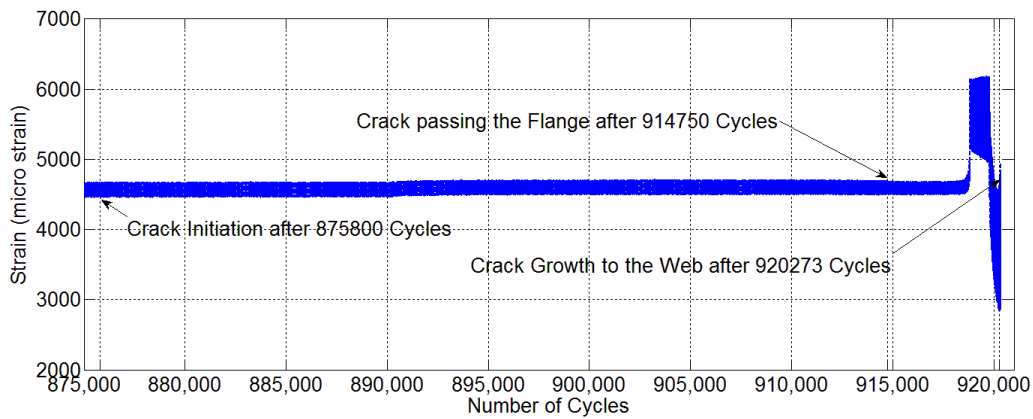


(c) Strain gauge (GS3)

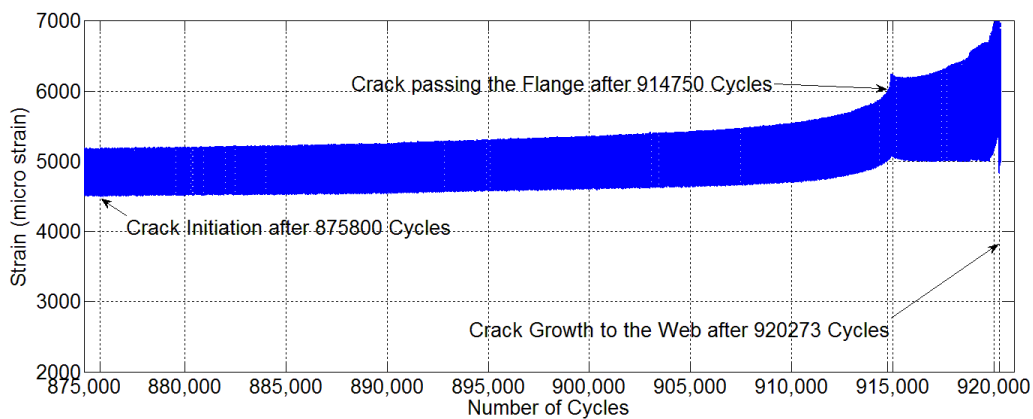
Figure 4.19. Strains vs. number of cycles for specimen 37%-C-M



(d) Strain gauge (GS4)

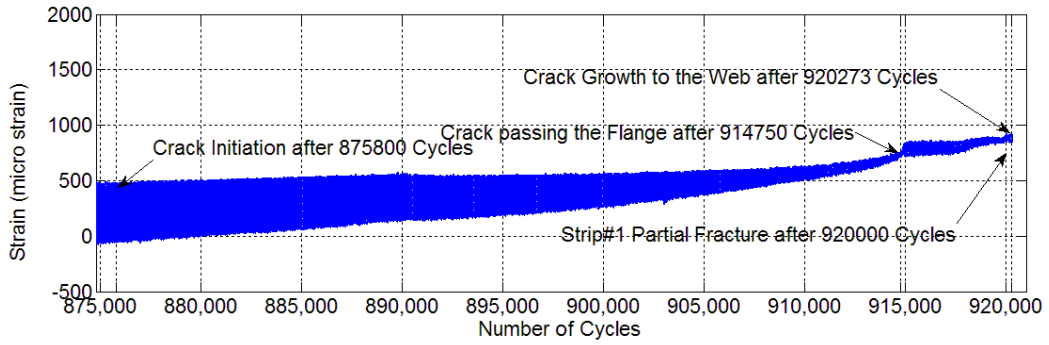


(e) Strain gauge (GS5)

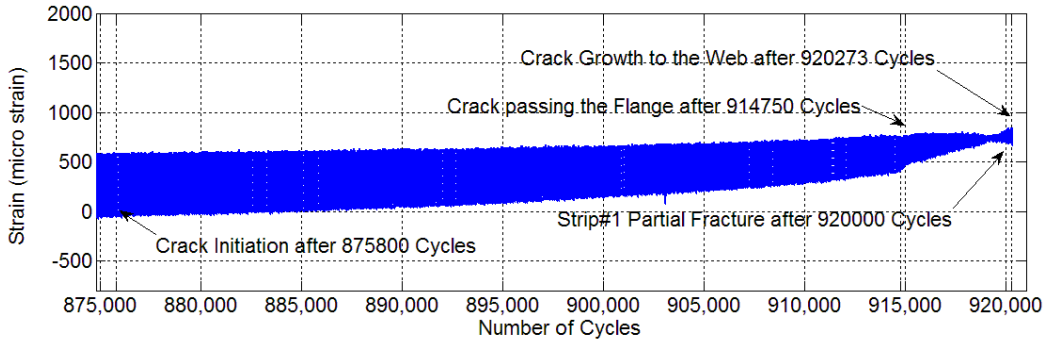


(f) Strain gauge (GS6)

Figure 4.19 (continued). Strains vs. number of cycles for specimen 37%-C-M



(g) Strain gauge (GB1)



(h) Strain gauge (GB3)

Figure 4.19 (continued). Strains vs. number of cycles for specimen 37%-C-M

Table 4.13. Summary of strain-life results for the specimen 37%-C-M

Gauge #	Occurrence	Cycle #	% life	$\epsilon$ min ( $\mu\epsilon$ )	$\epsilon$ max ( $\mu\epsilon$ )	$\Delta\epsilon$ ( $\mu\epsilon$ )
GS1 70 mm from end of strip #1	Crack Initiation	875800	95.2	3154	3383	229
	Crack Growth	914750	99.4	3175	3380	205
	Fracture	920273	100.0	3208	3364	156
GS2 225 mm from end of strip #1	Crack Initiation	875800	95.2	4521	4822	301
	Crack Growth	914750	99.4	4528	4817	289
	Fracture	920273	100.0	4703	5048	345
GS3 485 mm from end of strip #1	Crack Initiation	875800	95.2	4492	4900	408
	Crack Growth	914750	99.4	5579	6346	768
	Fracture	920273	100.0	1137	4259	3122
GS4 at the middle strip #1	Crack Initiation	875800	95.2	4496	5166	671
	Crack Growth	914750	99.4	5552	6514	962
	Fracture	920273	100.0	1391	4170	2779
GS5 1195 mm from end of strip #1	Crack Initiation	875800	95.2	4454	4668	213
	Crack Growth	914750	99.4	4505	4678	173
	Fracture	920273	100.0	2848	4756	1909
GS6 at the middle strip #2	Crack Initiation	875800	95.2	4514	5179	665
	Crack Growth	914750	99.4	5033	5967	934
	Fracture	920273	100.0	5064	6783	1719
GB1 at the middle of beam	Crack Initiation	875800	95.2	-40	473	513
	Crack Growth	914750	99.4	726	734	8
	Fracture	920273	100.0	875	900	25
GB3 Close to the weld toe	Crack Initiation	875800	95.2	-37	570	608
	Crack Growth	914750	99.4	446	735	289
	Fracture	920273	100.0	693	807	114

\* GBs are located on the beam and GSs are located on the strip

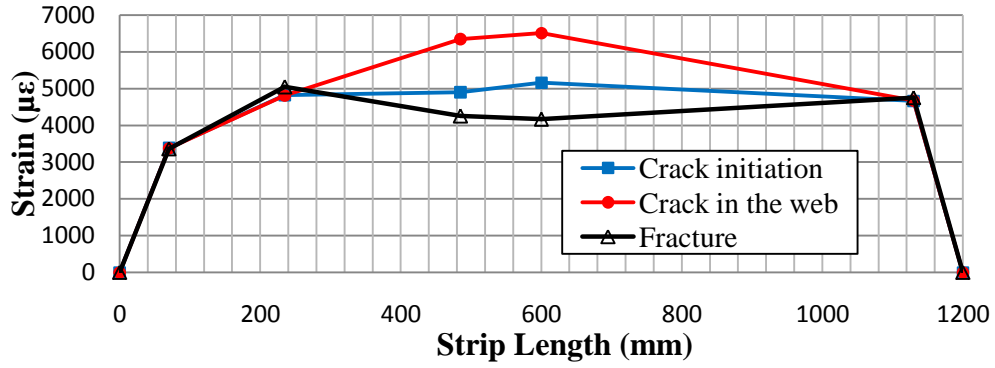


Figure 4.20. Strain variation along the CFRP strip length for specimen 37%-C-M ( $P_{max} = 280$  kN)

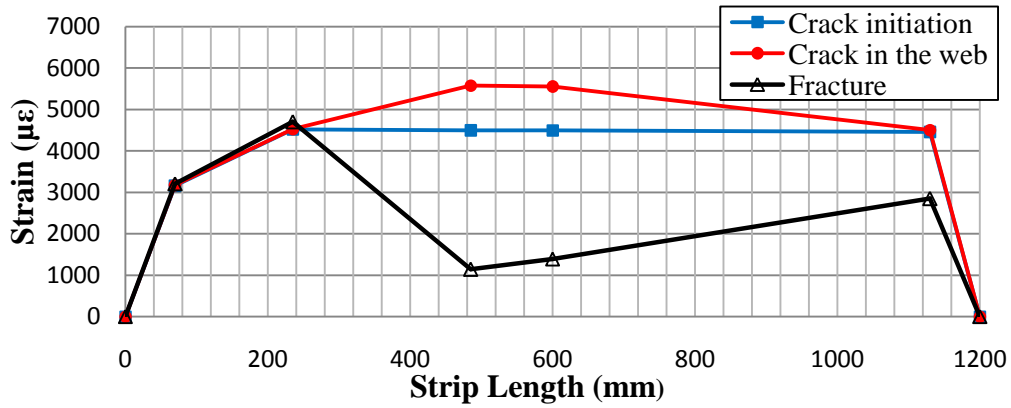


Figure 4.21. Strain variation along the CFRP strip length for specimen 37%-C-M ( $P_{min} = 32$  kN)

#### 4.3.4 Shear Stress-life

The shear stresses transferred through the epoxy during the fatigue tests ( $\tau_f$ ) were calculated using the measured strain range ( $\Delta\varepsilon_f$ ) based on Equation 4.1. The total shear stress ( $\tau_t$ ) was determined as the summation of the shear stress obtained during prestressing ( $\tau_p$ ) and the shear stress during the fatigue test ( $\tau_f$ ).

### 1) Specimen 15%-F-S

The shear stresses along the beam length for specimen 15%-F-S is shown in Table 4.14. GS1 was located at 125 mm from the live end of CFRP strip and the other gauges were located with the distance ( $\Delta x$ ) given in the table from the previous gauge. The total shear stresses were low at the ends compared to midspan confirming good bond between the strip and epoxy except for the location of debonding initiation, GS3-GS4.

Table 4.14. Total shear stress variation along the beam length during prestressing and fatigue testing for specimen 15%-F-S

Location	Occurrence	$\Delta x$ (mm)	$\Delta \varepsilon_f$ ( $\varepsilon$ )	$\tau_p$ (MPa)	$\tau_f$ (MPa)	$\tau_T$ (MPa)
GS1-GS2	Crack Initiation	250	1.0E-04	0.03	0.08	0.11
	Debonding	250	8.2E-05	0.03	0.07	0.10
	Fracture	250	7.1E-04	0.03	0.56	0.59
GS2-GS3	Crack Initiation	400	4.4E-04	0.01	0.22	0.23
	Debonding	400	9.3E-04	0.01	0.46	0.47
	Fracture	400	6.2E-04	0.01	0.31	0.32
GS3-GS4	Crack Initiation	400	4.9E-04	0.01	0.24	0.25
	Debonding	400	8.8E-04	0.01	0.44	0.44
	Fracture	400	3.5E-03	0.01	1.74	1.75
GS4-GS5	Crack Initiation	250	1.7E-04	0.07	0.13	0.20
	Debonding	250	1.8E-04	0.07	0.14	0.21
	Fracture	250	1.9E-04	0.07	0.15	0.22

### 2) Specimen 35%-F-M

The shear stresses transferred through the epoxy along the strip for specimen 35%-F-M are listed in Table 4.16. GS1 was located at 125 mm from the live end of CFRP strip and the other gauges were located with the distance ( $\Delta x$ ) given in the table from the previous gauge. At failure, or specimen fracture, strip#1 was already debonded at GS2-GS3 location; consequently compression (negative) strain values were recorded (Table 4.11). No shear



stress was transferred through the epoxy after strip debonding which is indicated as not available (--) in Table 4.15.

Table 4.15. Total shear stress variation along the beam length during prestressing and fatigue testing for specimen 35%-F-M

Location	Occurrence	$\Delta x$ (mm)	$\Delta \varepsilon_f$ ( $\varepsilon$ )	$\tau_p$ (MPa)	$\tau_f$ (MPa)	$\tau_T$ (MPa)
GS1-GS2	Crack Initiation	250	$1.8 \cdot 10^{-3}$	0.24	2.12	2.36
	Debonding Strip#1	250	$1.7 \cdot 10^{-3}$	0.24	2.01	2.24
	Debonding Strip#2		$1.7 \cdot 10^{-3}$	0.24	2.03	2.26
	Fracture	250	--	0.24	--	--
GS2-GS3	Crack Initiation	400	$5.1 \cdot 10^{-3}$	0.15	0.04	0.19
	Debonding Strip#1	400	$8.8 \cdot 10^{-3}$	0.15	0.64	0.79
	Debonding Strip#2		$1.2 \cdot 10^{-3}$	0.15	0.87	1.02
	Fracture	400	--	0.15	--	--
GS3-GS4	Crack Initiation	400	$2.5 \cdot 10^{-3}$	0.14	0.18	0.33
	Debonding Strip#1	400	$1.0 \cdot 10^{-3}$	0.14	0.74	0.88
	Debonding Strip#2		$1.3 \cdot 10^{-3}$	0.14	0.98	1.13
	Fracture	400	--	0.14	156.	--
GS4-GS5	Crack Initiation	250	$2.2 \cdot 10^{-3}$	2.68	2.62	5.30
	Debonding Strip#1	250	$1.9 \cdot 10^{-3}$	2.68	2.27	4.95
	Debonding Strip#2		$1.9 \cdot 10^{-3}$	2.68	2.22	4.90
	Fracture	250	$3.9 \cdot 10^{-3}$	2.68	4.56	7.23

\* (--) Gauge failed

From Table 4.15, it can be seen that the total shear stress at the middle of the strips was lower in comparison to the shear stress at the strip ends, especially at GS2-GS3 location before beam fracture. A very sudden increase in shear stress at GS3-GS4 location where the strip was partially fractured indicates a reduction in transfer of shear stress through the epoxy as expected.

### 3) Specimen 0%-F-M

The shear stress variations along the strips during fatigue for specimen 0%-F-M are reported in Table 4.16. GS1 was located at the beginning of the CFRP strip (live end) and the other gauges were located with the distance ( $\Delta x$ ) given in the table from the previous gauge. A

very small shear stress difference for the adjacent gauges of GS1-GS2 and GS2-GS3 indicates a good bond along the strip while a higher difference was mainly because of higher stress at GS2-GS3 location (midspan) than GS1-GS2 (end) due to the bending during the fatigue test.

Table 4.16. Shear stress variation along beam length during fatigue test, specimen 0%-F-M

Location	Occurrence	$\Delta\varepsilon_{max}$ ( $\varepsilon$ )	$\Delta x$ (mm)	$\tau_f$ (MPa)
GS1-GS2	Crack Initiation	$1.0 \cdot 10^{-3}$	600	0.50
	Crack in the Web	$2.4 \cdot 10^{-3}$	600	1.16
	Debonding Strip#1	$2.4 \cdot 10^{-3}$	600	1.17
	Fracture	--	600	--
GS2-GS3	Crack Initiation	$2.8 \cdot 10^{-3}$	100	0.83
	Crack in the Web	$7.0 \cdot 10^{-3}$	100	2.05
	Debonding Strip#1	$6.8 \cdot 10^{-3}$	100	2.00
	Fracture	--	100	--

\* (--) Gauge failed

The total shear stress was equal to the shear stress of fatigue test due to unstressed strips.

#### 4) Specimen 37%-C-M

The shear stress variation along the beam length for specimen 37%-C-M is given in Table 4.17. GS1 was located at 125 mm from the CFRP strip end (live end) and the other gauges were located with the distance ( $\Delta x$ ) given in the table from the previous gauge. Considering the shear stress variation in Table 4.17, it can be seen that the lower shear stresses at GS4-GS5 (dead end) in comparison with GS1-GS2 (live end) reveals the effectiveness of the fixed end clamping system application. The lowest transferred shear stress is at the midspan (GS3-GS4) while the highest transferred shear stress is at the end of CFRP strip (GS1-GS2).

However, the other end of CFRP strip did not exhibit the same transferred shear stress (GS4-GS5) where the fixed clamp was mounted, emphasizing the clamping systems effectiveness.

Table 4.17. Total shear stress variation along the beam length during prestressing and fatigue testing for specimen 37%-C-M

Location	Occurrence	$\Delta x$ (mm)	$\Delta \varepsilon_f$ ( $\varepsilon$ )	$\tau_p$ (MPa)	$\tau_f$ (MPa)	$\tau_T$ (MPa)
GS1-GS2	Crack Initiation	165	$1.4 \cdot 10^{-3}$	2.45	2.57	5.02
	Debonding	165	$1.4 \cdot 10^{-3}$	2.45	2.56	5.02
	Fracture	165	$1.7 \cdot 10^{-3}$	2.45	3.00	5.46
GS2-GS3	Crack Initiation	250	$7.8 \cdot 10^{-5}$	0.07	0.09	0.16
	Debonding	250	$1.5 \cdot 10^{-3}$	0.07	1.80	1.87
	Fracture	250	$7.9 \cdot 10^{-4}$	0.07	0.93	1.00
GS3-GS4	Crack Initiation	110	$2.7 \cdot 10^{-4}$	0.08	0.71	0.79
	Debonding	110	$1.7 \cdot 10^{-4}$	0.08	0.45	0.53
	Fracture	110	$8.9 \cdot 10^{-5}$	0.08	0.24	0.32
GS4-GS5	Crack Initiation	600	$5.0 \cdot 10^{-4}$	0.01	0.24	0.25
	Debonding	600	$1.8 \cdot 10^{-3}$	0.01	0.90	0.91
	Fracture	600	$5.9 \cdot 10^{-4}$	0.01	0.29	0.30

#### 4.3.5 Crack Growth and Beam Failure

In general, crack initiation occurred at 80% to 90% of each specimen's fatigue life. The crack initiated at the weld-toe of the cover plate in all cases. Asymmetrical crack propagation along the weld-toe due to unsymmetrical loading was observed for all specimens except for specimen 37%-C-M and specimen 0%-C-M. Cracking was followed by CFRP strip debonding from the beam surface. The strip debonding occurred at the same side as the crack. Beam failure occurred less than 0.5% of fatigue life after CFRP debonding in all cases except specimen 37%-C-M where debonding did not occur until the beam fractured. The location of the bonded CFRP strip had a significant impact on the effectiveness of the reinforcement. In this regard, specimen 37%-C-M experienced the highest fatigue life followed by specimen 0%-C-MM, which had a fatigue life that was higher than the best

result for the prestressed specimens with CFRP strips on the inside of flange. This phenomenon can be explained by considering a few factors, such as the uplifting force applied by the beam bending on the bond. In the case of the CFRP strip on the flange, as the beam tends to bend, a peel stress is applied to the bond as a consequence of this uplifting force, while the beam bending would introduce a negative peel stress (or squeezing stress) for the case of strip on the cover plates. Since the epoxy is a brittle material, it is possible that the applied peel stress accelerates the fatigue failure of the bond. Another possible reason might be the unbounded length of CFRP strip at the critical location, when the CFRP strip is on the cover plates. The peak stress is always near the crack tip, so that for the specimen with CFRP strips on the flange, as the crack reaches the epoxy, a significant local stress is transferred to the epoxy, which tends to break the epoxy and causes debonding as a result. After debonding, the effects of prestressing are diminished and specimen failure accelerated. Because of the unbonded CFRP strip length at the critical location, in the case of the specimens with CFRP strips on the cover plates, the described phenomenon never happens for this reinforcing configuration. Debonding occurred in the strip-to-epoxy interface at the midspan where the crack was initiated. The use of end clamps prevented debonding of the CFRP strips at the beam ends by reducing the local shear and peel stresses. The cracks observed during the fatigue testing were similar for all specimens; however, the amount of fatigue life improvement and the effects of the reinforcement on the failure mode were different. The specific observations for each specimen are presented in the following.

#### 1) Control specimen

The control beam cracked after 376520 (80% of fatigue life) cycles. The deflection rapidly increased as the crack propagated into the flange thickness at 407573 (0.5% of fatigue life)

cycles. The beam failed less than 2000 cycles later (less than 0.5% of the total fatigue life). The crack was initiated at a corner of the cover plate and propagated along the weld. Asymmetrical crack growth along the weld is shown in Figure 4.22. Crack propagation vertically through the web is shown in Figure 4.23.



Figure 4.22. Crack initiation and propagation along the weld for control specimen



Figure 4.23. Crack from the flange to the web of control specimen

## 2) Specimen 14%-F-M

For the specimen 14%-F-M, the crack was initiated at the corner of one cover plate (close to GB1) after 443250 cycles. Elliptical crack propagation through the flange thickness and crack growth across the beam are shown in Figure 4.24 and Figure 4.25. Such asymmetric crack growth maybe due to unsymmetrical loading and unequal prestressing force in the strips. Strip #2 was prestressed to about 14.5% and strip #1 was prestressed to about 13.2% of ultimate strength of the strip. The strip at the same side of the crack location (strip#1) started to debond as the crack was growing. The debonding started at the middle of strip and propagated to the strip ends after 571000 cycles. Following debonding of the strip, the crack propagated into the web and just after 4300 additional cycles (0.7% of fatigue life) failure occurred.

Figure 4.25 illustrates that: (1) the debonding was between the epoxy and the CFRP strip interface and that no debonding occurred between the epoxy and steel surface. (2) An elliptical crack shape was observed. Crack growth in a few cycles from the flange through the web is shown in Figure 4.26. The catastrophic failure shown in Figure 4.26 was the result of crack growth through the web in just 5 cycles.

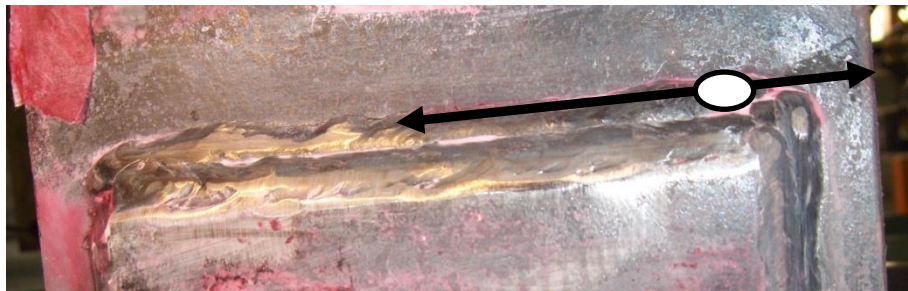


Figure 4.24. The location of crack initiation and the crack length at the point of debonding for specimen 14%-F-M



Figure 4.25. Elliptical crack growth pattern through the thickness of flange and interfacial debonding between epoxy and strips (specimen 14%-F-M)

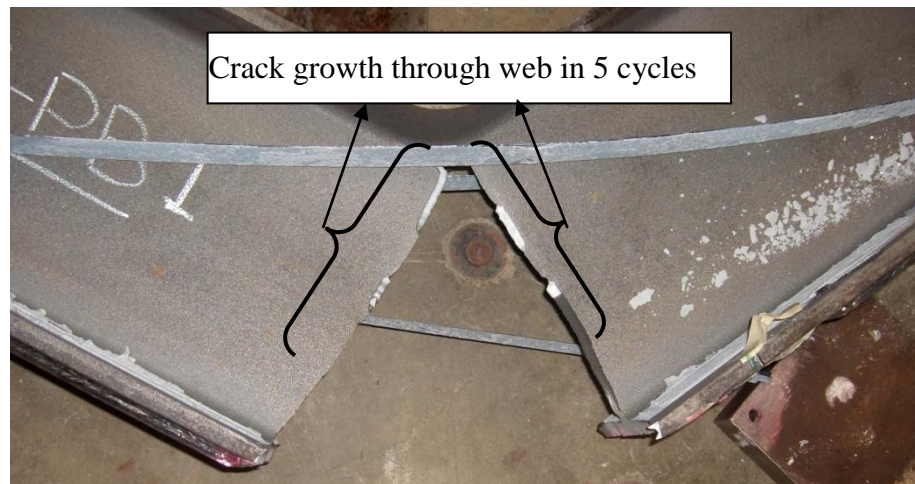


Figure 4.26. Rapid crack growth in few cycles in the web causing a catastrophic failure of specimen 14%-F-M

### 3) Specimen 15%-F-S

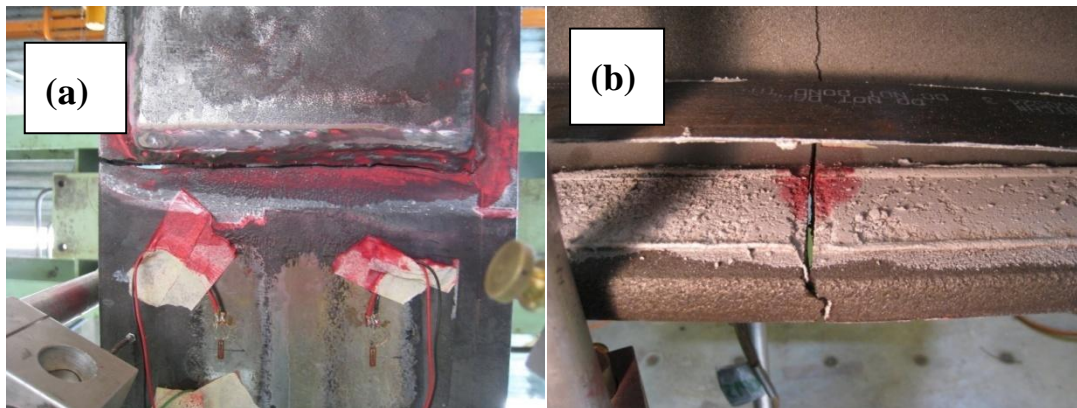
Similar behaviour to specimen 14%-F-M was observed for specimen 15%-F-S but with a lower fatigue life improvement. Using CFRP strips with a lower elastic modulus of elasticity

and premature debonding led to a shorter fatigue life. Asymmetric debonding of strip#1 while strip#2 is still bonded to the flange was observed as shown in Figure 4.27.



Figure 4.27. Debonding of strips for specimen 15%-F-S

Crack growth along the weld and through the flange/web are shown in Figure 4.28(a) and Figure 4.28(b). "Magnaflux dye penetrant" spray was used to make the cracking more visible. Debonding between the strip and epoxy occurred on the same side of the flange where crack initiation was observed. This illustrates the effect of cracking on the observed debonding of the strips.



(a) Asymmetric crack growth along the weld

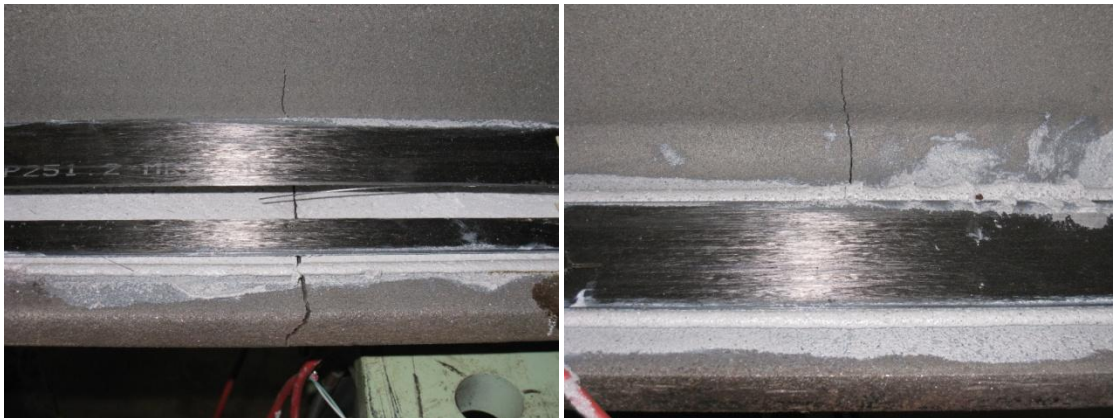
(b) Crack pattern through the Web/Flange

Figure 4.28. Crack growth pattern along the weld and through the flange (specimen 15%-F-S)



4) Specimen 35%-F-M

Specimen 35%-F-M exhibited debonding of both strips within a period of just 150 cycles as shown in Figure 4.29. Strip#1 first started debonding at 557100 cycles followed by the debonding of strip#2 just after 150 cycles later (557250 cycles). At failure, strip#1 was totally debonded and fractured while strip#2 was still bonded at the beam ends. Asymmetrical crack propagation across the flange was also observed, with the crack initiation on the same side of the specimen as strip#1, which was completely fractured.



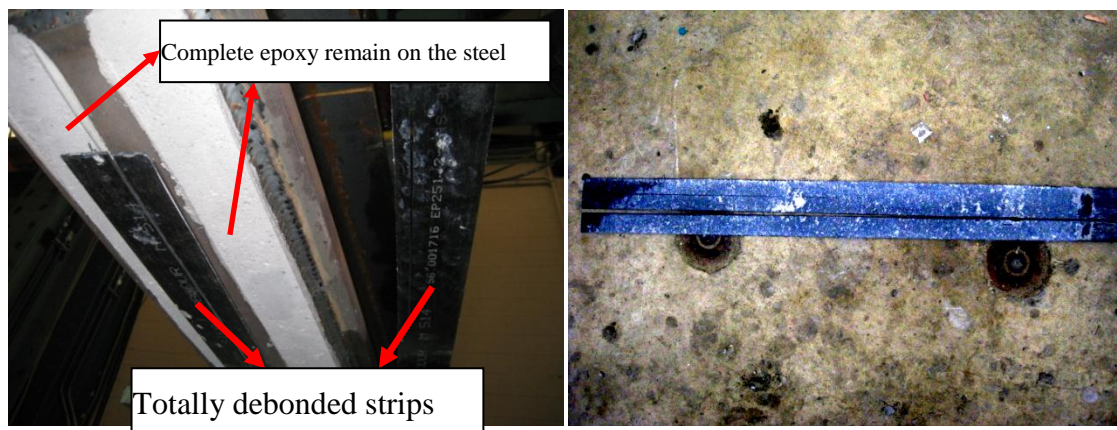
(a) Debonded strip fracture (Strip#1)

(b) Locally debonded Strip#2

Figure 4.29. Crack growth in both sides of the flange (specimen 35%-F-M)

### 5) Specimen 0%-C-M

To investigate the effects of strip location, two additional specimens were reinforced using the strips bonded onto the cover plates; the strips were unstressed (0%-C-M) or prestressed (37%-C-M). In contrast to the previous specimens, the CFRP strip debonding occurred only after crack growth into the web. Looking at Figure 4.30, a pure interfacial debonding between the epoxy and CFRP strips can be seen for the specimen 0%-C-M.



(a) Debonded and fractured strips after failure

(b) Pure debonding between epoxy and strip

Figure 4.30. Debonding of the strips after failure for specimen 0%-C-M

Debonding occurred after the crack reached the web. The crack growth into the web resulted in an increase in deflection and stress amplification at the strip-epoxy interface, which caused the strip debonding to occur. The beam failed at the onset of debonding.

### 6) Specimen 37%-C-M

A fatigue life improvement of 123% over the control beam was achieved for specimen 37%-C-M compared to an improvement of 56% for specimen 0%-C-M, illustrating the significant effect of prestressing on the fatigue life when the CFRP strip is on the cover plate. The

observations during fatigue testing for specimen 37%-C-M were similar to those for specimen 0%-C-M. Symmetrical and uniform crack propagation was observed. No debonding occurred before failure and the strip fracture resulted in beam fracture as shown in Figure 4.31. Figure 4.32, illustrates the effectiveness of the end clamping system in maintaining the CFRP prestress.

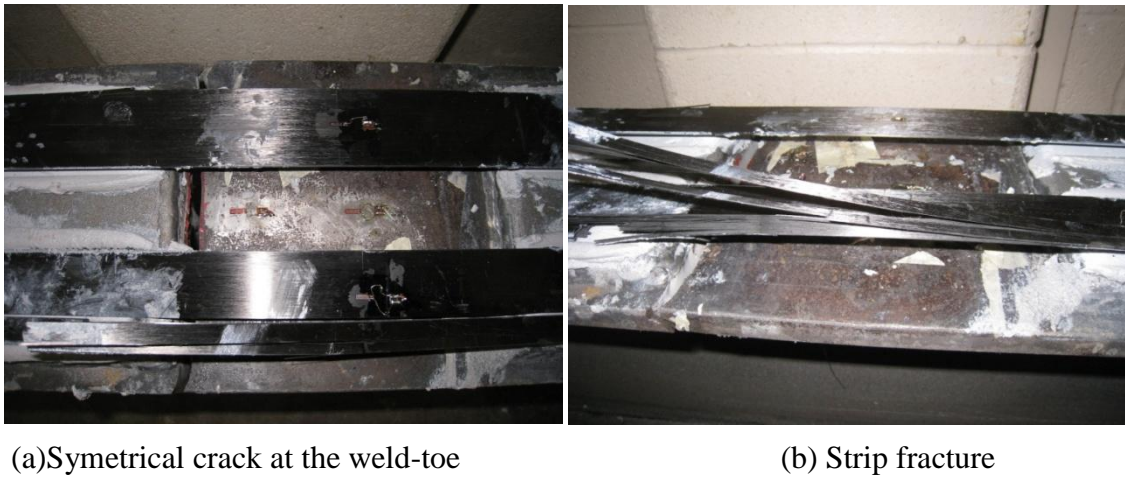


Figure 4.31. Crack growth and strip fracture for specimen 37%-C-M



Figure 4.32. Performance of end clamps after failure for specimen 37%-C-M

#### 4.3.6 Summary

Based on to the fatigue tests results and observations, the following key findings are noted: (1) the strengthening of steel girder using CFRP strips increases the fatigue life. (2) The maximum fatigue life improvement was for the specimen with the prestressed CFRP strips on the cover plates (specimen 37%-C-M with 123.3% fatigue life improvement). (3) The maximum fatigue life improvement in the case of CFRP strips on the flange was only 40.8% (versus 57.8% for the unstressed specimen with CFRP strips on the cover plates), indicating the significant influence of the CFRP strip location. (4) The CFRP strip elastic modulus is important: specimens with higher CFRP elastic modulus exhibited higher fatigue lives. (5) The dominate failure mode was CFRP strip debonding, followed by cracking of the steel. The crack initiated at the weld toe in all cases and grew through the flange thickness towards the web. For specimens with CFRP strips on the flange, debonding eventually occurred, while no debonding was observed prior to web cracking for the specimens with CFRP strips on the cover plates.

## **Chapter 5: Analytical and Numerical Modelling**

### **5.1 Introduction**

This chapter presents analytical and numerical models developed to predict the behaviour of W section steel girders with welded cover plate fatigue details reinforced using bonded stressed and unstressed CFRP strips. In Sections 5.2 and 5.3, analyses of the strains through the cross section after prestressing and under the imposed flexural load are performed, based on the concepts of strain compatibility and force equilibrium. In Section 5.4, stress distributions along the path of the fatigue crack are predicted using linear elastic finite element analysis (FEA) methods. Both approaches are validated by comparison with the available test data. As discussed in Chapter 4, varying the bonded strip location and CFRP elastic modulus among the test specimens resulted in gains in the fatigue life improvement that did not correlate well with the prestressing level in all cases. This led to difficulties in experimentally assessing the effect of the level of prestressing. As such, the models presented in this chapter are useful for examining and uncoupling the three parameters studied; namely, the level of prestressing, the location of applied strips, and the CFRP elastic modulus. Analytical and numerical studies of the bond behaviour and stress transfer through the epoxy are also discussed in this chapter, in Sections 5.5 and 5.6, respectively.

### **5.2 Static Analysis of Prestressed Cross Section (before Flexural Loading)**

To investigate the effects of the prestressed CFRP strips bonded to the steel beam, a static analysis was first carried out, based on the work of Al-Saidy et al. (2004) and Täljsten et al. (2008).

The calculated strain variations in the steel beams and CFRP strips and the deflection induced by prestressing were then compared with the experimental data.

### *5.2.1 Analysis Description*

The stress / strain distributions and specimen deflections were determined using strain compatibility / force equilibrium and load balancing analysis, respectively.

#### *5.2.1.1 Evaluation of Cross-Section Strain/Stress*

A static analysis based on the concepts of elastic strain compatibility and force equilibrium of steel beams reinforced using bonded CFRP strips is shown in Figure 5.1 and Figure 5.2. For this analysis, linear elastic behaviour was assumed and the self weight was considered.

This approach was employed herein to investigate the stress and strain changes in the specimen cross section after releasing the prestressing force to the beam. The assumed material properties of the CFRP and steel were as described in Chapter 3 and shown in Figure 3.1 and Figure 3.2. Two locations along the beam length were considered, the midspan ( $x = L/2$ ) and one of the quarter points ( $x = L/4$ ) where the cover plate is present. The section was analyzed by conducting a layer by layer analysis. The number of elements in such an analysis is not critical, if linear elastic material behaviour is assumed. Hence, the cross section was divided into 20 elements for reasons of convenience to determine the strain at the locations of interests such as the bottom flange and CFRP strip surfaces. The analysis was done for the time of load release (i.e. just after the prestressing force was transferred to

the beam). Consequently, the calculated stress and strain distributions in the steel beam were due to the transferred prestressing force, while the calculated stresses and strains in the strips were actually losses of prestressing force resulting from the deflection of the beam (elastic shortening). The deformation of the epoxy was neglected by assuming a perfect bond between the CFRP strips and the steel beam.

The bottom and top stresses produced by the eccentric prestressing force were calculated using Eq. (5.1) and Eq. (5.2).

$$\sigma_{bottom} = \frac{P}{A} + \frac{P \cdot e}{S_b} - \frac{M}{S_b} \quad (5.1)$$

$$\sigma_{top} = \frac{P}{A} + \frac{P \cdot e}{S_t} + \frac{M}{S_t} \quad (5.2)$$

where A is the cross sectional area of the steel and  $S_t$  and  $S_b$  are the section moduli of the steel with respect to the top and bottom extreme fibres, respectively. Since no external moment was imposed during the prestressing process, the external moments,  $\frac{M}{S_b}$  and  $\frac{M}{S_t}$ , only include moments due to the beam self weight. To do this, the beam self weight, W, is used to calculate the associated moment, M, where  $M = \frac{W \cdot L^2}{8}$  at midspan ( $x = L/2$ ) and

$M = \frac{3 \cdot W \cdot L^2}{32}$  at quarter length of the beam ( $x = L/4$ ). The stresses at any location in the cross section and the corresponding strains can be determined using the obtained bottom and top stresses to facilitate comparison with the experimental results using the equation of  $\varepsilon = \frac{\sigma}{E}$ , where E is the elastic modulus of material. The geometric properties of sections for

all specimens at the midspan ( $x = L/2$ ) and one of the quarter points ( $x = L/4$ ) are tabulated in Appendix C, along with a sample calculation in Excel.

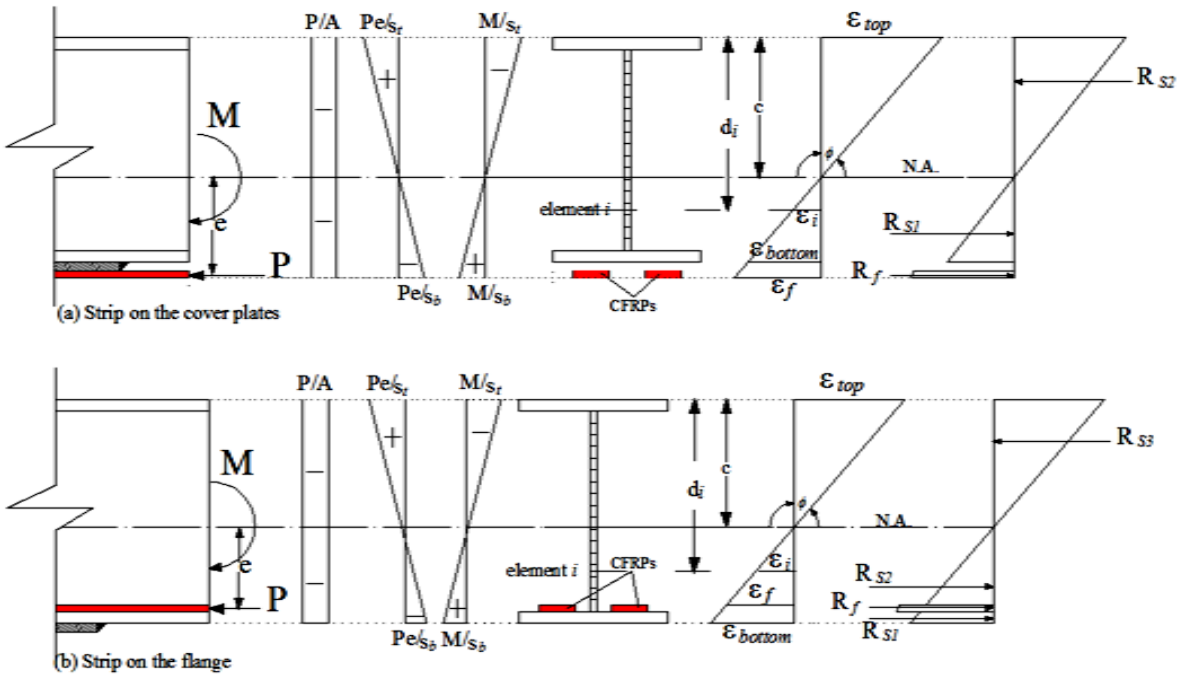


Figure 5.1. Cross section analysis at  $x = L/2$  (midspan)

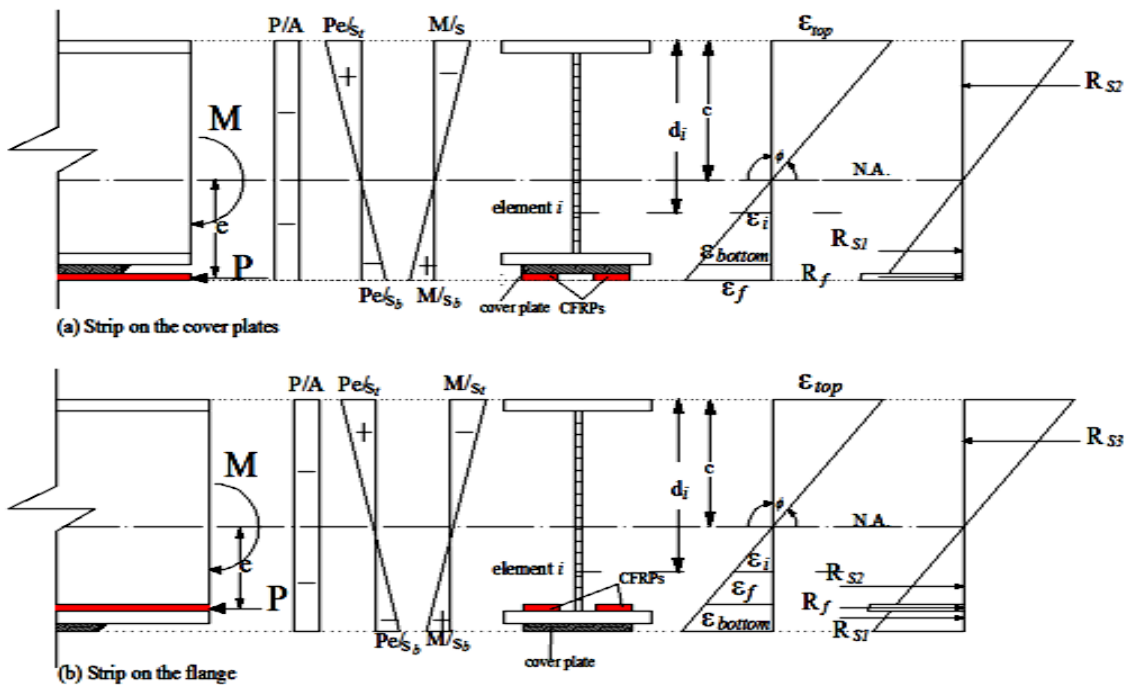


Figure 5.2. Cross section analysis at  $x = L/4$  (quarter point)



### 5.2.1.2 Prestressing Camber Calculation

The camber during prestressing was analytically calculated based on static analysis of a deformed beam, as shown in Figure 5.3. Since the CFRP strips were not bonded all along the beams, the actual location of the prestressing force was not exactly at the end of the beam. However due to the low prestressing force compared to the size of the beam, the camber tends to be very small, as will be shown later. Consequently, a uniform cross-section subjected to an eccentric prestressing force was assumed, as shown in Figure 5.3. The camber was then calculated based on the following equation.

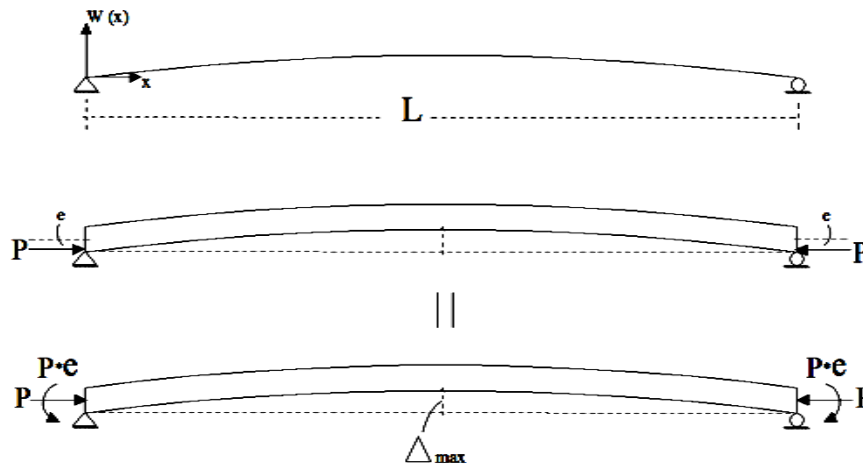


Figure 5.3. Deflection produced by prestressing force

Deflection along the beam corresponding to the prestressing force associated with the eccentricity ( $e$ ) can be calculated as follows:

$$W(x) = \frac{P \cdot e}{2 \cdot E \cdot I_{(x)}} \cdot x^2 - \frac{P \cdot e \cdot L}{2 \cdot E \cdot I_{(x)}} \cdot x \quad (5.3)$$

where  $E = 200$  GPa and the moment inertia of section  $I_{(x)}$  varies along the beam length due to the presence of the cover plates and CFRP strips. The maximum deflection (camber) at the midspan can be calculated as follows:

$$\Delta_{\max} = \frac{-P \cdot e \cdot L^2}{8 \cdot E \cdot I} \quad (5.4)$$

To account for the self weight effect on the camber, Eq. (5.5) was used to determine the positive deflection of the beam due to self weight shown in Figure 5.4

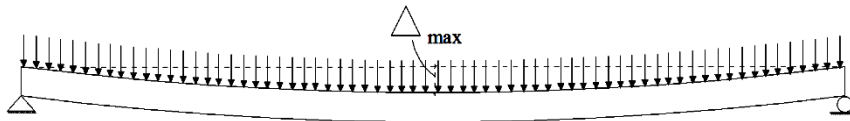


Figure 5.4. Deflection due to self weight

$$\Delta_{\max} = \frac{5 \cdot w \cdot L^4}{384 \cdot E \cdot I} \quad (5.5)$$

The net camber during prestressing, accounting for self weight, was then calculated based on the summation of Eq. (5.4) and Eq. (5.5)

Since the camber during prestressing was not measured directly, the recorded strain at the midspan of the beams was used to determine the produced camber, including the self weight effect, derived according to elastic strain analysis, as illustrated in Figure 5.1. From Figure

5.1, it can be identified that  $\phi = \frac{\varepsilon_{bottom}}{h-c}$ , where the curvature ( $\frac{1}{\rho}$ ) is equal to  $\phi$ . The

maximum camber at the midspan ( $\Delta$ ) shown in Figure 5.4 can be calculated using Eq. (5.5).

$$\Delta = r - \frac{\sqrt{4 \cdot r^2 - L^2}}{2} \quad (5.5)$$

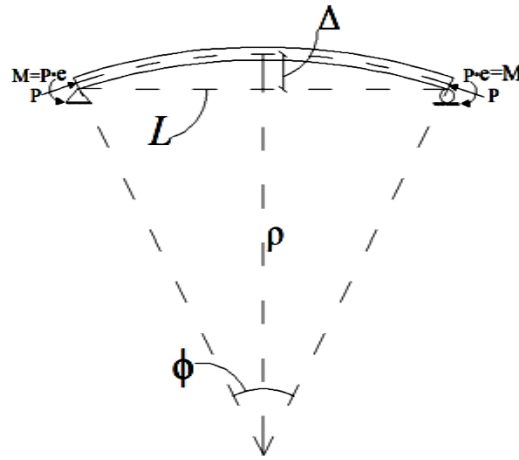


Figure 5.5. Bent beam from which relation for elastic curve is obtained

### 5.2.2 Comparison of Predicted and Measured Strain and Deflection

The change in strain due to release of the prestressing force to the steel beam after epoxy curing represents the prestress strain transferred to the epoxy. These strains can be calculated based on Eq. (5.1) and Eq. (5.2). Since the maximum deflection (camber) was at the middle of the beam, the strip strain changes at midspan location (GS3) were higher than that at the quarter point (GS1), as shown in Table 5.1. Actually, at release, the strains near the ends of the CFRP strips primarily decrease due to force transfer over the transfer length, and to a lesser degree, due to elastic shortening of the beam. Outside of the transfer length (i.e. at the midspan), the strains in the CFRP strip are reduced at release due to elastic shortening and camber of the beam. This latter condition is considered a form of prestress loss. At release,

the change in strain in the steel results from the fact that the prestress is now transferred to the beam through shear in the epoxy rather than through the prestressing hardware. Since the prestress in the CFRP strips is reduced due to elastic shortening, the steel beam strains are also affected by elastic shortening.

Table 5.1. Analytically and experimental change in strain after prestressing release

P (kN)	Specimen	Analytical			Experimental		
		$\Delta\varepsilon(\mu\varepsilon)$ GB1*	$\Delta\varepsilon(\mu\varepsilon)$ GS3**	$\Delta\varepsilon(\mu\varepsilon)$ GS1	$\Delta\varepsilon(\mu\varepsilon)$ GB1	$\Delta\varepsilon(\mu\varepsilon)$ GS3	$\Delta\varepsilon(\mu\varepsilon)$ GS1
23.0	15%-F-S	-25	-26	-17	-34	-15	-54
23.2	14%-F-M	-25	-21	-13	-72	-8	-76
62.6	35%-F-M	-70	-58	-37	-51	-80	-2143
65.3	37%-C-M	-79	-83	-58	-125	-19	-1058

\*GB1 is a strain gauge located on the beam

\*\*GS1 and GS3 are strain gauges located on the CFRP strips

Comparing the change in strains in the beam and CFRP strip at the midspan (gauges GB1 and GS3), the general trends appear to be captured reasonably well by the analysis. Since the experimental strains for specimens 35%-F-M and 37%-C-M were recorded within the transfer length, a large strain change was observed. The experimental change in strains during load release were expected to be slightly lower, due to the self supporting system used for prestressing procedure. Using this system, some of the prestressing strain is already transferred to the beams through the support reactions, prior to releasing the prestressing strips. In addition, it is possible that some of the strain may have been absorbed by the epoxy deformation.

Comparing the strains in Table 5.1, two results stand out for which the comparison between the analytical and experimental strains is particularly poor. Under the higher prestressing

forces (35-37%), there is a huge difference in the prestressing strain losses in the CFRP strip ends (gauge GS1). The analytical equation assumes perfect bond between strip and beam; hence, the calculated change in strains are significantly lower than the experimental strain losses

The beam camber was calculated using static analysis of the cross-section (section 5.2.1.2) for all prestressed specimens as tabulated in Table 5.2. The beam camber during prestressing was calculated based on measured strains at the midspan as given in Table 5.3.

Table 5.2. Prestressing camber calculation based on static analysis

Specimen	P (kN)	e (mm)	I (mm <sup>4</sup> ) × 10 <sup>6</sup>	W (kN/m)	$\Delta_{prestressing}$ (mm)	$\Delta_{self\ weight}$ (mm)	$\Delta_{total}$ (mm)
15%-F-S	23.0	135	$1.66 \times 10^8$	0.727	-0.052	-0.045	-0.047
14%-F-M	23.2	134	$1.67 \times 10^8$	0.727	-0.049	-0.045	-0.046
35%-F-M	62.6	134	$1.67 \times 10^8$	0.727	-0.126	-0.045	-0.121
37%-C-M	65.3	167	$1.68 \times 10^8$	0.727	-0.162	-0.045	-0.158

Table 5.3. Prestressing camber calculation based on measured strains

Specimen	$\epsilon$ ( $\mu\epsilon$ )	$\rho$ (mm)	$\Delta_{max}$ (mm)
15%-F-S	17	9.0E+06	-0.054
14%-F-M	15	9.9E+06	-0.050
35%-F-M	27	5.7 E+06	-0.087
37%-C-M	38	4.4 E+06	-0.113

Comparing Table 5.2 and Table 5.3, the maximum camber occurs in specimen 37%-C-M. It can be seen that the experimental and calculated cambers are generally in good agreement. The differences in the analytical and experimental cambers are mainly due to assuming a

perfect bond between the CFRP strip and beam. The prestressing camber is generally small and barely visible indicating very minor effect of prestressing on the specimens stiffness.

### 5.3 Static Analysis of the Bending Test

#### 5.3.1 Analysis Description

The beam specimens in this study were tested in four point bending under nominal load cycles ranging from 28 kN to 280 kN. The test scheme and the static analysis formulations required for further considerations are shown in Figure 5.5.

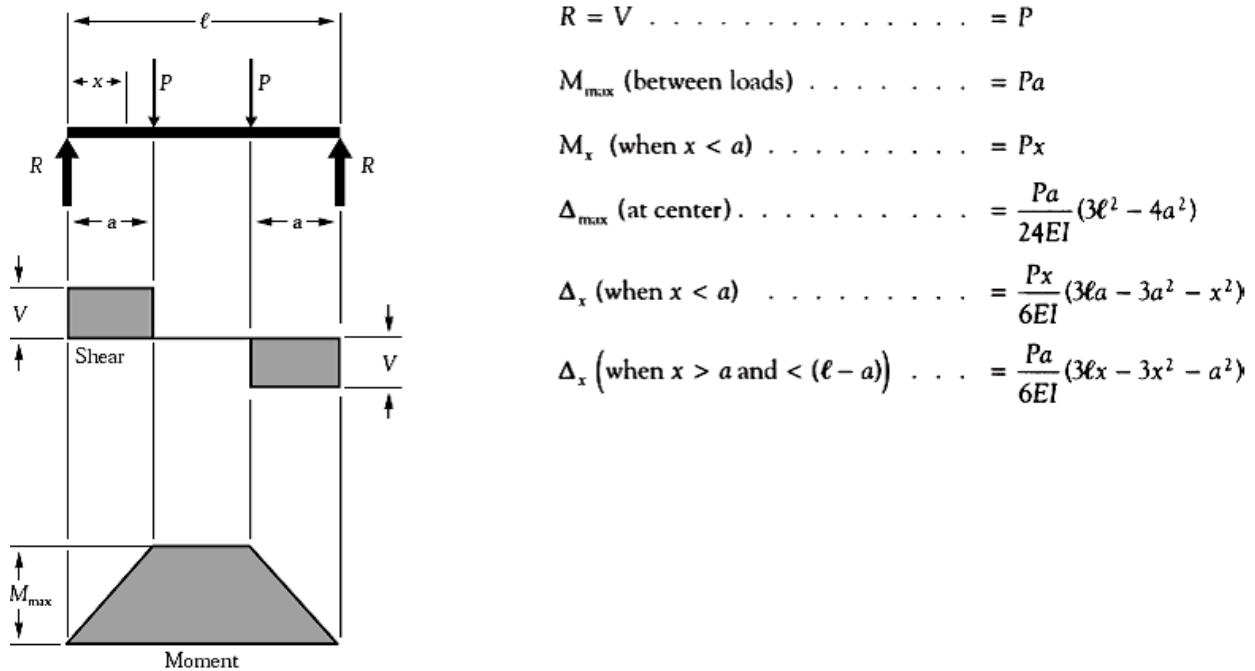


Figure 5.6. Fatigue test scheme and formulations (NDS, 2005)

In Figure 5.6,  $L$  (or  $\ell$ ) = 2000 mm,  $a$  = 800 mm,  $P_{\min}$  = 16 kN,  $P_{\max}$  = 140 kN,  $E$  (steel) = 200000 MPa and the other properties vary with the strengthening configuration.

The same concepts of static analysis described in Section 5.2.1 based on strain evaluation were employed to assess the behaviour of the specimens during the flexural fatigue loading, except that in this case, the external applied loads, including the prestressing force and vertical load, were considered. This approach was validated using strain data obtained prior to the initiation of fatigue cracking. Once the bottom and top fibre stresses are obtained, the stresses and corresponding strains at any other location can be determined for comparison with the test data.

### *5.3.2 Comparison of Predicted and Measured Strain and Deflection*

The stresses and strains due to prestressing, prestressing loss, and bending moments during fatigue testing were determined using Eq. (5.1) and Eq. (5.2). The total strains are then calculated by summing the strains from each stage (Table 5.4). The strains values for the prestressing stage were calculated based on the stress strain relation,  $\varepsilon = \frac{\sigma}{E_{cfp}}$ . The strains produced by the applied bending load were calculated using Eq. (5.1) and Eq. (5.2) with the prestressing force,  $P$ , taken as zero. Losses and transferred strains are taken from Table 5.1.

The measured total strain recorded during fatigue flexural loading are given in Table 5.5.

Table 5.4. Calculated strains under flexural loading

Prestressing	x = L/2 (midspan)				x = L/4	
Specimen	$\varepsilon(\mu\varepsilon)$ -GB1		$\varepsilon(\mu\varepsilon)$ -GS3		$\varepsilon(\mu\varepsilon)$ -GS1	
Control	0		0		0	
15%-F-S	0		2329		2271	
14%-F-M	0		1664		1625	
35%-F-M	0		4284		2824	
0%-C-M	0		0		0	
37%-C-M	0		4443		3124	
Applied load	x = L/2 (midspan)				x = L/4	
	$M_{max}$		$M_{min}$		$M_{max}$	$M_{min}$
Specimen	$\varepsilon(\mu\varepsilon)$ -GB1	$\varepsilon(\mu\varepsilon)$ -GS3	$\varepsilon(\mu\varepsilon)$ -GB1	$\varepsilon(\mu\varepsilon)$ -GS3	$\varepsilon(\mu\varepsilon)$ -GS1	$\varepsilon(\mu\varepsilon)$ -GS1
Control	530	0	62	0	0	0
15%-F-S	519	548	61	64	372	43
14%-F-M	514	426	75	62	290	34
35%-F-M	514	426	75	62	290	34
0%-C-M	509	534	74	78	382	53
37%-C-M	509	534	74	78	382	53
Losses & Transferred	x = L/2 (midspan)				x = L/4	
Specimen	$\varepsilon(\mu\varepsilon)$ -GB1		$\varepsilon(\mu\varepsilon)$ -GS3		$\varepsilon(\mu\varepsilon)$ -GS1	
Control	0		0		0	
15%-F-S	-25		-26		-17	
14%-F-M	-25		-21		-13	
35%-F-M	-70		-58		-37	
0%-C-M	0		0		0	
37%-C-M	-79		-83		-58	
Total Strains	x = L/2 (midspan)				x = L/4	
	$M_{max}$		$M_{min}$		$M_{max}$	$M_{min}$
Specimen	$\varepsilon(\mu\varepsilon)$ -GB1	$\varepsilon(\mu\varepsilon)$ -GS3	$\varepsilon(\mu\varepsilon)$ -GB1	$\varepsilon(\mu\varepsilon)$ -GS3	$\varepsilon(\mu\varepsilon)$ -GS1	$\varepsilon(\mu\varepsilon)$ -GS1
Control	530	0	62	0	0	0
15%-F-S	494	2851	36	2367	2626	2297
14%-F-M	489	2069	50	1705	1902	1646
35%-F-M	444	4652	5	4288	3077	2821
0%-C-M	509	534	74	78	382	53
37%-C-M	430	4894	-5	4438	3448	3119

\*GB is the strain gauge located on the beam

\*\* GS is the strain gauge located on the CFRP strip



Table 5.5. Measured total strains under flexural loading

Total Strains	x = L/2 (midspan)				x = L/4	
	M <sub>max</sub>		M <sub>min</sub>		M <sub>max</sub>	M <sub>min</sub>
Specimen	ε(μϵ)-GB1	ε(μϵ)-GS3	ε(μϵ)-GB1	ε(μϵ)-GS3	ε(μϵ)-GB1	ε(μϵ)-GS3
Control	542	0	89	0	0	0
15%-F-S	488	2792	23	2386	2455	2290
14%-F-M	454	2115	-14	1716	-	-
35%-F-M	462	4727	7	4330	3060	2854
0%-C-M	525	581	28	66	358	41
37%-C-M	361	4976	-75	4503	3357	3152

\*GB is the strain gauge located on the beam

\*\* GS is the strain gauge located on the CFRP strip

\*\*\*(-) Failed gauge

In general, the calculated and measured total strains in Tables 5.4 and 5.5 compare well. The strain values are close in magnitude, and the trends are similar. The tensile stresses in the beam decrease as the level of prestressing increases. Specimen 37%-C-M, which had the highest prestressing level, experienced the lowest bending strains (GB1) at the midspan. The deflection ranges for  $\Delta P = 248$  kN at the midspan during the fatigue tests were calculated

including the self weight ( $\Delta_{max} = \frac{5 \cdot w \cdot L^4}{384 \cdot E \cdot I_{transferred}} + \frac{F \cdot a}{24 \cdot E \cdot I_{transferred}} \cdot (3 \cdot L^2 - 4 \cdot a^2)$ ) and are

given in Table 5.6. In general, the measured and predicted deflection ranges compare well. The predicted deflections were systematically slightly greater than the measured deflections. A possible explanation for this is that the pin and roller restraints used in the actual tests provided more restraint than assumed in the analysis.

Table 5.6. Analytical and experimental deflections

Specimen	Deflection Range (mm)	
	Measured	Predicted
Control	1.178	1.194
15%-F-S	1.104	1.173
14%-F-M	1.063	1.180
35%-F-M	1.066	1.173
0%-C-M	0.838	1.165
37%-C-M	0.695	1.165

#### 5.4 Bond Behaviour and Analytical Solutions for Shear Stress Distributions

Due to practical difficulties, strains were not recorded during prestressing at the end of the strips. Based on the observations and experienced debonding during prestressing, a proper end clamp configuration was found to be essential to control the shear and peel stresses and mitigate debonding at that location. In this section, a debonding analysis is presented to explain the observed behaviour. In Section 5.6, the results of this analysis are compared with similar FEA results. Täljsten et al. (2008) modified an approach to calculate shear and peel stresses based on the work of Hart-Smith (1973) and Albat et al. (1999). The shear stress in the adhesive is defined by Eq. (5.7).

$$\tau = G_a \cdot \gamma \quad (5.7)$$

where  $G_a$  is the shear modulus of adhesive and  $\gamma$  is the shear strain.

For a given single lap joint (see Figure 5.7), modelled as the end of a CFRP strip bonded to a steel surface, where the prestressing force is introduced as a tension force,  $T$ , the shear strain,  $\gamma$ , can be determined employing the following equations for the elastic region:

$$\gamma(x) = C_1 \cdot \sinh(\beta x) + C_2 \cdot \cosh(\beta x) \quad (5.1)$$

and for the inelastic region:

$$\gamma(x) = \frac{\beta^2}{2 \cdot G_a} \cdot \tau \cdot x^2 + \left( \frac{T}{t_a \cdot E_f \cdot t_f} - \frac{\beta^2}{G_a} \cdot \tau \cdot L_{pl} \right) + \gamma_y \quad (5.2)$$

where  $\gamma_y$  is the yield strain,  $L_{pl}$  is the plastic length, which is zero for the elastic region and:

$$G_a = \frac{E_a}{2(1+\nu)} \quad (5.3)$$

$$\beta = \sqrt{\frac{G_a}{t_a} \cdot \left( \frac{1}{E_f \cdot t_f} + \frac{1}{E_s \cdot t_s} \right)} \quad (5.4)$$

$$C_1 = \frac{1}{2 \cdot \beta \cdot \cosh(\beta c)} \cdot \left[ \frac{T}{t_a} \cdot \left( \frac{1}{E_f \cdot t_f} - \frac{1}{E_s \cdot t_s} \right) - \frac{\beta^2}{G_a} \cdot \tau \cdot L_{pl} \right] \quad (5.5)$$

$$C_2 = \frac{1}{2 \cdot \beta \cdot \sinh(\beta c)} \cdot \left[ \frac{T}{t_a} \cdot \left( \frac{1}{E_f \cdot t_f} - \frac{1}{E_s \cdot t_s} \right) - \frac{\beta^2}{G_a} \cdot \tau \cdot L_{pl} \right] \quad (5.6)$$

$$C = \frac{2c - L_{pl}}{2}$$

Once the shear strain distribution is derived, the shear stress distribution may be obtained by multiplying the elastic portion of the response by the shear modulus, and setting the shear stress to equal  $\tau$  in the inelastic region. Because it is assumed that the adhesive has yielded only at one end, the above equation is valid until the shear stress at  $x = c$  ( $c = L/2$ ) reaches the yield stress. The solution for the case in which all the adhesive remains elastic can be obtained by assuming the for plastic length ( $L_{pl}$ ) equal to zero.

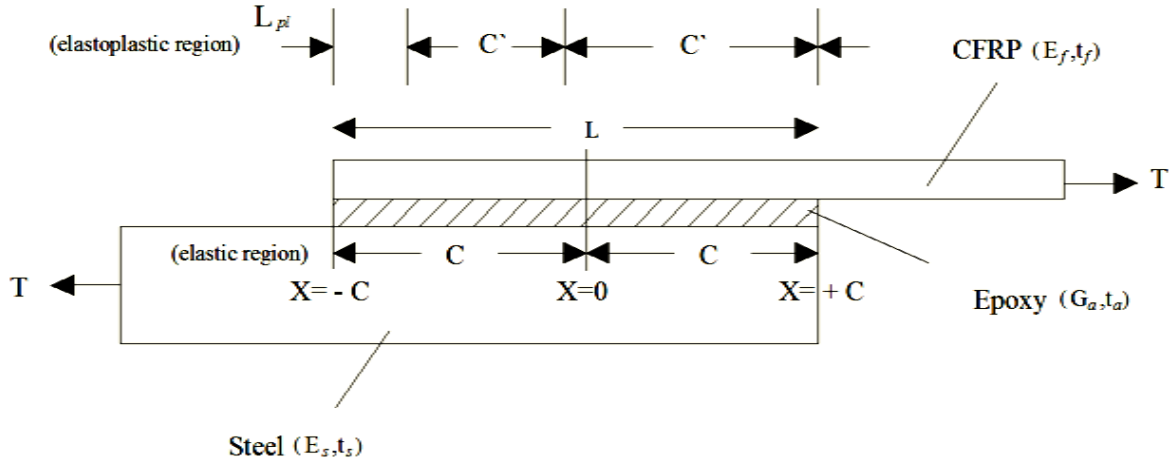


Figure 5.7. Schematic view of single lap joint model: geometric parameters

The simplified equations for elastic and plastic effective bond length are as follow:

$$L_{el} = \frac{4.6}{\beta} \quad (5.7)$$

$$L_{pl} = \frac{1}{\beta} \cdot [\sqrt{2 \cdot (\gamma_0 - 1) + 1} - 1] \quad \text{while} \quad L_{pl} \leq \frac{1}{\beta} \cdot \left[ \frac{E_s \cdot t_s}{E_f \cdot t_f} - 1 \right] \quad (5.8)$$

where:

$$\gamma_0 = \frac{\gamma_{ult}}{\gamma_y} \quad \text{and} \quad \beta = \sqrt{\frac{G_a}{t_a} \cdot \left( \frac{1}{E_f \cdot t_f} \right)} \quad (5.9)$$

The shear stresses along the bond joint obtained by using the described procedure were determined for two specimens with 37% prestressed and 14% prestressed CFRP strips. The ends of the CFRP strips used in the experimental study were considered as single lap joints to investigate the shear stresses at that location. The material properties of Sikadur-30 with the shear stress of  $\tau_y = 15$  MPa, Poisson's ratio of  $\nu = 0.3$ , elastic modulus of  $E_a = 4.5$  GPa, thickness of  $t_a = 2$  mm and Sika Carbodur MM 514 with elastic modulus of  $E_f = 210$  GPa, thickness of  $t_f = 1.4$  mm were used in the modelling of the single lap joint with a length,  $L =$

100 mm (see Figure 5.7). The plastic length for the 14% prestressed strip was determined using Eq. (5.8) to be 26 mm while the yield strain,  $\gamma_y$ , was calculated as  $\gamma_y = \tau_y/G_a = 0.00333$  and the ultimate strain of 0.01 led to 3 for  $\gamma_0$  in Eq. (5.9). The variation of shear stress along the bond length were compared in Figure 5.8. Increasing the prestressing force from 14% to 37% shifted the plastic length from the end of the joint (where the shear stress exceeds 15 MPa) from 2 mm to 21 mm.

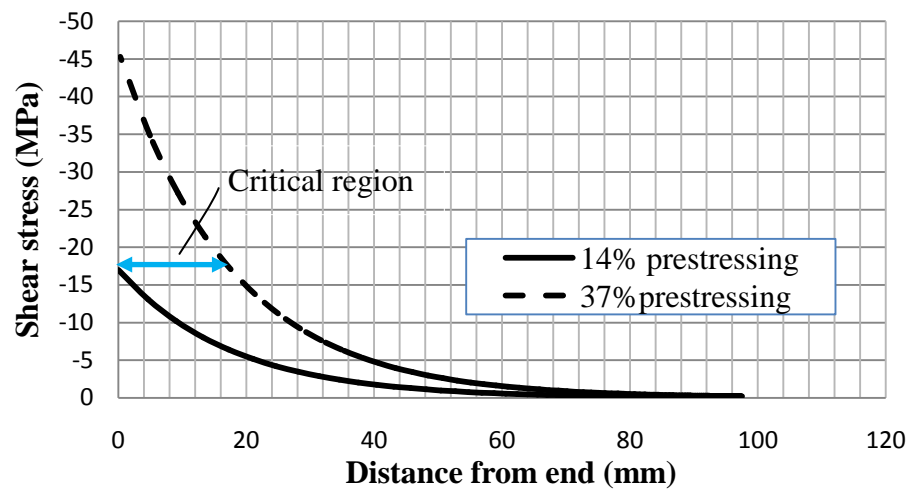


Figure 5.8. Shear stress variation along the bond length

Another stress type of shear present at the end of the strip is the peeling stress. Exceeding the elastic deformation of the adhesive in the inelastic region in an out-of-plane direction leads to debonding, as illustrated in Figure 5.9.

The evaluation of peel stress is performed to evaluate the stresses after the load release in the prestressing system. Clamping devices were mounted at the strip ends in order to prevent the high peel stresses, which means that only shear stresses were imposed when the prestressing system was released. Shear and peel stresses in double lap joints with uniform adherent

thickness including thermal mismatch effects, have been dealt with in the literature, in particular by Hart-Smith (1973). The formulation presented herein was modified to represent the single lap joint examined the current study (see Figure 5.7).

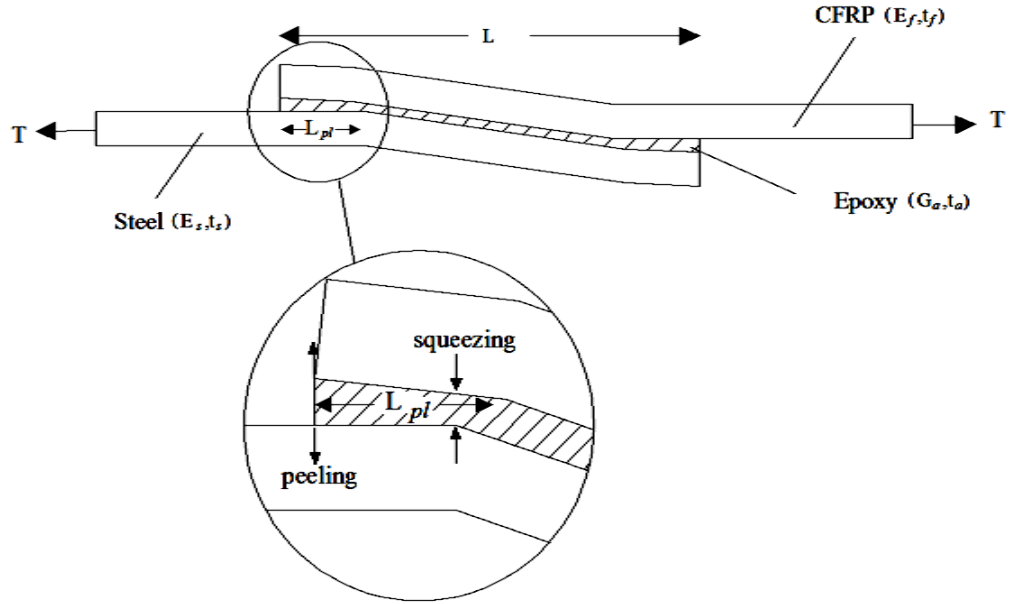


Figure 5.9. Schematic view of single lap joint model: debonding failure

The peel stresses in the reinforced joint were obtained from US Research Laboratory Composite materials handbook (2002). The exact form of the solution is discarded in this reference in favour of the following approximate solution:

$$\sigma_b = \sigma_{b,\max} \cdot \left[ (\cos \gamma_d \cdot \frac{x}{t} \cdot e^{-\gamma_d} \cdot \frac{x}{t}) - \left( \frac{1}{2} \cdot \cos \gamma_d \cdot \frac{x-1}{t} \cdot e^{-\gamma_d} \cdot \frac{x-1}{t} \right) \right] \quad (5.10)$$

Where

$$\gamma_d = \left( 3 \cdot \frac{E_a}{E_f} \cdot \frac{t_f}{t_a} \right)^{\frac{1}{4}} \quad (5.11)$$

The maximum peel stress,  $\sigma_{b,max}$  can , can then be found through the theory developed by Hart-Smith (1973) and Cadei et al. (2004), using the following expressions:

$$\sigma_{b,max} = \tau_{max} \cdot \left( \frac{3 \cdot E_a \cdot (1 - \nu_f^2) t_f}{E_f \cdot t_a} \right)^{\frac{1}{4}} \quad (5.12)$$

Where

$$E_a = \left[ \frac{(1 - \nu_a)}{(1 + \nu_a) \cdot (1 - 2\nu_a)} \right] \cdot E_a \quad (5.13)$$

Once the shear stress distribution is determined, the peel stresses in the joint can be obtained from Eq. (5.10). The resulting peel stress distribution at the end of the reinforcing strip with 37% prestressing level is illustrated in Figure 5.10. The material properties assumed were chosen to match those of the materials used in the laboratory tests. The assumed maximum tensile and compressive strengths of the epoxy were 24.8 MPa and 48.0 MPa, respectively.

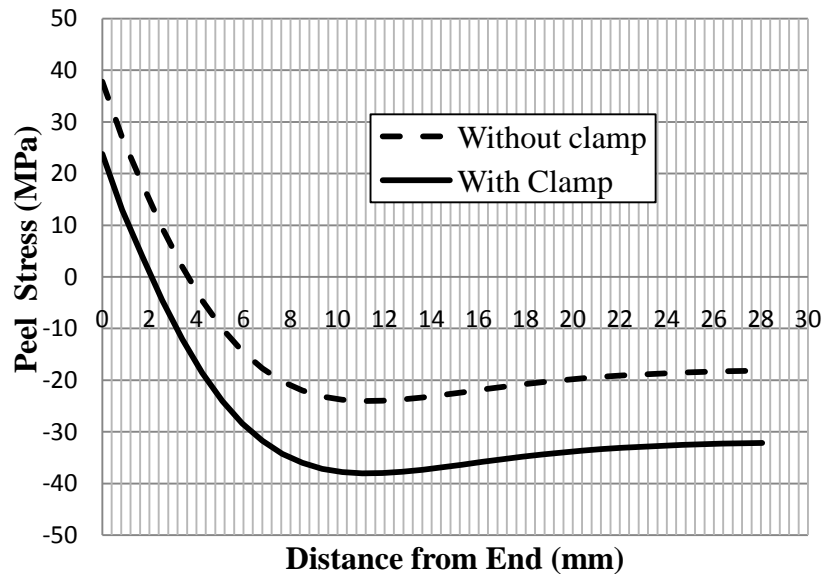


Figure 5.10. Peel stress variation at the end of strips (37% prestressing) with and without end clamp

Looking at Figure 5.10, it can be seen that up to 1.8 mm from the bonded end, the peel stress exceeds the maximum tensile strength of the epoxy (24.8 MPa) indicating a critical bond length susceptible to debonding due to peel stress. To mitigate the debonding a compressive pressure (14 MPa) was applied at this location to work against the peel stress. However the clamping pressure should not exceed the maximum compressive strength of the epoxy (48 MPa). Since the maximum peel stress in the specimen with 14% prestressing was equal to 18.3 MPa, which is less than maximum tensile strength of the epoxy, debonding was not observed at failure.

## **5.5 Elastic Finite Element Analysis (FEA) of Fatigue Specimens**

### *5.5.1 FEA Model Description*

Finite element analysis (FEA) is recognized as a useful tool for determining local stresses and strains in complex structural analysis problems. ABAQUS (revision 6.7.1) FEA program was used to model the steel beams strengthened by stressed and unstressed CFRP strips. In this section, FEA modelling and FEA results are presented and compared with the available test data and the analysis results presented in Sections 5.1 and 5.2.

The finite element analysis was performed in two stages. In the first stage, the unreinforced specimen was modelled and a mesh refinement was performed to evaluate the adequacy of the mesh. In the second stage, analyses were performed wherein all of the test variables were modelled. The models for each specimen type were analyzed separately for the cases of prestressing and vertical (flexural) loading.



Linear elastic material behaviour was assumed in the analyses, which made it possible to perform the analyses under unit loads and use the principal of superposition to combine the results for prestressing and vertical loading. Due to symmetry, it was only necessary to model a quarter of each specimen, in order to reduce the time required for each analysis. A schematic view of the model and the boundary conditions is presented in Figure 5.11.

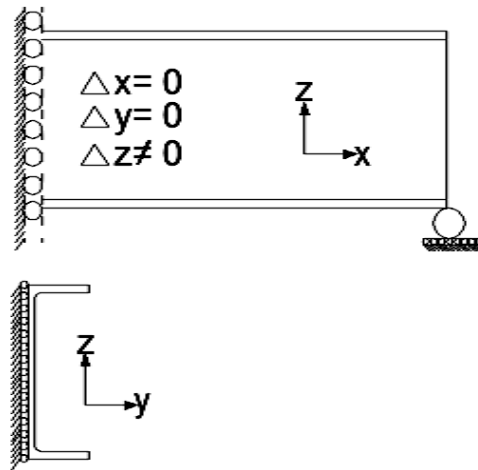


Figure 5.11. Symmetrical modelling of quarter beam and boundary conditions

All of the test conditions, including the loading and support plates, were considered in the analysis. In the first modeling effort, an attempt was made to model the fillets in the wide flange (W section) cross section precisely, as shown in Figure 5.12 (a). 3D quadrilateral brick elements (C3D20R) were used to model the W section, cover plate, welds, and loading/support plates. With a coarse mesh, it was found that the tracking of the curved fillet by the automatic meshing feature in ABAQUS was inconsistent. Thus, this approach was subsequently abandoned for a simpler approach, where these fillets were not considered. The effect of this assumption was expected to be negligible.

In the next modeling attempt, the revised geometry was discretized uniformly, with quadrilateral elements forced to maintain an aspect ratio of 1:2. Due to the relatively low thickness of the web, this resulted in an increased number of elements and a very time consuming simulation (see Figure 5.12 (b)). Allowing the use of tetrahedron (C3D4) elements, and relaxing the element aspect ratio limit, a third mesh was generated.

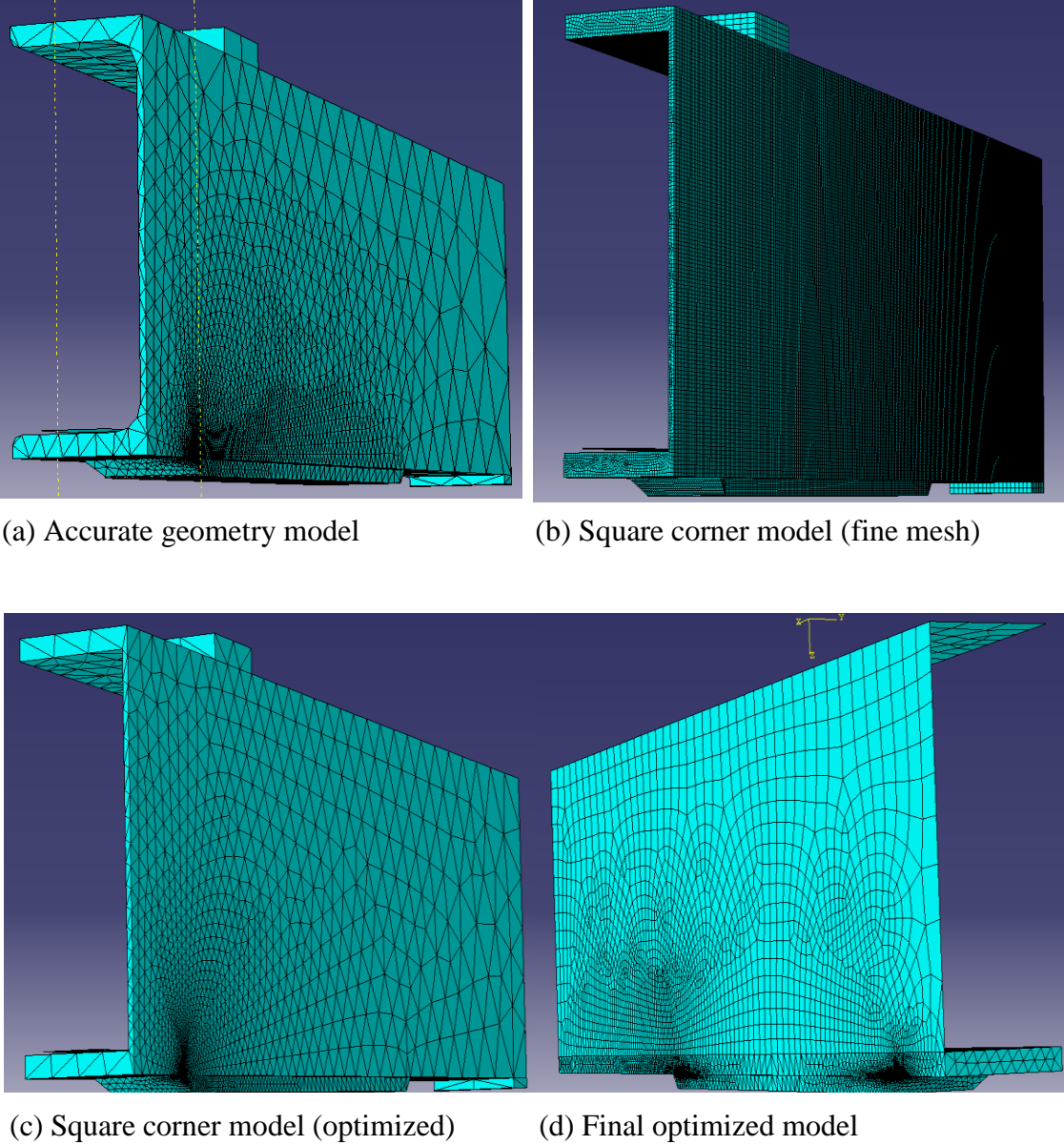


Figure 5.12. Various iterations of the beam specimen FEA model

In order to reduce the number of elements, the edges of the various model features were “seeded”, so that the elements would be concentrated in the region of the eventual fatigue crack (i.e., the weld toe and flange at the location of the cover plate and weld, see Figure 5.12(c)). Finally, it was recognized that, since the primary output desired from the analysis was the stress distribution along the anticipated crack path through the bottom flange, the web and top flange plates could be modelled with 2D plate elements (S4), resulting in significant increase in the analysis speed, with little loss of accuracy, see Figure 5.12(d).

A convergence test was employed to identify the optimal number of elements (Chandrupatla et al. 2002). The stress distribution at the weld toe was a main object of this FEA study so the convergence test was implemented considering a very fine mesh at this location. The mesh adopted in the end consisted of 539363 elements.

The assumed crack path along which the stress distributions were recorded is shown in Figure 5.13. Figure 5.14 presents the stress distributions for the optimized model (see Figure 5.12(d)) and the model believed to be the most accurate (see Figure 5.12 (c)) for the case of a unit vertical load. Note that since the quarter model only contains one load point, a unit of vertical load of 1 N applied the model actually translates to a total vertical load of 2 N in the specimen, since the load was applied to the specimen at two load points. A good agreement is seen in Figure 5.14; the difference in the peak stress at the surface is 1.3%.

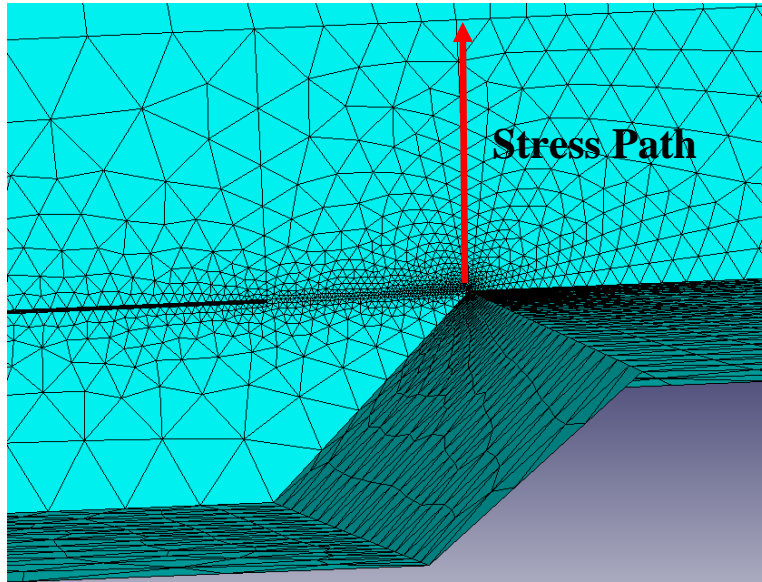


Figure 5.13. Stress path through the flange thickness at the weld toe

In modelling the strengthened specimens the CFRP strip was modelled as a shell element using tie constraints to connect it to the beam, as shown in Figure 5.15.

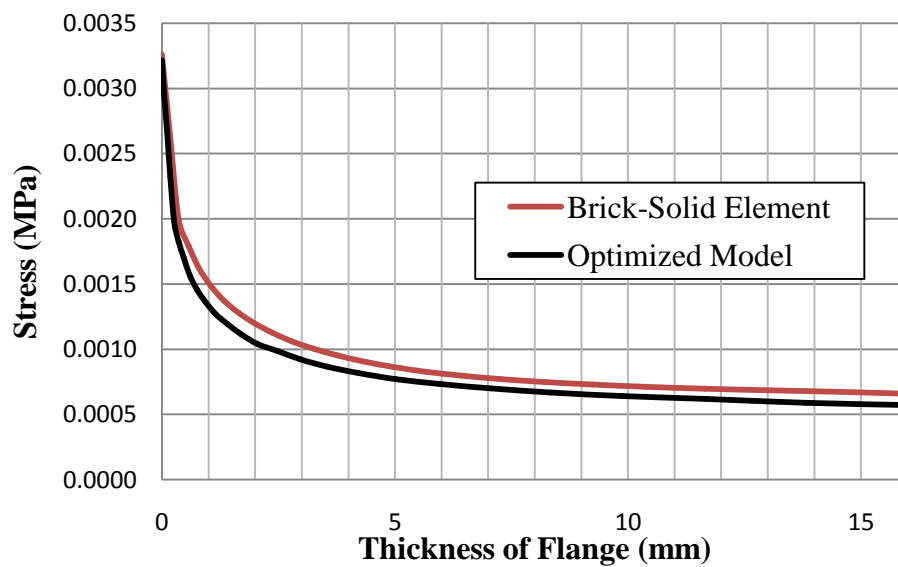


Figure 5.14. Comparison between optimized and most accurate models

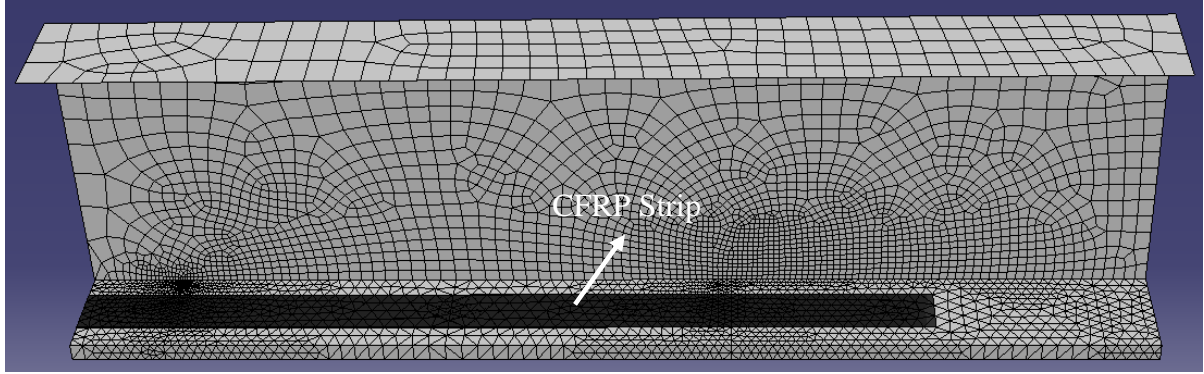


Figure 5.15. Shell element modelling of the strip

Because the exact mechanical characteristics of the interfacial bond between the epoxy and the CFRP strip and steel were not known, a perfect bond was simplistically assumed between the CFRP strip and the structural steel. The strip was located at a distance from the flange surface equal to the thickness of the epoxy plus half of the CFRP strip thickness. To make the models more realistic, the prestressing procedure was introduced in two steps, simulating the two steps used in the actual prestressing procedure performed in the laboratory, see Figure 5.16 and Figure 5.17. In the first step, the end of the strip was restrained at one end and pulled at the other. In the second step, the tie constraints between the nodes in the strip and the top surface of the flange were introduced and the prestressing force was removed.

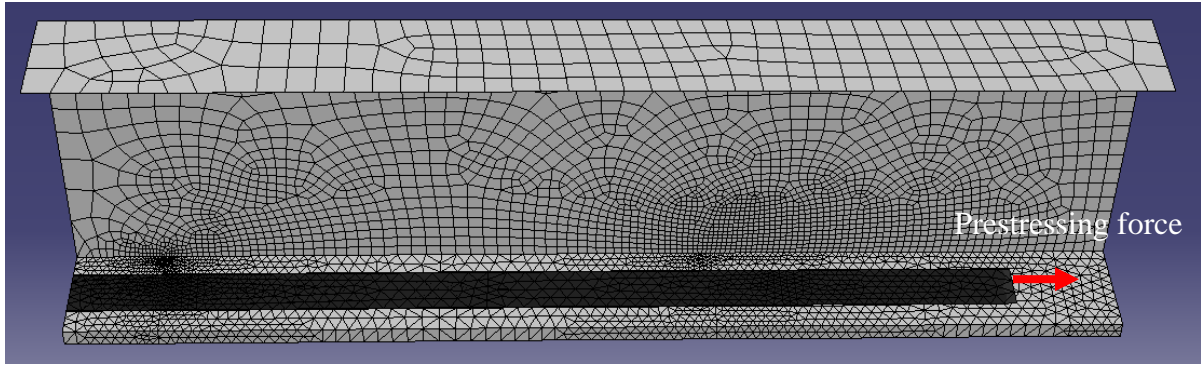


Figure 5.16. Prestressing Step 1 – introduction of prestressing force

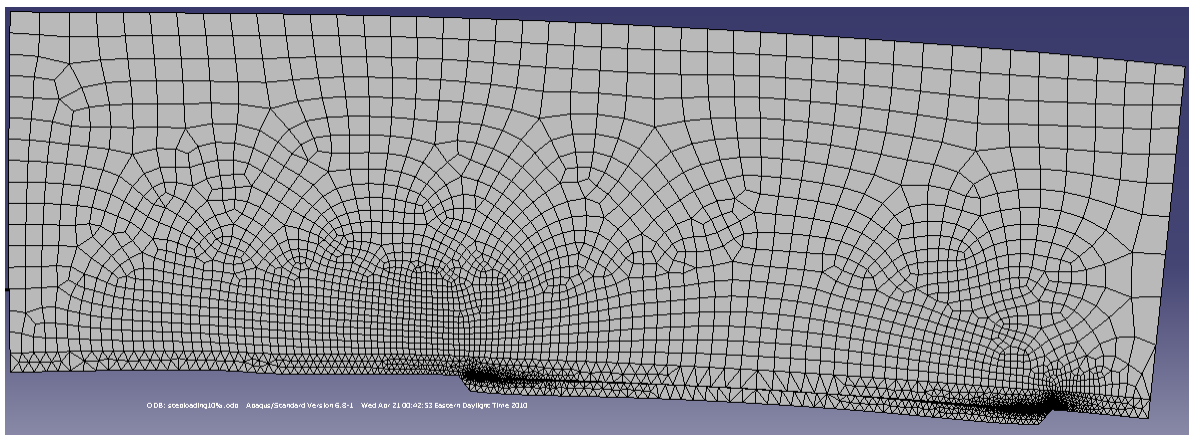


Figure 5.17. Prestressing Step 2 – camber in beam after force released

Looking at Figure 5.17, it can be seen that a camber due to releasing the prestressing force is produced (note: the camber in this figure is scaled up, so that it is visible). Vertical loading of the model beam was performed in one step. Tie constraints were applied for bond modelling and the vertical load was introduced as indicated in Figure 5.18. A deflection similar to the actual deflection during the tests was observed.

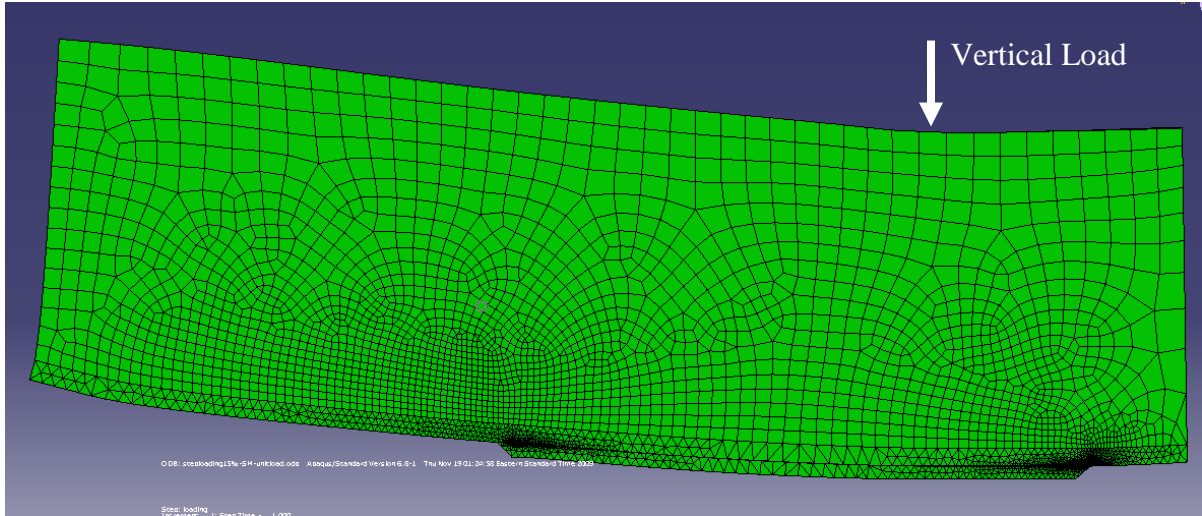


Figure 5.18. Deformed shape of the beam model under vertical load

### 5.5.2 Predicted and Measured Strain and Deflection Comparison

Even though a perfect bond was assumed between the CFRP and steel in the FEA work, losses still occurred in the prestress, due to the elastic deformation of the beam after release of prestressing force. In order to have the same stress in the CFRP strips as in the experiments, a higher initial force was applied in the FEA. As can be seen in Table 5.7, to reach final stresses in the strips equal to the experimental values, the initial applied forces were slightly higher in the FEA than the experimental applied force.

Table 5.7. Comparison of the experimental and FEA applied force

Specimen	Experimental	FEA	
	P (kN)	Initial P (kN)	Final P (kN)
15%-F-S	23.0	25.3	23.0
14%-F-M	23.2	25.5	23.2
35%-F-M	62.0	62.5	62.0
37%-C-M	65.3	66.15	65.3

A comparison of the camber during prestressing based on the FEA results, analysis results

and experimentally derived results are given in Table 5.8. It is evident that the “FEA” and “Analysis” values are the closest.

Table 5.8. Comparison of prestressing cambers determined by various means

Specimen	Experimental Camber (mm)	Analysis Camber (mm)	FEA Camber (mm)
15%-F-S	0.054	0.047	0.045
14%-F-M	0.042	0.046	0.048
35%-F-M	0.087	0.121	0.107
37%-C-M	0.110	0.158	0.137

The strains for the prestressed and vertically loaded beam models corresponding to the tests specimens (with actual prestress and vertical load levels) are given in Table 5.9.

Table 5.9. The prestressing and bending strains from FEA

Prestressing	x = L/2 (midspan)				x = L/4	
	M <sub>max</sub>		M <sub>min</sub>		M <sub>max</sub>	M <sub>min</sub>
Specimen	ε(μϵ)-GB1	ε(μϵ)-GS3	ε(μϵ)-GB1	ε(μϵ)-GS3	ε(μϵ)-GS1	ε(μϵ)-GS1
Control	0	0	0	0	0	0
15%-F-S	-30	2329	-30	2329	2271	2271
14%-F-M	-28	1664	-28	1664	1625	1625
35%-F-M	-72	4284	-72	4284	2824	2824
0%-C-M	0	0	0	0	0	0
37%-C-M	-81	4443	-81	4443	3124	3124
Applied load	x = L/2 (midspan)				x = L/4	
	M <sub>max</sub>		M <sub>min</sub>		M <sub>max</sub>	M <sub>min</sub>
Specimen	ε(μϵ)-GB1	ε(μϵ)-GS3	ε(μϵ)-GB1	ε(μϵ)-GS3	ε(μϵ)-GS1	ε(μϵ)-GS1
Control	533	0	53	0	0	0
15%-F-S	517	547	59	63	209	24
14%-F-M	508	532	58	61	163	19
35%-F-M	512	425	59	49	163	19
0%-C-M	508	532	58	61	214	25
37%-C-M	508	532	58	61	214	25



The total strains in the strips and beams can be determined by summing the prestressing and bending strains as shown in Table 5.10. The total strains obtained by simple analysis and FEA are compared with the experimentally measured strains listed in Table 5.10.

Table 5.10. Total strain comparison at three strain gauge locations

Experimental Strains	x = L/2 (midspan)				x = L/4	
	M <sub>max</sub>		M <sub>min</sub>		M <sub>max</sub>	M <sub>min</sub>
Specimen	$\epsilon(\mu\epsilon)$ -GB1	$\epsilon(\mu\epsilon)$ -GS3	$\epsilon(\mu\epsilon)$ -GB1	$\epsilon(\mu\epsilon)$ -GS3	$\epsilon(\mu\epsilon)$ -GS1	$\epsilon(\mu\epsilon)$ -GS1
Control	533	0	53	0	0	0
15%-F-S	397	2989	-26	2596	2798	2579
14%-F-M	425	2115	-12	1725	1926	1708
35%-F-M	338	4493	-99	4103	4303	4085
0%-C-M	501	709	50	71	217	22
37%-C-M	330	4920	-121	4282	4452	4256
Analytical Strains	x = L/2 (midspan)				x = L/4	
	M <sub>max</sub>		M <sub>min</sub>		M <sub>max</sub>	M <sub>min</sub>
Specimen	$\epsilon(\mu\epsilon)$ -GB1	$\epsilon(\mu\epsilon)$ -GS3	$\epsilon(\mu\epsilon)$ -GB1	$\epsilon(\mu\epsilon)$ -GS3	$\epsilon(\mu\epsilon)$ -GS1	$\epsilon(\mu\epsilon)$ -GS1
Control	530	0	62	0	0	0
15%-F-S	494	2851	36	2367	2626	2297
14%-F-M	489	2069	50	1705	1902	1646
35%-F-M	444	4652	5	4288	3077	2821
0%-C-M	509	534	74	78	382	53
37%-C-M	430	4894	-5	4438	3448	3119
FEA Strains	X = L/2 (midspan)				X = L/4	
	M <sub>max</sub>		M <sub>min</sub>		M <sub>max</sub>	M <sub>min</sub>
Specimen	$\epsilon(\mu\epsilon)$ -GB1	$\epsilon(\mu\epsilon)$ -GS3	$\epsilon(\mu\epsilon)$ -GB1	$\epsilon(\mu\epsilon)$ -GS3	$\epsilon(\mu\epsilon)$ -GS1	$\epsilon(\mu\epsilon)$ -GS1
Control	542	0	89	0	0	0
15%-F-S	488	2792	23	2386	2455	2290
14%-F-M	454	2115	-14	1716	-	-
35%-F-M	462	4727	7	4330	3060	2854
0%-C-M	525	581	28	66	358	41
37%-C-M	361	4976	-75	4503	3357	3152

\*GB is the strain gauge located on the beam

\*\* GS is the strain gauge located on the CFRP strip \*\*\*(-) Failed gauge

In general, although the analytical and FEA-based strains are not identical to the experimentally determined strains, the predictions are reasonably close. A number of factors were not considered in the analysis, which may have a significant impact on the results, and thus explain the differences in Table 5.10, including: variations in material properties and geometry, imperfections in the test set up, inaccuracy in the data recording, and human errors during specimen fabrication such as welding, sandblasting, and epoxy application.

### *5.5.3 Predicted Stress Distributions along the Crack Path*

One of the main reasons for performing the FEA work presented in the previous section was to determine the elastic stress distributions along the anticipated crack path due to the prestressing and the subsequent applied cyclic loading. These stress distributions were required inputs for the fracture mechanics analysis presented in Chapter 6, which was undertaken to facilitate fatigue life predictions for the various specimen types, as well as parametrical studies, where the various model parameters could be varied. The results of FEA for the model specimens are given in Appendix B.

Typical applied stress distributions for the 0%-C-M specimen are reported in Figure 5.19. Looking at Figure 5.19, the effect of reinforcement without prestressing on the stress distribution along the anticipated crack path can be seen. CFRP reinforcement appears to have no significant effect on the stress distribution. Figure 5.20 and Figure 5.21 show stress distributions along the crack path for specimen 37%-C-M, under actual (rather than unit) prestressing and vertical loads.

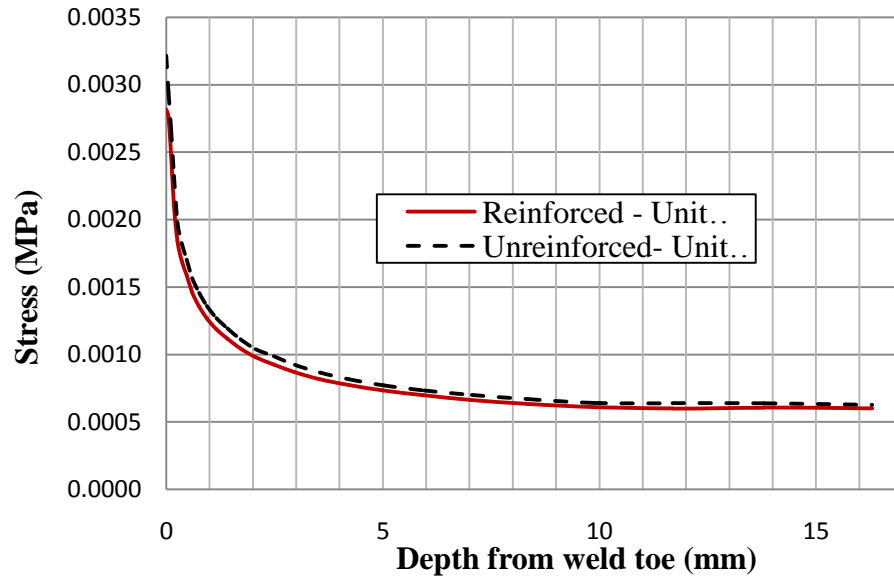


Figure 5.19. Stress distribution along crack path for specimen 0%-C-M

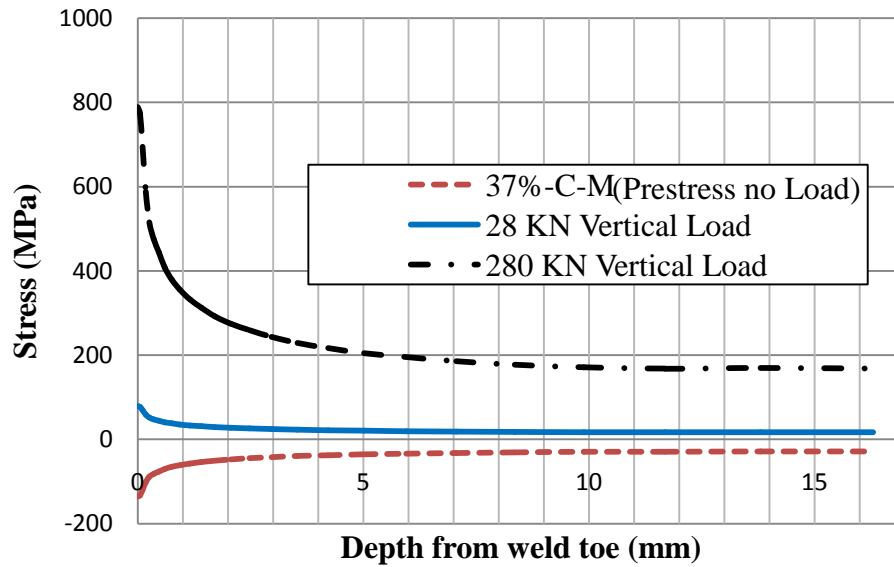


Figure 5.20. Stress distribution along crack path for specimen 37%-C-M

In Figure 5.20, the different stress distributions (prestress-no load, minimum vertical load of 28 kN, maximum vertical load of 280 kN) are shown separately. In Figure 5.21, the net stress

distributions are shown under the maximum and minimum loads. The net stress is the difference between the stress under minimum or maximum load and the stresses due to prestress only. Similar trend for the specimens with the medium modulus CFRP strips on the flanges were obtained, as shown in Figure 5.22 and Figure 5.23.

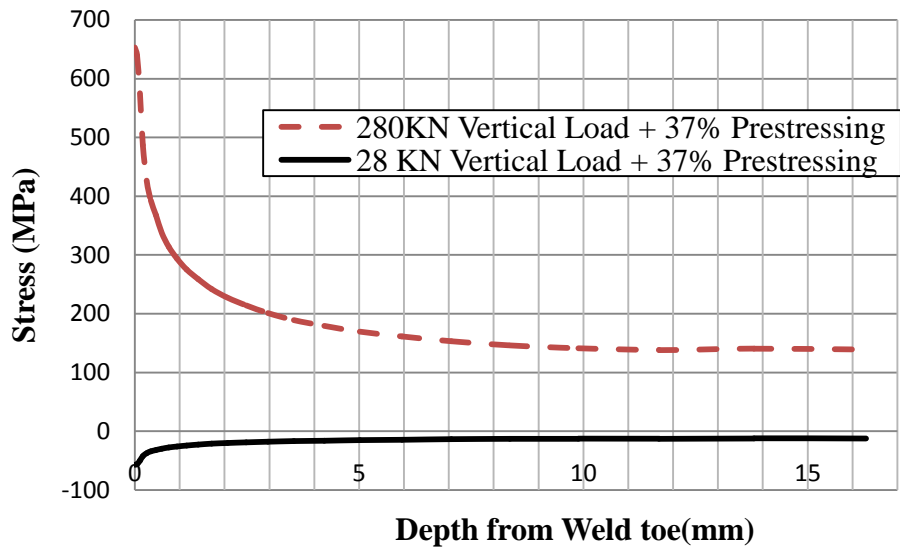


Figure 5.21. Net stress distribution for specimen 37%-C-M

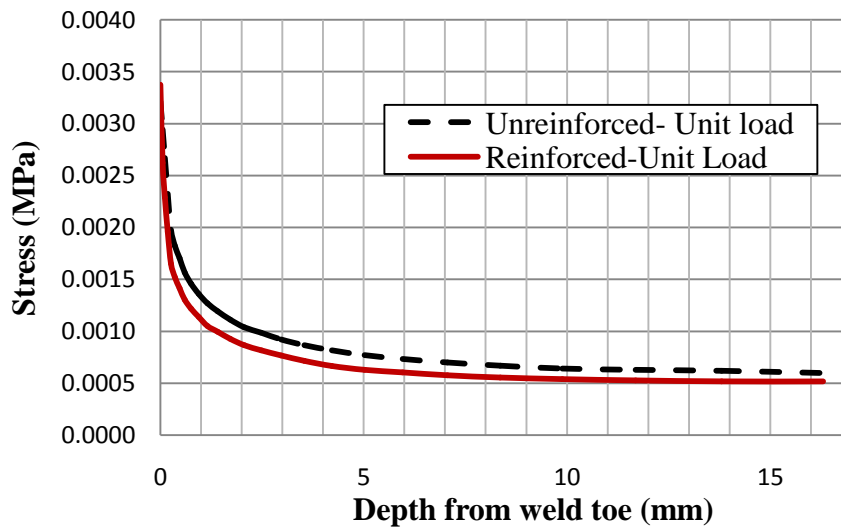


Figure 5.22. Stress distribution along crack path for 0%-F-M case

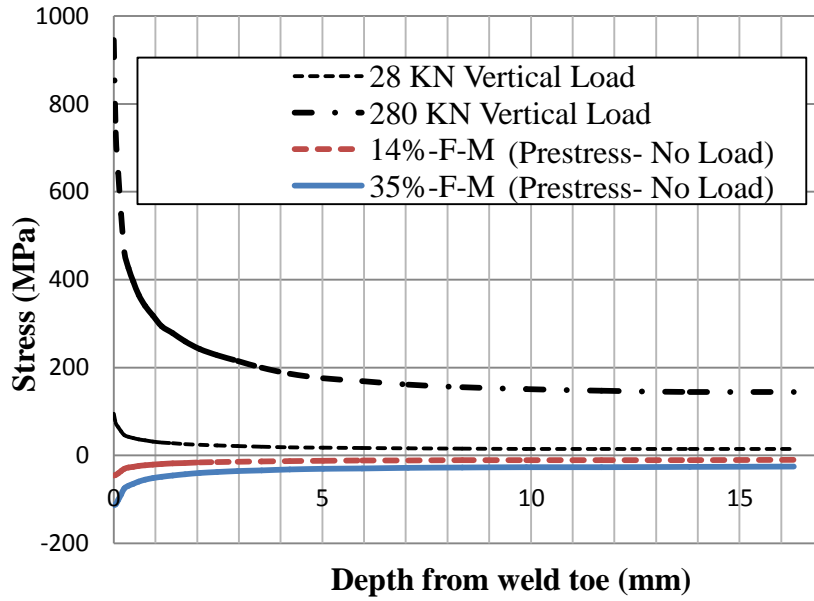


Figure 5.23. Stress distribution along crack path for specimen 14%-F-M

The difference stresses (prestress- no load, 28 kN vertical load, 280 kN vertical load) in specimen 15%-F-S, strengthened using S-CFRP strips attached on the flanges, are shown in Figure 5.24.

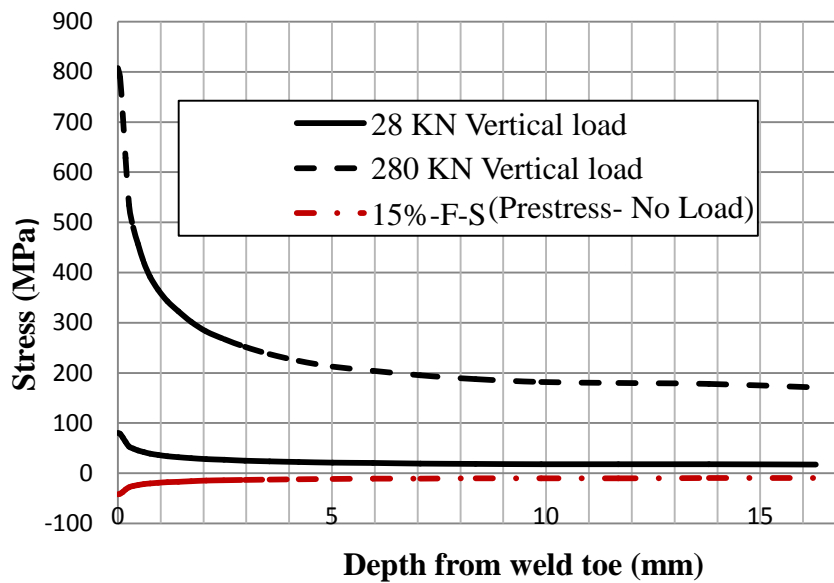


Figure 5.24. Net stress distribution along crack path for specimen 15%-F-S

#### 5.5.4 Predicted Stress Distributions along the Crack Path for Full-scale Girders

To investigate the effect of applying prestressed CFRP strips to improve the fatigue performance of deeper girders, the same FE analysis was performed for two “full-scale” girders with the same material properties and strengthening configuration but larger girder depths of 600 mm and 900 mm.

The FEA results for the unreinforced and reinforced (but not prestressed) cases are summarized in Figure 5.25. Looking at this figure, it can be seen that the stress is reduced as the size of the girder increase as expected. This trend can be explained by the fact that the unit load is the same for each girder, whereas the section modulus, which is a function of the moment of inertia and the girder depth, increases as the girder depth increases.

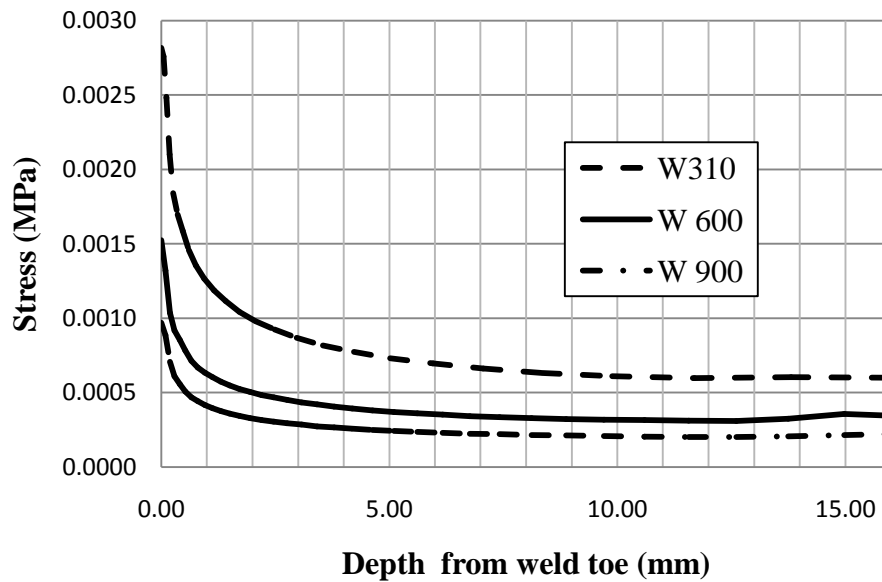


Figure 5.25. Stress distribution along crack path for different girder depths

The effect of prestressing on the full-scale girders was investigated through the analysis of reinforced models with 37% prestressing, see Figure 5.26. Based on these results, it can be concluded that the prestressing effects decrease as the size of the girder increases, if the area of the prestressed CFRP strips is held constant, up to a certain girder depth, beyond which, the distributions tend to converge. In practice, it is possible that a larger CFRP strip area would be used on full-scale girders. However, by keeping the CFRP strip area constant and only increasing the girder depth, it was possible to study the effect of varying one parameter with respect to the other on the effectiveness of the reinforcement.

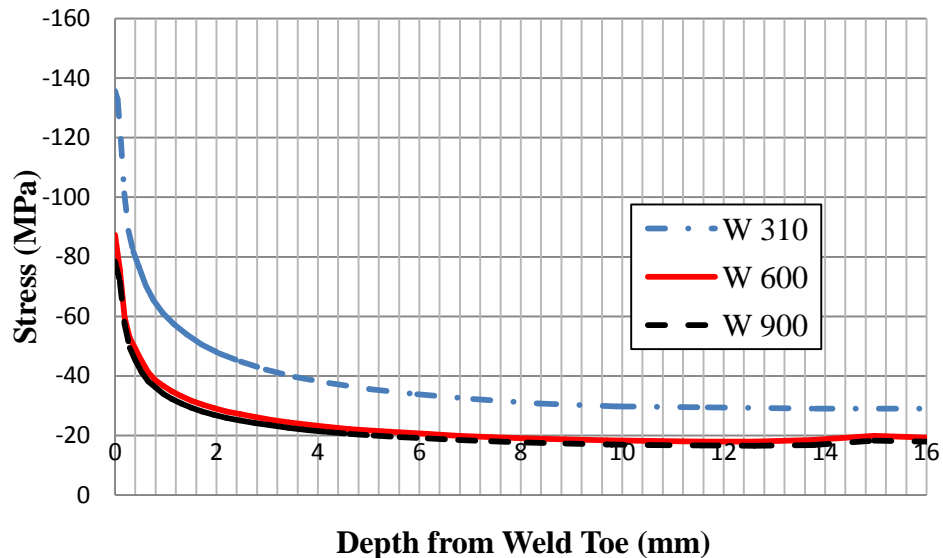


Figure 5.26. Effect of girder depth on stress distribution due to prestressing

### 5.6 FEA Modelling of CFRP Strip End Debonding

The most critical problem encountered during prestressing was the debonding observed at the time of releasing the prestressing load to the beam. An analytical approach was employed previously to study the bond behaviour at the location where CFRP strip terminated on the

beam (strip end) in detail. The interfacial shear and peel stress distributions at the end strip were determined using this approach.

To evaluate the validity of the analytical results, the CFRP strip end was analyzed using FEM as shown in Figure 5.27. The shear and peel stress distributions for a prestressing force of 37% were drawn as shown in Figure 5.28 and Figure 5.29. Very similar patterns can be observed for the analytical and FEM analysis results, as seen in this figure.

The critical location was 2.5 mm from the end for peel stress where the stresses exceed the tensile strength of the epoxy (24.5 MPa). Looking at Figure 5.29, it can be seen that the shear stress never exceeds the maximum epoxy shear capacity (15 MPa). This suggests that end clamps which is expected to reduce peel stress should be effective in preventing bond failures after prestressing release.

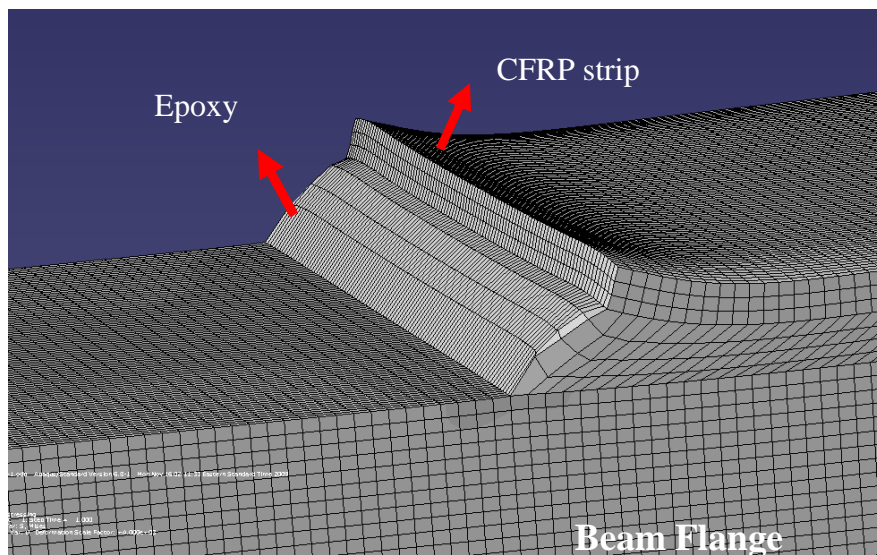


Figure 5.27. End bond deformation modelled using FEA



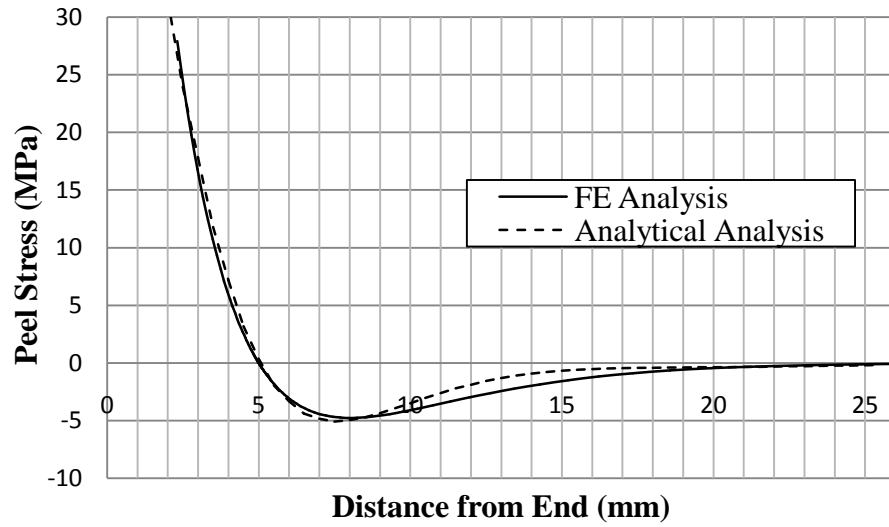


Figure 5.28. Peel stress distribution obtained using analytical and FEA methods

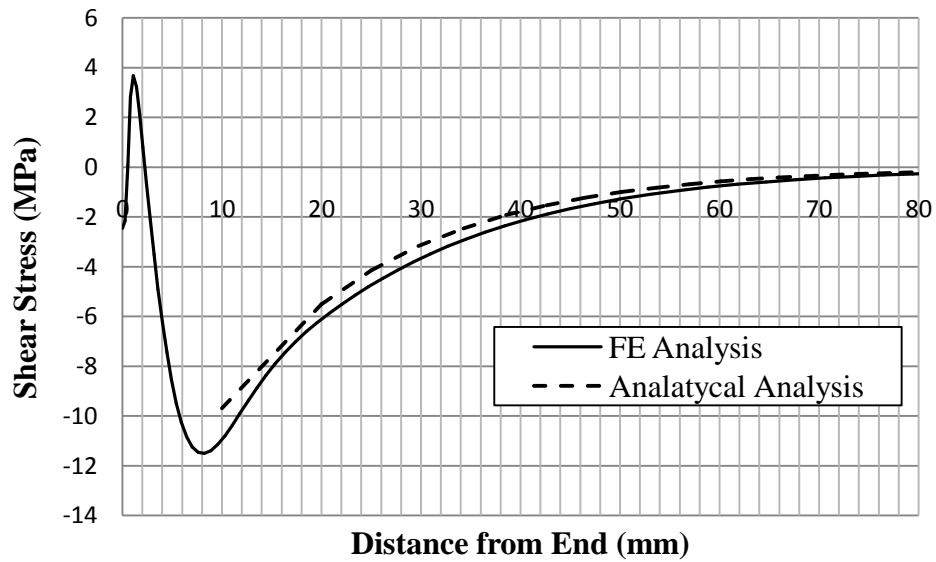


Figure 5.29. Shear stress distribution obtained using analytical and FEA methods

## **Chapter 6: Fatigue and Fracture Mechanics Analysis**

### **6.1 Introduction**

In the test program described in Chapters 3, only a small number of fatigue tests were performed, due to cost and time constraints and the relatively large specimen size. Although the test results for the reinforced specimens show the potential of this retrofitting strategy (Chapter 4), questions remain, due to the high uncertainties associated with the weld shape, loading range, crack size, and welding residual stresses, prestressing stresses, and material properties. In order to assess the significance of these uncertainties, a linear elastic fracture mechanics (LEFM) analysis was employed to model the fatigue behaviour of unreinforced and reinforced welded cover plate details similar to those studied in the laboratory test program. In the following sections, the LEFM model is briefly described, the model sensitivity to the various input parameters is studied, and then the model is applied to predict the fatigue performance improvement under various conditions not examined in the test program. These conditions include: various stress ranges and ratios, prestressing levels greater than 37%, and prestressing applications to full-scale girders.

### **6.2 Comparison of Test Results with Design S-N Curves**

Prior to conducting the fracture mechanics analysis of the test specimens, the test results were compared with design stress-life (S-N) curves for welded fatigue details from the Canadian Handbook of Steel Construction (CISC 2007). According to the S-N curve method for fatigue design, fatigue life is determined by comparison with a design curve that relates

the fatigue life to the applied nominal stress range. Nominal stress, in this case, is the stress applied in the general vicinity of the fatigue detail, but does not include the additional stresses due to the local stress concentration introduced by the fatigue detail. The design curves used in this approach are based on large volumes of test data. Typically, the design curves are taken as lower bounds of the test data, representing a 95% or a 97.5% survival probability. According to (CISC 2007), welded cover plates should be designed using Detail Category 'E' design curve if the plate thickness is less than 25 mm.

In Figure 6.1, the test results are compared with Detail Category 'D' and 'E' design curves. Looking at this figure, it can be seen that the S-N data point for the unreinforced specimen falls just slightly below the Detail Category 'E' curve. Normally, we would expect the data point to fall above the design curve. Possible explanations for the below average result include: below average weld quality or specimen misalignment causing a higher local stress level at the location along the weld where the fatigue crack eventually initiated.

Not only the fatigue life improvement for the reinforced specimen is clearly evident but also it can be stated that a proper reinforcement using prestressed CFRP strip bonded on the cover plates upgraded the specimen from category "E" to "D".

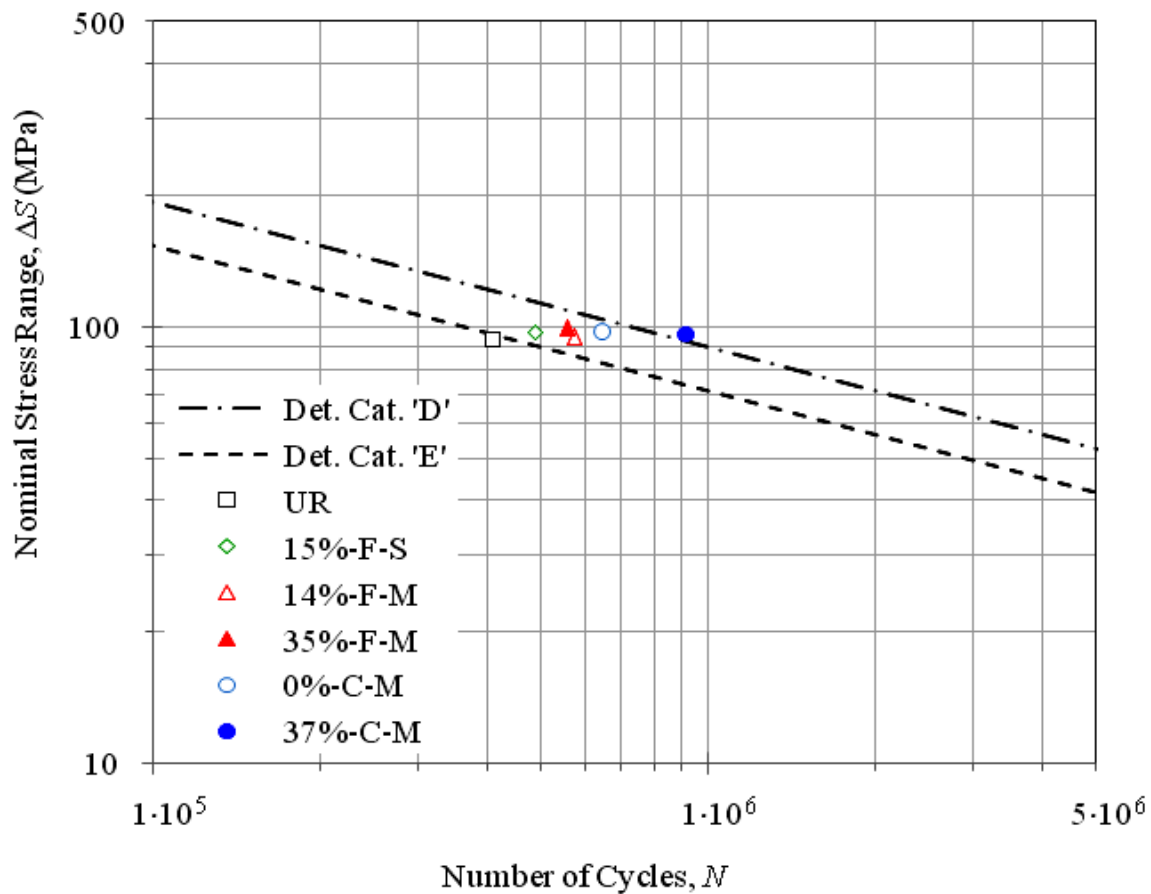


Figure 6.1. Comparison of design S-N curves and test results

### 6.3 LEFM Analysis of Fatigue Tests

#### 6.3.1 Model Description

A linear elastic fracture mechanics (LEFM) model was used to predict the results of the fatigue tests. A similar model was used previously to predict the effects of peening treatments on the fatigue performance of welds (Walbridge 2008). The model is based on the Paris-Erdogan crack growth law (Paris et al. 1963), modified to account for crack closure

effects and a threshold stress intensity factor (SIF) range,  $\Delta K_{th}$ . The number of cycles to failure,  $N$ , is calculated by numerically integrating the following expression over the crack depth range ( $a_i$  to  $a_c$ ):

$$N = \int_{a_i}^{a_c} \frac{da}{C \cdot \text{MAX}(\Delta K_{eff}^m - \Delta K_{th}^m, 0)} \quad (6.1)$$

The effective SIF range,  $\Delta K_{eff}$ , is calculated as follows:

$$\Delta K_{eff} = K_{max} - \text{MAX}(K_{op}, K_{min}) \quad (6.2)$$

where  $K_{max}$ ,  $K_{min}$ , and  $K_{op}$  are the SIFs corresponding to the maximum, minimum, and crack opening stress levels for each stress cycle, respectively. The various SIFs are determined in terms of an elastic weight function,  $m(b,a,c)$  (Shen and Glinka, 1991), and the stress distribution along the crack path,  $\sigma(b)$ , integrated over the crack depth:

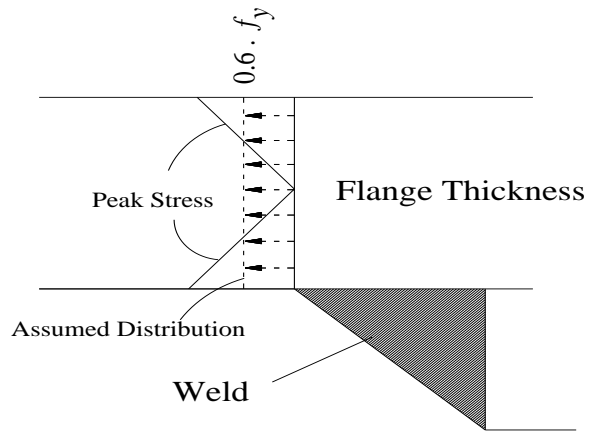
$$K = \int_0^a \sigma(b) \cdot m(b,a,c) \cdot dx \quad (6.3)$$

where  $a$  is the crack depth,  $\sigma(b)$  is the stress at depth,  $b$ , and  $c$  is half of the semi-elliptical crack width. The weight functions for semi-elliptical surface cracks from Shen and Glinka (1991) are used in the model. The model requires knowledge of the applied and residual stress distributions along the crack path. The latter includes the residual stress distribution due to the welding process, plus the residual stress due to the CFRP prestressing. These stress distributions are superimposed to obtain the total stress distributions associated with the maximum and minimum applied load level.

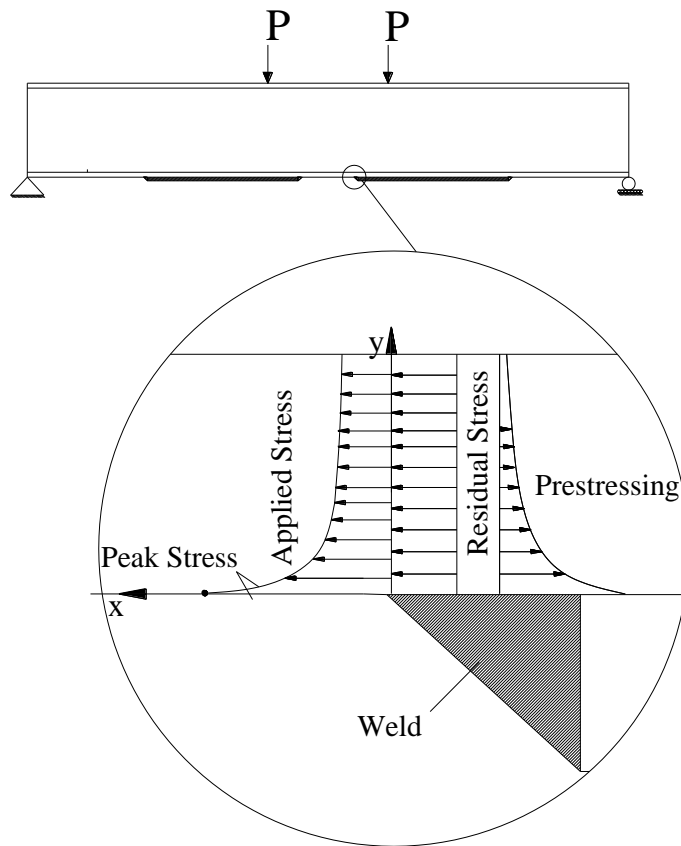
The stress distributions at the weld toe, through the flange thickness, created by welding, prestressing, and the applied vertical load are schematically drawn in Figure 6.2. It has been observed in many studies that the residual stress distribution created by welding is not constant and tends to form as shown in Figure 6.2(a) (Kulak et al. 1993, Monin et al. 2008, Paradowskaa et al. 2006, Roy 2003, Stacey 2000).

More specifically, the residual stress distribution due to welding is generally tensile at the surface and near zero or even compressive at the mid-depth. The tensile stresses at the surface can be as high as the yield stress of the steel ( $f_y$ ). However, a 60% of the yield stress is a more typical value (Stacey 2000). In this study a uniform residual stress distribution due to welding is conservatively assumed, as a simplification, with a magnitude of  $0.6 \cdot \sigma_y$  (Walbridge 2008).

The stress distribution generated by the prestressed and bonded CFRP strips is obtained from the FEA analysis presented in Chapter 5. This stress distribution is a function of the prestressing level, the material and geometric properties of the strip, and the strip location.



(a) Welding residual stress distribution



(b) The various stress distributions

Figure 6.2. Schematic view of stresses distributions through the flange thickness

The crack opening SIF is calculated using formulas from Newman (1994). These require knowledge of the “flow stress” of the material,  $\sigma_0$ , which can be taken as the average of  $\sigma_y$  and  $\sigma_u$ . In calculating  $K_{op}$ , rather than the stress ratio:  $S_{max} / \sigma_0$ , the SIF ratio:  $K_{max} / K_0$  is used as proposed by McClung (1989), where  $K_0 = \sigma_0 \cdot \sqrt{(\pi \cdot a)}$ . The crack shape constant  $a/c$  is assumed to be equal to 0.2, similar to the work by Walbridge (2008).

For the application of the crack closure model, the nominal yield and ultimate strength properties of CSA 350W steel were assumed (CISC 2007). A uniform tensile residual stress due to the welding process was simplistically assumed with a magnitude of 60% of the steel yield stress, based on Stacey (2000) and Walbridge (2008).

For each crack depth and stress level, the maximum, minimum, and crack closure SIFs are calculated. Using these parameters,  $\Delta K_{eff}$  and  $da/dN$  are then determined. The fatigue life is then obtained by numerically integrating Eq. (6.1). Table 6.1 summarizes the initially assumed values for the various model parameters.

Table 6.1. Model parameters assumed for LEFM analysis

Parameter	Value	Units	Reference
$T$	16.3	mm	(CISC 2007)
$\sigma_y$	350.0	MPa	(CISC 2007)
$\sigma_u$	450.0	MPa	(CISC 2007)
$\sigma_{weld} / \sigma_y$	0.6	-	(Stacey 2000, Walbridge 2008)
$C$	$3.1 \times 10^{-13}$	N, mm	(Walbridge 2008)
$m$	3.0	-	(Walbridge 2008)
$\Delta K_{th}$	80.0	MPa $\cdot\sqrt{\text{mm}}$	(Walbridge 2008)
$a_i$	0.15	mm	(Walbridge 2008)
$a_c$	$T / 2$	mm	(Walbridge 2008)
$a/c$	0.2	-	(Walbridge 2008)



### 6.3.4 Sensitivity Studies of Key Model Parameters for Control Specimen

Due to the high levels of uncertainty associated with the various model parameters, many of which were not measured in this study, sensitivity studies were performed, in order to determine the significance of the various parameters on the analysis results. The reasons that variations in the model parameters can be expected include variations in the: specimen geometry, welding process and quality, and material properties of steel obtained from different sources. Based on previous research (Walbridge 2008), it was determined that the following parameters either vary significantly or have a significant influence on the analysis results: the crack growth constants:  $C$ ,  $m$ , and  $\Delta K_{th}$ , and the crack geometry parameters:  $a_i$  and  $a/c$ . Table 6.2 summarizes values for Paris' crack growth constants ( $C$  and  $m$ ) assumed in various other studies for fatigue fracture in structural steel. Looking at this table, it can be seen that  $C$  typically ranges from  $0.137 \times 10^{-13}$  to  $5.21 \times 10^{-13}$  when units of N

and mm are used;  $m$  ranges from 3.0 to 3.6.

Table 6.2. Values for  $C$  and  $m$  reported or assumed by others

Reference	Steel Type	$C$ (N·mm)	$m$
BS 7910 (1999)	steel in air	$5.21 \times 10^{-13}$	3.0
Hobbacher (2005)	steel	$5 \times 10^{-13}$	3.0
Radaj et al. (1990)	structural	$3 \times 10^{-13}$	3.6
Radaj et al. (1990)	St. 37	$0.137 \times 10^{-13}$	3.3
Bremen (1989)	structural	$4.7 \times 10^{-13}$	3.0
Dubois (1994)	structural	$3.48 \times 10^{-13}$	3.0
Gurney (1979)	structural	$1.83 \times 10^{-13}$	3.0
Bhuyan (1989)	350W	$1.33 \times 10^{-13}$	3.0

To study the effect of varying these parameters on the predicted fatigue behaviour, analyses were repeated for the unreinforced specimen, with  $C$  and  $m$  varied, based on Table 6.2. The results of these analyses are summarized in Figure 6.3.

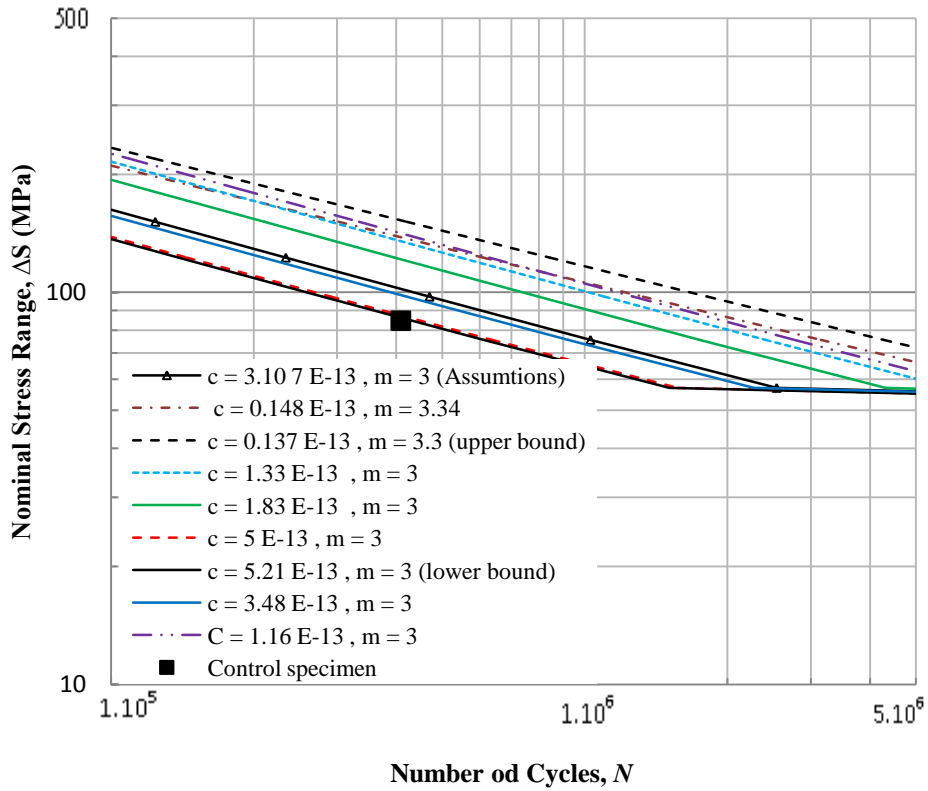


Figure 6.3. S-N curves for various  $C$  and  $m$  values

Looking at Figure 6.3, it can be seen that varying the Paris' crack growth constants ( $C$  and  $m$ ) causes a significant shift in the S-N curve position determined by the fracture mechanics analysis. In general, the S-N curve position shifts downwards as  $C$  is increased. Comparing the envelope of the analysis-based S-N curves with the data point associated with the fatigue test, it is confirmed that the data point falls within the envelope, closer to the lower bound and slightly below the curve associated with the parameter assumptions made for this study.

Table 6.3 summarizes assumptions made for the threshold stress intensity factor range ( $\Delta K_{th}$ ) in various other studies for structural steel. In these references,  $\Delta K_{th}$  is given either as a range, or as a function of the applied stress ratio,  $R$ . For design purposes, it is generally considered safe to under-estimate  $\Delta K_{th}$ . Thus, this parameter is often taken as zero, or the lower bound of the range is used (or the value associated with a high applied stress ratio).

Table 6.3. Values for  $\Delta K_{th}$  reported or assumed by others

Reference	Steel Type	$\Delta K_{th}$ (MPa $\cdot\sqrt{\text{mm}}$ )
BS 7910 (1999)	steel in air	63 ( $R > 0.5$ ) 170 – 214 $\cdot R$ ( $0 \leq R < 0.5$ ) 170 ( $R < 0.0$ )
Hobbacher (2005)	steel	144-190
Bremen (1989)	structural	70-130
Dubois (1994)	structural	100-160

Figure 6.4 shows the results of analyses performed with three values for  $\Delta K_{th}$  assumed: 0, 80, and 160 MPa $\cdot\sqrt{\text{mm}}$ . In these analyses, the originally assumed values for  $C$  and  $m$  were used. Looking at the curves in this figure, it can be seen that changing this parameter has no effect at the higher applied stress ranges. The main influence of this parameter is that it introduces a “constant amplitude fatigue limit”, below which, the predicted fatigue life is infinite.

Comparing the analysis curves with the test data point, it can be concluded that  $\Delta K_{th}$  is likely

less than  $160 \text{ MPa}\cdot\sqrt{\text{mm}}$ . With no additional information available regarding this parameter, the pre-assumed value is retained in the subsequent analyses, as it is thought to be a reasonable estimate of the average value for this parameter, based on experience.

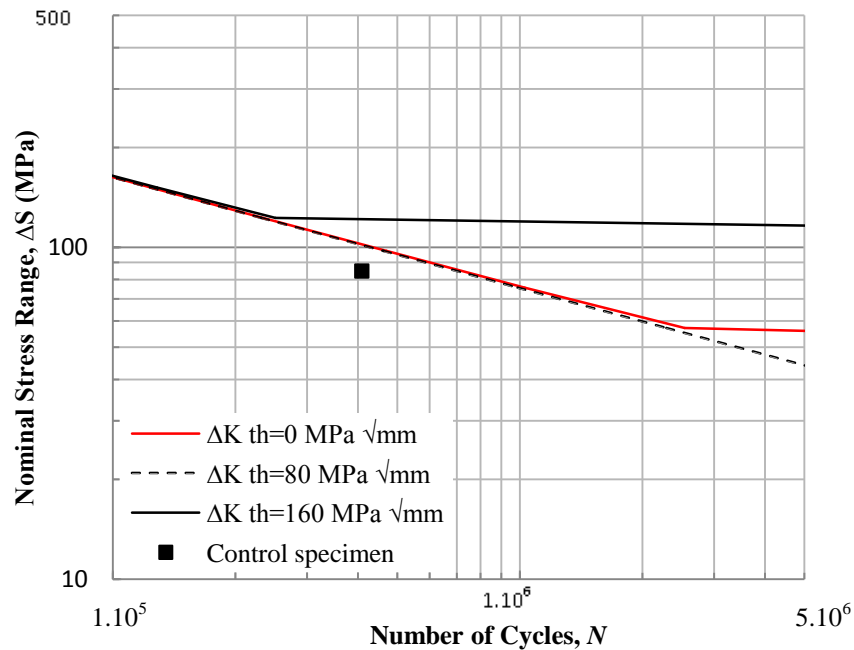


Figure 6.4. S-N curves for various  $\Delta K_{th}$  values

Similar analyses were performed to investigate the effects of the initial crack depth,  $a_i$ , and crack shape,  $a/c$ , on the predicted fatigue behaviour of the unreinforced specimen. The results of these analyses are presented in Figures 6.5 and 6.6. Looking at Figure 6.5, it can be seen that the predicted fatigue life decreases (i.e. the S-N curve shifts downwards) as the assumed initial crack depth increases. In general, however, this shift is small compared to the shift resulting from varying the crack growth constants over their expected ranges. Looking at Figure 6.6, it can be seen that the predicted fatigue life decreases as  $a/c$  decreases. With no measurements available for the initial crack depth and crack shape parameters, typical values

based on the literature review were employed (Walbridge 2006). Although the actual crack parameters applicable to the test specimens may differ, the effect of varying these parameters on the predicted fatigue behaviour is small.

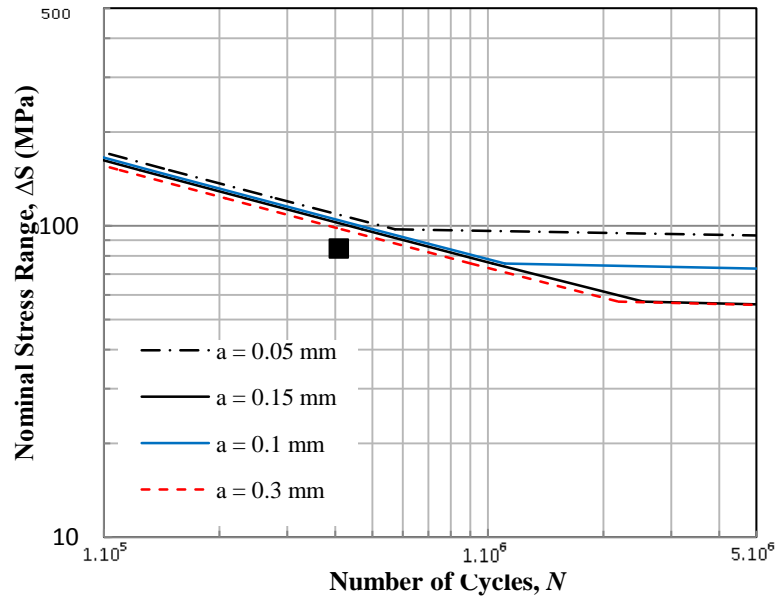


Figure 6.5. S-N curves for various  $a_i$  values

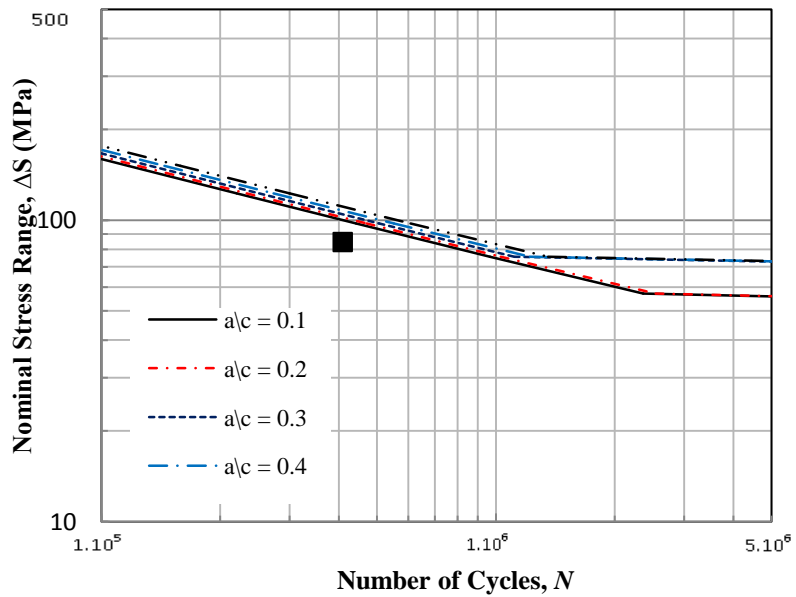


Figure 6.6. S-N curves for various  $a/c$  values

Upper and lower bound S-N curves were derived based on the parameter values in Table 6.4. Analyses were performed using the upper and lower bound values for the various parameters. The results are presented in Figure 6.7. Looking at this figure, it can be seen that the test data point falls between the pre-assumed and lower bound curves. No attempt was made to “fit” the analysis curve to the test data point, since the analytical model employs such a large number of input parameters, and it could not be determined with any certainty, which parameter to calibrate. Nevertheless, the analysis performed with the pre-assumed values for the input parameters gives a reasonable estimate of the test result for the unreinforced specimen. On this basis, the pre-assumed values (Table 6.1) were retained for the subsequent parametric studies.

Table 6.4. Parameters used for upper, lower, and assumed S-N curves derivation

Parameters	$a_i$ (mm)	$a/c$ (mm)	$m$	$C$ (N,mm)	$\Delta K_{th}$ (MPa $\cdot\sqrt{\text{mm}}$ )
Upper bound	0.05	0.5	3.3	$0.137 \cdot 10^{-13}$	160
Lower bound	0.3	0.1	3.0	$5.21 \cdot 10^{-13}$	0.0
Pre-assumed	0.15	0.2	3.0	$3.107 \cdot 10^{-13}$	80

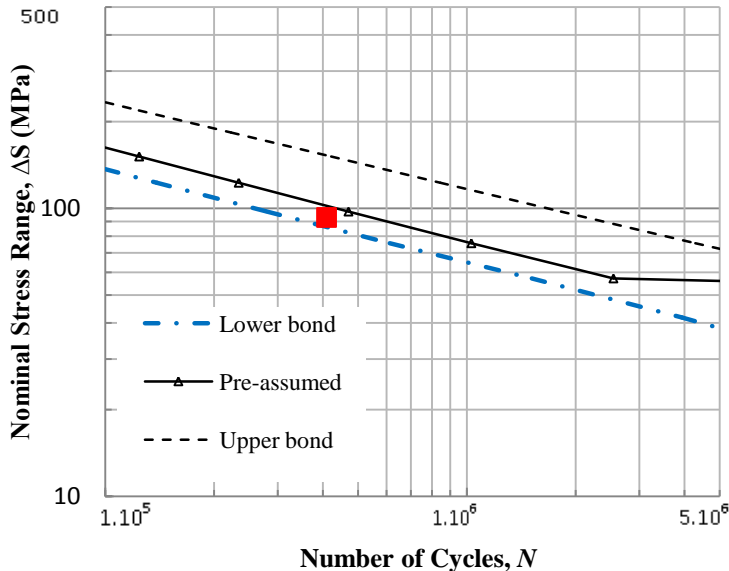


Figure 6.7. The upper, lower and best fit S-N curves

### *6.3.5 Analysis of Retrofitted Specimens using the LEFM Model*

Following the sensitivity studies presented in the previous section, analyses were performed for the reinforced specimens. For these analyses, the compressive stress distributions due to the prestressed CFRP strips obtained by FE analysis, as discussed in Chapter 5, were used to modify the residual stress distributions used in the analysis. The results of these analyses are presented in Figure 6.8. Looking at this figure, it can be seen that, in general, the fatigue life increase due to the CFRP reinforcing is predicted reasonably well by the analysis. Certain trends are also closely predicted. Specifically, the model predicts that the CFRP reinforcing will be more effective if placed on the cover plate, rather than the flange. This is consistent with the general trend observed in the tests. In general, the analysis predicts that the fatigue life increases with the prestressing level. This trend was not systematically observed in the fatigue tests. Based on the analyses presented in this section, it can now be concluded with greater certainty that the reason for this discrepancy is likely the normal statistical scatter inherent to fatigue testing. It is believed that if a larger number of repetitions were performed of each test type, the general trends observed in the analysis results would be apparent in the test results.

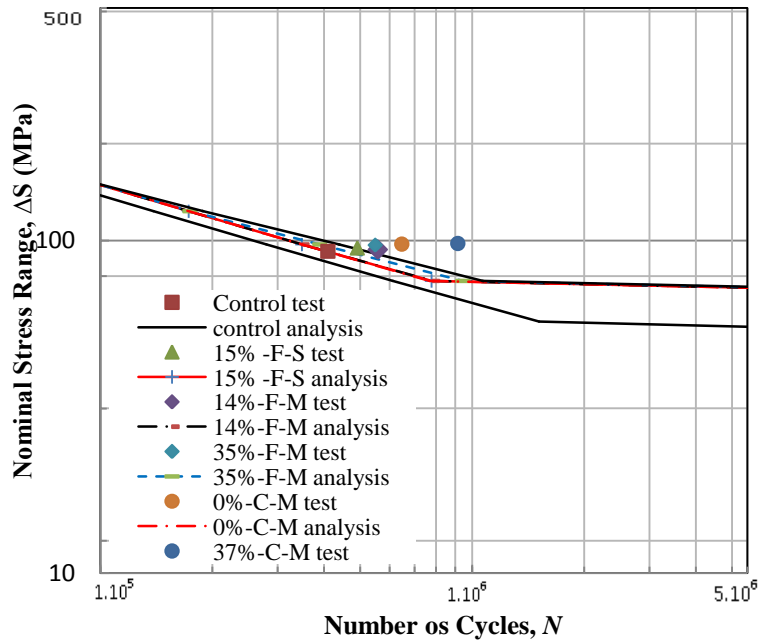
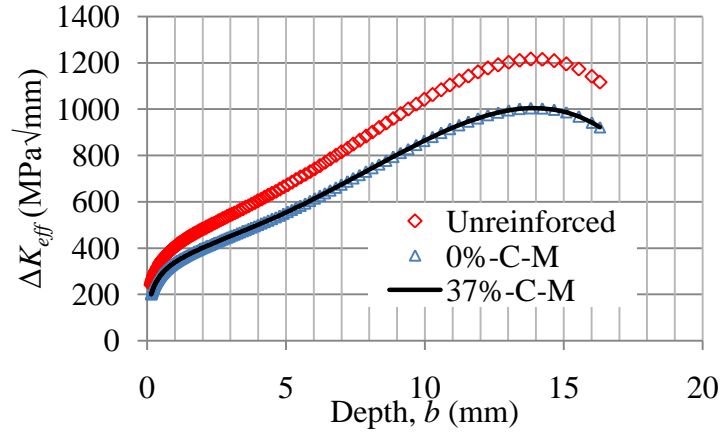


Figure 6.8. Comparison of LEFM analysis and test results

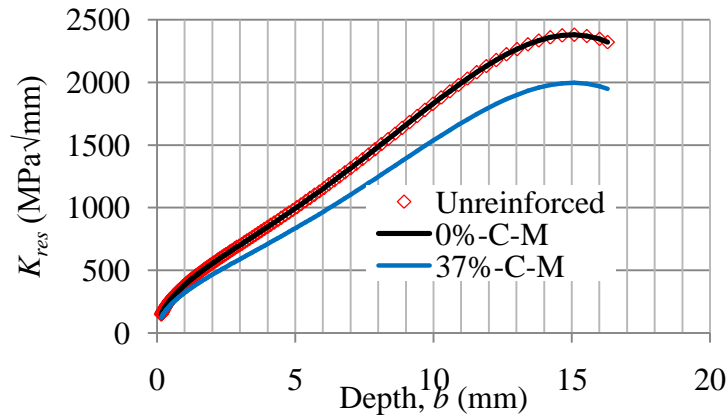
The reinforcement and prestressing effects on the effective stress intensity factor range ( $\Delta K_{\text{eff}}$ ) and the residual intensity factor range ( $\Delta K_{\text{res}}$ ) are presented in Figure 6.9. The  $\Delta K_{\text{eff}}$  and  $\Delta K_{\text{res}}$  curves are plotted for the unreinforced, 0%-C-M, and 37% -C-M cases under an applied load with  $R = 0.1$  and  $\Delta S = 100$  MPa. The  $\Delta K_{\text{eff}}$  curves (Figure 6.9(a)) show that under these loading conditions, most of the fatigue life increase is coming from the addition of the CFRP strips and not the prestressing, since the  $\Delta K_{\text{eff}}$  curves are basically identical for the 0% and 37% prestressing cases. However, the prestressing may also have more pronounced influence on  $\Delta K_{\text{eff}}$  if the residual stress due to welding is lowered to 30%.  $K_{\text{res}}$  is the SIF due to the residual stresses ( $\sigma_{\text{res}}$ ) including welding and prestressing effects calculated based on equation 6.4.

$$K_{\text{res}} = \int_0^a \sigma_{\text{res}}(b) \cdot m(b, a, c) \cdot dx \quad (6.4)$$





(a)  $\Delta K_{eff}$  versus crack depth curves



(b)  $\Delta K_{rds}$  versus crack depth curves

Figure 6.9. Comparison of  $\Delta K_{eff}$  and  $\Delta K_{rds}$  versus crack depth curves

Looking at Figure 6.9(b), it can be seen that the 37% prestressing influences  $K_{res}$ . The result shows that the prestressed specimen has better performance in lower stress ranges and ratios.

## 6.4 Parametric Study with the LEFM Model

### 6.4.1 Applied Stress Range and Ratio

The applied stress range and ratio were studied for the most effective strengthening configuration (strips on the cover plates) to investigate the effects of prestressing on the fatigue life. Analyses were performed for unstressed and 37% prestressed reinforced specimens. The results of these analyses are presented in Figures 6.10 and Figure 6.11. The figures illustrate that the fatigue life increase due to the CFRP reinforcing is predicted reasonably well by the analysis. Certain trends are also closely predicted. Specifically, the model predicts that the CFRP reinforcing will be more effective in the case of lower applied stress range. Regardless of the level of prestressing, the fatigue life goes to infinite when the stress range is lower than 25 MPa. This is consistent with the general trend observed in the tests. In general, the analysis predicts that the fatigue life increases with the prestressing level. This trend was not systematically observed in the fatigue tests. For the prestressed specimen model, the fatigue life increases as the stress ration ( $R$ ) decreases while the stress ratio appears to have no effect for unstressed model specimen.

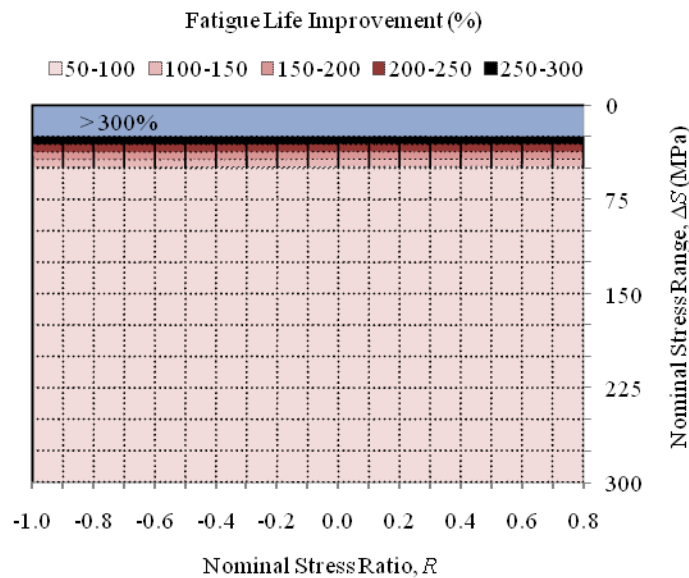


Figure 6.10. Stress range and ratio results for 0%-C-M case

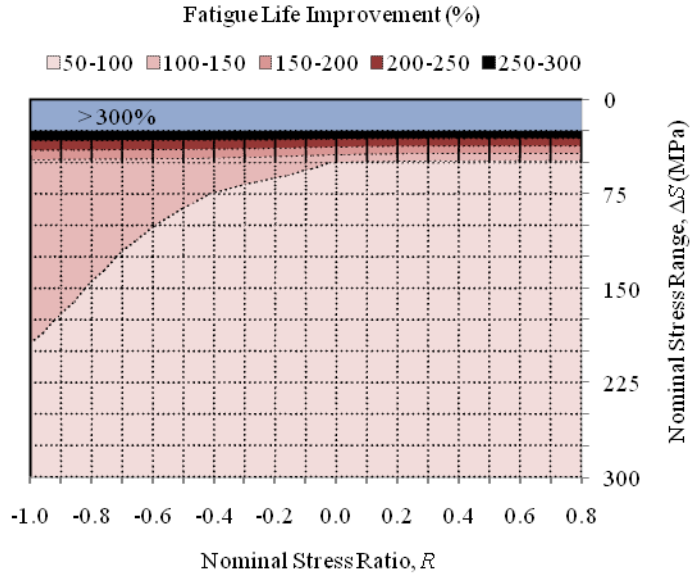


Figure 6.11. Stress range and ratio results for 37%-C-M case

#### 6.4.2 Prestressing Level Study

Figure 6.12 through Figure 6.14 show the results of analyses performed with three values for prestressing assumed: 40%, 60%, and 75%. Looking at the curves in these figures, it can be seen that changing this parameter has an effect at same applied stress ranges and ratios in fatigue life improvement. The fatigue life increases generally as the prestressing level increases. However the effects are more observable for the case with higher prestressing level (75%-C-M).

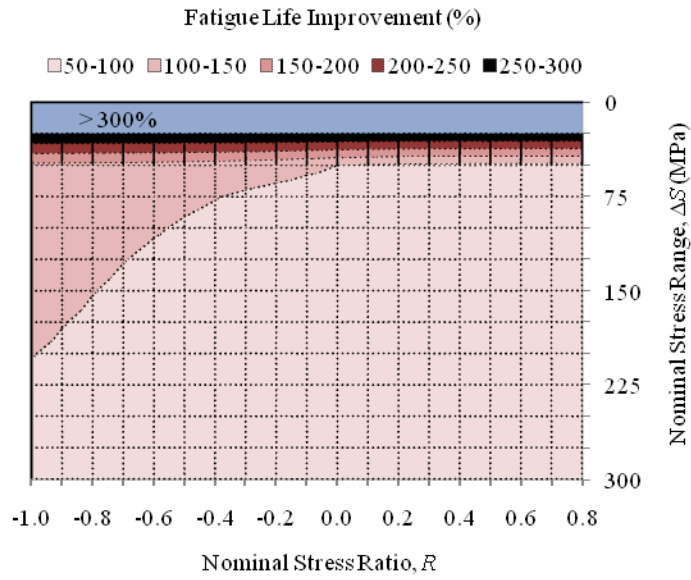


Figure 6.12. Stress range and ratio results for 40%-C-M case

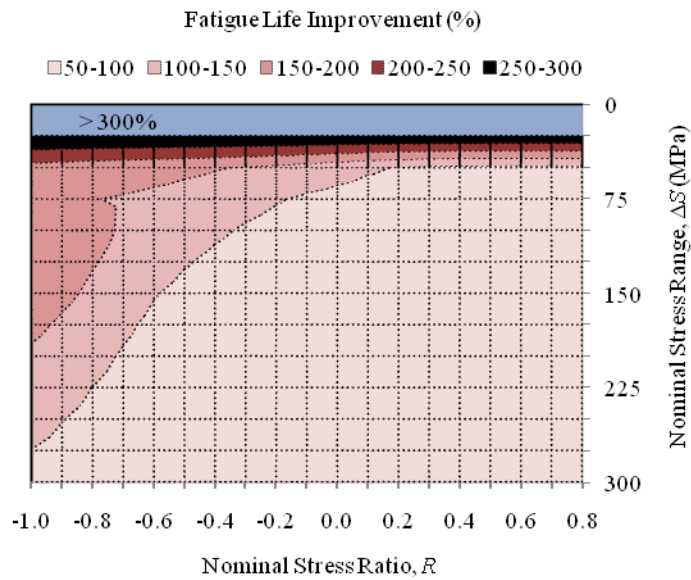


Figure 6.13. Stress range and ratio results for 60%-C-M case

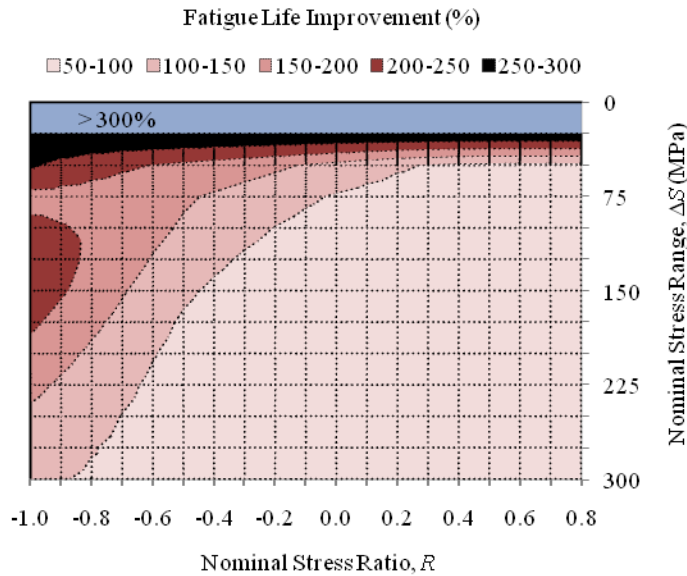


Figure 6.14. Stress range and ratio results for 75%-C-M case

#### 6.4.3 Analysis of Full-Scale Retrofitted Girder

Following the studies presented in the previous sections, analyses were performed for full-scale reinforced specimens. For these analyses, the compressive stress distributions due to the prestressed CFRP strips obtained by FE analysis, as discussed in Chapter 5, were used to modify the residual stress distributions obtained in the analysis. Two full-scale girders with retrofitted using M- CFRP strips bonded on the cover plates with 40% prestressing were considered. Similar materials and strengthening configurations applied previously were used to model the girders with 600 mm and 900 mm depth, respectively. The results of these analyses are presented in Figure 6.15 and Figure 6.16. The figures depict that the prestressing is still effective. Although the prestressing effect on fatigue life improvement for the larger

girder size is not as much as for the smaller girder size; nevertheless, the fatigue life increase due to the CFRP reinforcing is predicted reasonably well by the analysis.

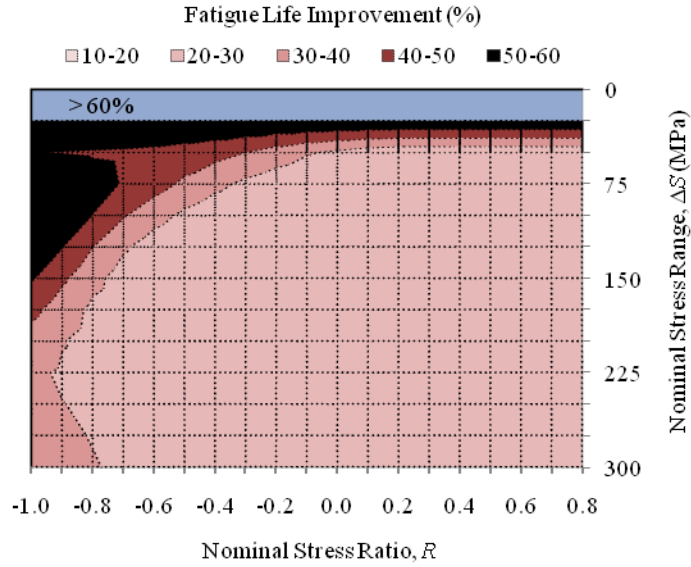


Figure 6.15. Results of full-scale retrofitted girder analysis ( $d = 600$  mm, 40%-C-M)

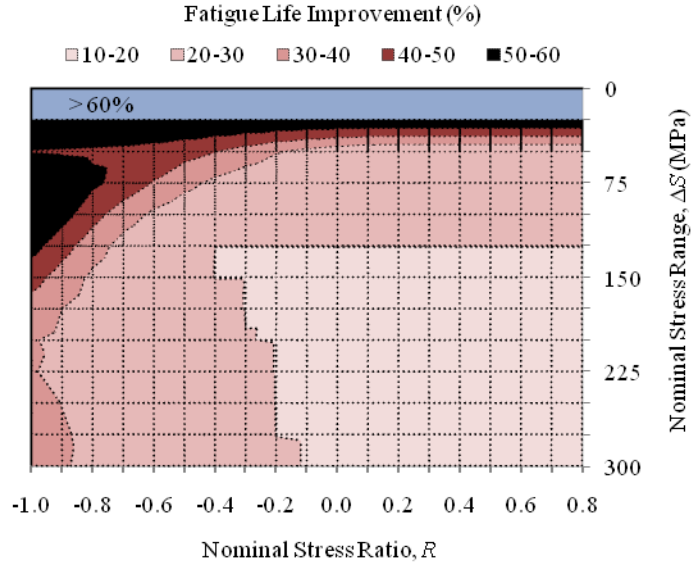


Figure 6.16. Results of full-scale retrofitted girder analysis ( $d = 900$  mm, 40%-C-M)

## **Chapter 7: Summary and Conclusions**

### **7.1 Summary**

The main objective of this study has been to evaluate the use of CFRP composite materials in strengthening steel girders. This included strengthening intact members using unstressed and stressed CFRP strips to increase their fatigue life. Both experimental and theoretical investigations have been carried out. In principle, the study demonstrates the potential of this strengthening technique. Also, the findings of this research program will enable engineers to make more informative decisions regarding the retrofitting of steel girders using prestressed, adhesively bonded CFRP strips and will assist in the development of reliable design guides.

The experimental investigation comprised two parts. Part one included the prestressing procedure. Five steel W-sections were strengthened using different configurations and modulus of CFRP strips. In the second part, the prepared specimens and control specimen were tested in cyclic four-point bending until fatigue failure. The study considered the effects of CFRP strip-type, location, and prestressing level on fatigue life.

Analytical and numerical models were developed and validated by comparison with the test data. The numerical (finite element) model was applied to investigate the stress distribution at the weld toe and bond behaviour at the end of the bond length. The analytical model was used to investigate the elastic cross section and bond behaviour. At the end of study, a LEFM analysis was employed to predict the fatigue life of each specimen. The models were then used in parametric studies to examine a wider range of parameters including other prestressing levels and girder depths.

## 7.2 Conclusions

### *7.2.1 Prestressing and Prestressing Force Release Procedures*

1. The simple gripping system is reliable for prestressing the CFRP strips up to 37% of the ultimate strength of the CFRP strip, using sandpaper to increase the friction between the steel plates and strips.
2. A proper surface preparation consisting of sandblasting the steel surface and wiping the CFRP strip surface with acetone prior to apply the epoxy is essential for achieving adequate bond behaviour.
3. The prestressing force should be released very slowly to avoid debonding.
4. Based on a numerical study, it is concluded that the debonding is caused by excessive peel stresses occurring within 2 mm from the bond end. The use of a physical clamp is shown to be a viable way of mitigating this debonding.
5. At load release, the prestress force transfers to the beam through the bond. The length required for this transfer to take place is known as the transfer length. This length varies, depending on the level of prestressing. The lowest transfer length was seen for specimen 14%-F-M to be equal to 150 mm and the greatest transfer length belonged to specimen 35%-F-M and was equal to 400 mm. The development length was far from the critical fatigue detail, and thus, did not play a role in the fatigue behaviour of the specimens. In practice, however, the transfer length should be kept in mind when designing prestressed CFRP reinforcements.



6. Most of the time dependent losses, including losses due to creep of the epoxy and elastic shortening of the steel beam, occurred within three days from load release. After three days, no noticeable losses were observed.
7. The cambers produced by the prestressed CFRP strips were very small, ranging from 0.05 mm to 0.113 mm, based on the measured strain data.

### *7.2.2 Fatigue Tests and Analytical Studies*

1. The M-CFRP strips increased the fatigue life of the investigated fatigue detail by 58% and 125% in the cases of unstressed and 37% prestressed CFRP strips located on the cover plates, respectively. A 41% fatigue life improvement was achieved for the specimen with 35% prestressed CFRP strips on the flange in this experimental study.
2. The M-CFRP strips were more effective than the S-CFRP strips in improving fatigue performance of the examined cover plate detail.
3. The location of the CFRP reinforcing strips was found to have a significant impact on the fatigue life. The beams with strips located on the cover plates showed a greater fatigue life improvement than those with strips located on the flange.
4. The control girder failed by flange fracture and crack growth from the weld toe towards the web. In the strengthened girders with the CFRP strips on the flange, debonding after 99.5% of fatigue life was followed by a rapid failure for the specimens strengthened with CFRP strips on the flange. Whereas the failure of the specimens strengthened with CFRP

strips on the cover plates involved crack growth through the flange thickness and into the web, followed by fracture of the beam and rupture of the strips.

5. Parametric studies using the validated LEFM model showed that the effectiveness of the CFRP strips is increased by prestressing the CFRP strip to a level of 37%. However higher prestressing can enhance the fatigue life even further.
6. Reinforcement using prestressed CFRP strips applied on the cover plates not only increased the fatigue life but also upgraded the detail category of girder from Detail Category E to D without additional welding or bolting.
7. The prestressed CFRP reinforcing effectiveness was seen to reduce as the girder depth was increased (if the area of CFRP is held constant), up to a certain depth, beyond which the reinforcing effectiveness is constant.
8. The residual stress due to the welding process decreases the beneficial effects of the CFRP prestressing. In the case of large-scale structures with higher residual stress levels due to the fabrication process, higher prestressing levels are essential.

### **7.3 Recommendations for Future Work**

The research work described in this thesis on the strengthening of steel girders using prestressed CFRP strips has demonstrated the potential of this approach. A number of major achievements have been accomplished in terms of developing a thorough understanding of the behaviour, failure modes, and modelling. Future research however, still needs to be carried out, however, on the following areas:

1. Optimization of the prestressing procedure and the development of an independent prestressing device, prestressing force release and end clamp arrangement are necessary.
2. A study on the effect of prestressed CFRP strips on delaying fatigue failure of steel girders or plates with different welding and stiffeners configurations is needed.
3. To investigate size effects, fatigue testing of large-scale steel-concrete composite girders strengthened or repaired using prestressed CFRP strips with various reinforcement ratio and prestressing levels would be of great interest.
4. A study of the effect of using prestressed CFRP strips on the behaviour of already fatigue damaged bridge girders is recommended.
5. Examination of the behaviour of CFRP-retrofitted girders under combined service loads and environmental conditions, including moisture and severe temperature gradient exposures is recommended.
6. The establishment of comprehensive design guidelines for steel girders strengthened using prestressed CFRP material would be made possible with the completion of the other future work items listed in this section.

## References

- Aalami, B.O. (1990), " Load Balancing: A Comprehensive Solution to Post-Tensioning.",  
Journal of Structures, ACI, 87(6): 662-670.
- Albat AM, Romilly DP. (1999), "A direct linear-elastic analysis of double symmetric  
bonded joints and reinforcements.", Composite Science Technology, (59): 1127–  
1137.
- Al-Saidy A. H., Klaiber F. W., and Wipf T. J.(2004), " Repair of Steel Composite Beams  
with Carbon Fibre-Reinforced Polymer Plates", Journal of Composites for  
Construction, ASCE, 8(2): 163–172.
- Allan R. C., Bird J., and Clarke J. D. (1988), " Use of Adhesives in Repair of Cracks in  
Ship Structures.", Journal of Materials Science and Technology, 4(10): 853-859.
- Armstrong K. B. (1983), "Carbon Fibre Fabric Repairs to Metal Aircraft Structures.",  
Third Technology Conference on Engineering with Composites, London,  
England, SAMPE European Chapter, 8.1-8.12
- Bakht B., Sweeney R. A. P., Saunders W. W., Yule R. B., Byers W. G., Mosese F.,  
McKeel W. T., Higgins M., Kahn L., and Heins C. P. (1979), "Repair and  
Strengthening of Old Steel Truss Bridges." American Society of Civil Engineers,  
New York.
- Benachour A., Benyoucef S., Tounsi A., Adda bedia E.A. (2008), " Interfacial stress  
analysis of steel beams reinforced with bonded prestressed FRP plate. ", Journal  
of Engineering Structures, (30): 3305-3315.

- Bhuyan G. S., Swamidas A. S. J. and Vosikovsky O. (1989), "Influence of environmental and mechanical variables on fatigue crack growth rates in CSA G40.21M 350 WT steel.", *International Journal of fatigue*, 88(010037): 0142-1123.
- Bisby L. A. (2003), "Fire Behaviour of FRP Reinforced or Confined Concrete.", PhD. Thesis, Department of Civil Engineering, Queen's University, Kingston, Ontario, Canada.
- Bremen U. (1989), "Amelioration du Comportement a la Fatigue D'assemblages Soudes: Etude et Modelisation de L'effet de Contraintes Residuelles.", These No. 787, Ecole Polytechnique de Lausanne, Lausanne.
- Brook D. (1982), "Elementary Engineering Fracture Mechanics.", Published by Martinus Nijhoff Publishers, The Hague. ISBN 90-247-2580-1
- Brown A. R. G. (1974), "The Corrosion of CFRP-to-Metal Couples in Saline Environments.", *Proceedings of the 2nd International Conference on Carbon Fibres*, London, England February 18(20): 230-241.
- BS 7910. (1999), "Guide on methods for assessing the acceptability of flaw in metallic structures.", *British Standard*. ICS 25.160.40.
- Cadei J.M.C., Stratford T.J., Hollaway L.C. & Duckett, W.G. (2004), "Strengthening Metallic Structures using Externally Bonded Fibre-Reinforced Polymers.", London, England: CIRIA.

- Chandrupatla R. T., Belegundu A. D. (2002), "Introduction to Finite Elements in Engineering.", 2nd Ed., Prentice-Hall, ISBN 0-13-061591-9.
- Colombi P., Bassetti A, Nussbaumer A. (2003), "Analysis of Cracked Steel Members Reinforced by Pre-stress Composite Patch.", *Journal of Fatigue and Fracture of Engineering Materials Structures*, 26: 59–66.
- Dawood M., Rizkalla S. (2006), " Bond and Splice Behaviour of CFRP Laminates for Strengthening Steel Beams.", *Third International Conference on FRP Composites in Civil Engineering (CICE)*, December 13-15 2006, Miami, Florida, USA.
- Dawood M. (2005), "Fundamental Behaviour of Steel–Concrete Composite Beams Strengthened with High Modulus Carbon Fibre Reinforced Polymer (CFRP) Materials.", Master's thesis, North Carolina State University, Raleigh (NC).
- Deng J., Marcus M.K. (2007), "Fatigue Performance of Metallic Beam Strengthened with a Bonded CFRP Plate.", *Journal of Composite Structures*, 78 (2007): 222–231.
- Dowling, N. (2009), "Mechanical Behaviour of Materials.", (4th Ed.), 912p, ISBN-13: 9780131863125.
- Dubois V., (1994), "Fatigue de Détails Soudés Traités Sous Sollicitations D`amplitude Variable.", These No. 1260, Ecole Polytechnique de Lausanne, Lausanne.
- Fam A., Witt S., and Rizkalla S. (2006), "Repair of Damaged Aluminum Truss Joints of Highway Overhead Sign Structures using FRP.", *Construction and Building Materials*, 20 (10): 948-956.

- Fawzia S., Al-Mahaidi R., Zhao X.L., Rizkalla S. (2007), "Strengthening of Circular Hollow Steel Tubular Sections using High Modulus CFRP Sheets.", *Construction and Building Materials* 21: 839–845.
- Grabovac I., Bartholomeusz R. A., and Baker A. A. (1991), "Fibre Composite Reinforcement of Metallic Plates of Varying Thickness and Contour.", *International Conference of Aircraft Damage Assessment and Repair*, Melbourne, Australia, 26(28): 231-238.
- Gurney T.R. (1979), "Fatigue of Welded Structures", Text book, Second edition, ISBN1 0521 22558 2.
- Haghani R., Al-Emrani M., Kliger R. (2008), "Interfacial Stress Analysis of Geometrically Modified Adhesive Joints in Steel Beams Strengthened with FRP Laminates.", *Journal of Construction and Building Materials*, 10(1016): 1413–1422.
- Hart-Smith LJ. (1973), "Non-classical adhesive-bonded joints in practical aerospace construction.", Technical Report NASA CR-112238, NASA; January 1973.
- CISC (2007), " Limit State Design of Steel Structures.", *Handbook of steel Construction*, Ninth Edition, ISBN 978-0-88811-124-1.
- Hanel J. J. (1975), "Crack Propagation in Single and Multistage Cyclically Loaded Plates, Taking Special Account of Partial Crack Closure.", (German), Report 27, publi .Institu. fur statik und stahlbau, TH Darmstadt.

- Hashim S. A. (1999), "Adhesive Bonding of Thick Steel Adherents for Marine Structures.", *Marine Structures*. 12, 405-423.
- Hobbacher A. (2005), "Recommendations for Fatigue design of Welded Joints and Components.", International Institute of Welding, IIW document XIII-1965-03 / XV-1127-03.
- Hollaway I. C. and Cadei J., Maunsell F., Beckenham (2002), "Progress in the Technique of Upgrading Metallic Structures with Advanced Polymer Composites.", *Journal of Progressing Structural Engineering Material*, 4: 131–148.
- Hoult, N., Sherwood, E.G., Bentz, E. and Collins, M.P. (2008), "Does the Use of FRP Reinforcement Affect the One-Way Shear Behaviour of Reinforced Concrete Slabs? ", *Journal of Composites for Construction*, ASCE, 12( 2): 125-133.
- Hwegler G., Berset T. (2000), "The use of Prestressed CFRP-Laminates as Post-Strengthening.", Paper presented at the 16th Congress of IABSE Luzern, Switzerland September 18(21): 200-240.
- Jones S. C. J. and Civjan S. A. (2003), "Application of Fibre Reinforced Polymer Overlays to Extend Steel Fatigue Life.", *Journal of Composites for Construction*, ASCE, 7(4): 331–338.
- Karbhari V. M., and Shulley S. B. (1995), "Use of Composites for Rehabilitation of Steel Structures – Determination of Bond Durability.", *Journal of Materials in Civil Engineering*, ASCE, 7(4): 239-245.



- Kulak G.L. and Smith I.F.C. (1993), "Analysis and Design of Fabricated Steel Structures for Fatigue: A Primer for Civil Engineers.", Structural Engineering Report, University of Alberta No. 190. July 1993.
- Kulak G.L. and Grondin G.Y. (2002), "Limit States Design in Structural Steel, Canadian Institute of Steel Construction.", Alliston, Ontario, Canada 63. Lam, C.C.A.,
- Linghoff D., Haghani R., Al-Emrani M. (2008), "Carbon-fibre Composites for Strengthening Steel Structures.", Journal of FRP Strengthened Metallic Structures, ASCE, 47( 10): 1048-1058.
- Liu. H.B., Zhao X.L and Al-Mahaidi R. (2005), "The Effect of Fatigue Loading on Bond Strength of CFRP Bonded Steel Plate Joints.", International Institute for FRP in Construction (BBFS).
- McClung R.C., (1989), "Finite element analysis of specimen geometry effects on fatigue crack closure. Fatigue and mechanics.", Proceedings of the JSCE. (1): 13-21.
- Miller T. C. Michael J., Mertz D. R. and Hastings J. N. (2001), "Strengthening of a Steel Bridge Girder using CFRP Plates.", Journal of Bridge Engineering, ASCE, 6( 6): 0514–0522.
- Monfared A., Soudki K., and Walbridge S. (2008), " CFRP Reinforcing to Extend the Fatigue Lives of Steel Structures.", Fourth International Conference on FRP Composites in Civil Engineering (CICE2008), Zurich, Switzerland.

- Monin V.I., Grova T., Castello X., Stefen S.F. , (2008), "Analysis of residual Stress State in Weld Steel plates by X-RAY Diffraction Method.", Journal of Revelation in Advance Materials , SCI, 19(2009): 172-175.
- Naaman A. E., (2004), " Prestressed Concrete Analysis and Design.", Text Book, Second Edition, Techno Press 3000, ISBN 0-9674939-1-9.
- NDS, (2005), "Beam Design Formulations with Shear and Moment Diagrams.", National Design Specification for Wood Construction, American Wood Council, Edition 2005.
- Newman J.C., (1994), "A Crack Opening Stress Equation for Fatigue Crack Growth.", International Journal of Fracture, 24(1994): R131-R135.
- Nordin H. (2005), "Strengthening Structures with Externally Prestressed Tendons.", Luleå University of Technology. Technical Report.
- Nozaka K., Shield K. C. and Hajjar J. F. (2005), "Effective Bond Length of Carbon-Fibre-Reinforced Polymer Strips Bonded to Fatigued Steel Bridge I-Girders .", Journal of Bridge Engineering, ASCE, 10(2): 2–195.
- Nozaka K., Shield K. C. and Hajjar J. F. (2004) ," Repair of Fatigued Steel Bridge Girders with Carbon Fibre Strips", Technical Report Published by Minnesota Department of Transportation Office of Research Services, February 2004.
- Paradowskaa A.M., Price J.W.H, Ibrahim R., Finlayson T.R., (2006), "The effect of heat input on residual stress distribution of steel welds measured by neutron

diffraction.", *Journal of Achievements in Materials and Manufacturing Engineering*, AMME, 17(2): 385–388.

Paris P. and Erdogan F., (1963), "A critical analysis of crack propagation laws.", *Journal of Basic Engineering*, Transactions of the American Society of Mechanical Engineers, 528-534.

Phares B. M., Wipf T. J., Klaiber F., Abu-Hawash A., Lee Y. (2003), " Strengthening of Steel Girder Bridges Using FRP.", *Mid-Continent Transportation Research Symposium*, Ames, Iowa, August 2003.

Radaj D. and Sonsino S. M., (1990), "Design and Analysis of Fatigue Resistant Welded Structures.", Text book, Abington Publishing, ISBN1 85573 0049.

Roy S., (2006), "Experimental and Analytical Evaluation of Enhancement in Fatigue Resistance of Welded Details Subjected to Post-Weld Ultrasonic Impact treatment.", PhD Thesis, Lehigh university, January 2006.

Schnerch, D. (2005), "Strengthening of Steel Structures with High Modulus Carbon Fibre Reinforced Polymer (CFRP) Materials.", Ph.D. dissertation, North Carolina State University, Raleigh, North Carolina.

Schnerch, D., Dawood, M., Rizkalla, S., and Sumner, E. (2007), "Proposed Design Guidelines for Strengthening of Steel Bridges with FRP Materials.", *Construction and Building Materials*, 21(5): 1001-1010.

- Schnerch, D., Dawood, M., Rizkalla, S., Sumner, E., and Stanford, K. (2006), "Bond Behaviour of CFRP Strengthened Steel Structures.", *Advances in Structural Engineering*. 9 (6): 805-817.
- Schwegler G., Berset T. (2000), "The Use of Prestressed CFRP-Laminates as Post-Strengthening", 16th Congress of IABSE, Luzern, Switzerland, September 18-21
- Sen R., Liby L. and Mullins G. (2001), "Strengthening Steel Bridge Sections Using CFRP Laminates.", *Journal of Composites*, part B (32): 309-322.
- Shen G. and Glinka G., (1991), "Weight functions for a surface semi-elliptical crack in a finite thickness plate.", *Journal of Theoretical and Applied Fracture Mechanics*, 15 (1991): 247-255.
- Shulley S. B., Huang X., Karbhari V. M. and Gillespie J. W. (1994), "Fundamental Consideration of Design and Durability in Composite Rehabilitation Schemes for Steel Girders with Web Distress.", *Proceedings of the Third Materials Engineering Conference*, San Diego, California, November 13(16): 1187-1194.
- Sika Canada Inc. (2009), "Carbon fibre laminate for structural strengthening.", *Product Data Sheet*, Edition 07.2009, CSC Master Format 03 01 30.
- Stacey A., Barthelemy J.Y., Leggatt R.H., Ainsworth R.A. (2000), "Incorporation of Residual Stresses into the SINTAP Defect Assessment Procedure.", *Engineering Fracture Mechanics*, 67 (2000): 573-611.

- Täljsten B., Skodborg C., Schmidt J. W. (2008), "Strengthening of Old Metallic Structures in Fatigue with Prestressed and Non-Prestressed CFRP Laminates.", *Journal of Construction and Building Materials* 23(2009): 1665–1677.
- Tavakkolizadeh, M., and Saadatmanesh, H. (2003a), "Repair of Damaged Steel-Concrete Composite Girders Using Carbon Fibre Reinforced Polymers Sheets.", *Journal of Composites for Construction*. ASCE, 7(4): 311-322.
- Tavakkolizadeh M., and Saadatmanesh H. (2003b), "Fatigue Strength of Steel Girders Strengthened with Carbon Fibre Reinforced Polymer Patch.", *Journal of Structural Engineering*, ASCE, 129( 2): 186–196.
- Tavakkolizadeh, M., and Saadatmanesh, H. (2001), "Galvanic Corrosion of Carbon and Steel in Aggressive Environments.", *Journal of Composites for Construction*. ASCE, 5(3): 0200–0210.
- Throop J. F. and Miller G. A. (1970), "Optimal Fatigue Crack Resistance," ASTM STP 467, American Society for Testing and Materials, Philadelphia.
- Walbridge S. (2008), "Fatigue Analysis of Post-Weld Fatigue Improvement Treatments Using a Strain-Based Fracture Mechanics Model", *Engineering Fracture Mechanics*, (75): 5057-5071.
- Wolf E. (1971), "The significance of crack closure, damage tolerance in aircraft structures.", *Journal of American Society for Testing of Materials*, ASTM STP, vol. 486.

US Research Laboratory, Composite materials handbook (2002), "Polymer matrix composites, materials usage, design, and analysis.", volume 3. US Army Research Laboratory.

Zhao X., Zhang L. (2006), "State-of-the-Art Review on FRP Strengthened Steel Structures ", Journal of engineering structures, 29 : 1808–1823.

Zheng Y., Ye L., Lu X., Yue Q. (2006), "Experimental Study on Fatigue Behaviour of Tensile Steel Plates Strengthened with CFRP Plates.", Third International Conference on FRP Composites in Civil Engineering (CICE 2006), December 13-15 2006, Miami, Florida, USA.

## Appendix A

### A.1 Material Mechanical Properties

The stress-strain diagrams for the M-CFRP and S-CFRP strips are plotted in Figure A.1 and Figure A.2 based on the applied prestressing force and the strain measured during prestressing. From these figures the elastic modulus values are determined to be equal to 165570 MPa and 209410 MPa for the S-CFRP and M-CFRP strips, respectively. These values are in agreement with the material supplier's data sheet.

Poisson's ratio of the CFRP strip was also determined using measurements from longitudinal and transverse strains on the strip during prestressing. The slope of the curve shown in Figure A.3 is the Poisson's ratio of M-CFRP and S-CFRP strips and it is equal to 0.3136.

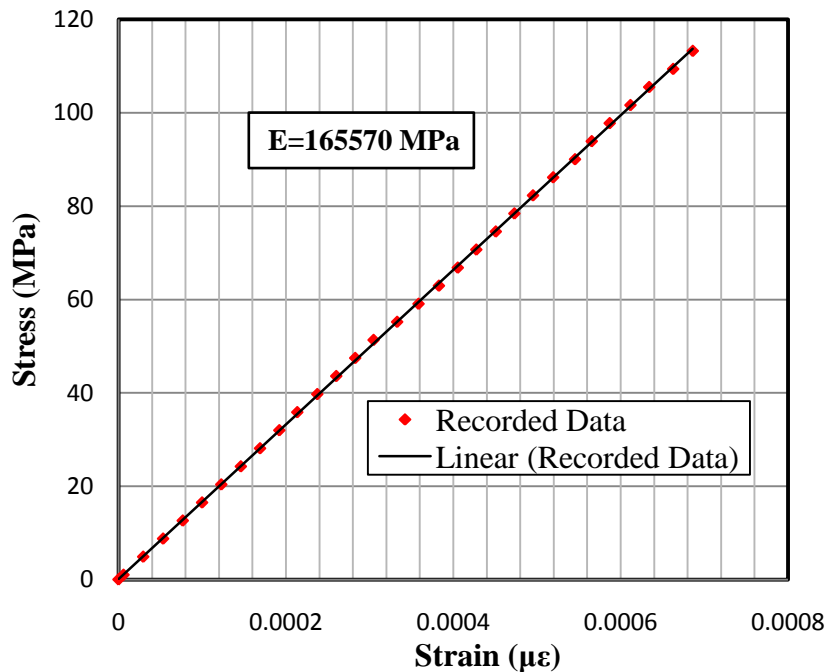


Figure A.1. Elastic modulus calculation based on stress-strain diagram for S-CFRP strip

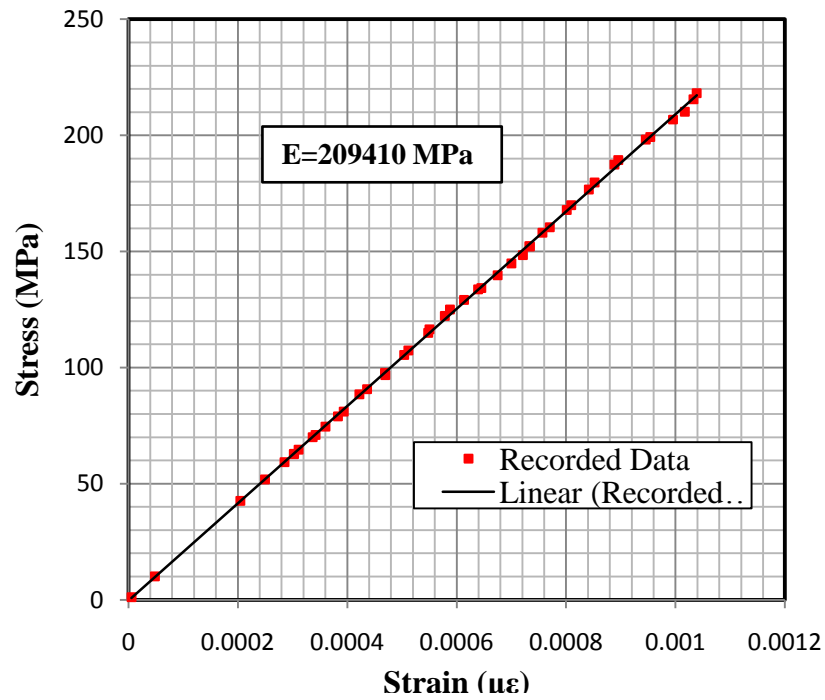


Figure A.2. Elastic modulus calculation based on stress-strain diagram for S-CFRP strip

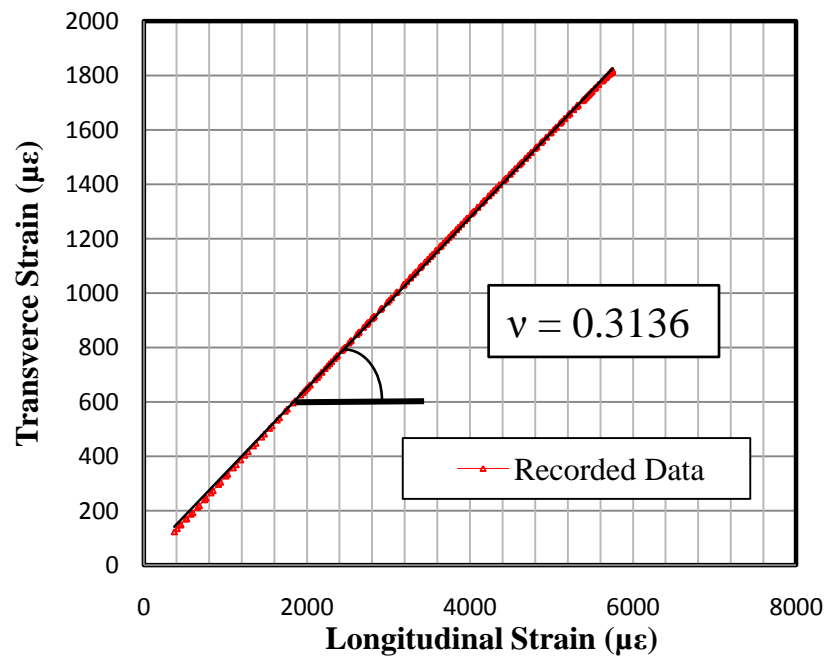


Figure A.3. Poisson's ratio calculation for S-CFRP and M-CFRP strips



## A.2 Gripping Tests

The gripping system was initially tested in a vertical tension test, as shown in Figure A.4. The value of the bolt tightening force to ensure minimal sliding was considered the main goal of this test. Two types of CFRP strips, S512 and M514 were tested. A 556 mm long standard modulus (S512) strip was tested first. Then, the gripping system was examined using the same length of high modulus (M514) strip.

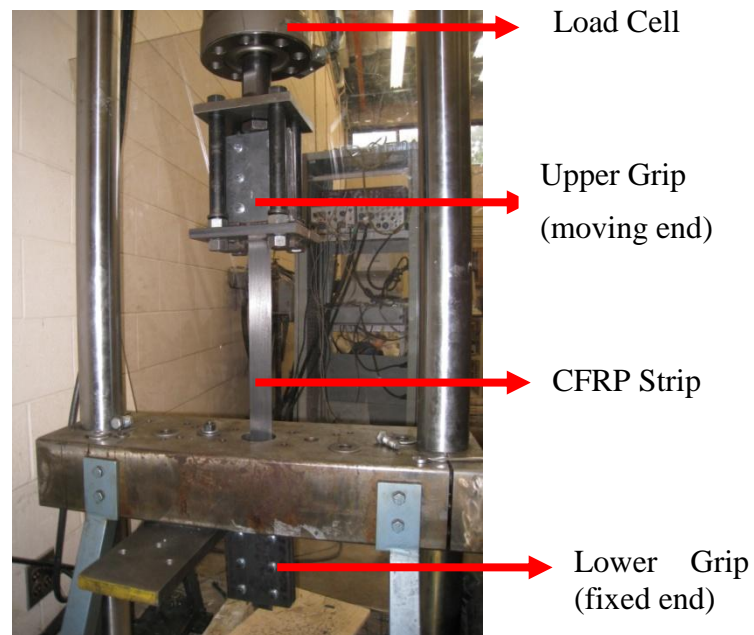
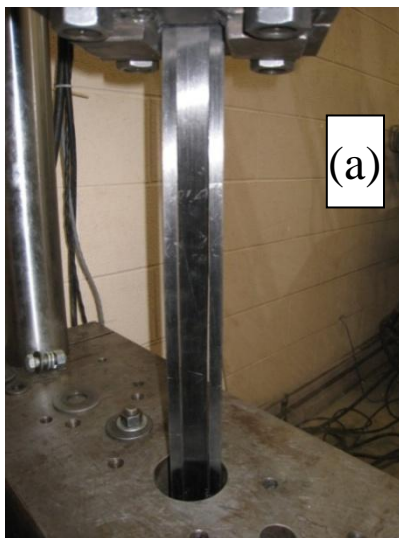


Figure A.4. Gripping test setup

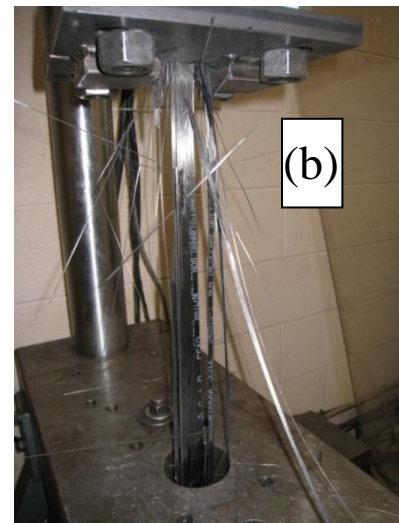
### A.2.1 Observations

The load was applied to the strip by moving the upper end upward. Increase of the applied load to the CFRP strip was transferred to the interface of steel plates, aluminum plates, and strips as shear stress resisted by the interfacial friction between the surfaces. The bolt tightening force played a significant role in the performance of the gripping system. Higher

levels of applied pressure to the strips by additional tightening of bolts can increase the interfacial friction but can also produce a camber at the steel plates, introducing a non-uniform pressure distribution. Consequently, a premature failure of slippage can result as shown in Figure A. 5(a). Since the pressure at both edges of the strip was higher than that at the center, the middle part of the strip, where the pressure was less than at the edges, started to slide. On the other hand, a proper use of annealed aluminum plates to prevent strip crushing and adequate tightening force can lead to the best results. Figure A.5 (b) illustrates a combined failure mode of sliding and strip crushing with the maximum applied load. In Figure A.6 the black marks on the aluminum plates show the location of sliding at the strip edges. In spite of better pressure distribution, the sliding was due to non-uniform pressure distribution that still exists. It could be mitigated using very thick steel plates. However, because of practical difficulties with the prestressing set up such as weight and workability, the minimum steel plate thickness and size was chosen.



(a) Premature sliding



(b) Combination of sliding and strip fracture

Figure A.5. Failure of gripping test

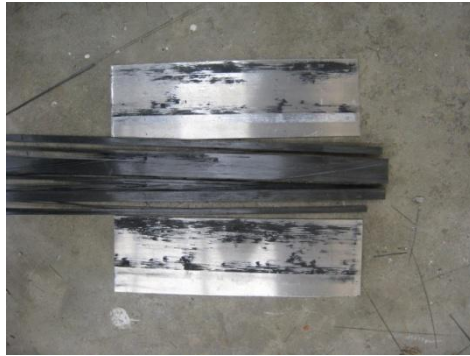


Figure A.6. Sliding at the edges

The proper tightening force should be about 25.5 kN for each bolt. This tightening force was applied using a calibrated torque wrench. According to the manufacture's data sheet, to achieve a 25.5 kN tightening force, a torque of 70 lb-ft should be applied. The anchorage configuration and the load applied using a torque wrench is shown in Figure A.7.

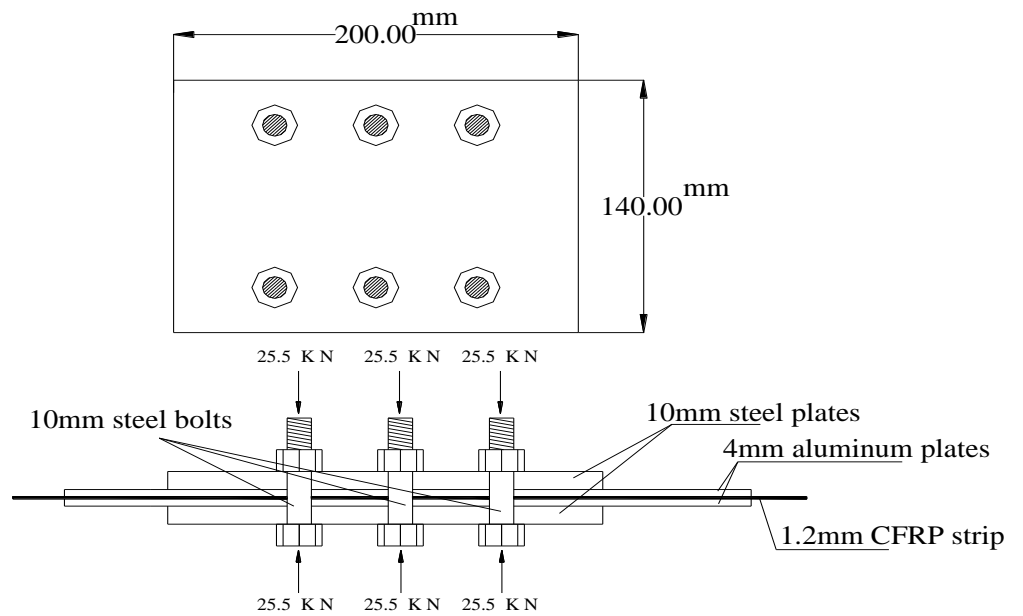


Figure A.7. A schematic view of gripping

### A.2.2 Load vs. Displacement Behaviour

Load versus displacement diagrams are drawn based on the gripping test results shown in Figure A.8. The maximum applied load without any sliding tends to be sufficient for the required prestressing force. The greatest required prestressing load was about 60% of the ultimate load resistance of the CFRP strip. Thus, the minimum applied load, without any sliding, tended to be equal to 60% of the ultimate strip load bearing capacity. 95.7 kN of applied load for the test using S512 strip compared to its ultimate load bearing capacity of 168.3 kN resulting in a satisfactory condition. Likewise with the M514 strip, the maximum load was about 117.5 kN that was about 66.6% of ultimate strip load bearing capacity equal to 176.4 kN. Perfect elastic behaviour for both tests up to the sliding point (point A) revealed a perfect anchorage performance while inelastic behaviour was observed after sliding. At the point of partial strip fracture, a dramatic drop in the load-displacement curves was observed, meaning that the strip could not take any more loads (point B).

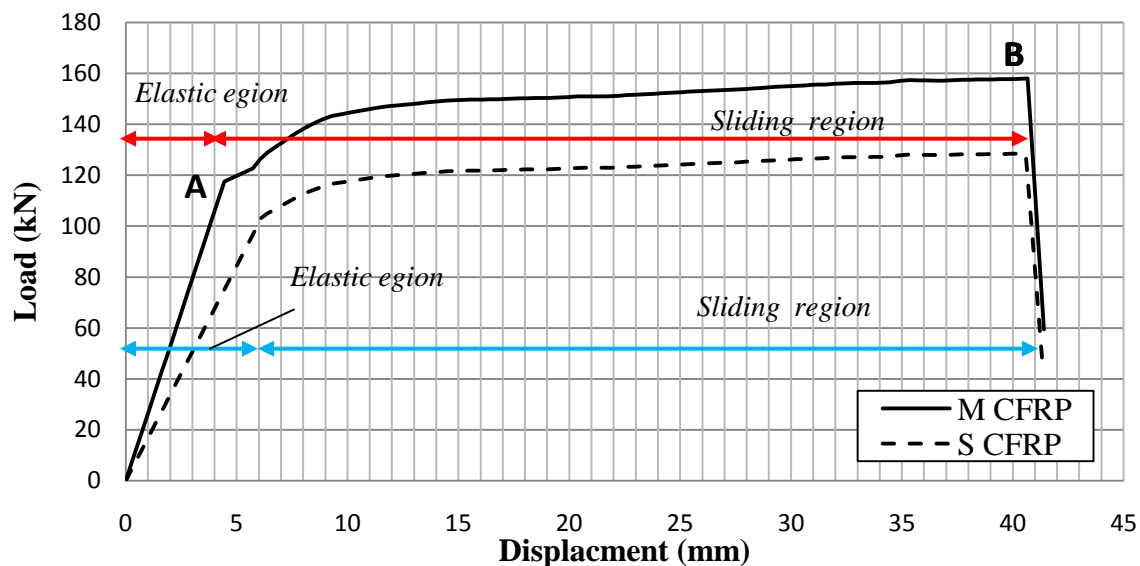


Figure A.8. Tensile load Vs. displacement curves for CFRP strip-anchor assemble

## Appendix B

The stress distributions through the flange thicknesses obtained from FEA are presented in the following tables.

Table B.1. Stress distributions through the flange thickness for the specimen strengthened using attached M-CFRP strips on the cover plates

M-CFRP (E = 210 GPa), Strips on the Cover Plates			
Vertical load: 1 kN		Vertical load: 1 kN	Vertical load: NO
Unreinforced		Reinforced	Reinforced
-----		0% prestressed	37% prestressed
Depth (mm)	Stress (MPa)	Stress (MPa)	Stress (MPa)
0.00	0.003214	0.00282	-135.64
0.05	0.002944	0.00276	-132.91
0.11	0.002671	0.00248	-119.51
0.18	0.002324	0.0021	-101.25
0.26	0.00198	0.00184	-88.68
0.35	0.001826	0.0017	-81.73
0.47	0.001703	0.00159	-76.47
0.60	0.001566	0.00146	-70.30
0.76	0.001456	0.00136	-65.37
0.94	0.001359	0.00127	-61.14
1.16	0.001268	0.00119	-57.28
1.41	0.001194	0.00112	-53.95
1.71	0.001113	0.00104	-50.42
2.06	0.001039	0.00098	-47.40
2.48	0.000986	0.00092	-44.75
2.97	0.000922	0.00087	-42.07
3.54	0.000867	0.00082	-39.60
4.22	0.000817	0.00077	-37.55
5.02	0.000772	0.00073	-35.53
5.95	0.000733	0.0007	-33.85
7.06	0.000699	0.00066	-32.20
8.36	0.000668	0.00063	-30.74
9.89	0.000641	0.00061	-29.68
11.69	0.000639	0.0006	-29.40
13.81	0.000638	0.00061	-29.00
16.30	0.000627	0.0006	-29.00

The stress distributions for specimens 14%-F-M and 35%-F-M are reported in Table B.2.

Table B.2. Stress distributions through the flange thickness for the specimen strengthened using attached M-CFRP strips on the flanges

M-CFRP (E = 210 GPa)-Strips on the Flange				
Vertical load: 1 kN		Vertical load: 1 kN	Vertical load: NO	Vertical load: NO
Unreinforced		Reinforced	Reinforced	Reinforced
-----		Unstressed	14% prestressed	35% prestressed
Depth (mm)	Stress (Mpa)	Stress (MPa)	Stress (MPa)	Stress (MPa)
0.00	0.00321	0.00338	-45.51	-113.8
0.05	0.00294	0.00262	-44.41	-111.0
0.11	0.00267	0.00229	-40.41	-101.0
0.18	0.00232	0.00196	-35.39	-88.5
0.26	0.00198	0.00165	-30.09	-75.2
0.35	0.00183	0.00152	-27.60	-69.0
0.47	0.0017	0.00141	-25.72	-64.3
0.60	0.00157	0.0013	-23.69	-59.2
0.76	0.00146	0.00122	-22.06	-55.2
0.94	0.00136	0.00114	-20.60	-51.5
1.16	0.00127	0.00105	-19.32	-48.3
1.41	0.00119	0.001	-18.20	-45.5
1.71	0.00111	0.00093	-17.04	-42.6
2.06	0.00104	0.00086	-15.99	-39.9
2.48	0.00099	0.00082	-15.15	-37.9
2.97	0.00092	0.00077	-14.29	-35.7
3.54	0.00087	0.00071	-13.51	-33.8
4.22	0.00082	0.00066	-12.76	-31.9
5.02	0.00077	0.00063	-12.16	-30.4
5.95	0.00073	0.00061	-11.75	-29.4
7.06	0.0007	0.00058	-11.27	-28.2
8.36	0.00067	0.00055	-10.93	-27.3
9.89	0.00064	0.00054	-10.68	-26.7
11.69	0.00063	0.00053	-10.66	-26.7
13.81	0.00062	0.00052	-10.50	-26.2
16.30	0.0006	0.00052	-10.2	-25.3

Similar table drawn for the specimen strengthened using S-CFRP strips attached on the flanges as shown in Table B.3. The stress distribution for unreinforced, reinforced and

reinforced with 37% prestressed CFRP strip full-scale beams, 600W and 900W, are given in Tables B.4, B.5 and B.6.

Table B.3. Stress distributions through the flange thickness for the specimen strengthened using attached S-CFRP strips on the flanges

Depth (mm)	S-CFRP (E = 165 GPa)-Strips on the Flange	
	Vertical load: 1 kN	Vertical load: 1 kN
	Reinforced	Reinforced
	Unstressed	15% prestressed
	Stress (MPa)	Stress (MPa)
0.00	0.00288	-41.87
0.05	0.00282	-40.86
0.11	0.00256	-37.18
0.18	0.00224	-32.55
0.26	0.00191	-27.68
0.35	0.00175	-25.39
0.47	0.00163	-23.67
0.60	0.0015	-21.79
0.76	0.0014	-20.29
0.94	0.0013	-18.95
1.16	0.00122	-17.77
1.41	0.00115	-16.75
1.71	0.00108	-15.68
2.06	0.00101	-14.71
2.48	0.00096	-13.94
2.97	0.0009	-13.15
3.54	0.00085	-12.42
4.22	0.0008	-11.74
5.02	0.00076	-11.18
5.95	0.00073	-10.81
7.06	0.0007	-10.37
8.36	0.00067	-10.05
9.89	0.00065	-9.83
11.69	0.00064	-9.81
13.81	0.00064	-9.70
16.30	0.00061	-9.23

Table B.4. Stress distributions through the flange thickness for unreinforced full-scale girders under a vertical applied unit load

Depth (mm)	W600	W900
	Stress (MPa)	Stress (MPa)
0.0	0.001524	0.0009700
0.1	0.001321	0.0008857
0.2	0.001038	0.0007078
0.3	0.000919	0.0006105
0.4	0.000853	0.0005568
0.5	0.000783	0.0005088
0.7	0.000715	0.0004700
0.8	0.000669	0.0004443
1.0	0.000636	0.0004176
1.1	0.000604	0.0003969
1.3	0.000575	0.0003779
1.5	0.000549	0.0003603
1.7	0.000526	0.0003442
1.9	0.000505	0.0003303
2.2	0.000485	0.0003173
2.5	0.000469	0.0003062
2.8	0.000452	0.0002955
3.1	0.000435	0.0002860
3.4	0.000421	0.0002747
3.8	0.000406	0.0002664
4.6	0.000381	0.0002507
5.1	0.000371	0.0002435
6.2	0.000354	0.0002318
6.8	0.000343	0.0002252
7.4	0.000336	0.0002212
8.1	0.000329	0.0002163
8.9	0.000323	0.0002127
9.7	0.000319	0.0002088
10.6	0.000317	0.0002060
11.6	0.000313	0.0002036
12.6	0.000311	0.0002029
13.7	0.000326	0.0002074
15.0	0.000357	0.0002167
16.3	0.000342	0.0002237



Table B.5. Stress distributions through the flange thickness for reinforced full-scale girders under a vertical applied unit load

Depth (mm)	W600	W900
	Stress (Mpa)	Stress (Mpa)
0.0	0.001419	0.0009057
0.1	0.001230	0.0008278
0.2	0.000968	0.0006620
0.3	0.000858	0.0005717
0.4	0.000797	0.0005219
0.5	0.000732	0.0004774
0.7	0.000669	0.0004415
0.8	0.000627	0.0004176
1.0	0.000596	0.0003930
1.1	0.000568	0.0003740
1.3	0.000541	0.0003565
1.5	0.000517	0.0003404
1.7	0.000496	0.0003256
1.9	0.000477	0.0003128
2.2	0.000458	0.0003009
2.5	0.000444	0.0002908
2.8	0.000428	0.0002810
3.1	0.000413	0.0002723
3.4	0.000400	0.0002620
3.8	0.000387	0.0002544
4.2	0.000376	0.0002470
4.6	0.000364	0.0002400
5.1	0.000354	0.0002334
6.2	0.000339	0.0002225
6.8	0.000329	0.0002165
7.4	0.000322	0.0002127
8.1	0.000315	0.0002081
8.9	0.000310	0.0002046
9.7	0.000306	0.0002009
10.6	0.000303	0.0001980
11.6	0.000299	0.0001956
12.6	0.000297	0.0001946
13.7	0.000310	0.0001982
15.0	0.000337	0.0002059
16.3	0.000323	0.0002120

Table B.6. Stress distributions through the flange thickness for 37% prestressed full-scale girders

Depth (mm)	W600	W900
	Stress (MPa)	Stress (MPa)
0.0	-87.34	-78.34
0.1	-75.69	-71.58
0.2	-59.51	-57.22
0.3	-52.74	-49.39
0.4	-48.96	-45.07
0.5	-44.93	-41.21
0.7	-41.08	-38.10
0.8	-38.43	-36.03
1.0	-36.56	-33.89
1.1	-34.79	-32.24
1.3	-33.12	-30.72
1.5	-31.67	-29.32
1.7	-30.35	-28.04
1.9	-29.17	-26.93
2.2	-28.00	-25.89
2.5	-27.10	-25.01
2.8	-26.13	-24.15
3.1	-25.21	-23.38
3.4	-24.40	-22.49
3.8	-23.54	-21.81
4.2	-22.85	-21.15
4.6	-22.12	-20.53
5.1	-21.50	-19.94
6.2	-20.53	-18.96
6.8	-19.87	-18.42
7.4	-19.44	-18.05
8.1	-18.98	-17.63
8.9	-18.61	-17.31
9.7	-18.34	-16.98
10.6	-18.17	-16.75
11.6	-17.95	-16.58
12.6	-17.93	-16.46
13.7	-18.43	-16.77
15.0	-19.84	-18.21
16.3	-19.05	-17.79

## Appendix C

Table C.1. Geometric properties of specimens at midspan ( $x = L/2$ )

Specimen	A (mm <sup>2</sup> )	I (mm <sup>4</sup> )×10 <sup>6</sup>	S <sub>b</sub> (mm <sup>3</sup> ) × 10 <sup>4</sup>	S <sub>t</sub> (mm <sup>3</sup> ) × 10 <sup>4</sup>	$\bar{y}$ (mm)	e (mm)
Control	9290	164	96.2	105.8	155.0	169.7
15%-F-S	9402	166.0	108.2	106.0	156.6	134.5
14%-F-M	9450	167.0	109.3	106.0	157.3	133.8
35%-F-M	9450	167.0	109.3	106.0	157.3	133.8
0%-C-M	9437	168.1	100.0	106.0	157.6	167.0
37%-C-M	9437	168.1	100.0	106.0	157.6	167.0

Table C.2. Geometric properties of specimens at the quarter points ( $x = L/4$ )

Specimen	A (mm <sup>2</sup> )	I (mm <sup>4</sup> )×10 <sup>6</sup>	S <sub>b</sub> (mm <sup>3</sup> ) × 10 <sup>4</sup>	S <sub>t</sub> (mm <sup>3</sup> ) × 10 <sup>4</sup>	$\bar{y}$ (mm)	e (mm)
Control	9290	164	96.2	105.8	155.0	169.7
15%-F-S	11202	197.6	141.4	108.4	182.2	108.9
14%-F-M	11250	197.9	142.0	108.3	182.7	108.4
35%-F-M	11250	197.9	142.0	108.3	182.7	108.4
0%-C-M	11250	199.0	140.0	108.6	183.2	141.5
37%-C-M	11250	199.0	140.0	108.6	183.2	141.5

### C.1 Sample strain calculation

Sample analytical section analysis for specimen 37%-C-M in excel at midspan ( $x = L/2$ ) is presented in follow. Based on the section specifications, bottom and top stresses using following equations can be derived.

$$\sigma_{bottom} = \frac{P}{A} + \frac{P \cdot e}{S_b} - \frac{M}{S_b}$$

$$\sigma_{top} = \frac{P}{A} + \frac{P \cdot e}{S_t} + \frac{M}{S_t}$$

To account for the self weight, the effect of self weight is added using the term of  $\frac{M}{S}$

where the 
$$M = \frac{W \cdot L^2}{8} = \frac{0.727 \cdot 2000^2}{8} = 363500(N - mm)$$

Using bottom and top stresses the stress and consequently, strains at any place over the section are calculated such as the strains at the flange and CFRP strip surface.

The section analysis is shown in details in Table c.3. and Table c.4 for the section at  $x = L/2$  and  $x = L/4$ , respectively.

Table c.3. Stress/Strain calculation (x = L/2)

inputs						
E <sub>epoxy</sub> =		12500				
E <sub>steel</sub> =		200000				
E <sub>cfRP</sub> =		210000		t <sub>cfRP</sub> (mm)= 1.4		
P(N)=		65268		M(N-mm)= 0		
H(mm)=		325.4				
Calculations				Strain & stress		
i	b (mm)	H (mm)	Y (mm)	A (mm <sup>2</sup> )	f <sub>i</sub> (MPa)	ε <sub>i</sub> (ε)
1	205	16.3	8.2	3341.5	-2.81	-1.4E-05
2	9.4	16.3	24.5	153.4	-2.51	-1.3E-05
3	9.4	16.3	40.8	153.4	-2.20	-1.1E-05
4	9.4	16.3	57.1	153.4	-1.89	-9.5E-06
5	9.4	16.3	73.4	153.4	-1.59	-7.9E-06
6	9.4	16.3	89.7	153.4	-1.28	-6.4E-06
7	9.4	16.3	106.0	153.4	-0.97	-4.9E-06
8	9.4	16.3	122.4	153.4	-0.66	-3.3E-06
9	9.4	16.3	138.7	153.4	-0.36	-1.8E-06
10	9.4	16.3	155.0	153.4	-0.05	-2.5E-07
11	9.4	16.3	171.3	153.4	1.42	7.1E-06
12	9.4	16.3	187.6	153.4	3.12	1.6E-05
13	9.4	16.3	204.0	153.4	4.81	2.4E-05
14	9.4	16.3	220.3	153.4	6.51	3.3E-05
15	9.4	16.3	236.6	153.4	8.20	4.1E-05
16	9.4	16.3	252.9	153.4	9.90	5.0E-05
17	9.4	16.3	269.2	153.4	11.60	5.8E-05
18	9.4	16.3	285.5	153.4	13.29	6.6E-05
19	205	16.3	301.9	3341.5	14.99	7.5E-05
20	105	1.4	324.7	147.0	17.36	8.3E-05
21	6.25	0.0	323.0	0.0	17.18	1.4E-03
Σ =				9437.56		
Sections specifications						
y bar (mm)	E (mm)	I (mm <sup>4</sup> )	S <sub>b</sub> (mm <sup>3</sup> )	S <sub>t</sub> (mm <sup>3</sup> )		
157.64	167.1	168102493	1002061	1066348		

transfer section	
n <sub>epoxy</sub> =	0.0625
n <sub>cfRP</sub> =	1.05

The bottom and top stresses are:

$f_{bot}(Mpa)=$	17.43
$f_{top}(Mpa)=$	-2.97

Stresses and strains at the level of flange surface and CFRP strip are:

	y (mm)	f (Mpa)	$\epsilon$ ( $\epsilon$ )
GB1 (steel)	310	-15.83	-7.92E-05
GS3 (CFRP)	325.4	-17.43	-8.30E-05

Sample analytical section analysis for specimen 37%-C-M in excel at a quarter of beams length ( $x = L/4$ ) where the cover plate exist, is presented in follow. Based on the section specifications, bottom and top stresses using following equations can be derived.

$$\sigma_{bottom} = \frac{P}{A} + \frac{P \cdot e}{S_b} - \frac{M}{S_b}$$

$$\sigma_{top} = \frac{P}{A} + \frac{P \cdot e}{S_t} + \frac{M}{S_t}$$

To account for the self weight, the effect of self wieght is added using the term of  $\frac{M}{S}$

where the  $M_x = \frac{W \cdot x}{2} \cdot (L - x) = \frac{0.727 \cdot 500}{2} \cdot (2000 - 500) = 272625(N - mm)$

Using bottom and top stresses the stress and consequently, strains at any place over the section are calculated such as the strains at the flange and CFRP strip surface.

Table c.4. Stress/Strain calculation ( $x = L/4$ )

inputs	
$E_{\text{epoxy}} = 12500$	
$E_{\text{steel}} = 200000$	
$E_{\text{cfRP}} = 210000$	$t_{\text{cfRP}}(\text{mm}) = 1.4$
$P(N) = 65268$	$M(N\text{-mm}) =$
$H(\text{mm}) = 325.4$	
Calculations	

transfer section
$n_{\text{epoxy}} = 0.0625$
$n_{\text{cfRP}} = 1.05$

i	b (mm)	H (mm)	Y (mm)	A (mm <sup>2</sup> )
1	205	16.3	8.15	3341.5
2	9.4	16.3	24.46	153.4
3	9.4	16.3	40.78	153.4
4	9.4	16.3	57.09	153.4
5	9.4	16.3	73.41	153.4
6	9.4	16.3	89.73	153.4
7	9.4	16.3	106.05	153.4
8	9.4	16.3	122.36	153.4
9	9.4	16.3	138.68	153.4
10	9.4	16.3	155.00	153.4
11	9.4	16.3	171.32	153.4
12	9.4	16.3	187.64	153.4
13	9.4	16.3	203.95	153.4
14	9.4	16.3	220.27	153.4
15	9.4	16.3	236.59	153.4
16	9.4	16.3	252.91	153.4
17	9.4	16.3	269.22	153.4
18	9.4	16.3	285.54	153.4
19	205	16.3	301.85	3341.5
20	105	1.4	324.70	147.0
21	6.25	2.0	323.00	12.5
22	150	12.0	316.00	1800.0
			$\Sigma =$	11250.06

Sections specifications				
y bar(mm)	e (mm)	I (mm <sup>4</sup> )	S <sub>b</sub> (mm <sup>3</sup> )	S <sub>t</sub> (mm <sup>3</sup> )
183.16	141.54	198972585	1398890	1086309

The bottom and top stresses are:

$$f_{\text{bot}}(\text{Mpa}) = 12.21033074$$
$$f_{\text{top}}(\text{Mpa}) = -2.45128814$$

Stresses and strains at the level of flange surface and CFRP strip are:

	y (mm)	f (Mpa)	$\epsilon$ ( $\epsilon$ )
GS1 (CFRP)	325.4	-12.21	-5.81E-05